



The
University
Of
Sheffield.

Zebrafish as a translational model of Parkinson's disease – a study of microRNAs

Lisa Trollope

Thesis submitted for the degree of Doctor of Philosophy

The University of Sheffield

Faculty of Medicine, Dentistry and Health

Department of Neuroscience

September 2015

Acknowledgements

I would firstly like to thank my supervisor, Professor Oliver Bandmann, who has been a fantastic mentor over the past 4 years. He supported and encouraged me throughout the PhD process, allowing me freedom to develop as a scientist while ensuring I stay focused.

I would also like to thank the University of Sheffield for funding this PhD project as part of the Sheffield Epigenetics Network. At the outset of my PhD, the Epigenetics Network meetings inspired my greater interest in the subject and allowed me to develop my skills and confidence in presenting my work.

Thank you to Heather Mortiboys for mentoring me in the lab in the first years of my PhD, and to Marcus Keatinge and Marc Da Costa for helping me in my transition into zebrafish research and for proof reading this thesis. I would also like to thank other members of both SITraN and the Bateson Centre, particularly Adrian Higginbottom, Caroline Gray, Richard Maguire and Stone Elworthy who have always gone out of their way to help me and answer my questions. Special thanks go to Phillippa Carling for her endless good advice and great friendship.

I owe my friends a great deal, for keeping me sane, offering support and making life extremely enjoyable both inside and outside of science.

Finally, my thanks go to my parents and to Mike for all their love, encouragement and support.

Abstract

Parkinson's disease (PD) is the second most common neurodegenerative disorder, currently there are no disease modifying treatments. It is thought that microRNAs may be implicated in pathogenesis of PD. In this thesis the function of three microRNAs, which may be relevant to PD, were investigated in zebrafish. These miRNAs are: miR-133b, thought to be involved in development of dopaminergic neurons through its target *PITX3*; miR-205, which has been shown to regulate the PD-associated gene *LRK2*; and miR-155, a key regulator of immune and inflammatory processes. Despite being more evolutionarily distant to humans than rodent models, the zebrafish has emerged as an effective model of human disease due to its low cost, fast development and transparency. A further aim of this thesis was to develop a high throughput imaging strategy to assess dopaminergic neuron number in the developing zebrafish brain, which can be used as a screening tool to identify potentially therapeutic compounds.

The effect of both miR-133b and miR-205 knockdown on the number of dopaminergic neurons was investigated. In wild type zebrafish miR-205 knockdown causes a slight but significant decrease in dopaminergic neurons whereas miR-133b knockdown causes a significant increase in dopaminergic neuron number. In a previously established zebrafish model of PD, miR-133b knockdown completely rescued a 15% decrease in dopaminergic neuron number. The expression of miR-155 was assessed in three different zebrafish models of PD. While no change was observed in *pink1*- or *parkin*-deficient zebrafish, an increase in this miRNA and related inflammatory markers was observed in both larvae and juvenile brains of *gba1*-deficient zebrafish. As this miRNA and inflammatory markers are shown to be upregulated before any neuron loss is detectable in these zebrafish, it is possible that miR-155-related inflammation contributes to neurodegeneration. A stable miR-155 mutant line was also generated which will be used to determine whether genetic ablation of this miRNA has a protective effect in *gba1*-deficient zebrafish.

A fluorescent reporter line expressing GFP in monoaminergic neurons has been validated for study of dopaminergic neurons. A fluorescence-based method developed using this line was able to reproduce data using a previously established *in situ* hybridisation-based method for neuron counting. To allow for more time and cost effective mounting of embryos for imaging, a mould has been developed. Use of this mould to mount embryos allows for high throughput imaging of the developing brain.

The miRNAs presented in this study may have therapeutic potential in PD through modulation of dopaminergic neuron survival or by regulating the expression of PD-associated genes. The development of a high throughput screening process may allow a PD-related drug or toxin screen to be performed in our group in the near future.

Contents

Chapter 1. Introduction	1
Chapter 2. Materials and Methods.....	44
Chapter 3. Investigating the role of miR-133b in dopaminergic neuron development and survival	78
Chapter 4. Investigating the interaction between miR-205 and <i>Irrk2</i> in zebrafish	132
Chapter 5. miR-155 and the role of neuroinflammation in neurodegeneration.....	156
Chapter 6. Developing a high throughput imaging system for zebrafish larval brains....	178
Chapter 7. General Discussion	210
Bibliography	221

List of Figures

Chapter 1

Figure 1. Parkinson's disease incidence and total prevalence in the UK.	4
Figure 2. Clinical symptoms and time course of Parkinson's disease progression.	8
Figure 3. Neuronal circuits for control of motor activity.	10
Figure 4. Overview of genetic variants associated with Parkinson's disease.	15
Figure 5. Cellular processes involved in Parkinson's disease pathology.	17
Figure 6. The adult zebrafish brain.	29
Figure 7. miRNA biogenesis and post-transcriptional repression.	34
Figure 8. DNA methylation, histone modification and the structure of chromatin.	36
Figure 9. miRNAs thought to be involved in the pathogenesis of Parkinson's disease.	42

Chapter 2

Figure 10. Fin clipping of embryos.	49
Figure 11. Using a graticule to measure injection volume.	50
Figure 12. Regions of the pri-miRNA transcript and MO design.	50
Figure 13. Injecting into the ventricles of a 24hpf embryo.	52
Figure 14. Plasmid map of dual reporter plasmid.	66
Figure 15. Location of <i>th</i> + neurons in 2 and 5dpf zebrafish.	70

Chapter 3

Figure 16. Identification of a feedback loop between miR-133b and PITX3 in midbrain dopaminergic neurons.	81
Figure 17. Summary of PITX3 network.	83
Figure 18. Polymorphisms conferring a significant risk or protective effect for PD in the <i>PITX3</i> genetic locus.	85
Figure 19. Protein homology and genetic locus synteny between human and zebrafish <i>pitx3</i>	86
Figure 20. Polymorphisms conferring a significant risk or protective effect for PD in the miR-133b containing genetic locus.	88
Figure 21. Possible mechanism of action of cocaine through miR-133b in zebrafish embryos.	89
Figure 22. Design of a WISH probe for <i>pitx3</i>	90
Figure 23. Conservation of miR-133b across species.	91
Figure 24. Gene synteny in the region surrounding human and zebrafish miR-133b.	92
Figure 25. Spatial expression of miR-133b at 3dpf.	93
Figure 26. Expression and localisation of <i>pitx3</i>	93
Figure 27. Knockdown of miR-133b using MO at 3dpf.	95
Figure 28. The effect of miR-133b knockdown on <i>th</i> mRNA levels.	95
Figure 29. miR-133b knockdown results in an increase of <i>th</i> + dopaminergic neurons at 3dpf.	96

Figure 30. Dopaminergic neuron number in uninjected and control MO injected embryos.....	96
Figure 31. Knockdown of miR-133b in <i>pink1</i> ^{-/-} embryos rescues <i>th</i> + dopaminergic neuronal loss.	97
Figure 32. Knockdown of miR-133b in MPP+ treated zebrafish is unable to rescue <i>th</i> + dopaminergic neuronal loss.	98
Figure 33. The effect of miR-133b knockdown on number of <i>th</i> + dopaminergic neurons at 36 and 48hpf.	99
Figure 34. miR-133b levels after miRNA mimic injection.....	101
Figure 35. FITC dextran injections into zebrafish ventricles.....	102
Figure 36. miR-133b levels after injection of miRNA mimic into ventricles.....	102
Figure 37. Number of <i>th</i> + dopaminergic neurons after miR-133b mimic injection.....	103
Figure 38. Localisation of miR-133b after miR-133b mimic injection.	104
Figure 39. A potential miR-133b binding site in zebrafish <i>pitx3</i> 3'UTR.....	105
Figure 40. Dual reporter plasmid maps.....	106
Figure 41. GFP and RFP fluorescence with control reporter plasmid.	107
Figure 42. MOs targeting <i>pitx3</i>	109
Figure 43. Testing of Abcam Pitx3 antibody.....	110
Figure 44. Initial testing of custom antibodies for Pitx3.	111
Figure 45. Optimisation of antibody incubation time.	112
Figure 46. Antibody ab164 specifically detects a band at 32kDa.....	113
Figure 47. Antibody ab164 specifically detects zebrafish Pitx3.	114
Figure 48. miR-133b knockdown does not increase <i>pitx3</i> mRNA levels at 3dpf.....	115
Figure 49. Assessment of miR-133b- <i>pitx3</i> interaction using reporter plasmid.....	116
Figure 50. miR-133b knockdown does not increase Pitx3 protein levels at 3dpf.	117
Figure 51. EdU incorporation into proliferating neurons.....	118
Figure 52. EdU incorporation into proliferating neurons in early development.....	119
Figure 53. EdU and TH in WT and miR-133b morphants.....	120
Figure 54. <i>neurogenin1</i> WISH and EdU staining at 13hpf.	121
Chapter 4	
Figure 55. Lrrk2 domain structure, domain functions and mutations associated with PD.	134
Figure 56. Conservation of amino acid sequences and functional domains of LRRK2 between human and zebrafish.	137
Figure 57. Design of a WISH probe for <i>lrrk2</i>	139
Figure 58. Conservation of miR-205 across species.	140
Figure 59. Spatial expression of miR-205 at 3dpf.....	140
Figure 60. Expression and localisation of <i>lrrk2</i>	141
Figure 61. Knockdown of miR-205 using MO.	142
Figure 62. miR-205 knockdown has no effect on <i>th</i> mRNA levels at 3dpf.	142
Figure 63. miR-205 knockdown results in a small decrease in <i>th</i> + dopaminergic neurons at 3dpf...	143

Figure 64. Validated and predicted binding sites for miR-205 in <i>lrrk2</i> 3'UTR.	143
Figure 65. RT-PCR analysis of the effect of the <i>lrrk2</i> MOs.	145
Figure 66. Effect of <i>lrrk2</i> MOs on the <i>lrrk2</i> transcript.....	145
Figure 67. Initial testing of <i>Lrrk2</i> antibody.	147
Figure 68. Investigating the specificity of the <i>Lrrk2</i> antibody using MOs.	147
Figure 69. miR-205 knockdown has no effect on <i>lrrk2</i> mRNA levels at 3dpf.	149
Figure 70. miR-205 knockdown has no effect on <i>Lrrk2</i> protein levels at 3dpf.....	149
Chapter 5	
Figure 71. Conservation of miR-155 across species.	159
Figure 72. Stability of zebrafish U6 snRNA and miR-24 in a range of samples.....	163
Figure 73. Reliability of qPCR results using accurate RNA quantification.	164
Figure 74. miR-155 expression levels are increased in <i>gba1</i> mutant brains and larvae.	164
Figure 75. Spatial expression of miR-155 in <i>gba1</i> mutants.....	165
Figure 76. miR-155 expression is not altered in PD zebrafish larvae and adult brains.	166
Figure 77. Expression of inflammatory markers in <i>gba1</i> mutant brains and larvae.	168
Figure 78. CRISPR/Cas9 gene editing system.	169
Figure 79. CRISPR sites in miR-155 region.....	170
Figure 80. Analysis of efficacy of miR-155 CRISPRs.....	171
Figure 81. Design and efficacy of miR-155 gRNA5.	172
Chapter 6	
Figure 82. Comparison of strategies for drug discovery.	181
Figure 83. Neuronal groups labelled by the <i>ETvmat2:GFP</i> reporter line.	184
Figure 84. Image analysis process with <i>ETvmat2:GFP</i> embryos.	186
Figure 85. <i>th+</i> dopaminergic neuron counts and fluorescence intensity in WT and miR-133b morphants.	188
Figure 86. <i>th+</i> dopaminergic neuron counts and fluorescence intensity in WT and MPP+ treated embryos.....	189
Figure 87. Image analysis methods with WT and <i>pink1</i> ^{-/-} embryos.	191
Figure 88. Using a 3D printed mould for zebrafish orientation for imaging.	194
Figure 89. Testing high throughput imaging of zebrafish embryos using the IN Cell Analyzer 2000.	196
Figure 90. Testing different concentrations of agarose to make wells.	199
Figure 91. Fluorescence intensity measurements using new mounting and imaging technique.	200
Figure 92. Contribution of area and intensity to total fluorescence intensity reading in WT and miR- 133b morphants.	203
Figure 93. Comparison of standard deviation from image analysis data from mould mounted and individually mounted zebrafish embryos.	206
Figure 94. Potential drug screening pipeline.....	209

List of tables

Chapter 1

Table 1. Prevalence of non-motor symptoms of Parkinson’s disease and related pathology.	11
Table 2. Monogenic forms of Parkinson’s Disease.	12
Table 3 Comparison of zebrafish with other model organisms.	26

Chapter 2

Table 4. Morpholinos used in this study.	51
Table 5. miRNA mimics used in this study.	52
Table 6. PCR/RT-PCR primers used in this study.	56
Table 7. qPCR primers used in this study.	57
Table 8. Taqman assays used in this study.	58
Table 9. Primers used to generate WISH probes.	60
Table 10. Exiqon LNA probes used.	61
Table 11. Antibodies used for fluorescent WISH and IHC.	64
Table 12. Components of the Click-IT® kit for EdU staining.	65
Table 13. Primers used for generation and analysis of reporter plasmids.	68
Table 14. Antibodies used for western blotting.	73
Table 15. Peptide epitopes of custom antibodies.	74
Table 16. Primers and ultramers used in CRISPR generation.	75

Chapter 3

Table 17. Potential targets of miR-133b of interest in Parkinson’s disease.	130
--	-----

Chapter 5

Table 18. Inflammatory markers increased in GD patients, <i>gba1</i> deficient mouse brains and PD patients with <i>GBA</i> mutations.	167
Table 19. Mutations caused by miR-155 CRISPR5.	173

Chapter 7

Table 20. Selected miRNA therapies currently in development.	219
---	-----

Abbreviations

-/-: homozygous mutant
+/-: heterozygous
+/+: wild type
3'UTR: 3' untranslated region
6-OHDA: 6-hydroxydopamine
AADC: aromatic amino acid decarboxylase
BBB: blood brain barrier
Cas9: CRISPR associated protein 9
cDNA: complementary DNA
CNS: Central nervous system
COR: C-terminal of ROC (domain of LRRK2)
CpG: cytosine-phosphate-guanine (a dinucleotide of C followed by G)
CRISPR: Clustered regularly interspaced short palindromic repeats
CSF: cerebrospinal fluid
D2: dopamine receptor 2
DAT: dopamine transporter
dpf: days post-fertilisation
EAE: experimental autoimmune encephalitis
EDS: excessive daytime sleepiness
EdU: 5-ethynyl-2'-deoxyuridine
EMT: epithelial to mesenchymal transition
ENU: N-ethyl-N-nitrosurea
EOPD: early onset PD
ER: endoplasmic reticulum
ESCs: embryonic stem cells
EtOH: ethanol
FOV: field of view
GAP: GTPase activating protein
GBA: glucocerebrosidase
gDNA: genomic DNA
GFP: green fluorescent protein
GPRD: General Practice Research Database
gRNA: guide RNA
GWAS: genome-wide association study
hpf: hours post-fertilisation
HTT: huntingtin
IHC: immunohistochemistry
iPSCs: induced pluripotent stem cells
LMP: low melting point
LNA: locked nucleic acid
LOPD: late onset PD
LPS: lipopolysaccharide
LRRK2: leucine rich repeat kinase 2
MCI: mild cognitive impairment
MDS-UPDRS: Movement Disorders Society unified Parkinson's disease rating scale
MeOH: methanol
miRNA/miR-: microRNA
MND: motor neuron disease
MO: morpholino

MPP+: 1-methyl-4-phenylpyridinium
MPTP: 1-methyl-4-phenyl-1, 2, 3, 6-tetrahydropyridine
mRNA: messenger RNA
NPC: non-pathogenic control
OR: odds ratio
PBS: phosphate buffered saline
PCR: polymerase chain reaction
PD: Parkinson's disease
PDD: Parkinson's disease with dementia
PFA: paraformaldehyde
PINK1: PTEN-induced putative kinase 1
PITX3: pituitary homeobox 3/paired-like homeodomain 3
pri-miRNA: primary microRNA
PTU: phenylthiourea
qPCR: quantitative real time PCR
RBD: REM sleep behaviour disorder
REM: rapid eye movement
RFP: red fluorescent protein
RISC: RNA induced silencing complex
ROC: Ras-like G-domain (domain of LRRK2)
RT-PCR: reverse transcription PCR
siRNA: small interfering RNA
SNCA: α -synuclein
TALEN: transcription activator-like effector nucleases
TH: tyrosine hydroxylase
UPS: ubiquitin-proteasome system
VMAT2: vesicular monoamine transporter 2
WISH: whole mount *in situ* hybridisation
WT: wild type

Chapter 1. Introduction

Contents

1.1 Parkinson's Disease.....	3
Incidence and economic burden of Parkinson's disease	4
Symptoms, diagnosis and treatment of Parkinson's disease	5
Pathology of Parkinson's disease.....	9
Causes and pathogenesis of Parkinson's Disease	12
1.2 Models of Parkinson's disease.....	18
Human cell culture models	18
Mammalian toxin induced models	20
Mammalian genetic animal models.....	21
Non-mammalian models of PD	23
1.3 Zebrafish as a model of neurodegenerative disease	25
Suitability of zebrafish as a model organism	25
Zebrafish genetic tools.....	26
Zebrafish as a model of neurodegeneration.....	28
1.4 microRNAs and human disease	32
Discovery and biogenesis of miRNAs	33
Epigenetics and non-coding RNAs	35
miRNA involvement in neurodegeneration	38
miRNAs relevant to Parkinson's disease.....	39
1.5 Aims and hypotheses	43

1.1 Parkinson's Disease

Parkinson's Disease (PD) is a common neurodegenerative disorder, affecting approximately 1% of the population in the western world (de Lau & Breteler 2006). The prevalence of PD is second only to Alzheimer's disease which affects approximately 4% of over 65s in Europe (Qiu et al. 2009).

PD was first described in 1817 by James Parkinson, after whom the disease is named. In his famous essay "An Essay on the Shaking Palsy" he systematically described 6 patients suffering with this condition. The disorder was not named Parkinson's disease until the mid-1800s when Jean-Martin Charcot refined Parkinson's early description and disseminated this information internationally. Parkinson had predicted that the "shaking palsy" was due to lesions in the cervical spinal cord (Parkinson 1817, subsequently reprinted in Parkinson 2002). We now know that many of the symptoms of PD are attributable to the progressive loss of dopaminergic neurons within the *substantia nigra pars compacta*. Although the disease is clinically defined by the characteristic motor symptoms, many non-motor symptoms are also associated with PD.

Since the clinical recognition of PD nearly 200 years ago tremendous effort has been put into understanding the causes and pathogenesis of this disease. However, there is still much that is unknown about this disorder. There are currently no disease modifying treatments for PD. Treatments, such as the dopamine precursor levodopa, are available to alleviate symptoms of the disease. Although treatment with levodopa is initially effective it becomes less effective over time and is associated with a number of side effects. The heterogeneous nature of PD has complicated drug discovery efforts as the pathology of the disease in patients may vary considerably (Kalia & Lang 2015). This highlights the need for a greater understanding of the range of pathologies associated with PD. In time this may allow for "personalised" medication.

In recent years, many advances have been made in the discovery of genetic risk factors for PD, developing research techniques and new animal models for study of PD (Shulman et al. 2011). As Shulman and colleagues state: "fortunately, the confusion that accompanies the crest of a rapidly advancing wave of discovery is usually transient, and in its wake comes a deeper understanding". We can be cautiously optimistic that new treatments for PD will be available in the not too distant future.

Incidence and economic burden of Parkinson's disease

In the UK the incidence of PD, as calculated in 2009 by the charity Parkinson's Disease UK, was 27.4 persons per 10,000 of the population over 20 years of age (Parkinson's UK 2009). Within the UK, this equates to a total of close to 127,000 cases of PD. The study performed by Parkinson's Disease UK calculated a higher prevalence of PD compared to others, which have reported a varied prevalence of between 10.5 to 17.8 persons with PD per 10,000 of the population in the UK (Hobson et al. 2005; Mutch et al. 1986). The variance between these studies is likely to be due to the small and geographically distinct populations used to calculate disease prevalence and the bias introduced by particular characteristics of these populations. The study performed by Parkinson's Disease UK used data from the General Practice Research Database (GPRD). In 2009, the GPRD contained data for over 7% of the population (3.4 million persons) and was considered representative of the UK population (Williams et al. 2012). Figure 1 shows the incidence and prevalence of PD in discrete age groups.

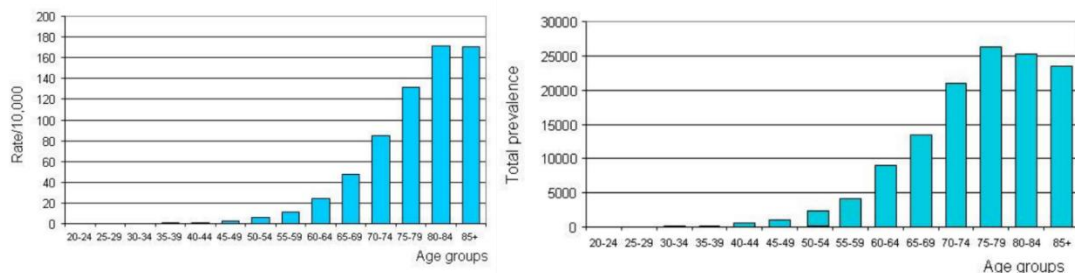


Figure 1. Parkinson's disease incidence and total prevalence in the UK. Reproduced from Parkinson's UK (2009)

PD is primarily a disease of the elderly with the majority of sufferers being over 70 years of age (Figure 1). Classical PD presents in people 60 years or older (Halliday & McCann 2010). A small number of patients who develop the disease before the age of 40 are classified as early-onset PD (EOPD) patients. EOPD is more commonly linked to familial PD (Schrag & Schott 2006).

Familial PD, defined as those cases where a first degree relative is also affected by PD, accounts for approximately 10% of all cases. The remaining 90% of cases are referred to as "sporadic" PD (Thomas & Flint Beal 2007). The single largest risk factor for sporadic PD is age. As the worldwide life expectancy increases the number of cases of PD, and other diseases of the elderly, will also increase. In rapidly developing nations such as China and India the number of PD cases is predicted to more than double by 2030 (Dorsey et al. 2007). Although the total population of the western world is rising less rapidly than that of developing

nations, the elderly population is growing more rapidly than any other age group. In 2010 there were approximately 10 million over 65s in the UK, 1/6th of the total population. This is expected to increase to approximately 19 million by 2050, equating to one in four people being in this age group (Cracknell 2010). The increased number of PD cases, which will inevitably result from the aging population, will result in increased pressure on primary care givers and an increased financial burden on patients and their health and social care systems. Furthermore, increased physical and emotional strain will be placed on patients and their families as these services are stretched.

In 2010 the total cost per PD patient in the UK over the course of their illness was calculated to be over €20,000. The majority of the cost of PD stems from what is termed as “direct non-medical” costs which includes the cost of social services, special accommodation and related care. This accounts for approximately 75% of the total cost of the disease. The remaining 25% is made up of direct medical costs and indirect costs for example early retirement (Fineberg et al. 2013).

The development of better drugs and other treatments to slow disease progression will not only help to improve the quality of life of PD sufferers and their families, but may also help to reduce the total cost of PD by increasing the independence of PD patients and thus limiting the “direct non-medical” costs.

Symptoms, diagnosis and treatment of Parkinson’s disease

PD is a chronic and progressive disorder with a highly variable disease course. Like many neurodegenerative diseases PD is clinically heterogeneous; some suggest that PD is likely to be a collection of related disorders rather than one distinct disease. In this section the major symptoms of the disease will be introduced. However, it is worth noting that not all patients develop all of the symptoms listed here in the same order, or indeed at all. Many efforts have been made to classify different subtypes of PD based on clustered clinical features, and in time this may aid research into distinct pathologies and aid treatment recommendations for individuals (Marras & Lang 2012).

PD has been traditionally regarded as a motor disorder and the motor symptoms are regarded as the cardinal symptoms of the disease. Bradykinesia, one of the main motor symptoms, describes a slowness of movement. This overarching symptom is also related to many secondary motor symptoms including: hypophonia (soft speech), hypomimia (reduced degree of facial expressions), micrographia (small, bunched handwriting), shuffling gait and

dysphagia (problems with swallowing) (Jankovic 2008). Together these symptoms may cause difficulty for patients in everyday activities. Resting tremor is the most apparent symptom and typically presents asymmetrically. Tremor characteristically disappears with movement or sleep (Askenasy & Yahr 1990; Sternberg et al. 2013). Rigidity is also a major motor feature and is often associated with pain. Shoulder pain is a common first manifestation of PD which is often, understandably, misdiagnosed as shoulder injury or arthritis (Stamey et al. 2008). Postural instability and freezing are further motor symptoms that mainly occur in later stages of the disease. These are common causes of falls and related injuries in PD sufferers (Williams et al. 2006).

With regard to motor symptoms, there are currently thought to be two major subtypes of PD: tremor dominant PD and non-tremor dominant PD. There are also patients who are intermediate of these two groups. Tremor-dominant PD patients demonstrate a relative absence of the other symptoms of PD; this is also associated with relatively slow disease progression. Non-tremor dominant PD patients generally display more dominant bradykinesia and rigidity (Marras & Lang 2012). While not all PD patients develop all of the above motor symptoms initially, the majority will suffer from them over the course of the disease. Some studies suggest that up to 25% of patients never experience a resting tremor (Hughes et al. 1993), however another study found that in all PD cases confirmed by autopsy a resting tremor had been detected at some stage in the disease course (Rajput et al. 1991).

There are a range of drugs available to treat motor symptoms. The most common of these is levodopa, a precursor to many catecholaminergic neurotransmitters. Treatment with levodopa is usually delayed for as long as the patient's quality of life is considered adequate. Although this treatment is initially effective in reducing motor symptoms and many patients benefit for several years, it is associated with potential motor complications such as dyskinesias (impairment of voluntary movement). Direct dopamine agonists are also effective for treatment but over time may result in peripheral oedema, impulse control disorders and excessive drowsiness (Massano & Bhatia 2012). Deep brain stimulation is also used as a treatment to alleviate motor symptoms in carefully selected patients (Lang et al. 2006).

Although less well known, PD also results in many non-motor symptoms that are equally damaging to patients' quality of life. Common non-motor symptoms include sensory abnormalities such as anosmia (loss of sense of smell), visuospatial abnormalities, autonomic dysfunction, sleep disturbances and depression. Many of these non-motor symptoms

present early in the course of PD and may precede motor symptoms by many years (Zesiewicz et al. 2006).

Pre-motor or prodromal phase symptoms may include constipation, sleep disturbances such as rapid eye movement (REM) sleep behaviour disorder (RBD) and excessive daytime sleepiness (EDS), impaired olfaction, visual dysfunction (for example impaired colour vision) and depression (Khoo et al. 2013). Less frequent bowel movements (<1 per day) have been shown to increase risk for PD approximately three-fold (Savica et al. 2009). Those who suffer with clinical depression are twice as likely to be diagnosed with PD in later life and approximately 70% of patients who experience both impaired colour vision and RBD develop PD or dementia within 5 years (Postuma et al. 2011; Noyce et al. 2012). The presence of these symptoms suggests that the pathology of PD begins well before the onset of motor symptoms. With further research these symptoms and the related pathology may be used to aid earlier diagnosis of PD.

With the progression of the disease and worsening of motor symptoms, further non-motor symptoms may manifest. Constipation is again a common complaint and other autonomic symptoms such as urinary incontinence and orthostatic hypotension (low blood pressure upon standing, resulting in dizziness or light-headedness) are present in some patients with advanced PD (Pfeiffer 2012). Cognitive impairment and dementia is also common in late stage PD; up to 80% of patients who have had PD for 20 years develop dementia (Hely et al. 2008). As well as dementia, a wide range of neuropsychiatric problems are associated with PD. These can be severely disabling and result in increased admission to nursing or care homes. In one study the 10-item Neuropsychiatric Inventory was used to assess over 500 PD patients with dementia (PDD). This study identified that nearly 90% of patients present with at least one NPI symptom, the most common of these were depression, apathy, anxiety and hallucinations (Aarsland et al. 2007).

Finally, further features of late-stage PD include both motor and non-motor complications. Impulsive and obsessive-compulsive behaviours and psychosis have been associated with PD. Although the pathology of these behaviours is not well understood they may be attributed to dopamine dysregulation and use of dopaminergic drugs (Spencer et al. 2011; Friedman 2013). Again, although there are currently no therapies that alter the disease course, there are available treatment options to manage the non-motor symptoms of PD. These are reviewed in detail by Kalia & Lang (2015). Figure 2 summarises the clinical symptoms and disease progression of PD.

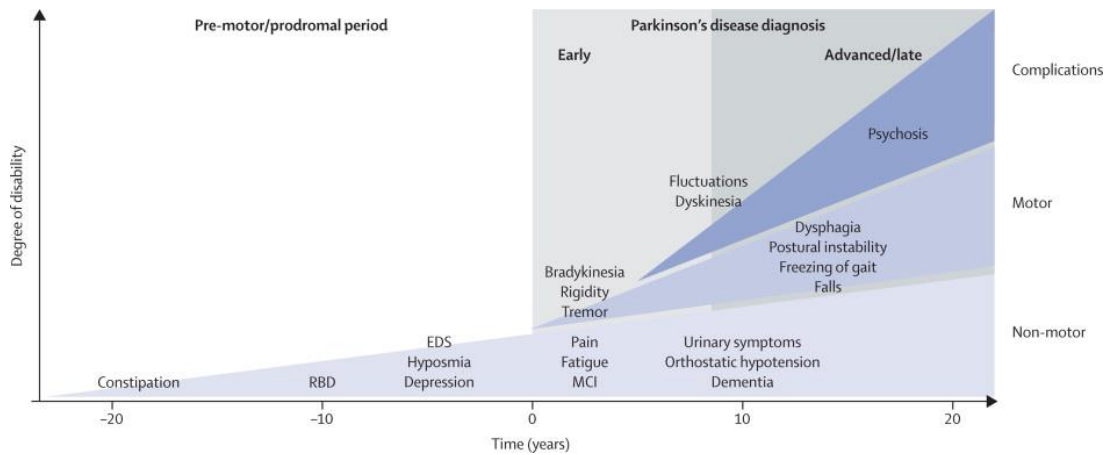


Figure 2. Clinical symptoms and time course of Parkinson's disease progression. EDS = excessive daytime sleepiness, RBD = REM sleep behaviour disorder, MCI = mild cognitive impairment. Reproduced with permission from Kalia & Lang (2015).

Currently, there are no simple diagnostic tests or biomarkers to aid the diagnosis of PD. Therefore, diagnosis is based on clinical presentation of the disease and the ruling out of alternate causes of the displayed symptoms. The diagnostic process is often hindered by the heterogeneous clinical presentation of the disease (Jankovic 2008).

Diagnosis is based on the presence of two or three characteristic motor symptoms of the disease; bradykinesia plus either resting tremor or rigidity. Using these symptoms alone does not distinguish PD from other forms of Parkinsonism such as multiple system atrophy, and progressive supranuclear palsy (Hughes et al. 1992). Additional criteria for diagnosis such as a positive response to levodopa treatment aid a correct diagnosis. The UK Parkinson's Disease Society Brain Bank provides a panel of exclusion criteria and supportive prospective criteria to aid diagnosis and distinguish PD from other similar disorders. However, this is still mostly based on the motor symptoms and includes many symptoms which are often present late in the disease course such as postural instability (Hughes et al. 1992). Berg and colleagues argue that PD needs to be redefined and suggest a three tiered approach taking into account clinical features, pathological findings and genetic and molecular mechanisms. Within the clinical tier, which will aid diagnostic efforts, they suggest that more emphasis needs to be placed on the non-motor symptoms that often precede the characteristic motor symptoms. However, the authors concede that this process will be challenging and more research needs to be performed to allow integration of the current body of knowledge to produce a comprehensive new definition of PD (Berg et al. 2013).

There are several rating scales to aid assessment of disease progression. The 5-stage Hoehn and Yahr scale is often used to compare groups of patients. Stage 0 indicates no signs of

disease and patients reach stage 5 when they are wheelchair or bedridden unless assisted. The Unified Parkinson's Disease Rating Scale (UPDRS), which assesses the overall disability of PD sufferers, is perhaps the most widely used and well established scale (Ebersbach et al. 2006). This scale was updated in 2007 by the Movement Disorder Society (now known as the MDS-UPDRS) to include a section for the non-motor symptoms of PD (Goetz et al. 2007).

Pathology of Parkinson's disease

The motor symptoms of PD strongly correlate with the loss of dopamine producing neurons in the *substantia nigra* and the related dopamine deficiency (Shulman et al. 2011). The neurons of the *substantia nigra* have ascending projections into the striatum. This signalling modulates neuronal circuits within the basal ganglia which facilitate movement. There are two neuronal circuits from the striatum, direct and indirect, which together regulate motor activity (Figure 3). The direct pathway stimulates motor activity and is stimulated by dopamine signalling. The indirect pathway inhibits motor activity and is inhibited by dopamine signalling. Therefore a loss of dopamine signalling from the *substantia nigra* results in a loss of motor activity through both pathways (Obeso et al. 2008).

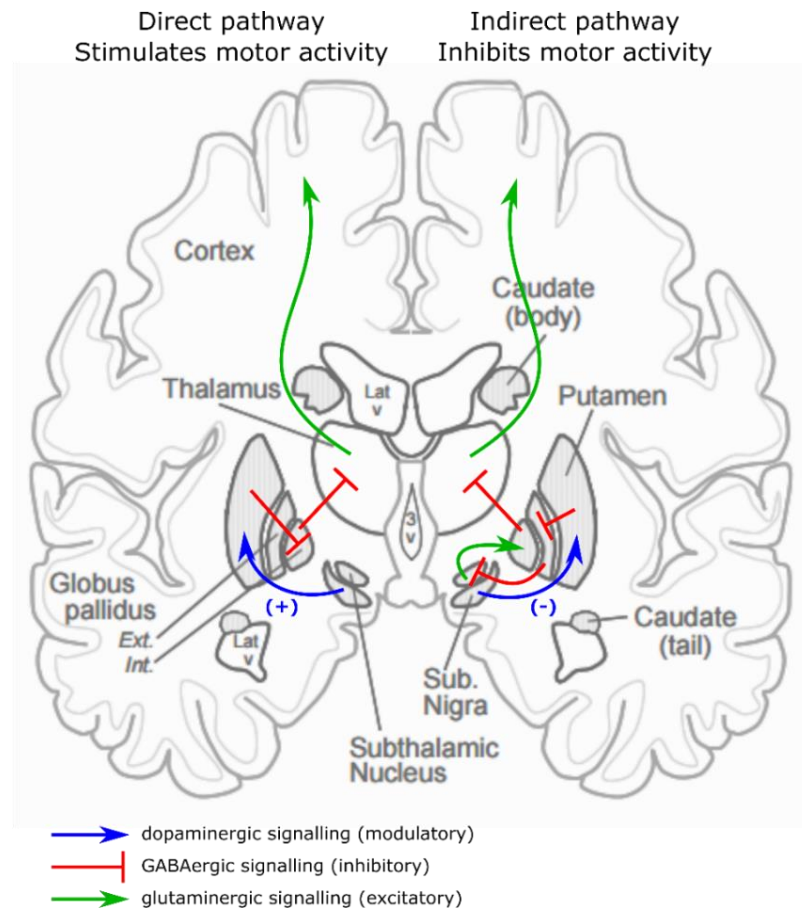


Figure 3. Neuronal circuits for control of motor activity. This figure shows a coronal section of the brain. Neuron populations involved in control of motor activity are labelled. The “direct” and “indirect” neuronal circuits which stimulate and inhibit motor signalling and are modulated by dopamine signalling from the substantia nigra (Sub. Nigra) are shown.

Alongside dopaminergic neuron loss, another major pathological hallmark of PD is the presence of Lewy bodies. Lewy bodies are inclusions of aggregated, abnormally folded proteins and are present in the majority of PD patients (Kalia & Lang 2015). Aggregates of PD-related proteins α -synuclein and Microtubule-associated protein tau (Tau) been shown to be the major components of Lewy bodies (Spillantini et al. 1997; Ishizawa et al. 2003). Prion-like spreading of Lewy body pathology has also been suggested as Lewy bodies have been identified within the grafted neurons of patients who had received healthy neuron transplants into their putamen (Visanji et al. 2013). It has also been suggested that it is pre-fibrillar α -synuclein intermediates which are harmful and that Lewy bodies are formed as a protective mechanism to remove this harmful protein (Dehay et al. 2015).

In the majority of cases Lewy bodies emerge in a predictable pattern within affected brains. These are grouped into Braak stages (Braak et al. 2003). In the pre-motor stages of the disease protein inclusions may be present in the olfactory bulb, dorsal motor nuclei of the vagal and glossopharyngeal nerves in the brainstem, and the pontine tegmentum.

Subsequently, as the motor symptoms of PD emerge, inclusions reach the *substantia nigra*, regions of the ventral forebrain, the hypothalamus, thalamus and regions of the cortex. As the disease progresses the pathology in these regions worsens (Braak et al. 2003). α -synuclein deposits are also present in the enteric nervous system. This is connected to the brain by the vagal nerve. However whether Lewy pathology begins here and spreads to the brain or *vice versa* is unclear (Del Tredici & Braak 2012). The pathology related to the non-motor symptoms of PD and the prevalence of these symptoms is summarised in Table 1.

Table 1. Prevalence of non-motor symptoms of Parkinson’s disease and related pathology. Adapted with permission from Berg et al. (2013).

Symptom	Prevalence	Related pathology
Olfactory dysfunction	>80%	Presence of Lewy bodies within in the olfactory bulb, amygdala and perirhinal cortex.
Visual dysfunction	Up to 90%	Dopamine deficit within the retina Thinning of retinal nerve fibre.
Sleep disorders: REM sleep behaviour disorder	30-50%	Presence of Lewy bodies in the nuclei of the lower brainstem.
Autonomic dysfunction: Constipation Urinary dysfunction	50-80% 27-39%	Lesions in the autonomic brainstem region and peripheral post-ganglionic neurons.
Depression	30-40%	Deficit of norepinephrine and serotonin in locus coeruleus and raphe nuclei.
Cognitive decline/ dementia	80% of PD patients with 20 year disease course	The spread of fibrillar α -synuclein pathology to limbic and neocortical structures. Up to 50% develop amyloid plaques and tau-tangles.

A future goal for PD research is to develop treatments which are able to slow or even halt the progression of the disease. As approximately 60-80% of dopaminergic neurons are already lost by the time motor symptoms present (Miller & O’Callaghan 2015), there is a great need for new diagnostic tools and biomarkers to halt PD in its earliest stages.

Causes and pathogenesis of Parkinson's Disease

The majority of PD cases are of unknown cause and are thought to arise from complex interplay between environmental and genetic risk factors (Shulman et al. 2011). As the era of genetic research has developed much progress has been made in determining genetic risk factors for PD. Studies of familial PD have also identified a number of monogenically-inherited forms of the disease (Verstraeten et al. 2015). In this section the known genetic and environmental causes and risk factors will be introduced.

The discovery of disease causing genes has proved extremely useful to aid understanding of the pathogenesis of the disease. Study of the function of these genes give researchers an insight into dysregulated pathways in PD. The effect of mutations in these genes may also be studied in animal models (Kalia & Lang 2015). So far, six genes have been associated with autosomal dominant forms of PD and four genes are linked to autosome recessive forms of PD, these are listed in Table 2.

Table 2. Monogenic forms of Parkinson's Disease.

Gene	Full protein name	Type of PD	References
Autosomal dominant inheritance of PD			
<i>SNCA</i>	α -synuclein	Early onset PD (EOPD)	(Polymeropoulos et al. 1997; Singleton et al. 2003)
<i>LRRK2</i>	Leucine-rich repeat kinase 2	Late onset PD (LOPD)	(Di Fonzo et al. 2005)
<i>VPS35</i>	Vacuolar protein sorting 35	LOPD	(Zimprich et al. 2011)
<i>EIF4G1</i>	Eukaryotic translation initiation factor 4- γ 1	LOPD	(Chartier-Harlin et al. 2011)
<i>DNAJC13</i>	Receptor-mediated endocytosis 8	LOPD	(Vilariño-Güell et al. 2014)
<i>CHCHD2</i>	Coiled-coil-helix-coiled-coil-helix domain containing 2	LOPD	(Funayama et al. 2015)
Autosomal recessive inheritance of PD			
<i>Parkin</i>	Parkin	Juvenile and EOPD	(Kitada et al. 1998)
<i>PINK1</i>	PTEN-induced putative kinase 1	EOPD	(Bonifati et al. 2005)
<i>DJ-1</i>	DJ-1	EOPD	(Bonifati et al. 2003)

Table 2 continued

<i>ATP13A2</i>	ATPase Type 13A2	Atypical PD/Kufor-Rakeb syndrome	(Di Fonzo et al. 2007)
----------------	------------------	----------------------------------	------------------------

SNCA, which encodes the α -synuclein protein, was the first PD gene to be discovered (Polymeropoulos et al. 1997). Missense mutations in *SNCA* and multiplications of the *SNCA*-containing genetic locus have been shown to cause PD (Singleton et al. 2003; Chartier-Harlin et al. 2004; Polymeropoulos et al. 1997). These mutations are thought to result in a toxic gain of function by increasing the likelihood of aggregation of the α -synuclein protein (Devine et al. 2011).

Mutations in *LRRK2* underlie the most common form of dominantly inherited PD. The G2019S mutation in this gene has shown to be responsible for up to 4% of all familial PD cases. However, prevalence of *LRRK2*-related PD varies considerably among different populations (Healy et al. 2008). Mutations in *LRRK2* are also thought to result in toxic gain of function. However, they are not completely penetrant, with 25% of carriers remaining disease free at 79 years (Kumari & Tan 2009). The function of *LRRK2* is discussed in more detail in the introduction to Chapter 4.

The most recent genes found to be associated with autosomal dominant PD are *VPS35*, *EIF4G1*, *DNAJC13* and *CHCHD2*. A single missense mutation in *VPS35* (Asp620Asn) has been identified in three families and segregates with PD. Three further missense mutations in this gene may confer a risk for PD. *VPS35* is a mediator of retrograde transport from the endosome to the trans-Golgi network (Zimprich et al. 2011). Recent evidence suggests that *VPS35* dysfunction prevents lysosomal degradation of α -synuclein (Miura et al. 2014). Two missense mutations in *EIF4G1*, which encodes a translation initiation factor, have also recently been implicated in PD. These mutations result in impaired binding of *EIF4G1* to *EIF4E* and *EIF3E*, suggesting a dominant negative loss of function mechanism of pathology. This may prevent cells from responding rapidly to stress through alteration of translation of mRNAs which aid cell survival (Chartier-Harlin et al. 2011). *DNAJC13* functions in similar pathways to *VPS35*. A missense mutation in this gene was discovered to segregate with the disease in a family of Dutch–German–Russian Mennonite ancestry (Vilariño-Güell et al. 2014). Finally, the most recent gene to be implicated in autosomal dominant forms of PD is *CHCHD2*, this encodes a mitochondrial protein (Funayama et al. 2015). As mutations in *DNAJC13* and *CHCHD2* have been identified very recently, further independent studies are

required to validate the association of these genes with PD and suggest mechanisms as to how mutations in these genes result in pathogenesis.

Mutations in *Parkin*, *PINK1* and *DJ-1* have been associated with autosomal recessive inheritance of PD (Kitada et al. 1998; Bonifati et al. 2005; Bonifati et al. 2003). Autosomal recessively inherited PD is more frequently an early onset disorder, with an age of onset of less than 40 years. Mutations in *Parkin* are the most common cause of EOPD; however the reported prevalence of these mutations in EOPD has varied considerably between studies (Lücking et al. 2000; Brooks et al. 2009). A study using a large UK cohort and a systematic review of many previous studies calculated that mutations in *Parkin* are present in 8.6% of EOPD cases. Mutations in *PINK1* and *DJ1* are rarer, and mutations in these genes are thought to be responsible for 3.7% and 0.4% of EOPD cases, respectively (Kilarski et al. 2012). These genes are all associated with mitochondrial pathways, providing an insight into important pathways underlying PD (Dodson & Guo 2007).

Rare mutations in number of other genes including *ATP13A2* are also associated with autosomal recessive PD. Patients carrying mutations in these genes often present with atypical features. For example, mutations in *ATP13A2* were originally demonstrated to result in a Parkinsonian disorder known as Kufor-Rakeb syndrome (Ramirez et al. 2006). This is an early onset disorder which presents with many typical features of PD with additional symptoms such as severe dementia, pyramidal signs and supranuclear gaze palsy. Studies have also identified mutations in this gene which are responsible for more typical EOPD with limited atypical symptoms (Di Fonzo et al. 2007).

The study of whole genomes and linkage analyses in families with inherited PD has facilitated the discovery of these rare mutations which confer high risk for the disease. However, familial PD is only responsible for approximately 10% of all cases (Thomas & Flint Beal 2007). Genetic risk factors also play a role in sporadic PD and a large number of genetic risk factors for PD have been identified. Genome-wide association studies (GWAS) using large number of subjects and subsequent meta-analyses have the power to identify common and medium frequency genetic variants which confer a small or medium increased risk for PD. Common variants in *LRRK2* and *SNCA* which confer a higher risk of PD (Satake et al. 2009) have been identified as well as over 25 other genetic risk loci for PD (Verstraeten et al. 2015). The average odds ratio (OR) for these common variants is approximately 1.3. Figure 4 summarises the frequency and risk conferred by known genetic variants associated with PD. Additionally, a comprehensive database, PDGene, lists a large number of polymorphisms

thought to be associated with PD has been created using data from a large, recent meta-analysis of GWAS (Nalls et al. 2014; Lill et al. 2012)

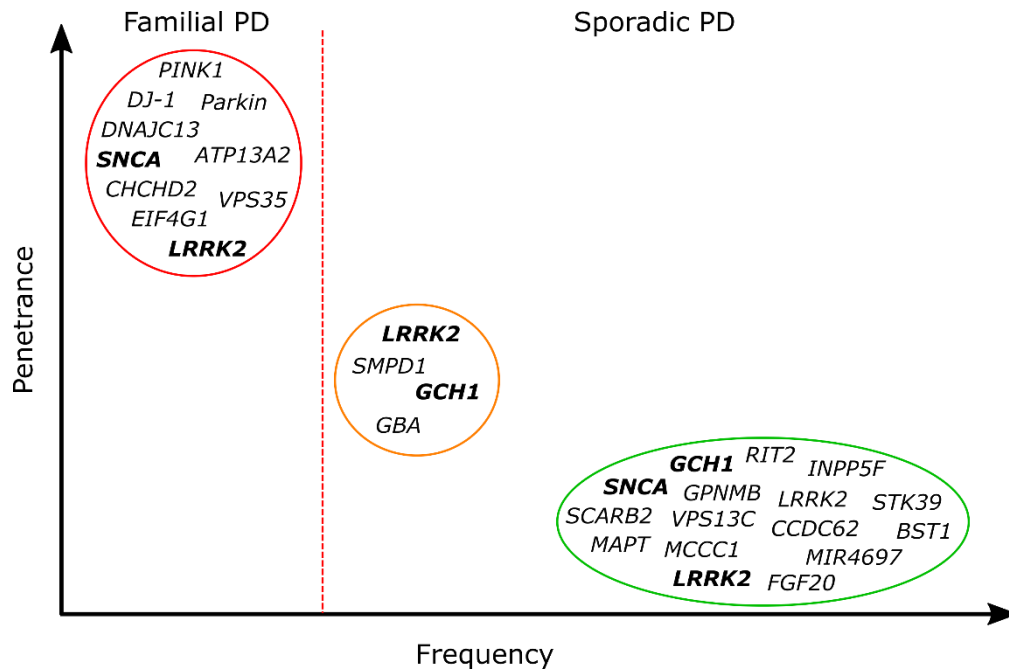


Figure 4. Overview of genetic variants associated with Parkinson's disease. This schematic indicates the penetrance and frequency of genetic variants associated with PD. A small number of rare alleles have been found that confer high risk for PD, while a larger number of common genetic variants have been shown to confer a small increased risk for PD. There are a number of intermediates (shown in the yellow circle). Genes in bold are pleomorphic, that is both rare high risk variants and common low risk variants are present at the same loci. Adapted with permission from Verstraeten et al. (2015).

A small number of variants have been identified with intermediate frequency and higher ORs. Mutations in *glucocerebrosidase (GBA)* are an important risk factor in PD. In the UK, approximately 4% of sporadic PD patients carry a mutation in this gene (Neumann et al. 2009). *GBA* mutations increase risk for PD approximately 20-fold, with *GBA*-related PD being very similar to idiopathic PD but with a slightly earlier age of onset and increased likelihood of cognitive decline (Schapira 2015). *GBA* is involved in glycolipid metabolism, and patients who are homozygous for mutations in this gene develop the lysosomal storage disorder Gaucher's disease. Heterozygous mutations in a related gene, *SMPD1*, have also been associated with a relatively high risk for PD in Ashkenazi Jewish population (OR = 9.4) (Gan-Or et al. 2013). Homozygous mutations in *SMPD1* are causative of another lysosomal storage disorder Niemann-Pick disease. The involvement of these genes in the risk for PD suggests an important role of lysosomal pathways.

Identification of genes involved in PD, together with pathological findings in PD patients, has helped determine some of the important cellular pathways that may underlie the disease. As discussed above a major pathological hallmark of PD is Lewy body pathology. The presence of protein aggregates in PD implicates impairment of protein folding and protein clearing mechanisms within the cell. These mechanisms include the ubiquitin-proteasome system (UPS) and autophagy pathways. Together these pathways function to degrade misfolded proteins, aggregates and dysfunctional organelles. Many PD genes, or risk variants for PD are involved in these pathways. Parkin is an E3 ubiquitin-ligase; addition of ubiquitin to proteins targets them for degradation, and thus mutations in Parkin may prevent the proper the degradation of its targets. Parkin has many targets linking it to both regulation of mitochondrial function and modulation of endoplasmic reticulum (ER) stress (Shin et al. 2011; Imai et al. 2001). Interestingly, α -synuclein has also been identified as a target of Parkin (Shimura et al. 2001), however Lewy body pathology is often absent in Parkin-related PD (Poulopoulos et al. 2012). As previously mentioned, GBA and SMPD1 are both involved in lysosomal function. A potential pathogenic feedback loop between GBA and α -synuclein has been identified. Accumulation of the GBA substrate glucosylceramide can stabilise α -synuclein, while α -synuclein is able to inhibit GBA activity (Mazzulli et al. 2011). LRRK2, VPS35, DNAJC13 and ATP13A2 are all thought to have roles in the lysosomal pathway.

Changes in mitochondrial function and mitophagy (a specialised form of autophagy which degrades dysfunctional mitochondria) are other key pathogenic pathways in PD (Ryan et al. 2015). Mitochondrial dysfunction is a key feature of many neurodegenerative diseases. It has been associated with PD since the early 1980s when it was found that a neurotoxin which causes Parkinsonism inhibits mitochondrial complex I (Langston et al. 1983; Nicklas et al. 1985). This discovery has proved to be very important as mitochondrial inhibitors, such as rotenone and MPP+, are now commonly used to mimic PD in animal models (Blesa & Przedborski 2014). In post mortem brain tissue from PD patients mitochondrial complex I activity was discovered to be reduced by approximately 30% (Schapira et al. 1989). Adding weight to the pathogenic role of mitochondrial dysfunction and impaired clearance of damaged mitochondria, many PD-associated genes act within these pathways. PINK1 is a key detector of mitochondrial damage and is thought to be able to activate the mitophagy pathway through interacting with Parkin (Eiyama & Okamoto 2015). Although the function of DJ-1 is less clear, this protein is also thought to be involved in the mitophagy pathway (McCoy & Cookson 2011).

Other involved pathways and cellular functions which may be dysregulated in PD include the protein and membrane trafficking pathway, synaptic function, transmission of dopamine signalling and inflammation (this is introduced more detail in Chapter 5). Figure 5 shows the key cellular pathways involved in PD pathogenesis and lists the PD-associated genes involved in these pathways.

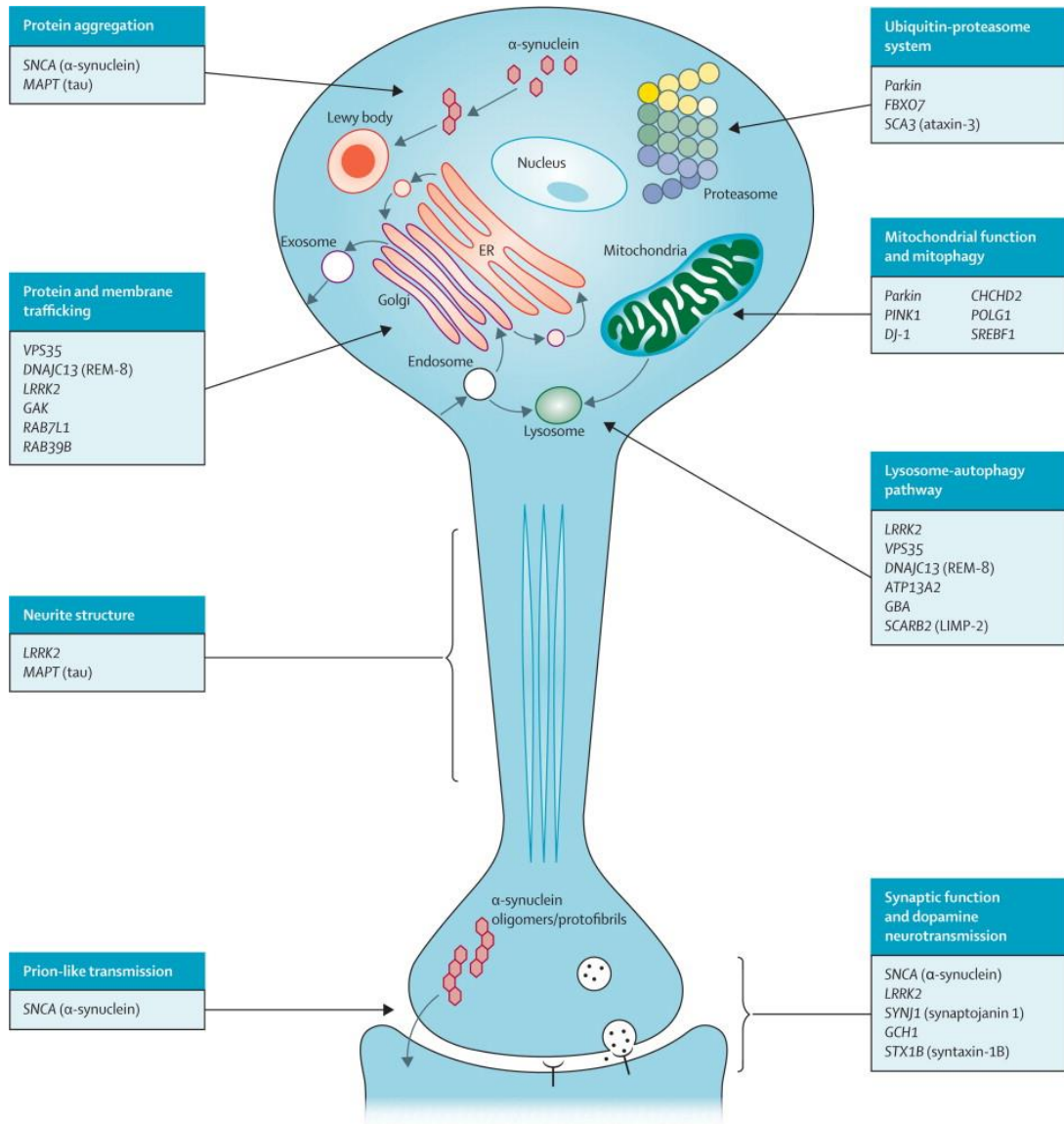


Figure 5. Cellular processes involved in Parkinson's disease pathology. Multiple genes have been associated with PD, this figure summarises their involvement in the many cellular processes that are implicated in PD pathology. Reproduced with permission from Kalia & Lang (2015).

Other non-genetic risk factors and protective factors have been identified, although the mechanisms of many of these are not well understood. Rural living and agricultural occupation confer an increased risk of PD; this may be related to increased pesticide exposure and well water drinking which are also known risk factors. Other factors that increase risk are prior head injury and beta-blocker use. Of these, pesticide exposure confers the highest risk. Protective factors include, smoking, coffee intake, alcohol consumption, use of non-steroidal anti-inflammatory drugs and calcium channel blocker use (Noyce et al. 2012). Understanding the mechanisms behind these risk factors and determining the interplay between them and genetic causes may help identify those who are at greater risk of PD.

Although a large number of genetic risk factors have been identified by GWAS studies, the overall heritability of PD is only estimated at approximately 27% (Keller et al. 2012). It is clear that there are unidentified genetic and environmental factors which increase the risk of developing PD.

1.2 Models of Parkinson's disease

As it is not possible to study the pathophysiology of PD progression in human patients, cell and animal models are used to aid understanding of the cellular mechanisms underlying dopaminergic neuron vulnerability. Through greater understanding of the underlying mechanisms of PD it is hoped that potential drug targets will be discovered. Large scale drug screens can also be performed in some model systems. In this section the models currently in use to study PD will be introduced. Zebrafish models of PD will not be discussed in this section, but will be introduced in detail in section 1.3.

Human cell culture models

Advantages of cell culture models derived from human tissue include the ability to study of sporadic PD and their suitability for small molecule screening. The power of using human dermal fibroblasts taken from patient skin biopsies has been demonstrated. Mitochondrial dysfunction has been observed in fibroblasts taken from patients with mutations in *Parkin* and *LRRK2* (Mortiboys et al. 2008; Mortiboys et al. 2010). Mitochondrial read outs were recently used for a drug screen which identified many drugs which were able to rescue the mitochondrial function in these cells. It is hoped that the UDCA, a drug identified as beneficial in this study and which already in clinical use for some liver disorders may be taken into clinical trials for PD patients in the near future (Mortiboys et al. 2013). A major limitation of fibroblasts is that they are not a relevant cell type. Although they do display some underlying

features of PD, such as mitochondrial dysfunction, they do not display the same vulnerability to these changes as neurons. They also may not express the same complement of genes as the relevant neurons and therefore may not be able to model some gene-gene interactions.

It is not possible to extract live neurons from patients, however, progress with production of induced pluripotent stem cells (iPSCs), which can be reprogrammed from fibroblasts, offers a major opportunity for the study of otherwise inaccessible cell types. iPSC-derived dopaminergic neurons, reprogrammed from somatic cells, have been characterised and are neurophysiologically similar to mature dopaminergic neurons. They are also susceptible to the PD-associated toxin MPTP (Hartfield et al. 2014). Unlike animal models where, typically, only one genetic alteration is made, iPSCs reprogrammed from patient cells contain the whole disease genome and have endogenous levels of gene expression. This may aid researchers understanding of the mechanisms behind sporadic PD and sub-types of PD resulting from defects in different cellular mechanisms.

One of the first iPSC models of genetic PD were cells derived from a patient containing a triplication of *SNCA*. Dopaminergic neurons derived from these cells exhibited PD-related phenotypes such as α -synuclein accumulation and oxidative stress (Byers et al. 2011). The effects of mutations in *PINK1*, *Parkin* and *LRRK2* on mitochondria have also been studied using iPSC-derived dopaminergic neurons. Cells derived from patients carrying *PINK1* mutations displayed reduced translocation of *Parkin* to the mitochondria after depolarisation of mitochondria (Seibler et al. 2011). Dopaminergic neurons containing mutations in *Parkin* demonstrated upregulation of monoamine oxidases and increased oxidative stress. Reduced dopamine uptake by *Parkin*-mutant cells compared to cells derived from healthy controls was also observed (Jiang et al. 2012). *LRRK2* mutations increased DNA damage in the mitochondrial genome (Sanders et al. 2014), increased oxidative stress and elevated levels of α -synuclein (Nguyen et al. 2011).

iPSCs have been used to study differences between monozygotic twins discordant for PD. Both twins carried a mutation in *GBA*. Dopaminergic neurons derived from both twins demonstrated elevated α -synuclein protein levels. Decreased levels dopamine levels were observed in cells from the affected twin. *Monoamine oxidase B (MAO-B)* was upregulated in the affected twin but not the unaffected twin; this may be due to epigenetic mechanisms. Inhibition of MAO-B and upregulation of *GBA* rescued the α -synuclein and dopamine phenotype (Woodard et al. 2014).

Neuronal cells derived from iPSCs have also been transplanted into other animal models of PD. This has been performed in a toxin-induced rat model of PD and in non-human primates. Human iPSC-derived neuronal stem cells transplanted into the rat striatum differentiated and integrated into the brain. This resulted in an improvement of motor impairment displayed in these rats (Han et al. 2015). In non-human primates, iPSCs derived from a Cynomolgus monkey differentiated to a dopaminergic phenotype were transplanted into the same animal after Parkinsonism was induced using MPTP. These neurons survived for at least 2 years (the duration of the study) and resulted in improvement of the motor features of the MPTP-treated monkeys (Hallett et al. 2015). These early studies suggest that neuronal transplant using iPSCs may be possible in the future.

Although iPSCs have not yet yielded any novel mechanistic insight study, the use of iPSCs to study PD is still in its early stages. As they are more widely used and new protocols developed they are likely to be a powerful model and may also be used for drug screening (Jacobs 2014).

Mammalian toxin induced models

The classical PD-inducing toxin is MPTP. This is a by-product of synthetic heroin production and was discovered in the early 1980s when a group of drug addicts developed Parkinsonism after injecting synthetic heroin contaminated with this by-product (Langston et al. 1983). MPTP is up-taken specifically into dopaminergic neurons through the dopamine transporter (DAT) and is metabolised to MPP+. MPP+ localises to mitochondria where it is able to inhibit mitochondrial complex I (Javitch et al. 1985; Richardson et al. 2007).

The particular strength of MPTP treatment is the specific and reproducible effect on the nigrostriatal system. MPTP-treated monkeys demonstrate PD-like motor defects and display features similar to the non-motor symptoms of PD patients including cognitive impairment and sleep disturbances. A specific loss of dopaminergic neurons in the *substantia nigra* and only mild loss of neurons in other regions is observed in MPTP-treated monkeys. Although no protein inclusions have been identified in these models α -synuclein mRNA and protein levels have been shown to be increased (Porras et al. 2012). MPTP is also used in other organisms, particularly the mouse. Although MPTP-mice do display motor defects and degeneration of dopaminergic neurons, they do not develop protein inclusions or presence non-motor features (Taylor et al. 2011).

Another classical toxin-induced PD model is the 6-hydroxydopamine (6-OHDA) treated rat. This model was developed earlier than MPTP models and a method for inducing loss of

dopaminergic neurons in rats using this toxin was first published in 1972 (Breese & Traylor 1972). 6-OHDA is a hydroxylated form of dopamine. 6-OHDA confers specific neurotoxicity to dopaminergic neurons in a similar manner to MPTP. It is transported into dopaminergic neurons through DAT where it causes oxidative stress and inhibits mitochondrial respiration (Rodriguez-Pallares et al. 2007). Unlike MPTP, 6-OHDA is unable to cross the blood brain barrier and therefore requires injection directly into the brain of animal models. The effects of this toxin are similar to those of MPTP and specific loss of dopaminergic neurons without presence of Lewy bodies is observed (Bové & Perier 2012).

Other toxin-induced models of PD include rotenone and paraquat models. Due to the increased risk of PD associated with pesticide exposure, the effect of these toxins, which are both present in some pesticides, on animal models is of interest (Nisticò et al. 2011). Like MPP+, rotenone is a mitochondrial complex I inhibitor while paraquat causes oxidative stress. Unlike MPTP and 6-OHDA models, rotenone and paraquat administration in rodents is able to induce intracellular inclusions resembling Lewy bodies (Manning-Bog et al. 2002; Sherer et al. 2003).

The toxin-induced PD models have proved invaluable in the last 3 decades for study of cellular pathways involved in advanced PD. While these models are unable to mimic the aetiology of PD, the involvement of mitochondrial function, oxidative stress, inflammation, and protein degradation pathways have been studied in these models (Bové & Perier 2012; Broom et al. 2011; Vila et al. 2008; McCormack et al. 2005). This has allowed for advances in our understanding of the mechanisms which may be behind dopaminergic neuron death. Limitations of toxin-induced models include the acute onset, lack of Lewy body pathology (in the majority of models), non-motor features and limited reproducibility in certain models (Bové & Perier 2012). Toxin-induced models are less useful for study of early symptoms of PD and for drug discovery efforts due to the acute nature of cell death. Another inherent issue with performing drug screening in toxin induced models is the possibility of drug-drug interactions obscuring a meaningful effect.

Mammalian genetic animal models

The discovery of monogenically-inherited PD genes and the development of genome editing techniques have enabled researchers to create mammalian models which may better simulate the processes which underlie genetic forms of PD. Knockout, conditional and systemic and knock-in animal models for many PD related genes have been generated. The continued development of molecular tools such as the Cre-LoxP system, viral vectors and the

CRISPR/Cas9 system has revolutionised the generation of genetic animal models (Feil et al. 2009; Löw & Aebischer 2012; Yang 2015).

As *SNCA*- and *LRRK2*-related PD are thought to be due to toxic gain of function of the encoded proteins, animal models overexpressing the mutant, or wild type (WT), forms of these genes are most commonly used. Expression of these genes can be induced in specific tissues by placing the transgene under control of a tissue-specific promoter.

Overexpression of *SNCA* has been studied in mice, rats, and non-human primates. Many transgenic *SNCA* mouse models have been created with mixed results. The phenotype of *SNCA* transgenic mice varies depending on the promoter, level of over expression and whether WT or mutated *SNCA* is used (Blesa & Przedborski 2014). Tetracycline-induced transgenic mice which overexpress mutant *SNCA* under the *PITX3* promoter display robust neurodegeneration and motor phenotypes. Other relevant pathologies observed in this model included the presence of α -synuclein inclusions, reduced dopamine release and an impairment of the autophagy/lysosome pathway (Lin et al. 2012). Rat models of *SNCA*-related PD, using viral-vectors to drive expression of *SNCA*, have generally proved to be more robust. The majority of these models demonstrate progressive loss of dopaminergic neurons, a motor phenotype and α -synuclein inclusions in stage-like manner. These inclusion are observed in the striatal axons and termini before cell body pathology appears (Decressac et al. 2012; Lo Bianco et al. 2002). Non-human primate models of *SNCA*-associated PD have been shown to be valuable models of PD. These models display a gradual worsening of motor coordination. Upon histological analysis, prominent degradation of striatal dopaminergic fibres was observed and ubiquitin containing aggregates were detected (Eslamboli et al. 2007). Early cognitive defects and anxiety phenotypes have also been observed in transgenic monkeys showing that these may be useful models for study of the pre-motor stages of the disease (Niu et al. 2015).

Knockout models of *LRRK2*, aiming to elucidate the function of this large complex gene, have failed to identify any neuronal loss. This suggests that this gene is not required for healthy neuronal function (Hinkle et al. 2012). Conversely, a neuroprotective role of *LRRK2* knockdown has been suggested. *LRRK2*-deficient rats were resistant to the neurodegeneration induced by lipopolysaccharide (LPS, an inflammatory stimulant which can induce dopaminergic neuron loss) treatment, through reducing the inflammatory response (Daher et al. 2014). Knock-in and overexpression (of both mutant and WT *LRRK2*) models in mice have again produced variable results. Some studies did not detect any neuron

loss while others observed neurodegeneration in an age dependant manner (Ramonet et al. 2011; Tong et al. 2009; Herzig et al. 2011). This variation may be due to the method used for overexpression, and the level of overexpression achieved. For example, viral-vector based models demonstrate the largest degree of neurodegeneration (Lee et al. 2010). Whether the neurotoxic effect of this is due to increased kinase activity or due to the absolute levels of LRRK2 is disputed. This is discussed in detail in Chapter 4.

PINK1, *Parkin* and *DJ-1* knock-out mouse models have also been generated. These models typically display a moderate decrease in striatal dopaminergic levels but do not model neurodegeneration or major motor defects (Yamaguchi & Shen 2007; Akundi et al. 2011; Gispert et al. 2009; Kitada, Pisani, et al. 2009). Mitochondrial dysfunction and abnormal expression of inflammatory genes, however, has been observed in *PINK1* deficient mice (Akundi et al. 2011; Gispert et al. 2009). Unexpectedly, a triple knockout of all three genes was also unable to model nigral degeneration (Kitada, Tong, et al. 2009). One mouse model generated using a bacterial artificial chromosome to express truncated *Parkin* in dopaminergic neurons demonstrated age-dependant and progressive dopaminergic neuron loss, accumulation of α -synuclein and motor symptoms (Lu et al. 2009). A similar neurodegenerative effect was seen as a result of overexpression of both WT and mutant *Parkin* in rats (Van Rompuy et al. 2014). Knockouts of these three genes have also been generated in rats. In contrast to the mice models, both *PINK1* and *DJ-1* deficient rats display progressive nigral degeneration with up to 50% of dopaminergic neurons being lost by 8 months; related motor impairments are also observed. However this is not seen in *Parkin*-deficient rats (Dave et al. 2014).

Non-mammalian models of PD

Small genetically tractable models such as the fruit fly *Drosophila melanogaster* and teleost fishes have also been used to model PD. As well as their genetic tractability other advantages of these models include their small size and low cost which makes them amenable to small molecule screens.

Both knockout models of recessive loss of function mutations and knock in models of dominant gain of function mutations have been created in *Drosophila*. Although flies have a relatively simple nervous system they do possess a population of dopaminergic neurons and there are well developed techniques to study neurophysiology (reviewed by West et al. (2015)). *Drosophila* models of PD have been instrumental in the implication of mitochondrial dysfunction and provided a demonstration that *pink1* and *parkin* act in the same pathway

(Yang et al. 2006; Park et al. 2006). Knockout of either *pink1* or *parkin* in *Drosophila* both display a shortened lifespan, locomotor defects derived from the degeneration flight muscles. This degeneration is thought to be related to mitochondrial dysfunction. Dopaminergic neurons were shown to degenerate in the *pink1* knockout model but not the *parkin* knockout model (Greene et al. 2003; Yang et al. 2006). The *parkin* knockout model also developed male sterility which was also related to mitochondrial dysfunction. *Drosophila* models expressing mutant forms of human *SNCA* and *LRRK2* have also been developed. These models have a shortened life-span, locomotor dysfunction, protein inclusions similar to Lewy-bodies, and specific loss of dopaminergic neurons (Liu et al. 2008). *SNCA Drosophila* models are reviewed by Mizuno et al. (2011).

Although *Drosophila* are a useful model to study cellular mechanisms, they are an invertebrate model and limitations of this model result from evolutionary distance from humans.

As well as zebrafish being a popular model for human disease (which will be discussed in detail in the following section) the medaka (*Oryzias latipes*), a Japanese freshwater fish has been utilised to study PD. Both toxin-induced and genetic models have been studied. As well as the standard PD toxins MPTP and 6-OHDA, lysosome and proteasome inhibitors have been used to model PD in medaka. Treatment with lysosome and proteasome inhibitors resulted in widespread protein inclusions and diencephalic dopaminergic neurons appeared to be more vulnerable to these inclusions. Specific loss of the dopaminergic neurons and a locomotor defect was observed (McNaught et al. 2004; Matsui, Ito, et al. 2010). Treatment with MPTP and 6-OHDA both resulted in reduced swimming and specific dopaminergic neuron loss, however protein inclusions were not detected (Matsui et al. 2009; Matsui, Ito, et al. 2010).

Loss of function mutations in *pink1* and *parkin* have also been created in medaka. However, the phenotype of these fish is mild and no dopaminergic neuron loss was detectable. Despite the lack of neurodegeneration, a late-onset decrease in spontaneous movement and a slightly decreased lifespan is observed in *pink1* mutant medaka (Matsui, Taniguchi, et al. 2010). Double *pink* and *parkin* mutants develop a more severe phenotype; this model displays a late-onset locomotion defect, a decrease in dopamine levels and a 30% decrease in dopaminergic neurons by 12 months. Mitochondrial dysfunction including enlarged mitochondria and reduced complex I and II activity function was detected at 12 months (Matsui et al. 2013).

1.3 Zebrafish as a model of neurodegenerative disease

The zebrafish (*Danio rerio*) is a small tropical freshwater fish native to the Himalayan region. It has been growing in popularity as a model of human disease over the past two decades after being initially developed as a model of development in the 1970s and 80s (Streisinger et al. 1981). Despite being less closely related to humans than their rodent, or indeed non-human primate counter-parts, the zebrafish hosts many advantages as a model for biomedical research. These advantages allow the zebrafish to be used as a powerful addition to existing models. Due to being classed as a “lower vertebrate”, zebrafish play an important role in the modern scientific and social climate where the 3Rs (replacement, reduction and refinement) movement aims to limit the number of animals used for research purposes. In this section both the advantages of the zebrafish as a model for neurodegenerative disease and what has been learnt from these models will be introduced.

Suitability of zebrafish as a model organism

Zebrafish embryos develop rapidly, with a full body plan established by 24 hours post-fertilisation (hpf). By 5 days post-fertilisation (dpf) the majority of development is complete. Embryos develop *ex utero* and are transparent. These are the qualities that first made them attractive as a model of development. The optical clarity of the zebrafish allows live imaging to be performed. When coupled with the use of fluorescent reporter lines this allows real-time imaging of developing pathologies and systems.

Zebrafish are cost-effective to house in large numbers and are capable of producing large numbers of progeny all year round. A single female can produce hundreds of eggs per week and breeding can be easily controlled by a light cycle. Sexual maturity is reached after 2.5-3 months resulting in a short generation time allowing mutant colonies to be established quickly. Despite the obvious differences between humans and zebrafish, they are a vertebrate model and over 70% of human genes have a recognisable orthologue in zebrafish (Howe et al. 2013).

The zebrafish offers a compromise between complexity and practical simplicity, representing an intermediate between rodent models, which, being mammals, are more closely related to humans than invertebrate models as *Drosophila*. Table 3 summarises the main strengths and weaknesses of fly, zebrafish and rodent models.

Table 3 Comparison of zebrafish with other model organisms. Reproduced with permission from Lieschke & Currie (2007). NB: since this figure was originally published advances in genome editing technology have allowed targeted gene modification to also be a relative strength in zebrafish models.

Attribute of disease model	Model organism			
	Fly	Zebrafish	Mouse	Rat
Practical issues				
Husbandry infrastructure	\$	\$	\$\$\$	\$\$\$
Cost per animal per year	\$	\$	\$\$\$	\$\$\$
Characterized inbred strains	+	-	++++	+++
Outbred laboratory strains	+	+++	++	++
Anatomical similarity	-	+	++	++
Molecular or genetic similarity	+	++	+++	+++
Pathological similarity	-	++	+++	+++
Storage; for example, freezing sperm	No	Yes	Yes	Yes
Molecular biology tools				
Transgenesis*	++	++	++	++
Targeted gene modification*	+	-	++++	+
Transient <i>in vivo</i> assays*	++	++++	+	+
Allelic series from TILLING*	+++	++++	++	+
Feasibility of large-scale screens [†]	++++	+++	++	+
Affordability of large-scale screens [†]	++++	+++	+	-
Sequencing progress [§]	+++	++	+++	++
Annotation progress [§]	++	++	++++	++
Cell-biology tools				
Cell lines and tissue culture	++	+	++++	+
Antibody reagents	++	+	++++	++

*Reverse-genetics approach; [†]forward-genetics approach; [§]genome sequence; -, not relevant, or not a strength; \$, \$\$, \$\$\$ and +, ++, +++, relative cost (\$) and strength (+) of the model in each category; +++++, outstanding strength of the model; TILLING, targeting induced local lesions in genomes.

Drug screening capabilities are a major advantage of zebrafish models, especially for PD where the effect of small molecules on a distinct, relevant population of neurons can be studied at an early age. Many of the qualities described above make zebrafish particularly suitable for use in phenotypic drug screening. These particular qualities and the specific advantages of phenotypic drug screening are described in detail in chapter 6.

Zebrafish genetic tools

A range of different genetic tools are now available to generate genetic models of disease using zebrafish. Due to the availability of large numbers of zebrafish embryos, large forward and reverse genetic screens are feasible using zebrafish. Large scale *N*-ethyl-*N*-nitrosurea (ENU) mutagenesis can be used to generate mutations at random; the generated mutants

may then be characterised and the responsible gene identified. The Cambridge-based Sanger Centre is undertaking the Zebrafish Mutation Project which aims to create a loss of function mutation for each of the zebrafish's 26,000 protein-coding genes. To do this ENU mutagenesis is combined with high throughput exome sequencing (Kettleborough et al. 2013).

More recently precise genome editing techniques have been developed. The first of these were zinc-finger nucleases, which were quickly followed by more cost-effective TALEN (transcription activator-like effector nucleases) and CRISPR/Cas9 (clustered-regularly-interspaced-short-palindromic-repeats/CRISPR associated protein 9) systems. These systems are now widely used to generate both knockout mutant zebrafish lines quickly and easily. They also have the power to generate specific point mutations and knock-in mutant lines through homology directed repair (Auer & Del Bene 2014). Details of the CRISPR/Cas9 system, which was utilised in this thesis, are described in detail in Chapter 5 section 5.4.

Techniques are also available to allow generation of fluorescent reporter lines and drive expression of transgenes (for example mutated human genes responsible for disease). Transgenes can be expressed transiently by injection of mRNA or stable transgenic lines can be created by driving integration of a transgene-containing plasmid into the zebrafish genome. This is possible by exploiting the *tol2* transposon to drive insertion events (Kawakami et al. 2004). Expression of transgenes may be driven by endogenous elements, known as the enhancer trap method which is dependent on insertion of the transgene in close proximity to a regulatory elements (Wen et al. 2008). Transgenes may be also placed under the control of a promoter of choice which is inserted alongside the transgene. There are numerous examples of this technique in zebrafish research and most have demonstrated that expression is similar to the endogenous gene expression pattern of the promoter (Bandmann & Burton 2010). Conditional expression of transgenes is also possible using the Cre-LoxP and GAL4-UAS systems (Halpern et al. 2008; Hans et al. 2009).

Morpholinos (MOs) are a form of steric-block antisense oligonucleotides which are commonly used to generate transient knockdown of protein-coding and miRNA genes. They have been shown to be more specific and stable than siRNAs (Summerton 2007) and have proved to be a popular tool for generating fast, cost-effective knockdowns. Currently there are over 7000 publications using MOs (the MO publication database is accessible at <http://www.gene-tools.com/morpholino-publication-database>). For knockdown of protein coding genes, MOs can either be designed against the ATG start site to prevent translation

of the mRNA or to intron-exon/exon-intron splice sites to disrupt proper processing of the mRNA. MOs can be designed to a number of regions within the pri-miRNA to prevent proper splicing of this transcript into the mature miRNA (Eisen & Smith 2008). Some MOs have been shown to induce off-target toxic effects through p53 activation, and therefore care must be taken with investigation of cell death when using MOs (Robu et al. 2007). Another limitation of using MOs is that although knockdown is induced quickly the effect is transient and usually wears off after 3-5dpf.

This year (2015) two important publications which compared MO knockdowns to stable mutant lines have highlighted the need for care to be taken when investigating the effect of mutations. Kok and colleagues investigated the similarity of MO induced mutants with stable lines and found that many of these did not phenocopy one another (Kok et al. 2015). However it has recently emerged that deleterious mutations induced by the CRISPR/Cas9 system in certain genes resulted in the upregulation of compensatory genes, thus no phenotype was observed, whereas MO knockdown of the same gene did not and the effect of knockdown could be investigated (Rossi et al. 2015).

Zebrafish as a model of neurodegeneration

Of particular interest for research into neurodegenerative disorders the zebrafish brain shares some anatomical similarities with the human brain. A distinct fore-, mid- and hind-brain is present in the zebrafish. The telecephalon, diencephalon and cerebellum are clearly represented, however unlike human or rodent brains the zebrafish brain only contains a rudimentary cortex. The peripheral nervous and enteric nervous system is also present. Zebrafish also possess specialised sensory organs such as the eye, ear and olfactory system. Although zebrafish do display “higher” behaviours these are abstracted and simplified compared to human behaviours. However, laboratory tests exist to assess motor ability, anxiety, memory and social behaviours (Lieschke & Currie 2007). Figure 6 shows a diagram of the major regions of the adult zebrafish brain.

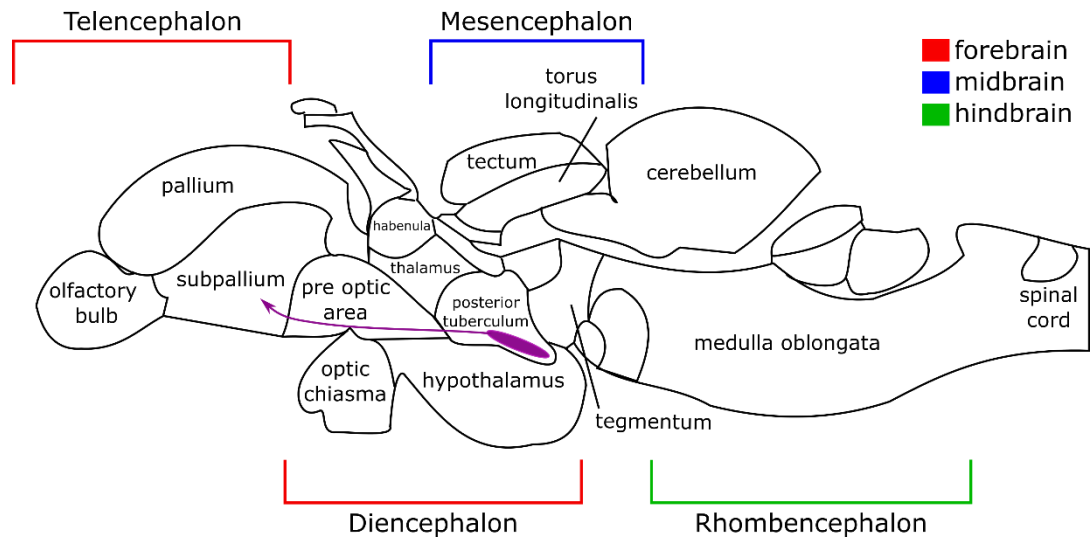


Figure 6. The adult zebrafish brain. The purple shaded area shows the location of the dopaminergic neurons with ascending projections into the subpallium (analogous to the human striatum).

Models of Alzheimer’s disease, Huntington’s disease, Motor Neuron Disease (MND) and PD have been established in zebrafish (Henshall et al. 2009; Schiffer et al. 2007; Bai et al. 2007; Paquet et al. 2009; Babin et al. 2014). The majority of these studies stated an overarching aim for using the disease model for compound screening to identify potential therapeutics for the disease of interest. As mentioned above (and in chapter 6) the ease of use of zebrafish in drug screening efforts is one of the major advantages of this model organism.

A CAG repeat expansion in *huntingtin* is the genetic cause of all cases of Huntington’s disease. The zebrafish has been used to study the function of *huntingtin* by generating a knockdown of this gene (Henshall et al. 2009). A zebrafish expressing a mutated form of human *huntingtin* has also been created. Similarly to human Huntington’s disease, this mutant protein formed aggregates in the zebrafish. This model has been used to screen compounds which may lessen the toxicity the aggregated protein (Schiffer et al. 2007). Zebrafish have also been used to investigate the toxic effects of Tau. Tau pathology is relevant to both Alzheimer’s disease, frontotemporal dementia and PD. Various transgenic lines expressing mutant forms of the Tau-encoding gene *MAPT* have been generated, and these models demonstrate relevant pathological features including hyper-phosphorylation of Tau, tangle formation and neurodegeneration in the spinal cord (Bai et al. 2007; Paquet et al. 2009).

Many genetic models of MND have been generated using zebrafish (Babin et al. 2014). The two most common genetic forms of MND involve mutations in *C9ORF72* and *SOD1*. Expression of the disease causing GGGGCC repeat expansion of *C9ORF72* in zebrafish results in RNA foci and neuronal death (Lee et al. 2013). *SOD1* models, including mutated zebrafish

sod1 and transgenic of human mutant *SOD1*, demonstrate hallmarks of MND. Increased oxidative stress, alteration at the neuro-muscular junctions and motor neuron loss was observed in these models (Ramesh et al. 2010; Da Costa et al. 2014).

Both genetic and toxin-induced zebrafish models of PD have also been established. Zebrafish possess a small population of ascending dopaminergic neurons with projections to the subpallium (analogous to the human striatum). Unlike in the human brain where these neurons are present in the *substantia nigra* in the midbrain, in zebrafish this population of neurons is present in the posterior tuberculum in the basal diencephalon (see Figure 6) (Rink & Wullimann 2001). In the embryonic brain this population is detectable by 18hpf and is an analogous position to the adult population (Rink & Wullimann 2002). In zebrafish embryos these neurons are easily identifiable by performing staining techniques (whole mount *in situ* hybridisation or immunohistochemistry) for markers of dopaminergic neurons. Fluorescent reporter lines which label this neuronal population are also available (Wen et al. 2008; Xi, Yu, et al. 2011). This allows the easy study of this neuron population. The use of one of these reporter lines, the *ETvmat2:GFP* line which expresses GFP in monoaminergic neurons, is described in Chapter 6. A recent paper describes a transgenic zebrafish which expresses mCherry in the mitochondria of dopaminergic neurons (Noble et al. 2015). This is likely to be a valuable tool for study of the mitochondrial phenotype in zebrafish models of PD.

Zebrafish are susceptible to the toxin MPP+. Treatment of zebrafish larvae with this toxin results in the specific loss of dopaminergic neurons and motor defects (Sallinen et al. 2009; Bretau et al. 2004). 6-OHDA has also been used to model PD in zebrafish. Larvae treated with this toxin displayed locomotor defect with reduced total swimming distance and an increase in time spent in the bottom portion of the tank being observed. While the number of dopaminergic neurons was not quantified, expression of *tyrosine hydroxylase (th)*, a marker of dopaminergic neurons, was demonstrated to be decreased after treatment. Treatment with Sinemet, a widely used drug for PD sufferers which contains levodopa, and Vitamin E, which has been used as an alternative therapy for PD, rescues the locomotor defect and *th* decrease in 6-OHDA treated zebrafish (Feng et al. 2014). However beneficial effects of vitamin E in PD patients have not been proven (Ricciarelli et al. 2007). The ease of toxin treatments in zebrafish are another benefit of this experimental system as they permeable and easily uptake compounds placed in the water.

Loss of function studies to model genetic forms of PD have also been performed in zebrafish. Zebrafish possess functional orthologues of many PD-associated genes. However they do not

possess a functional orthologue of *SNCA*. Rather than this being regarded as a limitation of zebrafish models of PD, it is seen as a unique opportunity to study the effects of PD-associated genes independent of *SNCA*-related pathology. Two studies induce a knockdown of parkin using a MO strategy (Flinn et al. 2009; Fett et al. 2010). Fett and colleagues did not observe any dopaminergic neuronal loss whereas Flinn and colleagues identified a specific loss of dopaminergic neurons (no change in pan neuronal marker HuC or numbers of motor neurons was observed) at 3dpf. This may be due to the increased level of knockdown achieved by Flinn and colleagues. Although no swimming abnormalities were detected, abnormal mitochondria and a complex I defect was observed *parkin* morphants (Flinn et al. 2009). Rodent models of *Parkin* deficiency do not display dopaminergic neuron loss, thus making the zebrafish the first vertebrate model to display dopaminergic neuron loss with *parkin* deficiency.

Another PD-associated gene which has been studied in zebrafish is *Irrk2*. Knockdown studies of *Irrk2* using MOs have been inconclusive. As regulation of *Irrk2* in zebrafish is one of the focuses of this thesis, these studies are discussed in chapter 4. *pink1* deficiency has also been studied using the MO strategy. Three independent groups have reported varying phenotypes. These range from a lack of dopaminergic loss but increases sensitivity to MPTP to a small decrease in dopaminergic neuron number to a 30% decrease in dopaminergic neuron number. The studies which observed a loss of dopaminergic neurons also reported either embryonic lethality in the morphants or developmental delay, deformity and increased apoptosis (Anichtchik et al. 2008; Xi et al. 2010; Sallinen et al. 2010). The discrepancies between the findings of these studies are likely to be due to off-target effects of the MO used in the latter studies and variation in the level of knockdown achieved.

To further study the effects of *pink1* deficiency a mutation generating a premature stop codon in zebrafish *pink1* was identified from an ENU mutagenesis screen (Flinn et al. 2013). By 3dpf a 25% decrease in dopaminergic neuron number is observed in *pink1* deficient zebrafish larvae. By 18 months old a 50% decrease was observed indicating a progressive loss of neurons. At 3 years a motor defect is seen in *pink1*-deficient zebrafish. Although the dopaminergic neuron number has not been quantified at this age the motor defect suggests that a dopaminergic neuron loss has progressed further. Mitochondrial defects in both larval and adult tissue are also apparent in this model. Mitochondria appear enlarged and a deficiency in complex I and III activity is present. Increased microglial activation in *pink1* deficient zebrafish suggests the involvement of inflammatory pathways. This model has also

been used to identify a novel pathway which may be involved in PD pathogenesis. *tigarB*, an inhibitor of glycolysis, was shown to be upregulated in *pink1* deficient zebrafish. Knockdown of *tigarB* was able to rescue the decrease in dopaminergic neurons observed in this model (Flinn et al. 2013). Overall, this model represents many features which are similar to human PD. As this model demonstrates a clear and easily quantifiable dopaminergic phenotype at 3dpf it has potential to be used in drug screening efforts to identify compounds which are able to rescue this phenotype.

1.4 microRNAs and human disease

microRNAs (miRNAs) are short non-coding RNAs which are able to post-transcriptionally regulate a large number of target genes through binding to target sites in the 3'UTR (He & Hannon 2004). miRNAs may target multiple transcripts and at least half of all human protein coding genes are thought to be regulated by a miRNA (Gurtan & Sharp 2013). This leaves tremendous scope for miRNA to be involved in the pathogenesis of disease.

Expression changes of miRNAs have been identified in the large majority of human diseases by miRNA profiling strategies. Rare miRNA gene variants have also been associated with some diseases (Cammaerts et al. 2015). It has also been shown that some miRNAs circulate in body fluids and display high levels of stability. These miRNA may be useful as biomarkers of disease (Kim 2015). As miRNAs are able to target many genes each, it is possible that therapies targeting miRNAs may be used as a "system level" therapy to rectify or change the expression levels of many genes in a pathway.

Normal development of the central nervous system (CNS) requires a highly regulated and precise coordination of many pathways. A large number of miRNAs have been shown to be expressed in the brain, therefore it is likely that they play an important role in CNS development and maintenance of neural populations. A number of studies have shown that preventing the proper biosynthesis of miRNA by removal of Dicer, many neural populations display defects in proliferation and/or increased levels of apoptosis (Huang et al. 2010; Davis et al. 2008; McLoughlin et al. 2012; Kim et al. 2007). Loss of Dicer also results in death of post-mitotic neurons (Schaefer et al. 2007; Kim et al. 2007).

The dopaminergic neuron population is no exception to this. In order to investigate the role of miRNAs in the development of midbrain dopaminergic neurons Kim and colleagues deleted Dicer in embryonic stem cells (ESCs) which were then induced to differentiate to a midbrain dopaminergic neural phenotype. In the ESC cultures which were Dicer deficient,

the dopaminergic phenotype was not detectable, as measured by expression of dopaminergic markers such as *TH*. Although other neuronal classes, such as the GABAergic neurons were also reduced, the development of these populations were not as severely affected. These findings were then replicated *in vivo* by creation of a conditional Dicer mutant; where Dicer was specifically deleted in DAT expressing neurons. Mice deficient for Dicer specifically in the midbrain dopaminergic neurons displayed progressive loss of dopaminergic neurons and developed a motor phenotype reminiscent of PD (Kim et al. 2007). These data suggest that miRNAs have an important role in the development and maintenance of neuronal populations which are lost in neurodegenerative diseases including PD. Therefore dysregulation of miRNAs may contribute to disease progression. In this section the relationship between miRNA and epigenetics and the involvement of miRNAs in neurodegenerative disorders will be introduced.

Discovery and biogenesis of miRNAs

miRNAs were first identified in the nematode worm *Caenorhabditis elegans* (Lau et al. 2001; Lee & Ambros 2001) and are well conserved in both plant and animal species. The miRBase database provides researchers with a searchable repository of known miRNA sequences and related annotation. This was set up in 2002 with just 218 entries. Now in its 21st version, miRBase contains nearly 30,000 entries (Kozomara & Griffiths-Jones 2014). A standard annotation system for naming new miRNA has also been introduced (Ambros et al. 2003).

The mature miRNA sequence, which is 21-25 bp in length, is derived from one arm of the primary transcript hairpin (pri-miRNA). miRNAs genes may be located in introns and are transcribed alongside their host gene, while others are located in intergenic regions. A single transcript may give rise to many mature miRNAs or a single miRNA (Marco et al. 2013). Figure 7 shows the microRNA biogenesis pathway and mechanism of post-transcriptional repression. The small interfering RNA (siRNA) pathway is also shown. siRNAs have many similarities to miRNAs. They are both dependant on Dicer for their maturation and are both able to post-transcriptionally regulate their targets through incorporation into the RNA induced silencing complex (RISC). Key differences are that siRNA are cleaved from fragments of double stranded RNA rather than processed from a single RNA transcript which forms a hairpin. This double stranded RNA may be exogenous or may be a bi-directionally transcribed endogenous RNA. siRNAs form a perfect duplex with their target and direct the cleavage of this mRNA, whereas miRNAs form imperfect duplex with a binding site in the 3'UTR of their

target. miRNAs most commonly repress their targets through translational repression, however some are able to direct mRNA cleavage (He & Hannon 2004).

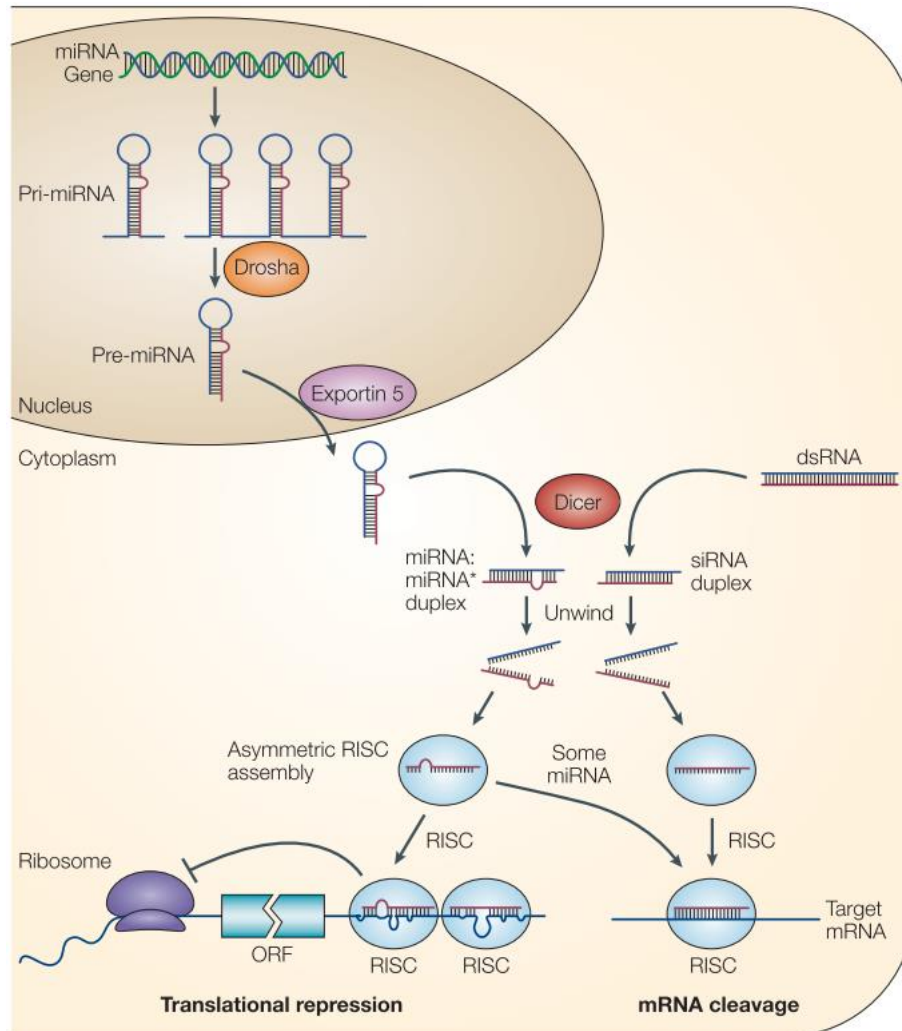


Figure 7. miRNA biogenesis and post-transcriptional repression. miRNA genes may be singular and transcribed alone or may be clustered and many miRNA cleaved from one transcript. The pri-miRNA, which folds into a hairpin secondary structure is cleaved in the nucleus by Drosha into a ~70bp pre-miRNA. This is exported from the nucleus to the cytoplasm by Exportin 5 the pre-miRNA undergoes further processing by Dicer. A miRNA:miRNA* duplex is formed. This duplex is then unwound and one strand is preferentially assembled into the RNA induced silencing complex (RISC). miRNAs target mRNAs in a specific manner by binding to partially complementary target sites within the 3'UTR of its targets. This results in either translational repression or mRNA cleavage. The siRNA biogenesis pathway is also shown. Reproduced with permission from He & Hannon (2004).

Validation of miRNA targets is costly and time consuming, therefore online programs to predict miRNA:mRNA interactions play an important role in identifying potential interactions of interest. As miRNA pairing with mRNA target sites is not perfectly complementary, prediction programs which can accurately identify likely miRNA targets have been

challenging to produce. A small region of the miRNA, nucleotides 2-8, is known as the seed sequence. This region is required for pairing with target sites (Lewis et al. 2003). The four main aspects which are common features for target prediction programs are complementarity of the seed region, conservation of the binding site, free energy and site accessibility. Although prediction software is a valuable tool which can predict potential targets with increasing accuracy, there are still major limitations which prevent them, so far, from being used for network analysis. The limitations of these tools are based on the weighting and number of factors used for prediction. Also, relatively few target prediction tools are able to incorporate information about the expression patterns of the miRNA and target of interest (Peterson et al. 2014). Databases of experimentally validated miRNA:mRNA interactions, such as miRTarBase, are also available as a tool for researchers (Hsu et al. 2014).

Epigenetics and non-coding RNAs

Epigenetics is defined as heritable changes in gene expression which do not involve alteration of the coding sequence. In 2007 Adrian Bird offered an alternate definition of epigenetics to ease confusion over the issue of heritability, especially regarding post-mitotic tissues. This definition is “the structural adaptation of chromosomal regions so as to register, signal or perpetuate altered activity states” (Bird 2007). This definition highlights the responsive, rather than proactive, nature of epigenetics to external or internal stimuli.

The two main epigenetic mechanisms are DNA methylation and histone modification. DNA methylation, addition of a methyl group to position 5 of the pyrimidine ring of cytosine, occurs at CpG sites (cytosine-phosphate-guanine) to create 5-methylcytosine (Razin & Riggs 1980). Large groups of CpG sites within close proximity to one another are known as CpG islands; these are found in approximately 70% of the promoters of mammalian genes (Saxonov et al. 2006). Methylation in the promoter region of the gene results in transcriptional repression. This is thought to have evolved as a protection mechanism against transposable elements and viral DNA (Bird 2002). As well as the known repressive action of methylation in promoter regions and in regions containing transposable elements or viral DNA, methylation is also detected in other regions. Large scale genomic mapping of DNA methylation has revealed DNA methylation in areas including transcriptional start sites and gene bodies. The effect of DNA methylation appears to be region specific as methylation in gene bodies is thought to be associated with active expression (Jones 2012).

Figure 8 shows DNA methylation (Figure 8A), the structure of chromatin and post-translational modification of histones tails. Figure 8B shows the nucleosome. This is made up

of DNA (red) wound around an octamer of histones (green). This octamer includes two of each histone H2A, H2B, H3 and H4. Post-translational modifications of the amino-terminal histone tails, which extend out from the structure can affect chromatin folding and/or can act as binding sites for other transcription factors. In Figure 8C histone tails are shown in dark green and modifications represented as coloured circles. The most well characterised histone modifications are acetylation and methylation. These are known to direct chromatin to a more transcriptionally active and more repressed state, respectively. Other histone modifications include sumoylation, phosphorylation and ubiquitination. This diverse histone code allows for fine tuning of gene expression (Jenuwein & Allis 2001). Figure 8C and D show how the DNA folds into a heterochromatin fibre; this is a tightly folded chromatin structure which prevents transcription factors accessing the genes in this region. Figure 8C shows the conformation of nucleosome referred to as “beads-on-a-string” formation. This is an active conformation of DNA which can be accessed by transcription factors allowing genes in this region to be expressed (Swygert & Peterson 2014).

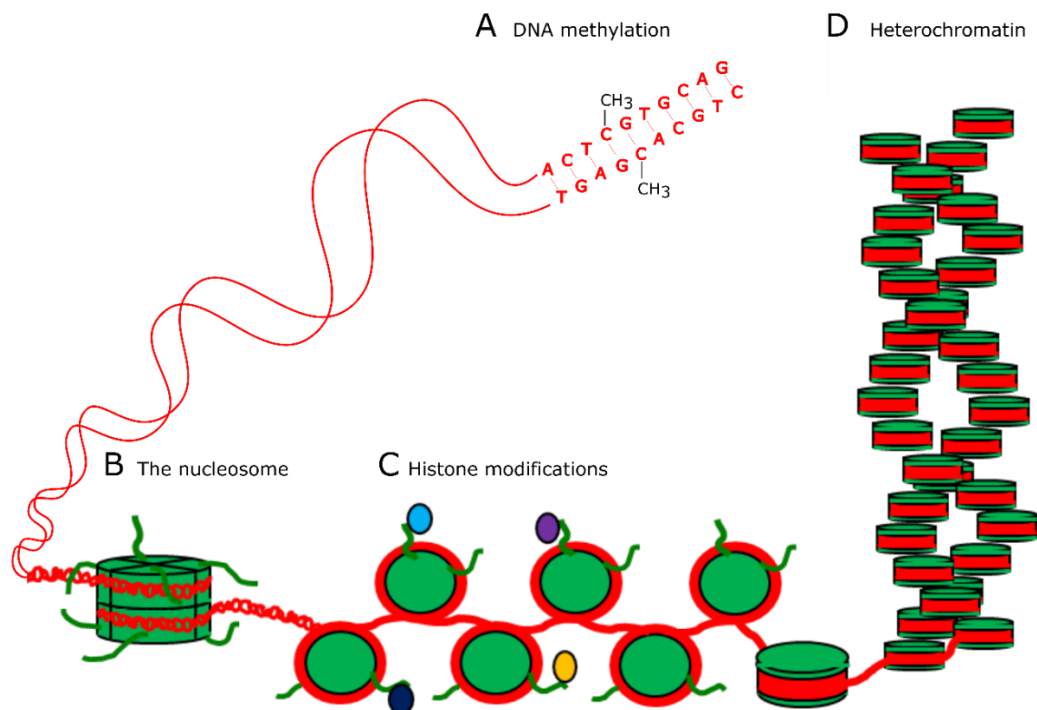


Figure 8. DNA methylation, histone modification and the structure of chromatin. *A* shows methylation of cytosine at a CpG site (cytosine followed by guanine). *B* shows the nucleosome, that is, DNA wrapped around an octamer of histone proteins. *C* shows various histone modifications (represented by coloured circles) present on the protruding histone tails. In *C* the chromatin is in the so-called “beads-on-a-string” formation which is transcriptionally active. *D* shows the folding of chromatin into a tightly packed fibre called heterochromatin. Genes in this region are in a transcriptionally repressed state.

Non-coding RNAs, including miRNAs have also historically been included as an epigenetic mechanism. Although there is no doubt that the effect of miRNAs is crucial for the regulation of gene expression, the increased understanding of their mechanism of action means that they are now not widely viewed as an epigenetic mechanism themselves but as a separate gene regulation mechanism which acts alongside epigenetics (Sætrom et al. 2007). Key differences between the mechanism of miRNAs and the classical epigenetic mechanisms are that miRNAs act to repress their targets post-transcriptionally, and as they are not directly associated with chromatin, that miRNAs are not inherited in the same manner as DNA and chromatin modifications. The initial inclusion of miRNAs being an epigenetic mechanism may stem from the discovery of this class of non-coding RNA in *C. elegans*. Unlike in other organisms, in *C. elegans* the effect of a miRNA is maintained for long periods of time and can even be passed onto offspring to maintain gene repression (Grishok et al. 2000). The persistence of non-coding RNA species in *C. elegans* is driven by the presence of an RNA dependent polymerase. This allows the continued production of RNA without *de novo* expression of additional RNAs (Sætrom et al. 2007). In mammals the average half-life of miRNAs has been shown to be approximately 5 days (Gantier et al. 2011).

A recent study has shown that miRNAs may be responsible, at least partly, for the inheritance of behavioural phenotypes induced by early trauma in mice. The behavioural effects, namely reduced avoidance and fear phenotype, of early traumatic stress were detectable in both the mice exposed to trauma (F1) and their offspring (F2). Some behavioural abnormalities were also detected in the F3 generation. Changes in miRNAs present in the sperm of the F1 mice compared to control were detected. To determine whether these miRNA changes were responsible for the behavioural phenotypes RNAs were purified from the sperm of F1 males and injected into wild type fertilised oocytes. Interestingly, the behavioural phenotype of the injected mice was similar to the F2 mice (Gapp et al. 2014). These data suggest that miRNAs play a role in transmission of behavioural phenotypes. However, in the F2 mice there were no changes in sperm miRNA, therefore the transmission of the behavioural phenotype to the F3 generation is by a different mechanism.

miRNAs have been shown to regulate genes involved in adding or removing histone modifications or methyl groups to DNA. For example, miR-29 has been shown to modulate DNA methylation by targeting DNA methyltransferases (Fabbri et al. 2007). Similarly, other non-coding RNA species are able to directly recruit polycomb repressive complexes, which are involved in chromatin remodelling via placing of repressive histone modifications. The

most notable example of this is *Xist* which has an essential role in X-chromosome inactivation in mammals (Peschansky & Wahlestedt 2014). Transcription of miRNAs may also be regulated by epigenetic mechanisms. To aid further study and increase understanding of the interaction of miRNAs and epigenetic mechanisms, a database, named EpimiR, has been created to collate information about mutual regulation between miRNAs and epigenetic mechanisms (Dai et al. 2014).

miRNA involvement in neurodegeneration

Although the involvement of miRNAs in human disease is most widely studied in the field of cancer, their involvement in neurodegenerative disorders is becoming increasingly apparent. Dicer, one of the key enzymes on microRNA biogenesis, is essential for proper development of the brain and for the maintenance of post-mitotic neurons (Petri et al. 2013). Several studies demonstrate that specific deletion of Dicer in a particular neuronal cell type results in the malformation or death of population of cells. This is true for dopaminergic neurons (Kim et al. 2007), motor neurons (Haramati et al. 2010) and Purkinje neurons of the cerebellum (Schaefer et al. 2007). Conditional loss of Dicer in the adult mouse forebrain results in the death of hippocampal neurons and cellular shrinkage in the cortex (Hébert et al. 2010; Davis et al. 2008), while Dicer ablation in *Wnt*-expressing neurons resulted in malformation of the midbrain and cerebellum (Huang et al. 2010). As miRNAs have such an important role in the survival of specific neuronal cell types it is no surprise that dysregulation of particular miRNAs have also been specifically implicated in many neurodegenerative disorders, including PD (discussed in detail in the next section), Huntington's disease, Alzheimer's disease and MND.

Gross transcriptional dysregulation is a key feature of Huntington's disease and this extends to miRNA dysregulation. A large number of miRNAs have been identified by miRNA profiling studies (Johnson et al. 2008; Packer et al. 2008; Martí et al. 2010). Alteration of four transcription factors, TP53, REST, E2F1 and GATA4, in Huntington's disease patient brains is likely to contribute to the transcriptional dysregulation of miRNAs, and other protein coding genes, observed (Sinha et al. 2012). miR-9/miR-9* may be involved in Huntington's disease pathology through their targets REST and coREST (Packer et al. 2008). In Huntington's disease patients REST is no longer sequestered in the cytoplasm and therefore can enter the nucleus and have a repressive effect its target genes (Buckley et al., 2010). Therefore, the reduced levels of miR-9/miR-9* observed in Huntington's disease patients may contribute to the transcriptional dysregulation observed.

miR-9 has also been implicated in both Alzheimer's disease; addition of amyloid- β peptides to primary neuron cultures result in the downregulation of this miRNA. In Alzheimer's disease miR-9 dysregulation may be involved in pathology through its target SIRT1 which is associated with the accumulation of hyperphosphorylated forms of Tau (Schonrock et al. 2010). Other miRNAs which have been consistently identified as dysregulated in Alzheimer's disease are: miR-107, miR-29, miR-181, miR-34, miR-106 and miR-146. Many of these miRNAs are implicated in the regulation of genes associated with Alzheimer's pathology (Goodall et al. 2013).

MND-associated proteins TDP-43 and FUS have been shown to interact with components of the miRNA biogenesis machinery, thus implicating dysregulation of miRNAs in MND pathology. Many miRNA expression changes are observed in MND brain tissue, however miRNAs in peripheral tissues are also thought to be important. The muscle-specific miR-206 is dysregulated in MND patient muscle tissue (Russell et al. 2013). This miRNA is thought to be involved in nerve-muscle communication and reinervation of muscles following nerve damage (Andrew H Williams et al. 2009). Another miRNA of interest which is thought to be involved in MND pathology is miR-155. The involvement of this miRNA in neurodegeneration is discussed in chapter 5.

miRNAs relevant to Parkinson's disease

Similarly to other neurodegenerative diseases miRNAs involved in PD have been identified by both large profiling screens and by directed studies to identify miRNA which target PD-associated genes. In this thesis three miRNAs of interest have been studied in zebrafish models. These miRNAs are: miR-133b, miR-205 and miR-155. These miRNAs were chosen as single, well conserved orthologues of these miRNAs and their major targets are present in zebrafish, thus allowing an easier comparison of their function in this model. The function of these miRNAs will be introduced briefly here and in more detail in the introduction to their respective chapters (Chapters 3, 4 and 5 respectively).

miR-133b is expressed in the midbrain and has been shown to directly target the transcription factor *PITX3*, which is involved in the development and maintenance of dopaminergic neurons. Inhibition of miR-133b in embryonic stem cell cultures resulted in increased expression of dopaminergic markers and dopamine release suggesting that this miRNA may be able regulate the development of a dopaminergic phenotype (Kim et al. 2007). This study aims to investigate the effect of miR-133b knockdown on dopaminergic neuron development in zebrafish.

miR-205 has been shown to directly target the PD-associated gene *LRRK2*. In the brain patients with sporadic PD, increased levels of LRRK2 protein and decreased levels of miR-205 were detected (Cho et al. 2013). As previously discussed LRRK2 is thought to exert a neurotoxic effect through a toxic gain of function. It was originally thought that toxic gain of function resulted from increased kinase activity however it is now argued that actual levels of LRRK2 protein may be a more important factor (Skibinski et al. 2014). This study aims to determine whether miR-205 knockdown in zebrafish results in increased levels of Lrrk2 protein and whether this has a neurotoxic effect on dopaminergic neurons.

miR-155 is a master regulator of inflammation and immune function (Vigorito et al. 2013). Neuroinflammation is a feature of many neurodegenerative diseases including PD. Increased expression of miR-155 has been detected in animal models of and the brains of patients with MND, Alzheimer's disease and MS (Butovsky et al. 2015; Junker et al. 2009; Guedes et al. 2014; Murugaiyan & Beynon 2011; Alexandrov et al. 2012). The aim of this study is to assess whether miR-155 is involved in inflammation in zebrafish models of PD.

Brain-enriched microRNAs miR-7 and miR-153 have been shown to directly target *SNCA* using a luciferase-tagged reporter plasmid containing the *SNCA* 3'UTR (Doxakis 2010). In a toxin-induced mouse model of PD miR-7 levels were decreased, suggesting possible mechanism for the observed increase of *SNCA* levels (Junn et al. 2009). These two miRNAs present possible therapeutic targets as they could be used to modify the expression level of *SNCA* in PD patients to reduce its pathogenic load.

LRRK2 has been shown to interact with Ago proteins, components of the miRNA processing pathway (Dächsel et al. 2007). Gehrke and colleagues demonstrated that mutant (G2019S) LRRK2 in *Drosophila* antagonised let-7 and miR-184, potentially through altered binding to Ago proteins (Gehrke et al. 2010). This resulted in the increase of E2F1 and DP1 protein levels. These proteins are involved in the cell cycle and aberrant expression of these proteins affects cell survival (Höglinger et al. 2007). The overproduction of these proteins in G2019S-LRRK2 *Drosophila* were shown to be critical for LRRK2 pathogenesis (Gehrke et al. 2010). However, the findings presented in this study are yet to be reproduced in a vertebrate model system or in patient derived cell models.

GWAS studies have previously identified an association between single nucleotide polymorphisms SNPs within the fibroblast growth factor 20 (*FGF20*) gene and PD (van der Walt et al. 2004). *FGF20* is preferentially expressed in the *substantia nigra* and involved in

the maturation and survival of dopaminergic neurons (Murase & McKay 2006). Subsequent genetic and functional analysis of SNPs in this region showed that a SNP in the 3'UTR of *FGF20* conferred the highest risk for PD (Wang et al. 2008). The identified SNP is within the recognition site for miR-433, thus preventing regulation by this miRNA which results in increased translation of *FGF20*. The increased levels of FGF20 protein correlated with increased α -synuclein levels in both cell models and PD patient brain (Wang et al. 2008). However, the interaction of FGF20 with α -synuclein or the association of the SNP in the miR-433 binding site with PD was not confirmed by a further study (Wider et al. 2009).

Two related miRNAs which were identified by miRNA profiling of PD patient brains are miR-34b/c. These miRNAs have been shown to be downregulated in PD patient brain in both early and advanced neuropathological stages. Therefore these changes are not thought related to treatment. The function of miR-34b/c was further studied in vitro in differentiated SH-SY5Y dopaminergic neurons. In these cells depletion of either miR-34b or miR-34c reduced cell viability and also altered mitochondrial function (Miñones-Moyano et al. 2011). This study also suggests that PD related genes *DJ1* and *Parkin* may be indirect targets of miR-34b/c. miR-34 has also been associated with aging in *Drosophila*. Loss of miR-34 resulted in accelerated brain aging, neurodegeneration and decreased survival (N. Liu et al. 2012). miR-34b and related miR-34a have also been implicated in Huntington's disease and Alzheimer's disease (Gaughwin et al. 2011; Zovoilis et al. 2011).

Finally, a group of miRNAs are thought to be involved in PD pathogenesis through their involvement in autophagy. These miRNAs are upregulated in PD brain and have been shown to target components of chaperone-mediate autophagy, *LAMP-2A* and *hsc70*, which are decreased in PD brain. Transfection of these miRNAs into an SH-SY5Y cell line which overexpresses α -synuclein resulted in decreased protein levels of LAMP-2A and hsc70 and increased accumulation of α -synuclein (Alvarez-Erviti et al. 2013). Figure 9 summarises the involvement of these miRNAs in the pathogenesis of PD.

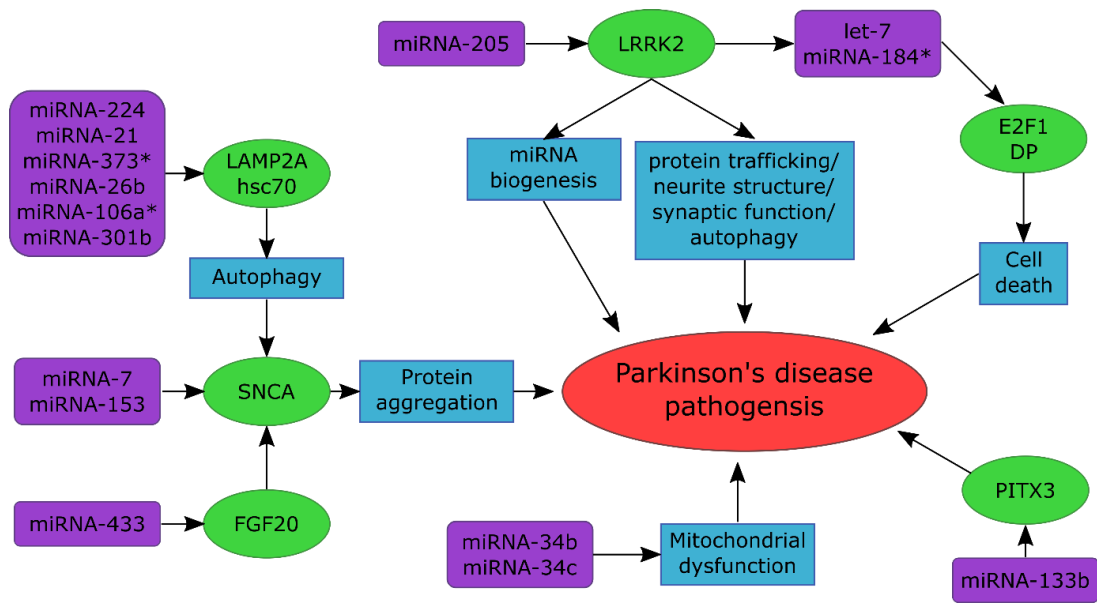


Figure 9. miRNAs thought to be involved in the pathogenesis of Parkinson's disease. Adapted from Goodall et al. (2013).

1.5 Aims and hypotheses

This main aim of this thesis is to study the effect of three miRNAs implicated in PD pathogenesis in zebrafish. These miRNAs are miR-133b, miR-205 and miR-155.

Aim 1: Investigate the role of miR-133b in dopaminergic neuron development and survival.

Hypothesis: Knockdown of miR-133b will increase dopaminergic neuron number through its target *pitx3*. I further hypothesise that knockdown of miR-133b will be able to rescue dopaminergic neuron loss observed in a previously validated zebrafish model of PD

Aim 2: Investigate the interaction between miR-205 and *lrrk2* in zebrafish.

Hypothesis: Knockdown of miR-205 will result in increased protein levels of its target Lrrk2. Increased levels of Lrrk2 protein will have a neurotoxic effect on dopaminergic neurons.

Aim 3: Investigate the role of miR-155 and neuroinflammation in neurodegeneration.

Hypothesis: miR-155, a marker of and driver of inflammation, will be upregulated in the brains of zebrafish models of PD and Gaucher's disease.

A further aim of this thesis is to develop a method allowing quantification of the number dopaminergic neurons a high throughput format.

Hypothesis: The development of such a method will facilitate future *in vivo* drug and toxin screens.

Chapter 2. Materials and Methods

Contents

Chapter 2. Materials and Methods	44
2.2 Materials	47
2.3 Zebrafish	47
2.3.1 Adult zebrafish husbandry	47
2.3.2 Zebrafish lines.....	47
2.3.3 Collection and maintenance of zebrafish embryos	48
2.3.4 Zebrafish anaesthesia.....	48
2.3.5 Genotyping of zebrafish larvae.....	49
2.4 Microinjection of zebrafish embryos	49
2.4.1 Preparation of injection apparatus	49
2.5 Transient knockdown of genes by Morpholino	50
2.6 Injection of miRNA mimic into embryos	51
2.7 Nucleic acid extraction and polymerase chain reaction (PCR)	52
2.7.1 gDNA extraction.....	52
2.7.2 RNA Extraction.....	53
2.7.2.1 From zebrafish embryos	53
2.7.2.2 RNA extraction from zebrafish brains.....	53
2.7.2.3 Lithium Chloride precipitation for RNA clean-up.....	54
2.7.3 cDNA synthesis	54
2.7.4 PCR/RT-PCR	54
2.7.5 DNA gel electrophoresis	54
2.7.6 qPCR	55
2.7.7 Primers used for PCR/RT-PCR/qPCR.....	56
2.7.8 miRNA taqman assays	57
2.8 MPP+ exposure	58
2.9 Embryo fixation	58
2.10 Whole Mount in situ Hybridisation	59
2.10.1 Synthesis of WISH riboprobes	59
2.10.2 Labelling of Exiqon LNA WISH probes for miRNA	60
2.10.3 Whole mount in situ hybridisation.....	61
2.11 Immunohistochemistry	62
2.11.1 Basic immunohistochemistry protocol.....	62

2.11.2 Combined fluorescent WISH and IHC.....	63
2.12 EdU exposure and staining	64
2.13 Generation of a fluorescent reporter for miRNA target analysis.....	65
2.13.1 Cloning of the pitx3 3'UTR into the reporter plasmid.....	66
2.13.2 Injection of the reporter plasmid and analysis of results	68
2.14 Imaging of stained/fluorescent embryos.....	69
2.14.1 Imaging embryos after WISH.....	69
2.14.2 Confocal microscopy for imaging fixed fluorescent embryos.....	69
2.14.3 Spinning disc confocal microscopy for imaging of live embryos	69
2.14.4 High throughput imaging of fluorescent embryos.....	69
2.15 Assessment of dopaminergic neuron number	70
2.15.1 Counting of dopaminergic neurons after WISH for th	70
2.15.2 Using the ETvmat2:GFP reporter line to assess dopaminergic neuron number	71
2.16 Western Blotting.....	71
2.16.1 Extracting protein from zebrafish embryos	72
2.16.1.1 Deyolking zebrafish embryos.....	72
2.16.2 Western blotting.....	72
2.16.2.1 Design and production of custom made antibodies.....	74
2.17 CRISPR/Cas9 genome editing technique.....	74
2.17.1 Design and purification of ultramers.....	74
2.17.2 Transcription of gRNA from ultramer.....	76
2.17.3 Injection of CRISPR	76
2.17.4 Determination of CRISPR efficiency	76
2.17.5 TOPO® TA cloning to determine mutations generated.....	77
2.18 Statistical tests and analysis	77

2.2 Materials

Unless otherwise stated, all chemicals are obtained from Sigma-Aldrich (Gillingham, UK); all enzymes and buffers from New England Biolabs; all plastic consumables from STARLAB Ltd (Milton Keynes, UK); and all polymerase chain reaction (PCR) primers and other DNA oligomers from Integrated DNA Technologies.

2.3 Zebrafish

2.3.1 Adult zebrafish husbandry

All adult zebrafish are housed in aquaria at the Bateson Centre at the University of Sheffield. Zebrafish are housed in tanks at a density of no more than four zebrafish per litre at a constant temperature of 28°C on a 14 hour light-10 hour dark cycle.

All experimental procedures are carried out in accordance with the UK Home Office Animals (Scientific Procedures) Act 1986 under project licence PPL 70/8437 held by Professor Oliver Bandmann and Personal Licence PIL I04FA191D held by Lisa Trollope.

2.3.2 Zebrafish lines

Unless otherwise stated all zebrafish referred to as wild type or WT are AB wild type zebrafish with the exception of wild type zebrafish which are the non-mutant siblings of any of the mutant lines used. Other zebrafish lines used in this study are:

The *ETvmat2:GFP* line, this line has green fluorescent protein (GFP) inserted between exon 2 and 3 of *vesicular monoamine transporter 2 (vmat2)* using the enhancer trap method (Wen et al. 2008). This line expresses GFP in monoaminergic neurons. This line is used with both a WT and *pink1*^{-/-} background.

The *pink1*^{-/-} mutant line. This line was generated from an ENU mutagenesis screen. A mutant containing a premature stop codon in the kinase domain of *pink1* was identified. Homozygote *pink1* mutant zebrafish are viable so homozygote mutants are generated from a homozygote in-cross. The WT siblings of these mutants, generated from a previous heterozygote in-cross are used as controls. The features of this mutant line are described in the following publication from the Bandmann lab (Flinn et al. 2013).

The *glucocerebrosidase1 (gba1)* mutant line. As homozygous *gba1* mutant zebrafish cannot produce viable progeny. Zebrafish which are heterozygous for the *gba1* mutation are in-crossed to generate embryos which are either WT (*gba1*^{+/+}), heterozygous (*gba1*^{+/-}) or

homozygous (*gba1*^{-/-}) for the *gba1* mutation. This line was generated by TALEN mutagenesis (Keatinge et al. 2015).

2.3.3 Collection and maintenance of zebrafish embryos

To collect embryos, either a marble tray is placed in the tank the previous evening to stimulate mating at the start of the light cycle in the morning, or, if embryos required careful staging, for example for injecting, zebrafish are pair mated by placing a male and a female on either side of a divided tank overnight. In the morning at the desired time the divider is removed and zebrafish are allowed to mate for the required time before the embryos are collected.

Embryos and larvae are kept at a constant temperature of 28°C in 1x E3 media (500µM NaCl, 17µM KCl, 33µM CaCl and 33µM MgSO₄, with 2 drops per litre methylene blue antifungal agent added) in 10cm petri dishes, at a density of no more than 60 zebrafish per plate (approximately 40ml).

With all embryos collected, especially those which have undergone injection at the one cell stage, the embryos are monitored at 8 hours post-fertilisation (hpf) when any unfertilised embryos can be identified and removed. Again, at 24hpf any dead embryos are removed, and a note is made if there is significant death in the injected group compared to control. To prevent any further death of embryos the E3 media is replaced.

If the embryos are to be used for imaging, and therefore a lack of pigmentation is desirable, phenylthiourea (PTU) is added at a final concentration of 4.3mM to the E3 media when then embryos are 8-24 hours old to prevent pigment from forming.

In accordance with the UK Home Office Animals (Scientific Procedures) Act 1986 larvae are not kept past 5.2dpf unless they are being raised to adulthood. To cull, live embryos are anaesthetised in tricaine (0.016%) before disposal in bleach.

2.3.4 Zebrafish anaesthesia

Tricaine or MS222 (PharmaQ Hampshire) is made up at a stock of 0.4% (w/v) in deionised distilled water. For embryo manipulation and sedation a 0.016% solution is used (that is 420µl of 0.4% stock solution is added to 10ml of E3 media. A lower concentration of 0.003% is used for mounting of zebrafish for imaging to induce a light sedation.

2.3.5 Genotyping of zebrafish larvae

In this study this technique was used to determine the genotype of embryo from an incross of *gba1* heterozygous mutants. 3dpf zebrafish larvae are anaesthetised in 0.016% tricaine. The anaesthetised larvae are placed under a Leica L7 dissecting microscope. A small section of tail is cut using a scalpel (Figure 10). This small section of tail is removed in 2µl of E3 media and placed in a 96 well PCR plate, the embryo is placed in the corresponding well of a regular 96-well plate. DNA is extracted from the tail section by the gDNA extraction method described in section 2.7.1. Once the genotypes have been determined the embryos are separated back into 10cm petri dishes by genotype.

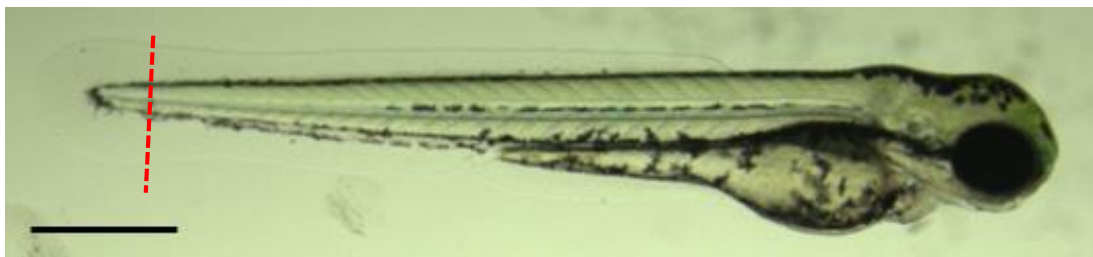


Figure 10. Fin clipping of embryos. The red line shows where a small section of the tail is cut. DNA is extracted from this section of tail. The scale bar represents 500µm.

2.4 Microinjection of zebrafish embryos

Microinjection of zebrafish embryos is a useful technique allowing various compounds, including Morpholinos for short-term knockdown of specific genes and the nucleoside analogue EdU (5-ethynyl-2'-deoxyuridine) for labelling proliferating cells (see section 1.4) to be injected into the zebrafish embryo at various embryonic stages.

2.4.1 Preparation of injection apparatus

Firstly microinjection needles are pulled from borosilicate glass capillaries (Kwik-Fil, World Precision Instruments, Inc., Hertfordshire, UK) using a micropipette puller (Model P-97, Sutter Instrument Co., USA).

Gel loading tips are used to pipette the solution which is to be injected into microinjection needle. The needle is loaded into the injection stand and adjusted so it can be lowered into the field of view of the microscope. The end of the needle is broken using fine tweezers. The injector air pump (Pv 820 Pneumatic pico-pump, WPI) is set to timed mode and the pressure and injection time can be adjusted to ensure one pump releases exactly 0.5nl or 1nl of injection solution. This is done by placing a drop of mineral oil onto a graticule and injecting some solution into the oil. The volume of the injected solution can be measured by lining up

the edges of the injected 'bubble' with the grid on the graticule. Volumes of 0.5nl or 4nl can be measured as shown in Figure 11.

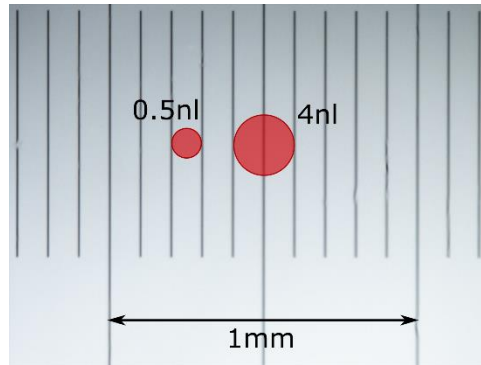


Figure 11. Using a graticule to measure injection volume.

2.5 Transient knockdown of genes by Morpholino

In order to create short-term knockdowns of particular genes in zebrafish, one cell-stage embryos were injected with Morpholino (MO), an antisense technology which prevents the correct splicing of the mRNA or primary microRNA (pri-miRNA) transcript. For protein coding genes MOs are either designed to target exon-intron/intron-exon boundaries to produce splicing defects assayable by RT-PCR. Alternatively, they may be designed to target the transcriptional start site to prevent translation of the mRNA. For miRNAs MOs can be designed to a number of regions in the pri-miRNA to prevent correct processing of the mature miRNA transcript (Figure 12).

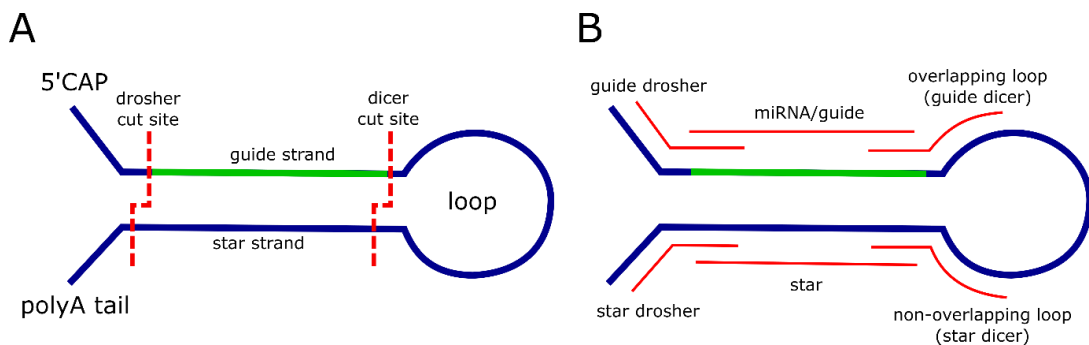


Figure 12. Regions of the pri-miRNA transcript and MO design. A shows the regions of a pri-miRNA transcript and the cut sites for processing enzymes drosher and dicer. B shows the potential binding sites of MOs which will disrupt processing of the pri-miRNA into its mature form.

All MOs are ordered from Gene Tools (Philomath, OR, USA). On arrival they are immediately resuspended to a concentration of 2mM in sterile water and stored at room temperature. The MOs used in this study are listed in Table 4. A standard control MO, designed to target human beta-globin is also used to control for any toxic effects of MO injection.

Once the injection apparatus is set so the required volume can be injected embryos are collected at the one cell stage. This is usually 20-40 minutes after the dividers have been removed from pair mating tanks or 20-40 minutes after the lights have been turned on in the aquarium if marble tanks are being used. If embryos from pair-mating tanks are embryos from at least two pairs of zebrafish are collected and pooled.

MO is made up to the optimal concentration (see Table 4) with distilled water and phenol red. 10% phenol red is added to enable the visualisation of the MO solution when it is injected to ensure it is injected into the yolk. 1nl of MO solution is injected into the yolk of embryos at the one cell stage. Injected embryos, and uninjected controls from the same batch of embryos are then left to develop at the desired time point.

Table 4. Morpholinos used in this study.

Target gene & region of MO binding	Sequence	Amount injected (in 1nl)
miR-133b miRNA/guide region	5'-CAGCTGGTTGAAGGGGACCAA-3'	1.8ng
miR-205 overlapping loop	5'-TGATTGAACAACACTACAGACTCCG-3'	5ng
Standard control MO (human beta-globin)	5'-CCTCTTACCTCACAGTTACAATTTATA-3'	Same as the MO it is controlling.
<i>Irrk2</i> Kinase domain	5'-CCCCTTCAGTATAAAACAC-3'	8ng
<i>Irrk2</i> WD40 domain	5'-AAATCTGCATGTTTTAGCACCTGGT-3'	8ng & 10ng
<i>pitx3</i> start site	5'-CGGTCTAGTGGAGGTAATCCTCGAA-3'	2ng
<i>pitx3</i> exon2-intron2 boundary	5'-GACATAAATATGAACTGACCACTGT-3'	4ng

2.6 Injection of miRNA mimic into embryos

A miRNA mimic is injected into embryos to determine the downstream effect of an up-regulation of this particular miRNA.

Firstly, the mimic is injected into the yolk in one-cell stage embryos, 1nl of 20mM mimic was chosen as the working concentration. The stock solution of miRNA mimic is diluted to the desired concentration with nuclease-free water and 10% phenol red to ensure the injected solution is visible. In order to allow persistence of miRNA mimic in the zebrafish brain the miRNA mimic is injected into the brain ventricles of 24 hour old embryos. These embryos are dechorionated, anaesthetised in 0.016% tricaine then mounted in 1% low melting point (LMP) agarose in a petri dish; this is to prevent leakage of the injection solution. The microinjection needle is able to penetrate the LMP agarose and enter the ventricle while the zebrafish embryo is in a lateral orientation (Figure 13). At this age 1nl of 10mM mimic is injected.

Table 5. miRNA mimics used in this study.

miRNA	Sequence	Company/cat no
miR-133b	5'-UUUGGUCCCUUCAACCAGCUA-3'	QIAGEN/MSY0001831



Figure 13. Injecting into the ventricles of a 24hpf embryo. The zebrafish is manipulated into a lateral orientation within the LMP agarose and the microinjection needle penetrates the ventricles from the side. The mimic is visualised using phenol red.

2.7 Nucleic acid extraction and polymerase chain reaction (PCR)

2.7.1 gDNA extraction

Genomic DNA (gDNA) is extracted from tissue (i.e. whole embryos, embryo fin clip or adult fin clips) by boiling in sodium hydroxide. Depending on the amount of tissue from which gDNA is being extracted 30-100µl NaOH is added to the tissue, the sample is heated to 95°C for 5 minutes before being vortexed vigorously to break up any remaining tissue. One tenth

of a volume 1M Tris HCl pH8 is added to neutralise the solution. The sample is then centrifuged at 1000xg for 1 minute to pellet any large debris. The supernatant is used for downstream applications.

2.7.2 RNA Extraction

2.7.2.1 From zebrafish embryos

RNA is extracted from zebrafish embryos using the trizol method. Around 20 embryos are placed into a 1.5ml Eppendorf tube and washed with DEPC-treated water. In a fume hood, 250µl TRI reagent® is added to the embryos and they are immediately homogenised by passing through a 25g needle. The sample is incubated for 3 minutes at room temperature. 50µl chloroform is added then tubes are inverted gently 10 times to mix. After a 3 minute incubation at room temperature the sample is centrifuged for 15 minutes at 16000xg at 4°C. After centrifugation layers separating the sample have formed; the top aqueous phase containing RNA, the interphase containing DNA and the lower organic phase containing protein and lipids. The aqueous phase is removed and is placed into a fresh Eppendorf tube. An equal volume of isopropanol is added. The tube is inverted gently to mix then incubated at room temperature for 10 minutes. The sample is centrifuged for 15 minutes at 16000xg at 4°C to collect the RNA pellet. The supernatant is removed completely taking care not to disturb the pellet. To wash 150µl of 75% ethanol is added to the pellet and centrifuged at 4500xg for 5 minutes at 4°C. The supernatant is removed completely then the RNA pellet is left to air-dry for around 3 minutes in the fume hood, or until all the excess ethanol has evaporated. The pellet is then resuspended in 15µl sterile DEPC-treated water, the concentration and purity of the RNA is determined using a nanodrop spectrophotometer (NanoDrop ND-100, Labtech International). The RNA is only used if the 260/230 and 260/280 ratios are above 2.0, indicating the RNA is free from contamination; if these ratios are lower lithium chloride precipitation to remove contamination is performed (section 2.7.2.3). RNA is stored at -80°C.

2.7.2.2 RNA extraction from zebrafish brains

RNA is extracted from zebrafish brains using the trizol method. The method differs from the method described above at the following steps. RNA was extracted from 1-2 brains in an 1.5ml Eppendorf tube, after TRI reagent® is added the brains are first broken up by passing through a 19g needle 20 times, they are then further homogenised by passing through a 25g needle 20 times. After homogenisation they are incubated with trizol for 5 minutes before addition of chloroform. The rest of the protocol is performed as above until the last step

where an extra ethanol wash is added (that is, remove supernatant, add 150µl 75% EtOH and centrifuge at 7000xg for 5 minutes).

2.7.2.3 Lithium Chloride precipitation for RNA clean-up

If the extracted RNA is not clean, as indicated by the 260/230 and 260/280 ratios given by the nanodrop, the RNA is cleaned up using LiCl precipitation. 30µl RNase free H₂O and 25µl LiCl precipitation solution (7.5M LiCl and 50mM EDTA pH8.0) (Ambion) is added to the contaminated RNA, this is mixed thoroughly and incubated at -20°C for 30 minutes. This is then centrifuged at 13000xg for 15 minutes at 4°C, the supernatant is removed and the pellet is washed with 100µl 75% EtOH as in the trizol protocol. The pellet is then resuspended in 10-20µl water and analysed using a nanodrop spectrophotometer.

2.7.3 cDNA synthesis

Complementary DNA (cDNA) is synthesised using the Verso cDNA synthesis kit (Thermo Scientific) according to the manufacturer's instructions. Briefly, 4µl of 5X reaction buffer, 2µl dNTP, 1µl RNA primer, 1µl enhancer and 1µl Verso enzyme mix is added to 11µl of RNA (maximum 1µg RNA in a 20µl reaction). This reaction is incubated at 42°C for 30 minutes then at 95°C for 2 minutes. cDNA is either used immediately for reverse transcription PCR (RT-PCR) or quantitative real-time PCR (qPCR) or stored at -20°C.

2.7.4 PCR/RT-PCR

On arrival primers are diluted to a 10µM working stock. In a 10µl reaction 5µl Biomix (Bioline) is used with 1µl of each the forward and reverse primer (working concentration 1µM), 1µl gDNA/cDNA template and 2µl ddH₂O. To optimise primer annealing temperature a gradient PCR is set up with temperatures between 55-65°C. The general temperature cycle is as follows: 93°C for 3 minutes followed by 30 cycles of 95°C for 30 seconds, annealing temperature for 30 seconds and 72°C for 1 minute, then to finish the reaction is incubated for 5 minutes of 72°C.

2.7.5 DNA gel electrophoresis

DNA gel electrophoresis is used to visualise PCR products and restriction digest products. To observe the DNA product 2µl of the reaction is run on a 1-2% agarose gel. The gel is made by dissolving agarose powder in TAE buffer (40mM Tris, 20mM acetic acid, 1mM EDTA) at the desired concentration (1-2% depending on expected DNA fragment size). Two drops of ethidium bromide are added per 100ml of agarose and mixed by swirling the molten agarose gel taking care to avoid splashing. The agarose is allowed to cool the poured into a gel mould

with a comb allowing wells to be formed. Once the gel has set the comb is removed and the DNA product can be loaded into the wells. If the DNA product is not present in a solution which contains loading dye (such as Biomix) 1/5th of a volume 5x loading dye is added to ensure that the DNA product sinks into the well and can be seen. Samples are electrophoresed at 150V for 15-30 minutes. DNA bands are visualised under UV light using the BIODOC IT™ imaging system (UVP).

2.7.6 qPCR

Quantitative PCR (qPCR) is used to quantitatively measure relative amounts of specific mRNA transcripts. A fluorescent dye (SYBR) which intercalates with double-stranded DNA is utilised and the fluorescence intensity is measured after each cycle to measure the quantity of PCR product. The number of cycles taken for the fluorescence intensity to reach the threshold intensity is calculated, this is called the Ct value.

To optimise PCR primers used for qPCR, primer pairs are tested at a range of concentrations between 100nM and 500nM. Secondly a standard curve is created using a range of concentrations of cDNA to ensure that the primer efficiency is close to 100% ($\pm 10\%$) and that there is a single peak on the dissociation curve, indicating only one product is being produced. Once the primers have been optimised the lowest successful concentration of primer and a concentration of cDNA that falls within the linear range of the standard curve is used in subsequent reactions.

Each 20 μ l reaction mixture contains 10 μ l SYBR green (Agilent), primer and cDNA at desired concentration, made up to 20 μ l with nuclease free dH₂O. The reactions are loaded into a qPCR plate (Geneflow) and the plate is briefly centrifuged to ensure the reaction mixture is in the bottom of the wells. The plate is loaded into the qPCR machine (Stratagene Mx3000P) and the reaction is cycled through 40 cycles of 30s at 95°C followed by 1 minute at 60°C. At the end of the cycles a melt curve is performed. Data are analysed using Stratagene MxPro 3000P (Stratagene).

Zebrafish *ef1a* is used as a reference gene. Fold changes are calculated using the delta-delta-Ct (ddCt) method. To calculate fold changes using this method the Ct value for the reference gene is subtracted from the Ct value for the gene of interest, this gives the delta-Ct value (dCt). To calculate the delta-delta-Ct (ddCt) value, the dCt value of the controls is subtracted from the dCt value of the “treated” or “mutant” groups. To calculate the fold change the following formula is used: fold change = $2^{(-ddCt)}$

2.7.7 Primers used for PCR/RT-PCR/qPCR

Primers are designed using Primer3 software v4.0.0 (<http://primer3.ut.ee/>) and a primer BLAST (NCBI) was performed to ensure the designed primers are specific for the gene of interest.

Table 6. PCR/RT-PCR primers used in this study.

Primer set	Sequence
miR-205 region	FWD 5'-AACCAAAGTGAGGTGGATGG-3' REV 5'- GCCTGCATTGATCCGTGTAT-3'
miR-133b region	FWD 5'-TGTTTGCTCTACATCCATGGA-3' REV 5'-ACATCAGCCAACACATTAAGCT-3'
<i>Irrk2</i> kinase domain	FWD 5'-GAGACGCTGCTGAAGAAA-3' REV 5'-GCAACTCACTGGGAAACT-3'
<i>Irrk2</i> WD40 domain	FWD 5'-ATGTTTATTCGTTCCGGTCTG-3' REV 5'-AGTGTCCCCTGCTGCTGTG-3'
<i>pitx3</i> 5'UTR-exon4	FWD 5'AGCCTTCACTCTCCGCTAAA-3' REV 5'-GCGGGCTTACATTCATGGAG-3'
miR-155 region seq and CRISPR1-4 analysis	FWD 5'-GGCATGATGGAAACTGTGCT-3' REV 5'-TCACACTCCAGCATGTCTTCT-3'
miR-155 CRISPR5 analysis primers	FWD 5'-GTGGATGTGCGTTGATCTCC-3' REV 5'-GATGTTCAGACGGTTCGCTC-3'
<i>gba1</i> genotyping primers	FWD 5'-AAAGCAGCACGATATGTCCA -3' REV 5'-ATGTCATGGGCGTAGTCCTC-3'

Table 7. qPCR primers used in this study

Primer set for qPCR	Sequence	Primer concentration used for qPCR
Zebrafish <i>ef1α</i> (reference gene)	FWD 5'-TGGTACTTCTCAGGCTGACT-3' REV 5'-TGACTCCAACGATCAGCTGT-3'	100nM
Zebrafish <i>pitx3</i>	FWD 5'-CCGGCAAAGGACACATTTC-3' REV 5'-GGCTTGCTGGTTCCTTTCTC-3'	100nM
Zebrafish <i>lrrk2</i>	FWD 5'-GCGCATACTAGAGCAGC-3' REV 5'-CGTTTCTCTCATTCTGCGGG-3'	100nM
Zebrafish <i>th</i>	FWD 5'-GAGGAGAGCGATGGAAAAGC-3' REV 5'-ATCCTTTGGTTTTTCGGCTGG-3'	100nM
Zebrafish CXCL8-I1	FWD 5'-TTAGAGATCCTTGCCACCTTGA-3' REV 5'-TCCGGGCATTCATGGTTTTTC-3'	100nM
Zebrafish CXCL8-I2	FWD 5'-GCTGGATCACACTGCAGAAA-3' REV 5'-TGCTGCAAACCTTTTCCTTGA-3'	500nM
Zebrafish <i>tnfa</i>	FWD 5'-GCGCTTTTCTGAATCCTACG-3' REV 5'-TGCCCAGTCTGTCTCCTTCT-3'	300nM
Zebrafish <i>tnfb</i>	FWD 5'-TCCTCAGACCACGGAAAAGTG-3' REV 5'-CCACCCATTTTCAGCGATTGTC-3'	300nM

2.7.8 miRNA taqman assays

Taqman assays are used to quantify the expression levels of miRNAs in zebrafish. These assays include a specific reverse transcription primer per miRNA and a single stem-loop qPCR primer.

RNA is extracted using the trizol method as described in section 2.7.2. RNA concentration is accurately quantified using the QuantiFluor™ RNA system (Promega) and the Qubit® fluorometer (Life Technologies). Exactly 100ng of total RNA is reverse-transcribed using the Taqman microRNA reverse transcription kit (Applied Biosystems) subsequently qPCR is performed using Taqman miRNA assays (Applied Biosystems). As with regular primers the qPCR is tested by running a standard curve of different cDNA concentrations to assess primer efficiency, the assays are only accepted if the efficiency is between 90-110%.

Table 8. Taqman assays used in this study.

Taqman assay	Sequence (mature miRNA)	Cat number
miR-133b	5'-UUUGGUCCCCUUAACCAGCUA-3'	002247
miR-205	5'-UCCUUCAUCCACCGGAGUCUG-3'	000509
miR-155	5'-UUA AUGCUAAUCGUGAUAGGGG-3'	000479
miR-146a	5'-UGAGAACUGAAUCCAUAGAUGG-3'	005396_mat
miR-24	5'-UGGCUCAGUUCAGCAGGAACAG-3'	000402
U6 small RNA	5'-GTGCTCGCTACGGTGGCACATATACTAAAATTGGAT CGATACAGAGAAGATTAGCATGGCCCCTGCGAAAGGA TGACACGCAAATCCGTGAAGCGCTCCATATTGCT-3'	custom assay

2.8 MPP+ exposure

MPP+ is a mitochondrial toxin that specifically targets the dopaminergic neurons. It is used to induce dopaminergic neuronal cell loss such as is seen in PD.

Embryos are exposed to a low dose, 3mM, of MPP+ at 48hpf or a high dose of 6mM at 24hpf, which is then replaced at 48hpf. Embryos treated with MPP+ are kept protected from light until they are fixed at 72hpf (see section 2.9).

2.9 Embryo fixation

In order to preserve embryos for whole mount *in situ* hybridisation or immunohistochemistry experiments 4% paraformaldehyde (PFA) in 1x phosphate buffered saline (PBS) is used as a fixative.

Embryos older than 18hpf are manually dechorionated with sharp tweezers, placed in a 1.5ml Eppendorf tube in groups of 20. All E3 media is removed before 1ml 4% PFA in PBS is added. Embryos younger than 24hpf are left inside their chorions. Embryos are incubated with agitation in PFA for 2 hours at room temperature or overnight at 4°C. PFA is removed and the embryos are dehydrated in 100% methanol for 20 minutes at room temperature, fixed embryos are then stored at -20°C.

If necessary, to remove excess pigment the embryos are bleached with 10% H₂O₂ and 0.5% KOH for 15 minutes directly after the PFA incubation, then gradually transferred into 100%

methanol (MeOH) via a 5 minute wash in 50% methanol in PBT (PBS with 0.1% tween-20) before dehydrating in 100% MeOH for 20 minutes. They are then stored at -20°C.

2.10 Whole Mount *in situ* Hybridisation

Whole mount *in situ* hybridisation (WISH) is used to visualise the expression pattern of various mRNAs and miRNAs in zebrafish embryos.

2.10.1 Synthesis of WISH riboprobes

Primers are designed to the cDNA sequence of a gene to generate a product 500-1000bp in length. A BLAST (NCBI) search is performed comparing the expected PCR product to the zebrafish transcriptome to ensure this is not present in any other genes. SP6 and T7 promoters (SP6 promoter: 5'-GATTTAGGTGACACTATAG-3', T7 promoter: 5'-TAATACGACTCACTATAGGG-3') are attached to the start of each primer to create a PCR product with SP6/T7 promoter on the start/end. These are used to initiate transcription so riboprobes both complementary (antisense) to the mRNA and the same sequence (sense) as the mRNA can be produced. The antisense probe is used to detect specific expression of the gene of interest while the sense probe is used as a control. RT-PCR reaction is performed to amplify a region of the cDNA (see section 2.7.4). The PCR products are then purified using the QIAquick PCR purification kit (QIAGEN) according to manufacturer's instructions. Briefly, 5 volumes of PB buffer is added to the PCR product and added to spin column, this is centrifuged at max speed (16000rcf) for 1 minute, the flow through is removed and 750µl PE buffer is added to the column, the column is then centrifuged again to wash the column. The flow through is removed then centrifuged once more to remove any remaining wash buffer. 20-30µl ddH₂O is added and incubated in the column for 1 minute then centrifuged to elute the purified PCR product. The concentration of purified PCR product is then checked using the nanodrop spectrophotometer.

The transcription reaction is then performed. Between 300-500ng of PCR product is diluted to 13µl with ddH₂O and 2µl 10x transcription buffer, 2µl 10x DIG labelled oligonucleotides, 1µl RNase inhibitor and 2µl of either SP6 or T7 polymerase (Roche) are added. This reaction is mixed thoroughly by pipetting then incubated for 2 hours at 37°C. To degrade DNA, 2µl DNaseI (Roche) is added and the mixture is incubated for a further 20 minutes at 37°C. To check the transcription reaction has worked 2µl of the mixture is run on a 1.5% agarose gel (15mins 150V). If RNA is present it is then purified by adding a mixture of 60µl 100% EtOH and 10µl 7.5M ammonium acetate, both ice cold, and inverting to mix. The mixture is then centrifuged for 15 minutes at 16000xg at 4°C to collect the RNA pellet. The supernatant is

removed completely taking care not to disturb the pellet. 100µl 100% ethanol is added to wash the pellet and centrifuged at 16000xg for 15 minutes at 4°C. The ethanol is removed without disturbing the pellet and the remaining ethanol is allowed to evaporate. The pellet is resuspended in 20µl nuclease free water. The concentration of the RNA is assessed using a nanodrop spectrophotometer. The concentrations of the sense and antisense probes are adjusted to ensure they are equal. This final solution is diluted 2.3x in formamide (Ambion). For use in WISH 100µl probe is added to 900µl of hybridisation buffer, the remaining probe is stored at -80°C.

Table 9. Primers used to generate WISH probes. SP6/T7 promoter sequence in bold and start/stop codon underlined.

WISH probe primers	Sequence
<i>Irrk2</i>	FWD 5'- GATTTAGGTGACTATAGCGGGAGCAAAACCAAAGACA -3' REV 5'- TAATACGACTCACTATAGGGTCAAAGTGCAGCAAGACACC -3'
<i>pitx3</i>	FWD 5'- TAATACGACTCACTATAGGGCGGTAGAGGTGATGGATTTTA -3' REV 5'- GATTTAGGTGACTATAGGAAATCTAGACGCATCGCTTCA -3'
<i>neurogenin1</i>	FWD 5'- TAATACGACTCACTATAGGGGACGCGTGCCATTATCTTCA -3' REV 5'- GATTTAGGTGACTATAGGGTGATGAAGACGACGAGGA -3'

2.10.2 Labelling of Exiqon LNA WISH probes for miRNA

Unlabelled locked nucleic acid (LNA) WISH probes for a selection of miRNAs were purchased from Exiqon.

To label the miRNA LNA probes the DIG Oligonucleotide 3'-End labelling kit is used (Roche). 100pmoles of unlabelled probe is diluted in ddH₂O to a final volume of 10µl. This is placed on ice and the following solutions from the labelling kit are added: 4µl reaction buffer, 4µl CoCl₂, 1µl DIG UTP and 0.5µl (200units) terminal transferase. The mixture is mixed carefully by pipetting then incubated at 37°C for 30 minutes. 5µl 0.1M EDTA pH8.0 is added to stop the reaction and the mixture is placed on ice. To purify the labelled probe and remove any unincorporated label Illustria™ MicroSpin™ G-25 (GE Healthcare Life Sciences) columns are used. The columns are prepared by vortexing to resuspend the resin. The cap is then loosened and the bottom closure removed and the column was vortexed at 750rcf for 1 minute. The prepared column is then placed in a new sterile collection tube, the labelled

probe is added to the resin and the purified probe is eluted by centrifuging the column for 2 minutes at 750rcf. The labelled, purified probe is then stored at -20°C.

Table 10. Exiqon LNA probes used.

miRNA	Sequence	Product code
miR-206	5'-ACACACTTCCTTACATTCCA-3'	88081-00
miR-205	5'-CAGACTCCGGTGAATGAAGGA-3'	18099-00
miR-133b	5'-TAGCTGGTTGAAGGGGACCAAA-3'	38579-00
miR-155	5'-CCCCTATCACGATTAGCATTAA-3'	35129-00

2.10.3 Whole mount *in situ* hybridisation

On the first day of whole mount *in situ* hybridisation (WISH) fixed embryos (see section 2.9) are rehydrated by successive 5 minute incubations in 75% MeOH in PBT, 50% MeOH in PBT, 25% MeOH in PBT, then 4 consecutive 5 minute washes in PBT. Embryos 24hpf and older are then digested in 10µl/ml proteinase K. The length of the incubation is dependent on the age of the embryos: 1dpf - 8 minutes, 2dpf – 18 minutes, 3dpf – 30 minutes, 4dpf – 40 minutes, 5dpf – 50 minutes. Embryos younger than 24hpf are not digested with proteinase K. The embryos are then re-fixed in 4% PFA in PBS for 20 minute and are washed 3 x 5 minutes with PBT. HybA (50% formamide, 5xSSC (750mM NaCl and 75mM trisodium citrate), 50µl/ml heparin, 0.1% Tween-20, 500µl/ml tRNA, pH6) is preheated to 68°C for RNA probes or 30°C below the stated RNA Tm for the Exiqon LNA miRNA WISH probes and added to the embryos. The embryos are pre-hybridised for 5 hours at the hybridisation temperature then the probe is added and hybridised overnight. Exiqon LNA probes are diluted 100x in HybA to give a final concentration of 50nM, RNA probes are diluted in HybA to give a final concentration of 0.8-1ng/µl.

On the second day of WISH, post hybridisation washes are performed at the hybridisation temperature. Firstly the embryos are briefly washed in HybB (HybA without heparin or tRNA) then embryos are transferred into 2xSSC (100mM NaCl and 30nM trisodium citrate at pH7) via successive 15 minute washes in 75% HybB in 2xSSC, 50% HybB in 2xSSC, 25% HybB in 2xSSC then 100% 2xSSC. Two 30 minute washes in 0.2x SSC are then performed at hybridisation temperature. The following washes are performed at room temperature on the shaker, the embryos are transferred into PBT via successive 10 minute washes in 75%

0.2xSSC in PBT, 50% 0.2xSSC in PBT, 25% 2xSSC in PBT then in 100% PBT. Next the embryos are blocked in PBT with 2mg/ml BSA and 2% sheep serum for 3 hours, then incubated with anti-DIG-AB FAB fragments (Roche) at 4°C overnight (5000x dilution in blocking solution).

On the third day of WISH, all washes are carried out on the rocker and the embryos are protected from light. Firstly the embryos are washed 6x 15 minutes in PBT, they are then equilibrated in NTMT (0.1M TrisHCl, 50mM MgCl, 0.1M NaCl, 0.1% Tween-20) via 2x 5 minute washes in NTMT in Eppendorf tubes. They are then transferred into a 12 well plate and one further 5 minute wash in NTMT is performed. The NTMT is then removed and staining solution (3.5µl BCIP and 4.5µl NBT (Roche) per ml NTMT) is added. The staining is monitored using the dissection microscope every 15 minutes. When staining is sufficient the staining solution is removed and the embryos are washed 3x 5 minutes in PBT. If any background staining has occurred the embryos can be cleared by bringing to 100% MeOH for 10-15 minutes or until the background staining has cleared, via a 5 minute wash in 50% MeOH. Once background staining has cleared the embryos are washed in 50% MeOH for 5 minutes then 3x 5 minute washes in PBT. The embryos are then moved back into eppendorf tubes and re-fixed for 20 minutes in 4% PFA in PBS. Finally, they are washed 3x 5 minutes in PBT then transferred into 75% glycerol for storage via 10 minute washes in 25% glycerol and 50% glycerol. Embryos are stored at 4°C.

2.11 Immunohistochemistry

Immunohistochemistry (IHC) is used to detect protein expression spatially in the zebrafish embryo. In this study it was used combined with either WISH, to detect co-localisation of mRNA and protein, and EdU staining to detect co-localisation of protein and proliferating cells.

2.11.1 *Basic immunohistochemistry protocol*

Fixed embryos are rehydrated and permeabilised by the desired method: either the method performed as part of the WISH protocol (section 2.10.3) or the EdU detection protocol (section 2.12), these protocols are performed until the blocking step when the following protocol is used.

To block, embryos are incubated for overnight at 4°C in PBDT (PBS with added 0.5% triton-100, 1% DMSO and 1% BSA) with 2% sheep serum (PBDTss) or 5% normal goat serum (PBDTngs). The primary antibody is diluted in PBDTss/ngs and incubated with the embryos overnight at 4°C with gentle agitation.

On the second day of staining the antibody solution is removed and the embryos are washed 6 x 20 minutes in PBDT. Secondary antibodies are then diluted in PBDT and incubated with the embryos at room temperature for 2 hours. The embryos are washed for 4 consecutive 20 minutes in PBDT followed by one 20 minute wash in PBT before re-fixing in 4% PFA in PBS and finally transfer into 75% glycerol for storage.

2.11.2 Combined fluorescent WISH and IHC

This technique is used to determine whether an mRNA and a protein are present in the same region by combining WISH to detect and visualise mRNA and IHC to detect and visualise protein.

The protocol is very similar to the single WISH protocol but differs in the following ways. At the end of day2 anti-DIG POD (Roche), to detect the dig-labelled nucleotides of the WISH probe and the antibody for the gene of interest are incubated with the embryos overnight at 4°C. After the primary antibody incubation the embryos are washed 6x 15 minutes with PBDT. To develop the staining of the WISH probe embryos are washed 3x 5 minutes in TNT (0.1M Tris-HCl pH7.5, 0.15M NaCl and 0.05% Tween20) before incubating in TSA-cy3 (Perkin-Elmer) for 2 hours. Embryos are then washed 3x 5 minutes in TNT and once in PBDT for 30 minutes before incubation with an Alexafluor tagged secondary antibody overnight at 4°C. All washes are performed in the dark with gentle shaking. After the overnight antibody incubation the embryos are washed 4x 15 minutes in PBT then refixed for 20 minutes in 4% PFA in PBS. Finally, they are washed 3x 5 minutes in PBT then transferred into 75% glycerol for storage via 5 minute washes in 25% glycerol and 50% glycerol. Embryos are stored at 4°C.

Table 11. Antibodies used for fluorescent WISH and IHC.

Target (and tag)	Species and type	Dilution factor	Company, Cat number
TH	Rabbit	1:500	Millipore ab152
TH	Mouse	1:2000	Immunostar
GFP	Rabbit	1:1000	Torrey pines (TP01)
Digoxigenin-POD tagged		1:5000	Roche
Secondary Antibodies			
Anti-mouse Alexafluor-568	goat	1:500	Invitrogen A21043
Anti-rabbit Alexafluor-488	goat	1:500	Invitrogen A11034
Anti-mouse Alexafluor-488	goat	1:500	Invitrogen A21121
Anti-rabbit Alexafluor-568	goat	1:500	Invitrogen A11035

2.12 EdU exposure and staining

EdU treatment was performed on either *ETvmat:GFP*;WT or WT zebrafish in order to detect proliferating neurons around the diencephalic catecholaminergic cluster, located by IHC for GFP or TH respectively. After treatment the embryos are fixed at the required time point. EdU is detected by the Click-iT® EdU Imaging kit (Invitrogen) and GFP/TH is detected using IHC (described in section 1.3).

5nl of 5mM EdU (2 volumes 10mM EdU:1 volume 0.3x Danieau's Solution:1 volume Phenol Red) is injected into the yolk of embryos at various time points (the preparation of microinjection equipment is described in section 2.4). The embryos are then left to develop at 28°C until the desired age is reached. At this point the embryos are fixed in 4% PFA in PBS for 2 hours at room temperature then dehydrated in 100% methanol. They are then stored at -20°C for at least 12 hours.

To detect EdU labelled cells the embryos are rehydrated the by successive 5 minute washes in 75% MeOH in PBT, 50% MeOH in PBT, 25% MeOH in H₂O. To permeabilise the embryos an

acetone crack is performed. To do this the embryos are suddenly incubated for 10 minutes in ice-cold acetone at -20°C. One quick wash in H₂O then 3 consecutive 5 minute washes in PBT are performed before the embryos are incubated in 1ml of Click-iT[®] reaction solution, protected from light, at room temperature for 3 hours. The Click-iT[®] reaction solution is made up as following and is used within 15 minutes of preparation:

Table 12. Components of the Click-iT[®] kit for EdU staining.

Reaction component	Storage details	Per 1ml of reaction solution
Click-iT [®] reaction buffer	Kit component D – stored at 4°C	43µl
H ₂ O		886µl
CuSO ₄	Kit component E – stored at 4°C	20µl
Alexa-fluor [®] 647 azide	Kit component B – stored at -80°C	1µl
Reaction buffer additive	Kit component F – stored at -80°C	50µl

After incubation in the Click-iT[®] reaction solution one wash in PBS is performed followed by 4 consecutive 15 minute washes in PBT. The protocol for IHC to detect GFP signal is then followed, beginning with an overnight blocking step in PBDBT + 5% sheep serum (see IHC section 1.3).

2.13 Generation of a fluorescent reporter for miRNA target analysis

A reporter plasmid was generated to determine whether miR-133b is able to target *pitx3* in zebrafish. A control dual reporter plasmid was kindly provided by the Giraldez lab. This plasmid contains both red fluorescent protein (RFP) and GFP. Downstream of RFP is a multiple cloning site into which a mock 3'UTR containing two perfect miR-133b binding sites have been placed, labelled on the plasmid map as miR-133b PTx2). GFP is present as a control as it does not have a 3'UTR therefore is not under the control of any miRNA. Figure 14 shows a plasmid map.

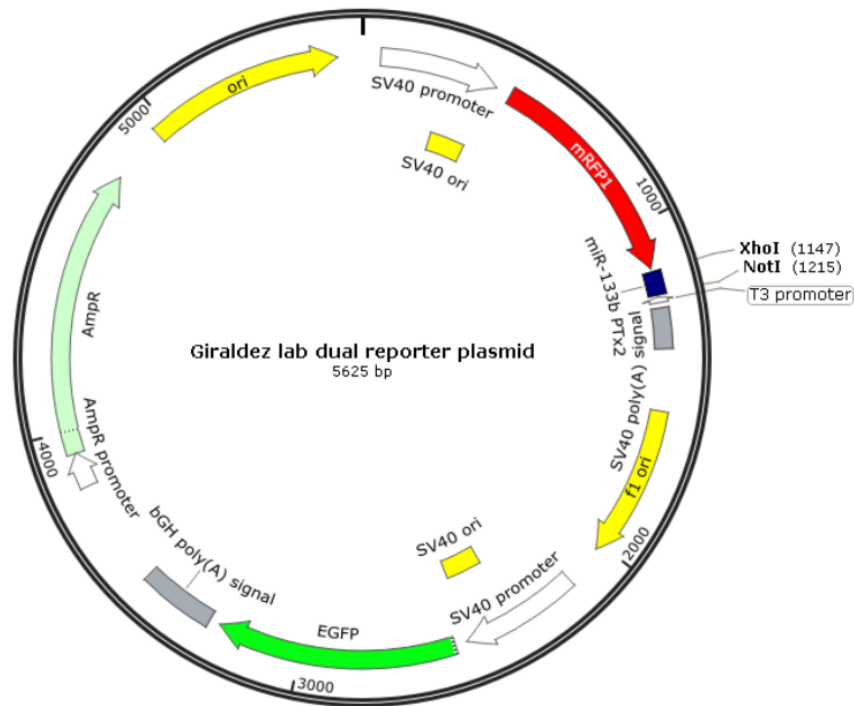


Figure 14. Plasmid map of dual reporter plasmid.

The control plasmid displayed above will express RFP under the control of miR-133b as the 3'UTR contains binding sites for this miRNA. To validate a specific miRNA-target interaction it is possible to clone in the 3'UTR of any gene of interest downstream of RFP between the *Xho1* and *Not1* restriction sites. This will help to determine whether this gene can be regulated by a particular miRNA. In this study the regulation of *pitx3* by miR-133b is being investigated. Therefore the 3'UTR of *pitx3* was cloned downstream of RFP in this vector.

2.13.1 Cloning of the *pitx3* 3'UTR into the reporter plasmid

Firstly, primers were designed to amplify the whole of the 3'UTR from the *pitx3* and to add a restriction site to each end so it is possible to cut both the plasmid and the PCR product with the same enzymes to allow targeted ligation. *Xho1* and *Not1* are the restriction enzymes used at the start and end of the 3'UTR fragment, respectively. The 3'UTR is amplified by PCR then both the PCR product and the plasmid are cut with the relevant restriction enzymes. The restriction reaction mix is as follows, 5µl 10x NEBuffer 4, 5µl 10x BSA, PCR product, 10U each restriction enzyme, the reaction mix is made up to 50µl with sterile water. The digestion products are then run on a 1% agarose gel at 100V for 30 minutes. The correct products are cut from the gel using a razor blade and are then extracted using the QIAGEN gel extraction kit according to the manufacturer's instructions. The digested 3'UTR and reporter vector are then ligated using NEB quick ligase using a 3:1 molar ratio of PCR product to linearised plasmid with a total of 100ng of DNA in the reaction. The reaction mixture is as follows: 5µl

buffer, 1µl enzyme, appropriate amounts of PCR and plasmid, made up to 10µl with sterile nuclease-free water. The reaction is incubated at room temperature for 5 minutes for ligation take place. The ligated vector and 3'UTR is then transformed into competent DH5β cells (NEB).

The transformation protocol is as follows: the competent cells are defrosted on ice for 30 minutes, 5µl of the ligation reaction is gently pipetted onto 50µl competent cells. The cells are incubated on ice for 30 minutes then heat-shocked at 42°C for 30 seconds. The cells are then incubated on ice again for 5 minutes to allow them to cool. Next the cells are recovered by placing 1ml of SOC media (NEB) and incubate at 37°C with agitation for 1 hour. Using aseptic technique, 100µl of the growth mixture is spread onto Ampicillin LB Agar plates. The rest of the cells are pelleted by centrifuging at 4000g for 1 minute and then re-suspended in 100µl media then this is all spread on a second agar plate. The plates are incubated overnight at 37°C to allow colonies to grow.

To produce plates 1 litre of LB-Agar (MP Biomedicals) is autoclaved then Ampicillin added to a final concentration of 0.1%. LB-Agar is cooled then plates are poured, left to set then dried at 37°C. 1 litre of LB-Agar contains 10g tryptone, 5g yeast extract, 0.5g NaCl and 15g Agar.

Several colonies are picked for screening to check for correct ligation. This is done by picking a small amount of the colony and placing it into a PCR using primers to regions either side of the insert. Therefore if the ligation has been successful the product will be the size of the 3'UTR plus the small region either side. 2-6 colonies that yield the correct size PCR product are selected and grown overnight at 37°C with agitation in 50ml LB (MP Biomedicals) with ampicillin.

The following day the plasmid is midi-prepped from the overnight culture, following manufacturer's instructions (QIAGEN). The plasmid is then analysed digestion with *Xho1* and *Not1* and finally by direct sequencing with to assess the insert is as expected.

Table 13. Primers used for generation and analysis of reporter plasmids.

Primer	Sequence
For sequencing multiple cloning site downstream of RFP and analysis of insert:	
AG plas RFP end FWD	5'-AAGACCGACATCAAGCTGGA-3'
AG plas RFP polyA REV	5'-TCACTGCATTCTAGTTGTGGT-3'
Zebrafish <i>pitx3</i> 3'UTR:	
Fwd primer + Xho1 (red)	5'-CAA CTCGAG AAGCGATGCGTCTAGATTTCTGA-3'
Rev primer + Not1 (red)	5'-ATAAGAAT GCGGCCGCT GAGACAAAGCAGGCTACACCAGGA-3'

2.13.2 Injection of the reporter plasmid and analysis of results

1nl of injection solution containing 1nl of 50ng/ μ l of plasmid, 50ng/ μ l *tol2* mRNA and either control MO, no MO or miR-133b MO is injected into one-cell stage zebrafish embryos. In some cells the plasmid will be incorporated into the genome. In these cells and descendants of these cells, GFP will be expressed freely as there are no regulatory sequences downstream of it. RFP will be expressed unless it is repressed by any post-transcriptional mechanism due to binding sites present in its 3'UTR.

Injected zebrafish embryos are imaged after 48 hours to assess fluorescence of GFP and RFP (see section 2.14.3). To determine whether a miRNA (in this case miR-133b) is able to interact with binding sites in the 3'UTR the ratio of RFP fluorescence intensity to GFP fluorescence intensity in plasmid containing cells is measured in the presence and absence of the miRNA of interest. In the presence of the miRNA of interest, if the miRNA is able interact with sites in its 3'UTR downstream of RFP, the levels of RFP will be reduced and therefore the RFP:GFP ratio will be reduced. In the absence of the miRNA of interest, or if this miRNA is not able to interact with binding sites in the 3'UTR downstream of RFP, RFP will not be repressed and the RFP:GFP ratio will be close to 1.

To measure the RFP:GFP ratio, a region containing GFP, and therefore expressing the plasmid, is selected. The fluorescence intensity of both GFP and RFP this region is measured using ImageJ. The ratio is calculated by dividing the RFP fluorescence intensity by the GFP fluorescence intensity.

2.14 Imaging of stained/fluorescent embryos

2.14.1 *Imaging embryos after WISH*

To capture images of zebrafish embryos and larvae after WISH a Nikon SMZ150 stereomicroscope was used. Embryos are placed in a watch glass in 75% glycerol and manipulated into the correct orientation using a mounted needle. At least 10 embryos/larvae from each group are imaged before selection of a representative image.

To take representative images of the larvae after WISH for *th* the Olympus Upright Epifluorescent microscope was used. In order to generate a colour image 3 bright field images were taken, one using each of the blue, red and green filters. The images are then combined to give a colour image.

2.14.2 *Confocal microscopy for imaging fixed fluorescent embryos*

To capture images of embryos after IHC, fluorescent WISH and EdU staining embryos are mounted dorsally onto microscope slides in glycerol and subsequently imaged using a Nikon Eclipse Ti confocal microscope.

2.14.3 *Spinning disc confocal microscopy for imaging of live embryos*

In order to capture images of live embryos expressing a fluorescent construct an UltraViewVoX spinning-disk confocal microscope (PerkinElmer Life and Analytical Sciences) was used. Anaesthetised embryos are mounted in the desired orientation on a glass coverslip in 1% LMP agarose.

2.14.4 *High throughput imaging of fluorescent embryos*

Mounting and individually imaging fluorescent embryos is a time consuming part of the experimental process. In order to increase the speed of imaging embryos and move towards a more high throughput imaging system a mould was created to create wells in agarose in a 96 well plate which are able to hold embryos in a dorsal position. The mould was designed by Westhoff and colleagues (2013), it was originally milled from brass, however a 3D printed version of the mould was later published (Wittbrodt et al. 2014).

The 3D printed mould, using the published design, was printed by WeDo3DPrinting (Sheffield, UK). In order to create wells in a 96 well plate 100µl of 1.6% LMP agarose in E3 (no methylene blue) is pipetted into each well of a Greiner µclear black walled 96 well. The mould is then placed into the 96 well plate and the agarose is left to set for around 15 minutes. Care is taken when removing the mould to ensure it is not tilted to disrupt any of

the wells. The moulds are used immediately or 50µl of E3 is pipetted into each well to prevent them drying out, the moulds can be stored in this state in the fridge for up to 24 hours.

Before mounting embryos are first anaesthetised in a low dose of tricaine (0.003%) before being transferred to the wells in the 96 well plate in a total of 150µl E3 media. To orient the zebrafish they are observed under a dissecting microscope and carefully adjusted using a mounted needle. Images are captured using an UltraViewVoX spinning-disk confocal microscope (PerkinElmer Life and Analytical Sciences).

2.15 Assessment of dopaminergic neuron number

2.15.1 Counting of dopaminergic neurons after WISH for *th*

To assess the number of *th+* dopaminergic neurons WISH for *th* is performed on 3dpf embryos. The heads of stained embryos are mounted dorsally onto microscope slides in glycerol. The Zeiss Axioplan microscope using a Plan-Neo FLUAR 20x/0.5 objective (Carl Zeiss Ltd, Jena, Germany) was used to visualise and count stained *th+* neurons. Only neurons from from Wulliman-Rink groups (1, 2, 4 & 5) were counted as these groups have ascending projections into the subpallium (analogous to the striatum in humans) thus representing the function of the neurons in the *substantia nigra* in humans (Figure 15) (Rink & Wullimann 2002).

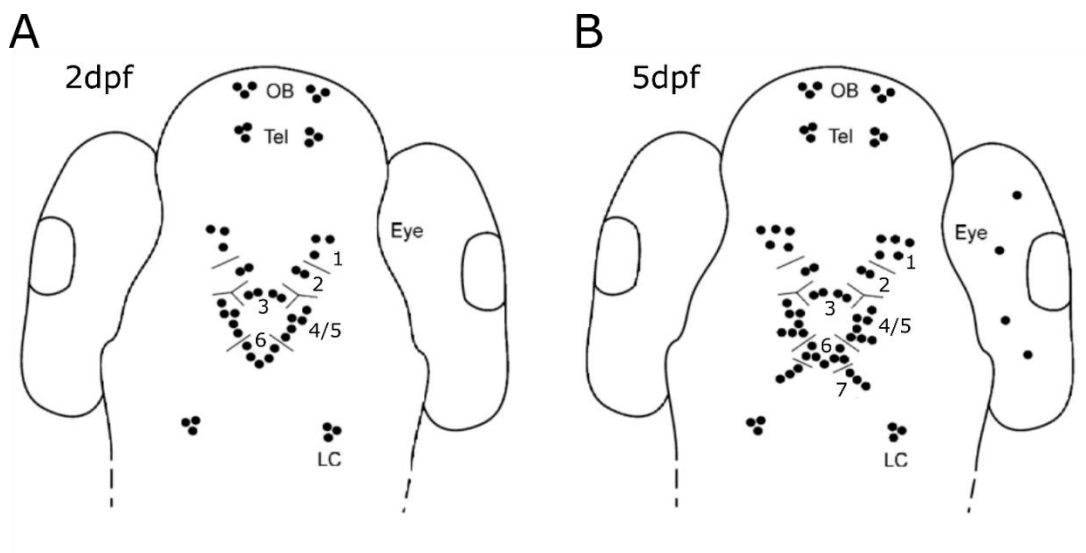


Figure 15. Location of *th+* neurons in 2 and 5dpf zebrafish. This figure shows the location of *th* expressing neurons at 2dpf (A) and 5dpf (B). In this study neurons from groups 1, 2, 4 and 5 are counted. OB = olfactory bulb, Tel = telencephalon and LC = locus coeruleus. Figure is adapted with permission from Rink & Wullimann (2002).

To avoid bias the investigator is blinded to the identity/genotype of the embryo being counted. In all experiments a minimum of 10 embryos are counted per group and the experiment is performed at least 3 times. The mean number of dopaminergic neurons in each group is calculated per biological repeat. The mean number of dopaminergic neurons is calculated for each group from each biological replicate. The average dopaminergic neuron count of the control groups is set to 100%; all other values are expressed as a percentage of this value.

*2.15.2 Using the *ETvmat2:GFP* reporter line to assess dopaminergic neuron number*

A number of methods can be used to assess the dopaminergic neuron number using the *ETvmat2:GFP* reporter line. The development of these methods is described in detail in Chapter 6.

Images of live zebrafish embryos containing the *ETvmat2:GFP* transgene are captured using the UltraViewVoX spinning-disk confocal microscope (PerkinElmer Life and Analytical Sciences). These images were processed in ImageJ. The image is cropped around the diencephalic catecholaminergic cluster and a substack is created which only contains neurons from this group.

Three methods of assessing dopaminergic neuron number can be performed using these processed images. Firstly, a maximum projection image can be created. From this image an intensity threshold is set. The mean fluorescence intensity of the region above the threshold and the number of pixels reaching the threshold value is measured. These values are multiplied together to give the total fluorescence intensity of the area above threshold value as a measure of dopaminergic neuron number. Secondly, the total fluorescent intensity reading can be measured from each slice of the substack. This method prevents loss of data where two neurons are present in the same X and Y position but different Z position. The total of these values can be used as a measure of dopaminergic neuron number. Thirdly, the number of dopaminergic neurons present in the substack image can be counted.

2.16 Western Blotting

In this study western blotting was used to determine Lrrk2 and Pitx3 protein levels in zebrafish embryos.

2.16.1 Extracting protein from zebrafish embryos

Whole embryos up to 3dpf are deyolked before extraction of protein. For brain-specific proteins such as Pitx3 the head of the 3dpf embryo is removed using a scalpel and protein extraction was performed on heads only to enrich for this protein of interest; in this case deyolking is not necessary.

4µl per embryo or 2µl per head of 2x Laemmli buffer (4% SDS, 10% 2-mercaptoethanol, 0.0004% bromophenol blue and 0.125M Tris-HCl pH 6.8) is added to the deyolked embryos/heads. Embryos/heads are passed through a 200µl pipette tip 5 times to break them up before sonication. Embryos/heads are sonicated 3x 10s with a 10 second rest between bursts at 25% amplitude. To remove any debris the samples are centrifuged at 4°C for 5mins at 13000rcf and the supernatant collected into a new Eppendorf tube. Samples are either used immediately for western blotting or stored at -80°C.

2.16.1.1 Deyolking zebrafish embryos

Up to 50 3dpf embryos are placed in a 1.5ml Eppendorf tube and the E3 media removed. 1ml of deyolking buffer (55mM NaCl, 1.8mM KCl and 1.25mM NaHCO₃) is added to each Eppendorf tube. Embryos are shaken for 5 minutes on a bench top vortex at 1000rpm. Embryos are centrifuged at 300g for 1 minute, the supernatant is carefully removed and discarded and replaced with 1ml wash buffer (110mM NaCl, 3.5mM KCl, 2.7mM CaCl₂ and 10mM TrisHCl pH8.5). Embryos are shaken for a further 2 minutes on a bench top vortex at 1000rpm before embryos are pelleted as above. One further wash is performed as above then all the wash buffer is removed. Deyolked embryos are then either snap frozen and stored at -20°C or immediately used for sample preparation.

2.16.2 Western blotting

Before loading into the gel the samples (between 10 and 40µl for optimisation) are heated to 95°C for 2 minutes then centrifuged briefly to ensure all of the sample is at the bottom of the tube.

The samples are then loaded into wells of a poly acrylamide gel alongside a protein ladder (Precision Plus Protein™ Dual Color Standard, BioRad). Pre-cast 4-15% polyacrylamide gels were used (BioRad). Electrophoresis is performed at a constant voltage of 150V for 30-45 minutes.

Once complete the protein is transferred from the gel to a polyvinylidene fluoride membrane (Merck Millipore). The membrane is briefly soaked in methanol then the transfer apparatus are assembled in transfer buffer (25mM Tris-base, 190mM glycine, 5-10% methanol). Proteins are transferred to the PVDF membrane by application of either 250mA (constant amps) for 1 hour or 90mA overnight. The membrane is then blocked with 5% non-fat milk powder (Marvel) in TBST (20mM Tris, 150mM NaCl and 0.1% tween pH7.6) blocking solution for 1-2 hours before incubation with the primary antibody. The membrane was incubated with the primary antibody for either 2 hours at room temperature or at 4°C overnight. The membrane is washed three times for 10 minutes in TBST before incubation with secondary antibody with an HRP tag for an hour at room temperature. The membrane is then washed again three times for 10 minutes in TBST. To visualise the protein the EZ-ECL Chemiluminescence detection kit for HRP (Biological Industries, Kibbutz Beit Haemek, Israel) was used according to manufacturer's instructions. The G:box (Syngene) was used for imaging. As a loading control the membrane was re-probed for Tubulin. The membrane was incubated with the anti-Tubulin antibody overnight at 4°C. The washes, incubation with secondary antibody and visualisation were performed as described above.

Table 14. Antibodies used for western blotting.

Protein	Species and type	Dilution factor	Company, Cat number
Pitx3	Rabbit monoclonal	1:500	Abcam ab134920
Pitx3 (custom)	Rabbit polyclonal	1:50	Eurogentec custom made antibody DSX-SUPR
Lrrk2	Mouse monoclonal	1:1000	NeuroMab N241A_34
Lrrk2 (custom)	Rabbit polyclonal	Not yet determined	Eurogentec custom made antibody DSX-SUPR
Tubulin	Mouse monoclonal	1:1000	Sigma T9026
Secondary Antibodies			
Goat anti-rabbit with HRP tag	Goat	1:5000	BIO-RAD #1706515
Goat anti-mouse with HRP tag	Goat	1:1000	BIO-RAD #1706516

2.16.2.1 Design and production of custom made antibodies

As commercially available antibodies specific to zebrafish Lrrk2 and Pitx3 were not available Eurogentec (Seraing, Belgium) were commissioned to produce custom antibodies for these proteins.

Eurogentec's peptide design service was used to generate a number of peptides from the supplied region of interest which are suitable for use as epitopes. These peptides were then assessed to ensure they are unique to the protein of interest using BLAST (NCBI). Per protein of interest two peptides specific to that protein were chosen. Polyclonal antibodies against these peptide epitopes were raised in rabbit. The antibodies were affinity purified against the peptide they were raised against before they were supplied.

Upon arrival the antibody was mixed with one volume of glycerol and stored at -20°C.

Table 15. Peptide epitopes of custom antibodies

Protein target/ antibody code	Peptide sequence	Stock concentration of antibody
Pitx3 ab164	Ac-ALSLSDSGTPQHDPGC-NH ₂	0.3mg/ml
Pitx3 ab165	H-CKGQDNSDTEKSHQNH-NH ₂	0.36mg/ml
Lrrk2 ab887	Ac-VAVQGKLPDPVKDYGC-NH ₂	0.2mg/ml
Lrrk2 ab888	Ac-PSSLSDHRPVIELPHC-NH ₂	0.14mg/ml

2.17 CRISPR/Cas9 genome editing technique

The CRISPR/Cas9 system is a method of generating stable mutant lines by inducing directed double stranded breaks in the DNA.

2.17.1 Design and purification of ultramers

CRISPR sites are identified by locating PAM sites (NGG) within the DNA. Cas9 nuclease will cut 3bp upstream of this sequence. Cas9 cut sites present within a restriction site were chosen as if the CRISPR generates a mutation the restriction site will be disrupted. The sequence of the 18bp upstream of the identified CRISPR site is used as a template, the reverse complement of this sequence is then placed into a gRNA template (see the underlined sequences in Table 16). The rest of this template contains the sequence for the

guide RNA which recruits Cas9 and the T7 promoter (shown in bold) from which the guide RNA is transcribed.

Table 16. Primers and ultramers used in CRISPR generation. For ultramers the underlined region is the target sequence and bold sequence is the T7 promoter.

Primer/ultramer	Sequence
General primers for ultramer amplification	FWD 5'- AAAGCACCGACTCGGTGCCAC-3' REV 5'-GCGTAATACGACTCACTATAG-3'
miR-155 upstream <i>Mwo1</i> gRNA1	5'-AAAGCACCGACTCGGTGCCACTTTTTCAAGTTGATAACGGACT AGCCTTATTTTAACTTGCTATTTCTAGCTCTAAAAC <u>CCAGCAGATTC</u> <u>TGCTCCTGCCCTATAGTGAGTCGTATTACGC-3'</u>
miR-155 exon <i>Bs1</i> gRNA2	5'-AAAGCACCGACTCGGTGCCACTTTTTCAAGTTGATAACGGACT AGCCTTATTTTAACTTGCTATTTCTAGCTCTAAAAC <u>GGTGCAGGTT</u> <u>TAATGCTACCCTATAGTGAGTCGTATTACGC-3'</u>
miR-155 exon <i>Bs1</i> gRNA3	5'-AAAGCACCGACTCGGTGCCACTTTTTCAAGTTGATAACGGACT AGCCTTATTTTAACTTGCTATTTCTAGCTCTAAAAC <u>GCACCAGGA</u> <u>GATCAACGCCCTATAGTGAGTCGTATTACGC-3'</u>
miR-155 downstream <i>Mwo1</i> gRNA4	5'-AAAGCACCGACTCGGTGCCACTTTTTCAAGTTGATAACGGACT AGCCTTATTTTAACTTGCTATTTCTAGCTCTAAAAC <u>AAAAGCAAC</u> <u>AAGTTGACCCCTATAGTGAGTCGTATTACGC-3'</u>
miR-155 exon <i>Hpy188III</i> gRNA5	5'-AAAGCACCGACTCGGTGCCACTTTTTCAAGTTGATAACGGACT AGCCTTATTTTAACTTGCTATTTCTAGCTCTAAAAC <u>ATCACGATTA</u> <u>GCATTAAACCCTATAGTGAGTCGTATTACGC-3'</u>

Upon arrival the ultramers are resuspended in 40µl dH₂O to a final concentration of 100µM. Ultramers are amplified with a standard set of primers in a 100µl PCR (50µl Biomix red, 38µl dH₂O, 5µl each forward and reverse primer and 2µl ultramer). The PCR reaction is 40 cycles using a 60°C annealing temperature. 2µl of the PCR reaction is electrophoresed on an agarose gel to ensure amplification has been successful. The remainder of the PCR is purified using the min-elute PCR purification (QIAGEN) according to manufacturer's instructions. The PCR product is eluted in 20µl of dH₂O then the concentration is measured using a nanodrop spectrophotometer. The amplified and purified ultramer can be stored at -20°C until it is needed.

2.17.2 Transcription of gRNA from ultramer

Transcription of the gRNA from the purified ultramer is performed using the MEGAscript T7 kit (Life Technologies). The transcription reaction mixture is as follows: 2µl buffer, 2µl each dNTP, 2µl enzyme, 1µl amplified ultramer (at least 30ng) and 7µl nuclease free water. The reaction is incubated at 37°C for at least 2 hours. After this incubation period 1µl of DNase is added to degrade the remaining ultramer. At this point 1µl of the mixture is run on an agarose gel to ensure the reaction has been successful. If RNA is present nuclease-free water is added to make up the reaction volume to 100µl. To purify the RNA 33µl ice cold 10M NH₄Ac and 350µl ice cold EtOH are mixed then added to the RNA. The RNA is precipitated in this mixture for at least 2 hours at -80°C. The RNA is pelleted by centrifuging at 13000rcf for 30 minutes at 4°C, the supernatant is removed and the pellet is washed in 70% EtOH as in the RNA extraction protocol (Section 2.7.2). The final pellet is air dried then resuspended in 10µl nuclease-free water. A 10x dilution of the RNA is made and the concentration of this dilution is measured using a nanodrop spectrophotometer. The gRNA is diluted to a concentration of 4-8µg/µl and stored at -80°C.

2.17.3 Injection of CRISPR

The gRNA is injected into one-cell stage embryos alongside Cas9 protein (NEB). The injection mixture contains 1µl of gRNA (4-8µg/µl), 1µl of Cas9 protein (stock concentration 18µM) and 0.5µl phenol red. 1nl of this mixture is injected into the yolk of one-cell stage embryos. The embryos are incubated in petri dishes at 28°C until 5dpf when they are transferred to tanks in the aquarium.

2.17.4 Determination of CRISPR efficiency

At 1dpf DNA is extracted from 8 CRISPR injected embryos and 8 uninjected embryos using the method described in section 2.7.1. PCR is performed on each sample with primers which surround the region which the CRISPR targets. The PCR products are electrophoresed on an agarose gel to determine if any large deletions are detectable. Secondly, the PCR products are digested with the relevant restriction enzyme. If the CRISPR is working effectively the restriction site is likely to be disrupted therefore an undigested band should still be present. The higher the ratio of undigested product to digested product, the more efficient the CRISPR.

2.17.5 *TOPO*[®] TA cloning to determine mutations generated

As injection of the CRISPR can generate a large number of different mutations within an individual embryo *TOPO*[®] TA cloning was performed to separate these mutations so they could be analysed individually. This helps determine the types of mutation generated by a particular CRISPR and whether they are likely to disrupt the function of the target gene.

The PCR products from CRISPR injected embryos are pooled and purified using the QIAquick PCR purification kit (QIAGEN) according to manufacturer's instructions. 4µl of the purified PCR product is combined with 1µl of the *TOPO*[®] vector and 1µl of a 4x dilution of the salt solution from the *TOPO*[®] TA cloning kit (Life Technologies). This reaction is incubated at room temperature for 30 minutes. This mixture is transformed into competent DH5β cells (NEB). This transformation protocol has previously been described in section 2.13.

The growth mixture was spread, under sterile conditions, on ampicillin-containing agar plates and incubated overnight at 37°C. Several colonies are picked for colony PCR. This is performed by picking a small amount of the colony and placing it into a PCR using the primers listed above to screen for mutations. Large insertions or deletions are visible after electrophoresis of the PCR product. Restriction digests were also performed to determine whether smaller mutations present disrupted the restriction site. If mutations were deemed to be present by analysis of the size of the PCR product or disruption of the restriction site the PCR product was sent for direct sequencing by the Core Genomics Facility at the Royal Hallamshire Hospital, Sheffield. Sequence data was analysed using FinchTV Version 1.4.0 (Geospiza, Inc.).

2.18 Statistical tests and analysis

All data analysis and statistical tests were performed using Graphpad prism V6.02 (Graphpad). The number of biological replicates of the experiments is denoted by the n number. Unless otherwise stated error bars represent the standard deviation of the mean. All data is analysed with an unpaired t-test, one way ANOVA or two way ANOVA unless otherwise states. Significance values are denoted as follows. Not significant (ns) $p > 0.05$, * $p < 0.05$, ** $p < 0.01$, *** $p < 0.001$.

Chapter 3. Investigating the role of miR-133b in dopaminergic neuron development and survival

Contents

3.1 Introduction	81
The implication of miR-133b in dopaminergic neuron development.....	81
PITX3 in dopaminergic neuron development and disease	81
Pitx3 in zebrafish.....	86
Functions of miR-133b.....	87
3.2 Characterisation of zebrafish miR-133b and <i>pitx3</i>	90
3.2.1 Optimisation	90
3.2.1.1 WISH probe for <i>pitx3</i>	90
3.2.2 Results	91
3.2.2.1 miR-133b sequence is conserved in zebrafish.....	91
3.2.2.2 Expression and localisation of miR-133b	92
3.2.2.3 Expression and localisation of <i>pitx3</i>	93
3.3 Knockdown of miR-133b and effect on dopaminergic neurons	94
3.3.1 Optimisation	94
3.3.1.1 Dosage optimisation of MO and validation of knockdown	94
3.3.2 Results	95
3.3.2.1 Effect of miR-133b knockdown on dopaminergic neurons in WTs	95
3.3.2.2 miR-133b knockdown is able to rescue dopaminergic neuron loss in <i>pink1</i> ^{-/-} zebrafish.....	97
3.3.2.3 miR-133b knockdown is unable to rescue dopaminergic neuron loss caused by MPP+ exposure	98
3.3.2.4 miR-133b knockdown results in an increase in <i>th</i> + neurons at 48hpf but not 36hpf.....	99
3.3.2.5 Validation of <i>th</i> + dopaminergic count using a the <i>ETvmat2:GFP</i> reporter line	100
3.4 Overexpressing miR-133b	100
3.4.1 Optimisation	100
3.4.1.1 Initial dosage optimisation.....	100
3.4.1.2 Optimisation of ventricle-injection technique and dosage of mimic	101
3.4.2 Results	103
3.4.2.1 Effect of miR-133b overexpression on dopaminergic neuron number	103
3.4.2.2 Localisation of miR-133b after injection of mimic.....	103
3.5 Effect of miR-133b knockdown on <i>pitx3</i>/Pitx3	104
3.5.1 Optimisation	105
3.5.1.1 Validation of reporter plasmid method using control plasmid	105

3.5.1.2 Western blotting	108
Morpholinos for <i>pitx3</i>	108
Testing of a commercially available antibody for Pitx3	109
Design and production of a custom Pitx3 antibody.....	110
Characterisation of custom Pitx3 antibodies - determining optimal working conditions.....	111
Characterisation of custom Pitx3 antibody ab164 – validating specificity for Pitx3	112
3.5.2 Results	114
3.5.2.1 Assessment of <i>pitx3</i> mRNA levels	114
3.5.2.2 Using a reporter plasmid to investigate the miR-133b- <i>pitx3</i> 3'UTR interaction	115
3.5.2.3 Assessment of Pitx3 protein levels	116
3.6 Effect of miR-133b knockdown on the proliferation of dopaminergic neurons	117
3.6.1 Optimisation	118
3.6.1.1 Determining time points to use for EdU analysis.....	118
3.6.2 Results	120
3.6.2.1 Comparison of proliferation between 12-48hpf in WT and miR-133b morphants.....	120
3.6.2.2 Comparison of proliferation between 12-13hpf in WT and miR-133b morphants.....	121
3.7 Discussion.....	122
Characterisation of miR-133b and <i>pitx3</i> in zebrafish.....	122
Knockdown of miR-133b and effect of dopaminergic neurons in WTs	123
Knockdown of miR-133b and effect of dopaminergic neurons in zebrafish models of PD.....	124
miR-133b overexpression experiments	126
Effect of miR-133b on Pitx3	126
Future work.....	129

3.1 Introduction

The implication of miR-133b in dopaminergic neuron development

miR-133b has been shown to be specifically expressed in midbrain dopaminergic neurons and depleted in the brain of PD patients. The confirmation of this finding in dopaminergic neuron deficient mouse models led to the identification of Pitx3 as a potential regulator of miR-133b. Overexpression of *Pitx3* in ESC cultures resulted in an increase in miR-133b precursor expression. It was confirmed that Pitx3 could regulate the miR-133b promoter using a luciferase reporter assay (Figure 16A). The study continued to demonstrate that miR-133b upregulation in ESC cultures resulted in a loss of dopaminergic markers and dopamine release and inhibition had the opposite effect, thus implicating miR-133b as a regulator of dopaminergic neuron development and function. Finally, Pitx3 was validated as a direct target of miR-133b using a luciferase reporter assay (Figure 16B), thus identifying a feedback loop between *PITX3* and miR-133b in dopaminergic neurons (Kim et al. 2007).

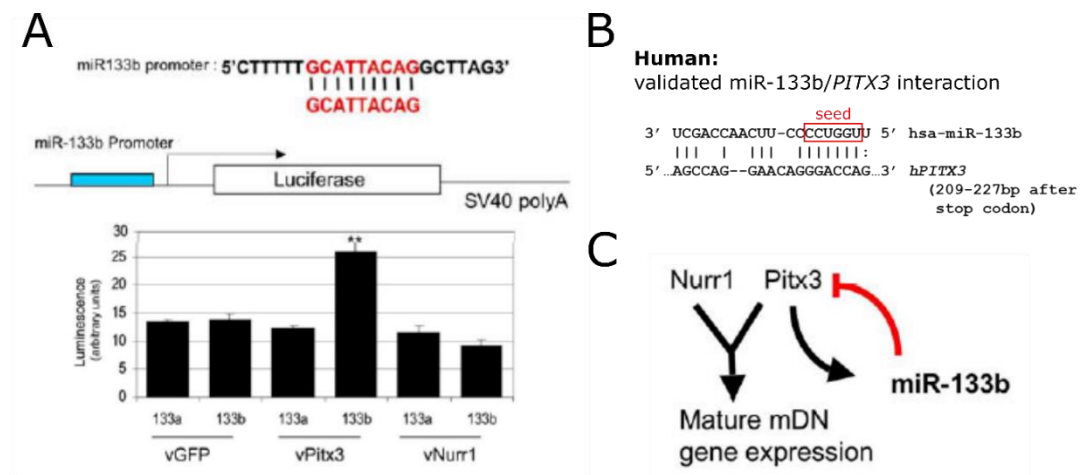


Figure 16. Identification of a feedback loop between miR-133b and PITX3 in midbrain dopaminergic neurons. This figure summarises the evidence for the feedback loop between miR-133b and PITX3. **A** shows evidence for regulation of the miR-133b promoter by PITX3. Upstream regulatory sequences from miR-133b or miR-133a were placed upstream of a luciferase reporter. The effect of addition of GFP, Pitx3 and Nurr1 containing vectors on luminescence from the miR-133a-luciferase construct was measured. No vector was able to increase luminescence from the miR-133a-luciferase construct and only Pitx3 was able to increase luminescence from the miR-133b-luciferase construct, thus confirming the specific upregulation of miR-133b by Pitx3 through this upstream regulatory element. **B** shows the validated binding site of miR-133b in the PITX3 3'UTR. **C** is a cartoon summarising the feedback loop between miR-133b and Pitx3. This figure is reproduced and adapted with permission from supplementary figures 4D, 6A and 6D of Kim et al. (2007).

PITX3 in dopaminergic neuron development and disease

In the mammalian system, PITX3 and NURR1 are master regulators of a sub-set of genes required for dopaminergic neurons. These genes are *TH*, aromatic amino acid decarboxylase (*AADC*), *VMAT2*, *DAT* and dopamine receptor 2 (*D2*); together these are responsible for the

synthesis, transport, detection and re-uptake of dopamine (Hwang et al. 2009; Jacobs et al. 2009; Lebel et al. 2001). NURR1 and PITX3 appear to work in concert to regulate these genes, and are able to target the same regions in the promoters of *TH*, *VMAT2*, *D2* and *DAT* (Jacobs et al. 2009). NURR1 is able to directly regulate PITX3 through a binding site in the *Pitx3* promoter, in the absence of NURR1, *Pitx3* expression is reduced (Volpicelli et al. 2012). Similarly, in the absence of PITX3, NURR1 exists in a repressed state through interactions with SMRT. SMRT interacts with HDACs to deacetylate and therefore repress their target genes. These data suggest that NURR1 requires PITX3 for activation by weakening the interaction of NURR1 with the SMRT repressive complex (Jacobs et al. 2009). PITX3 and NURR1 are essential for the development of midbrain dopaminergic neurons. PITX3 or NURR1 deficiency results in the loss of dopaminergic neurons specifically in the *substantia nigra* or the entire midbrain, respectively (Nunes et al. 2003; Castillo et al. 1998).

Transcription factors involved in specification of the dopaminergic phenotype have been shown to regulate PITX3. LMX1A and LMX1B have been shown to have a cooperative role in the specification of neural progenitors in the mammalian midbrain, through overlapping and cross-regulatory functions (Yan et al. 2011; Chung et al. 2009). *Lmx1a* forms an auto-regulatory loop with *Wnt1* and is able to positively regulate *Pitx3* expression through direct binding elements within the *Pitx3* promoter (Chung et al. 2009). This study also showed that *Lmx1b* was also able to bind the *Pitx3* promoter, thus confirming the previous suggestion of an interaction by Smidt and colleagues who found that that *Lmx1b*-deficient mice were not able to induce expression of *Pitx3* (Smidt et al. 2000). Another transcription factor capable of regulating *Pitx3*, is FOXP1. FOXP1 was identified as being differentially expressed in the PITX3 positive cells in embryonic mouse midbrain. In ESCs overexpression of *Foxp1* resulted in an increase in development of PITX3 positive cells, subsequently a binding site for FOXP1 was identified in the *Pitx3* promoter (Konstantoulas et al. 2010).

Neurotrophic factors GDNF and BDNF are also implicated in the *Pitx3* regulatory network. Two studies by Peng and colleagues place GDNF upstream of PITX3 and show that both GDNF and BDNF are regulated by PITX3 (Peng et al. 2007; Peng et al. 2011). Upregulation of these neurotrophic factors by PITX3 during development and adulthood illustrates its role in maintenance, as well as the development of, dopaminergic neurons.

Interestingly, and unexpectedly, PGC1 α has been shown to be a negative regulator of *Pitx3*. Overexpression of PGC1 α resulted in downregulation of *Pitx3* and increased sensitivity to MPTP toxicity. The authors suggest that this is due, in part, to decreased levels of BDNF, a

downstream target of PITX3. They discuss that as PGC1 α is a promising target for neuroprotection, the mechanism of PGC1 α regulation of PITX3 must be studied further (Clark et al. 2012).

Pitx3 is also able to positively regulate expression of the retinoic acid (RA) producing enzyme Aldehyde dehydrogenase (*Adh2*). *Adh2* is specifically expressed in dopaminergic neurons of the *substantia nigra*, these neurons specifically rely on Pitx3 for survival. Interestingly it was shown that through restoration of RA signalling in *Pitx3*-deficient mouse embryos, these neurons were able to survive, thus highlighting the importance of *Adh2* and RA in this population of neurons (Jacobs et al. 2011).

These data show that in the mammalian system, PITX3, as well as NURR1, is an important regulator which is involved in the terminal differentiation, survival and maintenance of dopaminergic neurons. The PITX3 network is summarised in Figure 17.

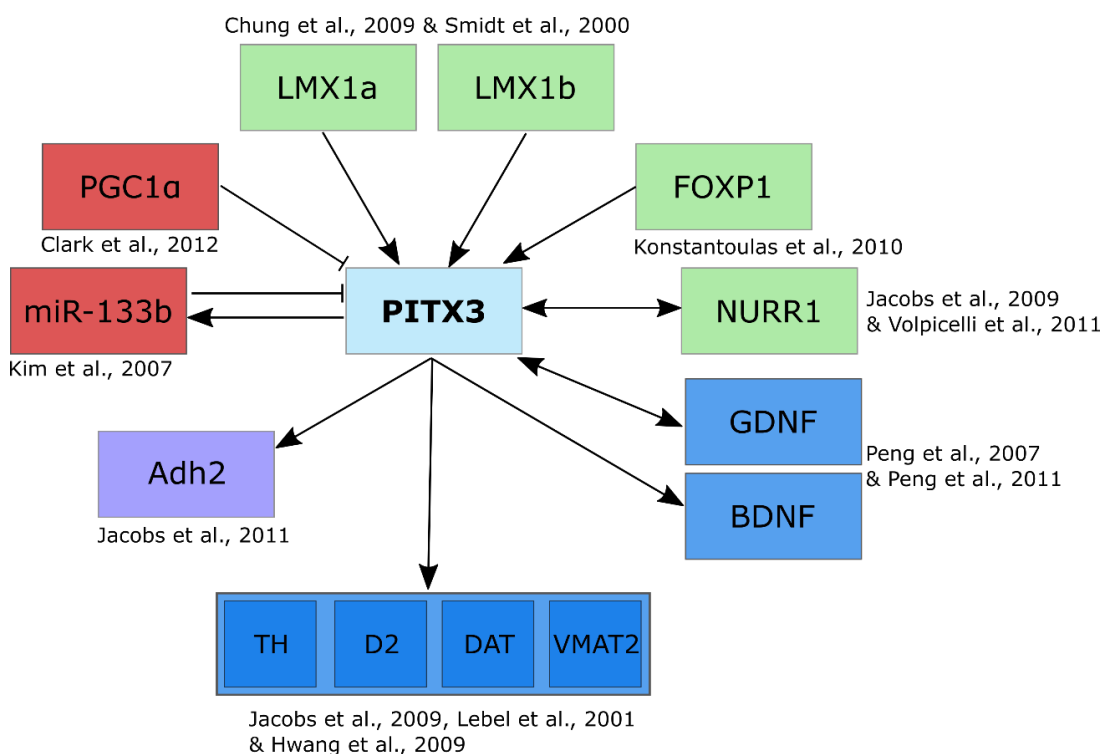


Figure 17. Summary of PITX3 network. This figure summarises the known activators, inhibitors and downstream targets of PITX3. Arrows represent an activation effect, blunt headed arrows represent an inhibitory effect and double headed arrows indicate a feedforward loop where a positive interaction has been identified in both directions.

Altered expression levels of *PITX3* have been associated with PD (H. Liu et al. 2012). This study measured the expression levels of *PITX3* and *NURR1* in peripheral blood lymphocytes of a cohort of over 250 Chinese PD sufferers and over 200 healthy controls. A significant decrease in the expression levels of both of these markers was detected in PD patients.

A number of SNPs in *PITX3* have been identified and their association with PD been investigated. In 2014, a meta-analysis was published which investigated the association between the three most commonly reported *PITX3* polymorphisms and PD (Jiménez-Jiménez et al. 2014). The meta-analysis did not find any of these polymorphisms to be significantly associated with LOPD, however a significant association between two of the polymorphisms and EOPD in Caucasians was revealed (Jiménez-Jiménez et al. 2014).

Four further polymorphisms were mentioned in this study, these were not included in the meta-analysis as they have only been investigated by two groups or fewer. Three of these polymorphisms were not determined to be associated with PD by these studies, however, the fourth polymorphism, C219>A, was determined to have an OR of 5.01 ($p < 0.001$) in Chinese population (Gui et al. 2012).

Moreover, the PDGene database (accessible at www.pdgene.org), recognises a number of polymorphisms which confer a significant risk ($OR > 1$) or protective effect ($OR < 1$) for PD in the *PITX3* genetic locus, shown in Figure 18. PDGene is a comprehensive data database aiming to provide extensive information on genetic association results from the most recent and largest meta-analyses of GWAS (Nalls et al. 2014). The original database is described in Lill et al. (2012). The presence of these polymorphisms further suggests that *PITX3* or the other genes present within this region may play a role in the development of PD.

The other genes present within the *PITX3*-containing locus are *NOLC1*, *ELOVL3* and *GBF1*. None of these genes have been previously associated with PD. Briefly, their functions are: *NOLC1*, synthesis of rRNA and the biosynthesis of ribosomes; *ELOVL3*, elongation of fatty acid chains; and, *GBF1* is a guanine nucleotide exchange factor involved in vesicular trafficking.

A Human chromosome 10q24.32



B

Polymorphism	Location (hg19)	Gene	Ethnicity	# Samples	# Studies	Allele contrast	1000G CEU	1000G CHB+JPT	Meta OR (95%CI)	I ² (95%CI)	Meta P-value
rs2296887	chr10:104005410	GBF1	All: C	108,990	15	C vs. T	0.1 (C)	0.3 (C)	1.12 (1.07-1.17)	34 (0-65)	4.43e-07
rs10748818	chr10:104015279	GBF1	All: C	108,990	15	G vs. A	0.092 (G)	0.333 (G)	1.12 (1.07-1.16)	39 (0-67)	8.61e-07
rs10883719	chr10:103977898	ELOVL3 [-8187bp]	All: C	108,990	15	T vs. C	-	-	0.89 (0.84-0.94)	32 (0-64)	3.14e-05
rs7913281	chr10:104010142	GBF1	All: C	108,990	15	G vs. A	0.117 (G)	0.308 (G)	1.09 (1.04-1.13)	39 (0-67)	5.83e-05
rs11598856	chr10:103940629	NOLC1 [+17002bp]	All: C	108,990	15	A vs. G	0.242 (A)	0.092 (A)	0.93 (0.89-0.96)	2 (0-54)	7.03e-05
rs10883718	chr10:103973851	ELOVL3 [-12234bp]	All: C	108,990	15	G vs. A	-	-	0.92 (0.88-0.96)	39 (0-67)	7.07e-05
rs10883717	chr10:103967590	ELOVL3 [-18495bp]	All: C	108,990	15	C vs. T	0.117 (C)	0.308 (C)	1.09 (1.04-1.13)	40 (0-67)	7.08e-05
rs71496537	chr10:103952323	NOLC1 [+28696bp]	All: C	108,990	15	T vs. G	0.283 (T)	0.108 (T)	0.93 (0.89-0.96)	7 (0-43)	9.69e-05
rs35523291	chr10:103957407	ELOVL3 [-28678bp]	All: C	108,990	15	G vs. A	-	-	1.08 (1.04-1.12)	5 (0-56)	9.76e-05
rs11593898	chr10:103958651	ELOVL3 [-27434bp]	All: C	108,990	15	C vs. T	0.267 (C)	0.108 (C)	0.93 (0.89-0.96)	4 (0-56)	9.88e-05
rs11594623	chr10:103960351	ELOVL3 [-25734bp]	All: C	108,990	15	T vs. C	-	-	1.08 (1.04-1.12)	5 (0-56)	9.98e-05
rs117507580	chr10:103941875	NOLC1 [+18248bp]	C	-	13	T vs. C	0.017 (T)	-	>1 (-)	2 (-)	<0.05
rs10883720	chr10:104010971	GBF1	C	-	13	C vs. G	0.117 (C)	0.308 (C)	>1 (-)	39 (-)	<0.05
rs11191243	chr10:103993035	PITX3	C	-	13	A vs. G	-	-	>1 (-)	45 (-)	<0.05
rs147188068	chr10:104000353	PITX3	C	-	9	A vs. T	-	-	<1 (-)	0 (-)	<0.05
rs77886504	chr10:103999779	PITX3	C	-	12	A vs. G	0.017 (A)	-	>1 (-)	41 (-)	<0.05
rs76637321	chr10:103963982	ELOVL3 [-22103bp]	C	-	13	A vs. G	0.017 (G)	-	<1 (-)	44 (-)	<0.05
rs144366339	chr10:103966145	ELOVL3 [-19940bp]	C	-	12	A vs. C	-	-	<1 (-)	0 (-)	<0.05
rs139387233	chr10:103973261	ELOVL3 [-12824bp]	C	-	12	A vs. G	-	-	>1 (-)	0 (-)	<0.05
rs116902041	chr10:103950714	NOLC1 [+27087bp]	C	-	13	T vs. C	0.133 (T)	-	<1 (-)	14 (-)	<0.05
rs3758549	chr10:104004195	GBF1 [-1094bp]	C	-	13	A vs. G	0.2 (A)	0.092 (A)	<1 (-)	0 (-)	<0.05
rs10883715	chr10:103960817	ELOVL3 [-25268bp]	C	-	13	T vs. C	0.133 (T)	0.3 (T)	>1 (-)	49 (-)	<0.05
rs142321508	chr10:103960278	ELOVL3 [-25807bp]	C	-	10	A vs. G	-	-	<1 (-)	0 (-)	<0.05

Figure 18. Polymorphisms conferring a significant risk or protective effect for PD in the PITX3 genetic locus. A shows the genes within the genomic region surrounding PITX3 on chromosome 10. **B** shows all polymorphisms which confer a significant risk or protective effect for PD. From PDGene, accessed August 2015 (Lill et al. 2012; Nalls et al. 2014). Legend: within ethnicity, C = Caucasian. Allele contrast “x” vs “y”, “x” refers to the allele with a protective or risk effect and “y” denotes the reference allele with an OR of 1. 1000G, allele frequency data from the 1000 genomes project. CEU, Utah residents with European ancestry. CHB, Han Chinese in Beijing. JPT, Japanese in Tokyo. OR = Odds ratio. I² = amount of heterogeneity between study-specific results that is beyond chance. CI = confidence interval.

Aphakia, meaning absence of a lens, mice harbour a naturally occurring mutation in the promoter of *Pitx3* (Semina et al. 2000). These mice demonstrate the progressive loss of dopaminergic neurons during development (Hwang et al. 2003). They also display motor impairments which can be ameliorated by levodopa (Van Den Munckhof et al. 2006). Additionally, these mice perform poorly in a number of cognitive tasks (Ardayfio et al. 2009). Taken together these findings show that *aphakia* mice display many symptoms that resemble those of PD.

Other functions of PITX3 include eye development, this is indicated by the failure of lens development in *Aphakia* mice. These mice naturally developed this phenotype which was later attributed to the deletion of a region upstream of *Pitx3* (Semina et al. 2000). In humans, mutations in *Pitx3* have been shown to be responsible for autosomal dominant congenital cataracts, presence of lens opacity of varying severity at birth, and anterior segment dysgenesis, the failure of normal development of the anterior segment of the eye (Verdin et al. 2014). While the role PITX3 plays in lens development is not fully understood studies in *Aphakia* mice demonstrate that a loss of proliferation and increased apoptosis is identifiable

at an early age. Expression of crystallins is also altered and the differentiation of lens cells is abnormal (Medina-Martinez et al. 2009). These data show that proper expression of *Pitx3* in the developing eye is critical for normal lens development.

Pitx3 in zebrafish

Zebrafish *Pitx3* shares many similarities with human *PITX3*. Firstly, it shares 63% amino-acid similarity with human *PITX3* (Figure 19A). Secondly, the genetic locus of zebrafish *pitx3* (on chromosome 13) is syntenic to the region of human chromosome 10 which contains *PITX3* (Figure 19B). Thirdly the expression pattern of zebrafish resembles the expression pattern described by mammalian studies. That is, a high level of expression is present in the developing lens and brain (Shi et al. 2005). Shi and colleagues aimed to identify the conserved function of *Pitx3* with respect to lens development in zebrafish. The authors found that the *pitx3* morphant phenotype includes defects in eye development, reminiscent of the *Aphakia* mouse phenotype. *pitx3*-deficient zebrafish also exhibit loss of differentiated neurons in the retina. This suggests a novel function of *Pitx3* in zebrafish (Shi et al. 2005). This study also hints towards a conserved role in zebrafish brain development.

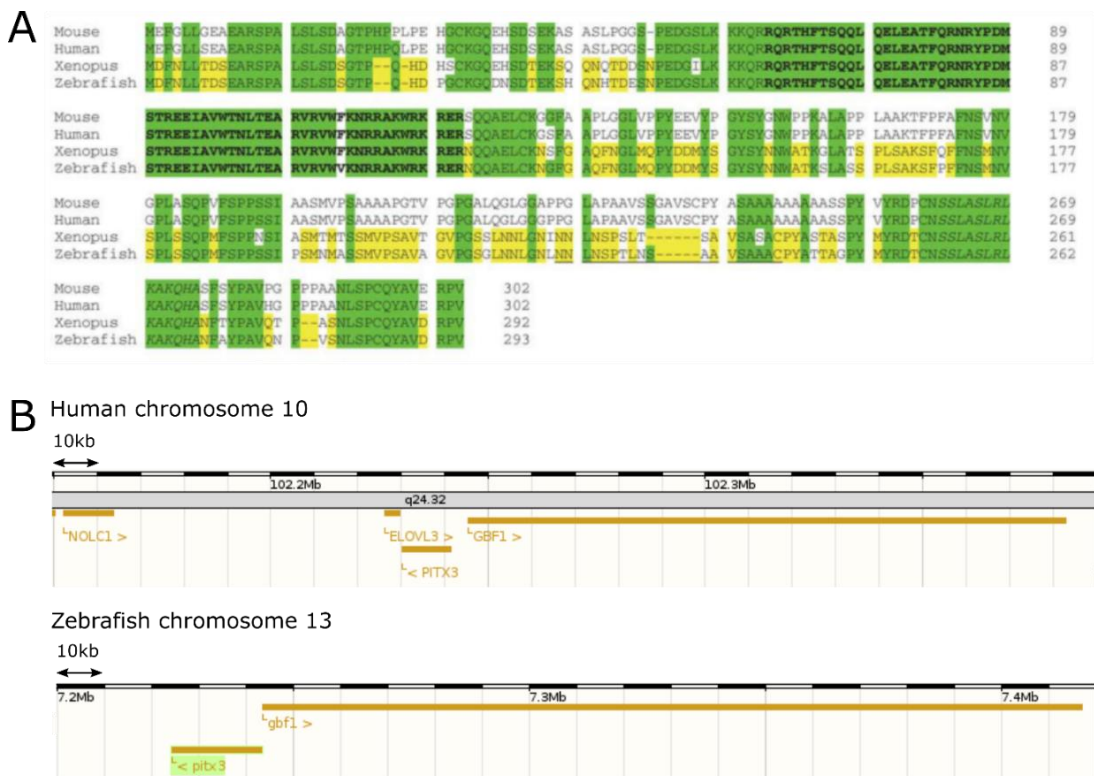


Figure 19. Protein homology and genetic locus synteny between human and zebrafish *pitx3*. **A** shows the protein homology between human, mouse, zebrafish and xenopus *Pitx3*. Green denotes conserved amino acids between all species and yellow denotes conservation between zebrafish and xenopus. The homeobox domain is shown in bold. Figure reproduced with permission from (Shi et al. 2005). **B** shows region synteny between the *pitx3* containing locus in humans and zebrafish. Zebrafish do not possess an orthologue of *ELOVL3*, however the orthologues of *NOLC1* is also present on chromosome 13, 2.4Mb away from *pitx3*.

Although the development of the dopaminergic system is well studied in the mammalian system, it is not as well characterised in zebrafish. In zebrafish, Pitx3 and Nurr1 do not seem to have the same roles in the differentiation of dopaminergic neurons as no co-localisation of TH and Pitx3 or Nurr1 is detectable in the diencephalic dopaminergic neurons (Filippi et al. 2007). However, they seem to have conserved roles in the maintenance of neural progenitors. *pitx3* knockdown by MO causes extensive, non-specific apoptosis in the zebrafish head and eye which can be ameliorated by concurrent knockdown of p53 (Filippi et al. 2007). Knockdown of zebrafish *lmx1b* orthologues causes a significant decrease in *pitx3* expression levels and a significant loss of dopaminergic neurons in both the diencephalon and the hindbrain. This suggests that Pitx3 and Lmx1b have some conserved roles in dopaminergic progenitor survival in zebrafish.

Functions of miR-133b

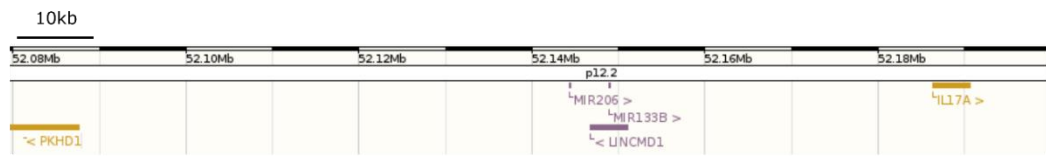
miR-133b is often referred to as a muscle-specific miRNA. Through interaction with a number of its targets it plays a role in myoblast differentiation, cardiomyocyte proliferation, cardiac hypertrophy and the cardiac conduction system. Moreover, dysregulation of miR-133b has been associated with a number of muscle diseases (Andrew H. Williams et al. 2009). miR-133b is thought to be transcribed in a bicistronic transcript with another “muscle-specific” miRNA, miR-206. MyoD, a transcription factor which plays a role in the regulation of muscle differentiation, has been shown to activate transcription of the bicistronic miR-133b/miR-206 transcript (Rosenberg et al. 2006).

miR-133b is now also recognised to have important roles other than those related to muscle (Kim et al. 2007; Chen et al. 2014; Guo et al. 2014). It has been suggested that miR-133b acts as a tumour suppressor and is downregulated in a number of cancers (Chen et al. 2014; Duan et al. 2013; Zhao et al. 2014). Significant downregulation of miR-133b was identified in colorectal cancer (Duan et al. 2013). This study validated *CXCR4* as a direct target of miR-133b and suggests that downregulation of miR-133b releases *CXCR4* from repression thus allowing it to promote tissue invasion and cancer-cell survival. In gastric cancer cell lines overexpression of miR-133b was able to inhibit metastasis. This metastatic-inhibition has been suggested to be through repression of a number of targets, including *Gli1*, *FSCN1* and *SP1* (Guo et al. 2014; Zhao et al. 2014; Qiu et al. 2014).

As discussed above miR-133b has also been implicated in the regulation of development of dopaminergic neurons (Kim et al. 2007). A recent large meta-analysis of GWAS studies has identified a number of polymorphisms within the miR-133b containing genetic locus (Lill et

al. 2012; Nalls et al. 2014). However, the effect of these polymorphisms has not been functionally validated.

A Human chromosome 6p12.2



B

Polymorphism	Location (hg19)	Gene	Ethnicity	# Samples	# Studies	Allele contrast	1000G CEU	1000G CHB+JPT	Meta OR (95%CI)	I ² (95%CI)	Meta P-value
rs115914526	chr6:52030789	MIR133B [+16950bp]	C	-	10	C vs. G	0.017 (C)	-	>1 (-)	0 (-)	<0.05
rs115563660	chr6:51980471	PKHD1 [+28048bp]	C	-	13	A vs. C	0.025 (C)	-	<1 (-)	4 (-)	<0.05
rs115085521	chr6:51982941	MIR206 [-26206bp]	C	-	13	C vs. G	0.033 (G)	-	<1 (-)	5 (-)	<0.05
rs150671504	chr6:52010772	MIR206 [+15400bp]	C	-	9	A vs. G	-	-	>1 (-)	0 (-)	<0.05
rs10484882	chr6:52011469	MIR206 [+22370bp]	C	-	13	A vs. G	0.142 (A)	0.1 (A)	>1 (-)	0 (-)	<0.05
rs75770430	chr6:52012042	MIR133B [-1679bp]	C	-	13	A vs. C	0.067 (A)	-	>1 (-)	24 (-)	<0.05
rs78884837	chr6:52011436	MIR206 [+2204bp]	C	-	13	A vs. G	0.067 (A)	-	>1 (-)	24 (-)	<0.05
rs78690722	chr6:51987178	MIR206 [-21969bp]	C	-	13	A vs. G	0.067 (A)	-	>1 (-)	38 (-)	<0.05
rs141796001	chr6:51971127	PKHD1 [+18704bp]	C	-	10	T vs. C	-	-	<1 (-)	11 (-)	<0.05
rs16882131	chr6:52008933	MIR206 [-214bp]	C	-	13	T vs. C	0.317 (T)	0.158 (T)	>1 (-)	0 (-)	<0.05
rs78922640	chr6:52010128	MIR206 [+896bp]	C	-	13	A vs. C	0.067 (C)	-	<1 (-)	27 (-)	<0.05
rs74382386	chr6:52010187	MIR206 [+955bp]	C	-	13	T vs. C	0.067 (T)	-	>1 (-)	25 (-)	<0.05
rs143733365	chr6:52047925	IL17A [-3260bp]	C	-	5	C vs. G	-	-	<1 (-)	65 (-)	<0.05

Figure 20. Polymorphisms conferring a significant risk or protective effect for PD in the miR-133b containing genetic locus. **A** shows the genes within the genomic region surrounding miR-133b on chromosome 6. **B** shows all polymorphisms which confer a significant risk or protective effect for PD. From PDGene, accessed August 2015 (Lill et al. 2012; Nalls et al. 2014). Legend: within ethnicity, C = Caucasian. Allele contrast “x” vs “y”, “x” refers to the allele with a protective or risk effect and “y” denotes the reference allele with an OR of 1. 1000G, allele frequency data from the 1000 genomes project. CEU, Utah residents with European ancestry. CHB, Han Chinese in Beijing. JPT, Japanese in Tokyo. OR = Odds ratio. I² = amount of heterogeneity between study-specific results that is beyond chance. CI = confidence interval.

In zebrafish, the function of miR-133b in muscle formation appears to be conserved. Disruption of miR-133b in zebrafish embryonic development interferes with sarcomeric actin organisation and a large number of muscle specific mRNAs were identified as direct targets of miR-133b (Mishima et al. 2009). Similar to the repressive role that miR-133b is thought to play in metastasis and cell survival in human cancer tissue, depletion of miR-133b in zebrafish has been shown to aid appendage and heart regeneration (Yin et al. 2008; Yin et al. 2012). The regeneration process may require some of the same pathways as cancer cells use to spread and invade. In contrast to the inhibitory function of miR-133b in fin regeneration miR-133b has been shown promote recovery of spinal cord injury in zebrafish (Yu et al. 2012). This difference in function is likely to reflect the differences in miRNA targets present in different tissues. In zebrafish miR-133b is upregulated after spinal cord injury, this is not the case in mammals, thus suggesting that the increased regenerative capacity of the zebrafish spinal cord compared to mammals may lie in the altered regulatory pathways that allow pro-regenerative factors to be expressed after spinal cord injury (Yu et al. 2012).

The function of miR-133b in regulation of dopaminergic phenotype also appears to be conserved in zebrafish. Work carried out by the Rodriguez group on addictive substances in zebrafish support the notion that *pitx3* is a target of miR-133b in zebrafish (Simon-Sanchez

et al. 2009; Barreto-Valer et al. 2012). In their study treatment of zebrafish embryos with cocaine or morphine resulted in an increase in dopamine receptors and a decrease in miR-133b expression. To test the hypothesis that this occurs through the interaction of miR-133b with *pitx3*, 100pg of *pitx3* 3'UTR was injected into zebrafish embryos. If miR-133b is able to bind the *pitx3* 3'UTR one would expect the exogenous 3'UTR to bind all of the free miR-133b thus releasing endogenous *pitx3* from repression. At 24 hours post injection of the *pitx3* 3'UTR the levels of miR-133b, *pitx3* and Pitx3 targets *th* and *dat* were assessed by qPCR. Levels of free miR-133b were decreased and *pitx3*, *th* and *dat* were increased. This data suggests that miR-133b is able to interact with the 3'UTR of *pitx3* in zebrafish.

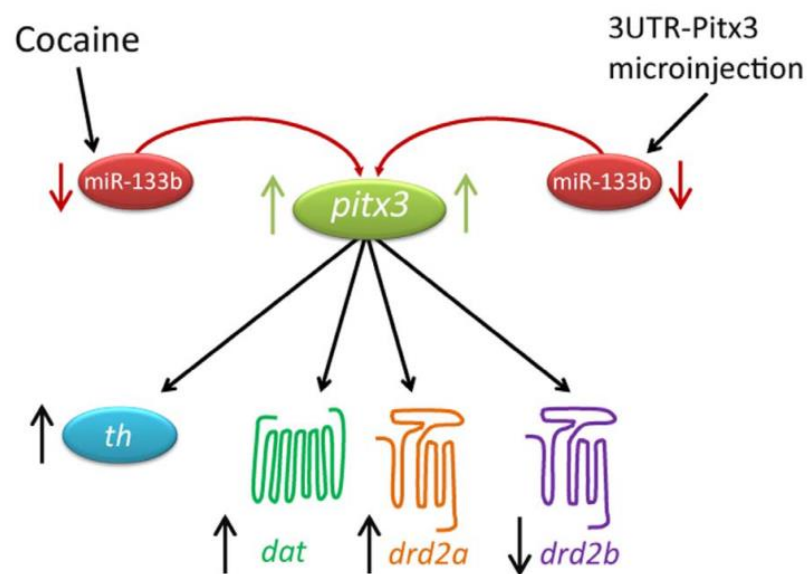


Figure 21. Possible mechanism of action of cocaine through miR-133b in zebrafish embryos. This figure summarises the findings of Barreto-Valer et al. They showed that exposure of zebrafish embryos to cocaine or microinjection of the 3'UTR of *pitx3* resulted in a decrease in miR-133b levels and an increase in *pitx3* and a number of its downstream targets: *th*, *dat*, *drd2a* and *drd2b*. This figure is reproduced from Barreto-Valer et al. (2012).

In this chapter the role of miR-133b in dopaminergic neuron development in zebrafish will be investigated. I hypothesise that, through an interaction with *pitx3*, knockdown miR-133b will result in increased development of dopaminergic neurons which may be protective in zebrafish models of PD.

3.2 Characterisation of zebrafish miR-133b and *pitx3*

In this section the homology of zebrafish miR-133b is explored and the expression patterns of miR-133b and *pitx3* are determined. For an interaction between miR-133b and *pitx3* to be possible they must share spatial and temporal expression.

3.2.1 Optimisation

3.2.1.1 WISH probe for *pitx3*

The design principles of WISH probes are described in detail in section 2.10. As *pitx3* is a relatively small gene consisting of only 4 exons a WISH probe for *pitx3* was designed to target the whole protein coding region of the gene. Forward and reverse primers designed to amplify the whole coding region of gene tagged with the T7 or SP6 promoter respectively (Figure 22). From this PCR product an antisense and sense control probe can be transcribed. Staining developed within 3 hours using the antisense WISH probe transcribed from the PCR product described. Within the same time scale, WISH performed with the sense control probe did not produce any staining, therefore indicating that staining produced with the antisense probe is specific for *pitx3*.

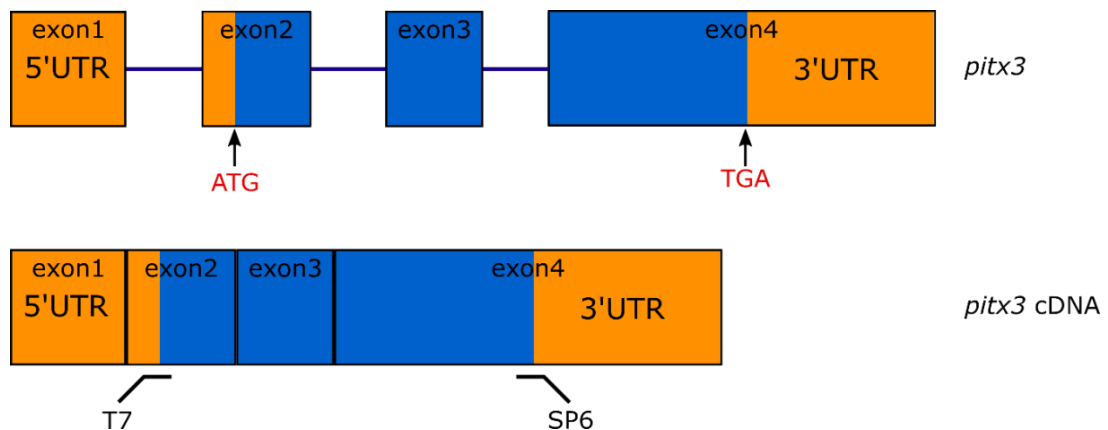


Figure 22. Design of a WISH probe for *pitx3*. The gene and cDNA sequence of *pitx3* are shown in this schematic. The location of the primers which amplify a region of the cDNA are shown. The resulting PCR product is used as a template from which the WISH probe is transcribed. The location of the start and stop codons are noted. Orange represents UTR and blue represents the protein coding region.

3.2.2 Results

3.2.2.1 miR-133b sequence is conserved in zebrafish

miR-133b is highly conserved across a wide range of species (miR-Base and Ensembl). There is good homology between the human and zebrafish miR-133b sequences, over the whole coding region there is an 80% similarity over 100% of the zebrafish sequence (the human sequence is 35bp longer). The mature miRNA sequence of zebrafish miR-133b is 100% homologous to human miR-133b (Figure 23A and B).



Figure 23. Conservation of miR-133b across species. **A** shows the sequence alignment of the whole miR-133b exon from human and zebrafish and **B** shows the mature miRNA sequences of human and zebrafish miR-133b.

Another indicator of conserved function between orthologues is gene synteny in the genomic loci of the gene of interest. The genomic loci of human and zebrafish miR-133b was compared. Human miR-133b is present of chromosome 6 and zebrafish miR-133b is present on chromosome 20. The immediate region, within 10kb of miR-133b, in both humans and zebrafish is remarkably similar (Figure 24). Although the gene order is reversed, miR-133b is close to miR-206 in both species. In humans miR-206 is present approximately 4.5kb upstream of miR-133b and in zebrafish it is approximately 1.2kb downstream of miR-133b. In both humans and zebrafish miR-133b is present within the coding region of another gene, in humans this is annotated as LINCMD1, however in zebrafish this has not yet been annotated. In zebrafish, unlike in humans, miR-206 is also present within this gene.

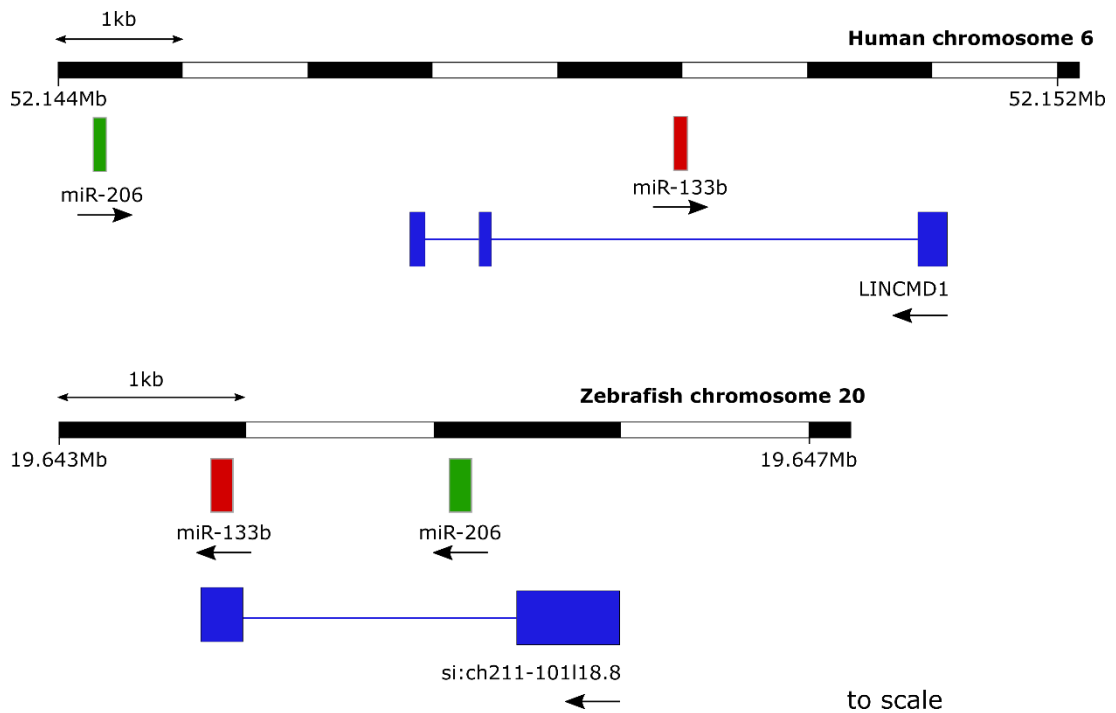


Figure 24. Gene synteny in the region surrounding human and zebrafish miR-133b. This figure shows the genes present in the immediate region around miR-133b in humans and zebrafish.

3.2.2.2 Expression and localisation of miR-133b

In humans, miR-133b was determined to have specific expression in the midbrain (Kim et al. 2007). To determine the miR-133b expression pattern in zebrafish WISH was performed. A LNA probe specific for miR-133b was used. As shown in Figure 25, miR-133b has strong expression in the somites and is also expressed in the developing lens and pharyngeal arches. Although the expression does not appear to be restricted to any specific region, miR-133b is expressed in the brain in zebrafish.

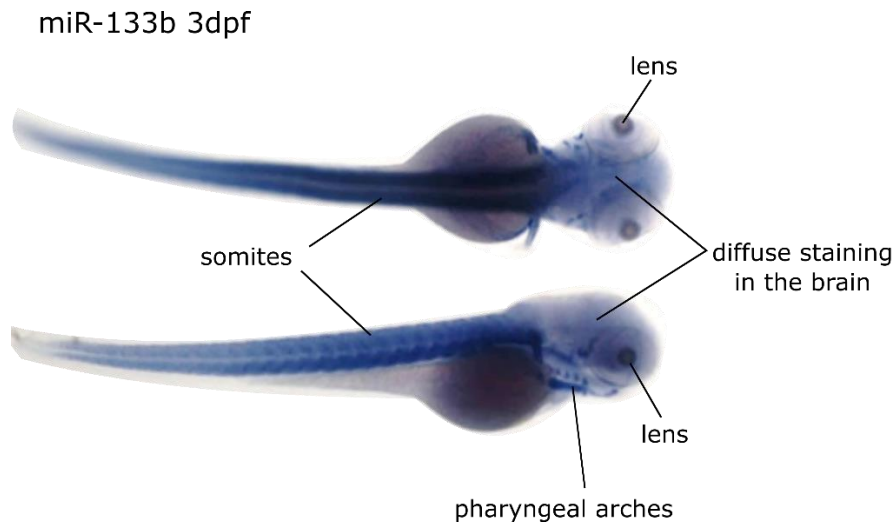


Figure 25. Spatial expression of miR-133b at 3dpf. This figure shows the spatial expression pattern of miR-133b at 3dpf, as determined by WISH. Staining is observed in the somites, pharyngeal arches, lens and the brain.

3.2.2.3 Expression and localisation of *pitx3*

For an interaction between miR-133b and *pitx3* to be possible these genes must be co-expressed. To determine whether miR-133b and *pitx3* share spatial and temporal expression patterns, the expression of *pitx3* was investigated by WISH at 3dpf and qPCR from 1-5dpf. As shown in Figure 26A, *pitx3* has a very distinctive expression pattern. It is expressed in specific areas of the developing diencephalon and in the pharyngeal arches and lens. The qPCR data, shown in Figure 26B, show that the expression of *pitx3* is relatively stable throughout embryonic and larval development.

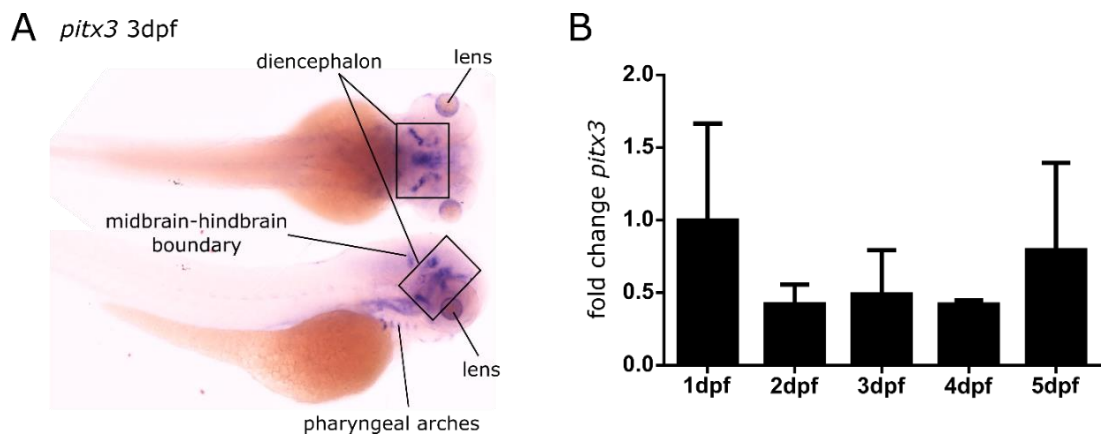


Figure 26. Expression and localisation of *pitx3*. **A** shows the spatial expression pattern of *pitx3*, as determined by WISH. Specific staining is observed in the diencephalon and lens. No staining was observed using a sense control probe. **B** shows the relative temporal expression pattern of *pitx3* from 1-5 days post fertilisation, as determined by qPCR. Error bars represent standard deviation.

The data shown in Figure 25 and Figure 26A indicate that both *pitx3* and miR-133b are expressed in the developing brain, lens and pharyngeal arches at 3dpf. Therefore, a direct physical interaction between these two genes is possible in these regions.

3.3 Knockdown of miR-133b and effect on dopaminergic neurons

In order to study the role of miR-133b in dopaminergic neuron development a MO was utilised to generate a transient knockdown of this miRNA. Once a knockdown had been validated the number of dopaminergic neurons present and miR-133b morphants was determined and compared to that of WT of control MO injected larvae.

3.3.1 Optimisation

3.3.1.1 Dosage optimisation of MO and validation of knockdown

There are a range of binding sites within the pri-miRNA transcript to which MOs can be designed (see Materials and Methods Figure 12). For miR-133b the MO used targets the mature miR-133b sequence. This MO was previously used by Mishima and colleagues; as described in the supplementary material of their paper (2009).

In order to assess the toxicity and optimise the dose of the miR-133b MO, it was injected at three different doses into one-cell stage embryos. These were: 0.9ng, 1.8ng and 3.6ng. Toxicity tests were performed by visual inspection of the embryos after injection; death rates were counted any deformities were noted. At the highest dose, 3.6ng of MO was not well tolerated. Embryos injected with this dose had a high death rate, approximately 50% of injected embryos 24 hours after injection. At 24hpf the surviving embryos displayed a severe developmental delay and gross deformities, including heart oedema, short curled tails and very small heads. At the two lower doses (0.9 and 1.8ng MO), the death rate was similar to control MO injected embryos; approximately 5-10%. Embryos injected with these doses display a mild developmental delay and have slightly smaller heads. However, these defects are very minimal and deemed acceptable. The highest tolerated dose, injection of 1.8ng of MO, was chosen; this was also the dose used by Mishima and colleagues. As the effects of MOs generally begin to wear off after 3dpf, the knockdown of miR-133b was assessed by qPCR at 3dpf. As shown in Figure 27, a knockdown of approximately 60% is achieved with this MO.

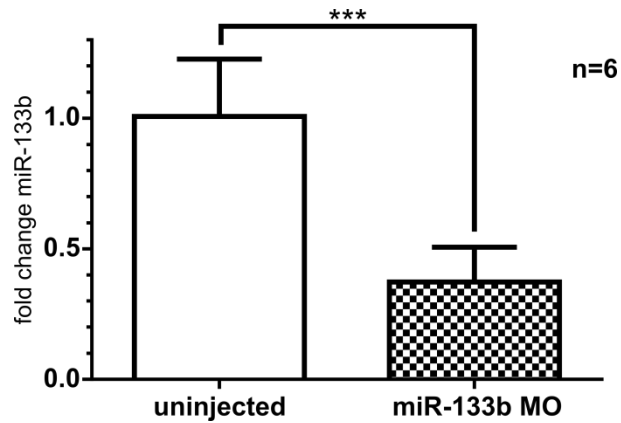


Figure 27. Knockdown of miR-133b using MO at 3dpf. A 60% knockdown of miR-133b after injection of MO is observed by qPCR. The data shown are from experiments using the chosen dose of MO, that is, 1.8ng miR-133b MO. miR-205 is used as reference gene. Error bars represent standard deviation. Data are analysed by an unpaired *t*-test with Welch's correction, *** = $p < 0.001$.

3.3.2 Results

3.3.2.1 Effect of miR-133b knockdown on dopaminergic neurons in WTs

PITX3 has been shown to be a direct target of miR-133b in both mice and humans (Kim et al. 2007), and therefore it was hypothesised that miR-133b knockdown will increase the level of Pitx3 protein in zebrafish embryos. As Pitx3 is thought to play a role in development of the dopaminergic system the effect of miR-133b knockdown on the zebrafish dopaminergic neuron population was investigated. Firstly, mRNA levels of *th* were assessed by qPCR in both WTs and miR-133b morphants. qPCR analysis demonstrated approximately a 40% increase in *th* mRNA level. These data, displayed in Figure 28 show that there was a trend towards an increase in *th* expression; however, this was not significant.

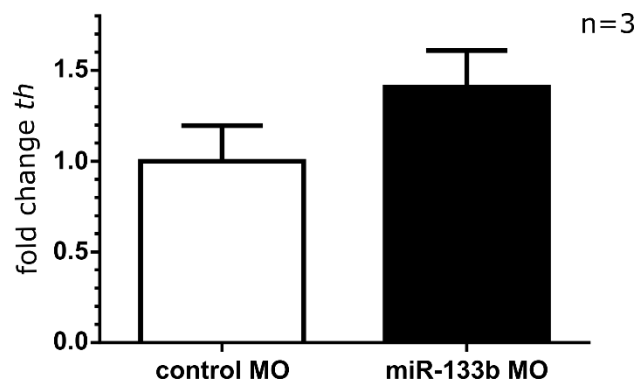


Figure 28. The effect of miR-133b knockdown on *th* mRNA levels. A 40% increase in *th* mRNA levels after knockdown of miR-133b is observed by qPCR. This is not statistically significant, $p > 0.05$. These data are from 3 biological replicates. Data is analysed by an unpaired *t*-test with Welch's correction.

In order to further investigate the effect of miR-133b knockdown on the *th+* dopaminergic neurons, WISH for *th* was performed and *th+* dopaminergic neurons were counted in WT zebrafish injected with either miR-133b MO or a control MO. This experiment revealed a significant increase in the number of *th+* dopaminergic neurons in the miR-133b knockdown embryos compared to the control MO injected embryos.

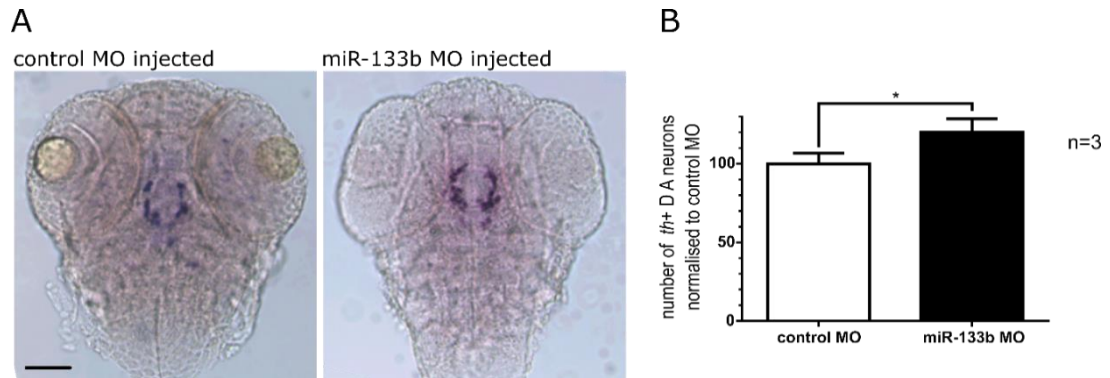


Figure 29. miR-133b knockdown results in an increase of *th+* dopaminergic neurons at 3dpf. **A** shows a representative image of the *th+* dopaminergic neurons in both control MO and miR-133b MO injected embryos. Scale bar = 100 μ m. **B** shows the quantified number of *th+* dopaminergic neurons normalised to control MO injected, an increase of 20% is observed in miR-133b MO injected embryos. Error bars represent standard deviation. These data are from three biological replicates. In each biological replicate the number of dopaminergic neurons is counted in 20 embryos and the average taken. Data are analysed with an unpaired t-test with Welch's correction. * = $p < 0.05$. On axis labels, DA = dopaminergic.

To confirm that the control MO does not cause a decrease in dopaminergic neurons itself, hence falsifying the increase in dopaminergic neurons seen with the miR-133b MO, *th+* neuron counts were compared between WTs and control MO injected embryos. The result of this analysis is shown in Figure 30. No change in neuron number is observed, therefore, for all future experiments miR-133b MO injected embryos are compared to WT uninjected embryos rather than a control MO.

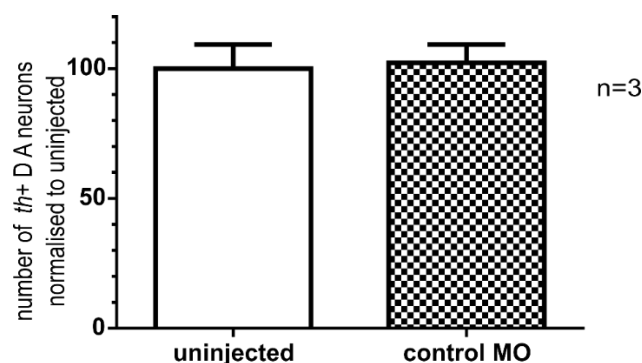


Figure 30. Dopaminergic neuron number in uninjected and control MO injected embryos. These data are from three biological replicates. In each biological replicate the number of dopaminergic neurons is counted in 20 embryos and the average taken. The data shown is normalised to uninjected. There is no significant difference in the neuron number between these two groups. Error bars represent standard deviation. On axis label DA = dopaminergic.

3.3.2.2 miR-133b knockdown is able to rescue dopaminergic neuron loss in *pink1*^{-/-} zebrafish

Knockdown of miR-133b significantly increases numbers of *th*⁺ dopaminergic neurons in WT zebrafish. It was hypothesised that this knockdown would be able to rescue the dopaminergic neuron loss observed in a previously established *pink1*^{-/-} zebrafish model of PD (Flinn et al. 2013).

Knockdown of miR-133b in *pink1*^{-/-} embryos was able to rescue the loss of dopaminergic neurons observed in uninjected *pink1*^{-/-} embryos. There is no significant difference in the number of dopaminergic neurons between the *pink1*^{-/-} with a miR-133b knockdown and WT uninjected embryos. This suggests that loss of miR-133b may have protective effect in a zebrafish model of PD.

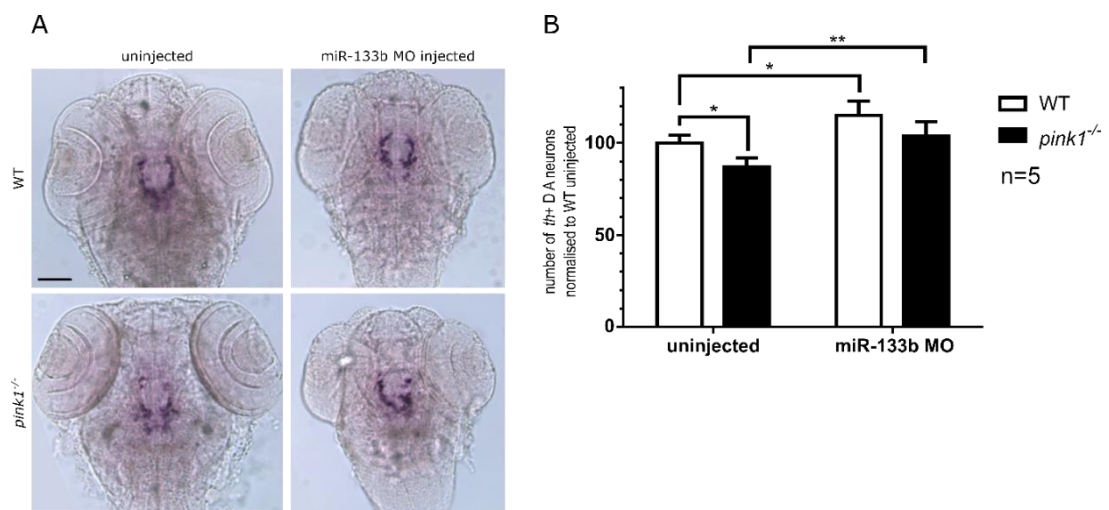


Figure 31. Knockdown of miR-133b in *pink1*^{-/-} embryos rescues *th*⁺ dopaminergic neuronal loss. **A** shows representative images of the *th*⁺ dopaminergic neurons in injected and uninjected WT and *pink1*^{-/-} embryos. Scale bar = 100 μ m. **B** shows the quantified number of *th*⁺ dopaminergic neurons normalised to WT uninjected. A decrease of 15% is observed in *pink1*^{-/-} embryos, this decrease is completely rescued by miR-133b MO injection into *pink1*^{-/-} embryos. Error bars represent standard deviation. These data are from five biological replicates. In each biological replicate the number of dopaminergic neurons is counted in 20 embryos and the average taken. Data are analysed with a 2-way ANOVA with Tukey post-tests. * = $p < 0.05$, ** = $p < 0.01$. On axis labels, DA = dopaminergic.

3.3.2.3 miR-133b knockdown is unable to rescue dopaminergic neuron loss caused by MPP+ exposure

As miR-133b knockdown is able to rescue the dopaminergic neuron loss seen in a genetic zebrafish model of PD, it was investigated whether this knockdown would be able to rescue the dopaminergic neuron loss caused by toxin exposure. For these experiments the toxic metabolite of MPTP, MPP+, is used as it has previously been shown to be a more potent toxin in zebrafish. This is thought to be due to the low levels of monoamine oxidase activity in the larval zebrafish brain which may limit conversion of MPTP to MPP+ (Sallinen et al. 2009). It has been previously demonstrated that treatment with 3mM MPP+ for 24hrs causes a loss of *th+* dopaminergic neurons (Bretaud et al. 2004). In this study, under the same condition, a similar decrease of *th+* dopaminergic neurons was observed after MPP+ treatment. In WT embryos, MPP+ treatment resulted in a 17% decrease in *th+* dopaminergic neuron number. Although miR-133b knockdown is able to rescue the decrease in dopaminergic neuron number caused by *pink1*-deficiency, it is unable to rescue neuronal loss caused by MPP+ exposure.

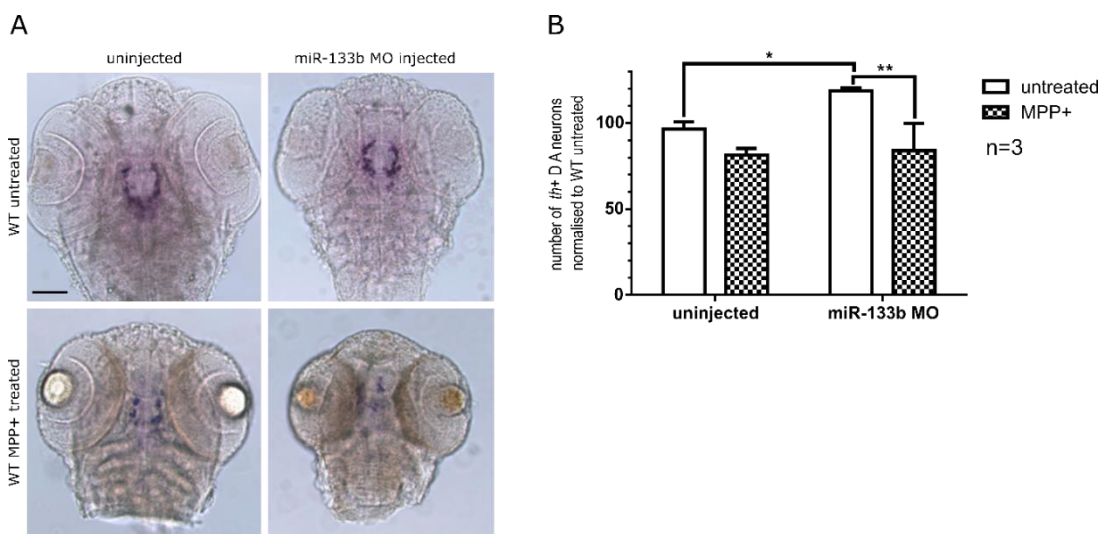


Figure 32. Knockdown of miR-133b in MPP+ treated zebrafish is unable to rescue *th+* dopaminergic neuronal loss. A shows representative images of the *th+* dopaminergic neurons in injected and uninjected, treated and untreated embryos. Scale bar = 100 μ m. B shows the quantified number of *th+* dopaminergic neurons normalised to WT uninjected. In uninjected embryos a decrease of 17% is observed in MPP+ treated embryos. In injected embryos there is nearly a 30% decrease in *th+* dopaminergic neuron number in the MPP+ treated group, this is due to the increase in neuron number in the injected untreated group. Error bars represent standard deviation. These data are from three biological replicates. In each biological replicate the number of dopaminergic neurons is counted in 20 embryos and the average taken. Data are analysed with a 2-way ANOVA with Tukey post-tests, * = $p < 0.05$ ** = $p < 0.01$. On axis labels, DA = dopaminergic.

3.3.2.4 miR-133b knockdown results in an increase in *th+* neurons at 48hpf but not 36hpf

All previous experiments examining the effect of miR-133b knockdown on *th+* dopaminergic neuron number have been performed at 3dpf. In order to determine at what age an increase in dopaminergic neuron number is detectable, embryos were injected with miR-133b MO and subsequently fixed at 24hpf, 36hpf and 48hpf. WISH for *th* was performed on these embryos and the neurons were counted. The 24hpf time point was excluded for technical reasons. At this age, the head is small and difficult mount without also including some yolk cells, these yolk cells obscure the view of the stained neurons. Also, there is a large variation in head size in the miR-133b morphants at this age. Neurons were counted in 36hpf and 48hpf embryos.

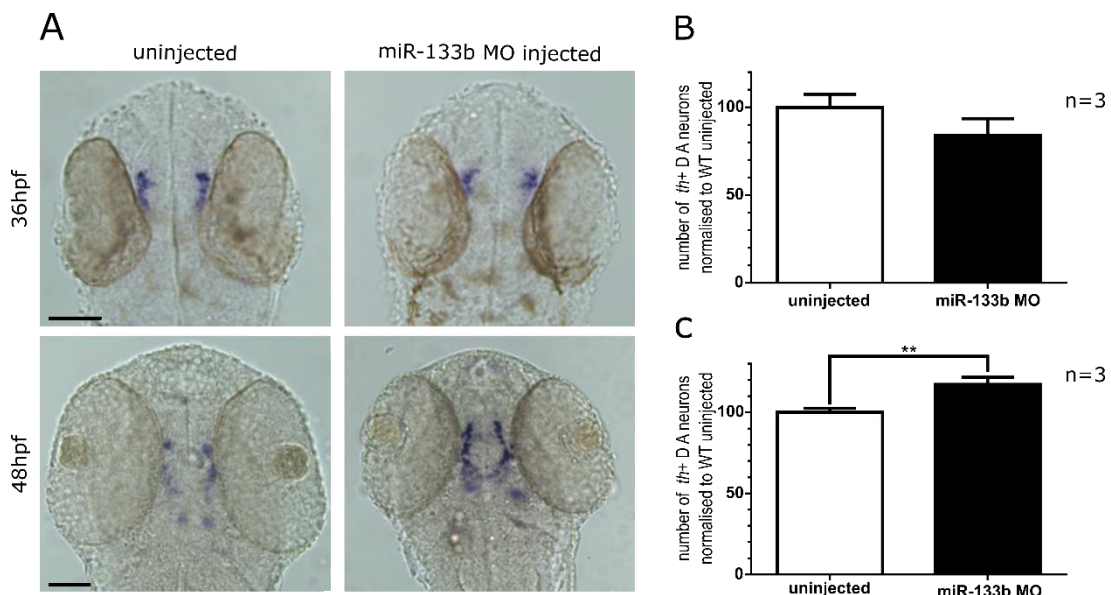


Figure 33. The effect of miR-133b knockdown on number of *th+* dopaminergic neurons at 36 and 48hpf. **A** shows representative images of the *th+* dopaminergic neurons in both uninjected and miR-133b MO injected embryos at 36 and 48hpf. Scale bar = 100 μ m. **B** and **C** show the quantified number of *th+* dopaminergic neurons normalised to uninjected at 36hpf and 48hpf respectively. There is no change in neuron number between the two groups at 36hpf however at 48hpf a significant increase of 17% is observed in miR-133b MO injected embryos. Error bars represent standard deviation. These data are from three biological replicates. In each biological replicate the number of dopaminergic neurons is counted in 20 embryos and the average taken. Data are analysed with an unpaired t-test with Welch's correction. ** = $p < 0.01$. On axis labels, DA = dopaminergic.

At 36hpf there is a slight, but non-significant, decrease in dopaminergic *th+* dopaminergic neuron number in miR-133b morphants (Figure 33A, and B), this is likely to be due to the variability in head size and slight developmental delay that these morphants demonstrate. At 48hpf there is a significant increase in neuron number between the two groups (Figure

33A and C). This suggests that proliferation or maturation of these neurons occurs between 36 and 48hpf and that miR-133b knockdown has an effect on this process.

3.3.2.5 Validation of *th*+ dopaminergic count using a the *ETvmat2:GFP* reporter line

To validate the observed neuron increase in miR-133b morphants, as measured by neuron WISH for *th* a second marker of the dopaminergic neuron population was used. The *ETvmat2:GFP* fluorescent reporter line expresses GFP in all *vmat2* expressing cells. *Vmat2* transports monoaminergic neurotransmitters, including dopamine, from the cytoplasm to the synapses and is therefore expressed in monoaminergic neurons. In Chapter 6 the expression of GFP in *th*+ dopaminergic neurons in the *ETvmat2:GFP* reporter line was validated (Figure 83). To determine whether the observed neuron increase can also be detected using this reporter line, thus using a second marker to validate this finding, miR-133b MO was injected into *ETvmat2:GFP* embryos. The method for measuring dopaminergic neuron number using this line is discussed in detail in Chapter 6 section 6.2.1.2. Briefly, in this reporter line all monoaminergic neurons, including the *th*+ dopaminergic neurons are labelled by GFP therefore is possible to approximate neuron number by analysing the fluorescence intensity of the GFP in the diencephalic catecholaminergic cluster. A significant increase in fluorescence intensity (40%, $p < 0.01$) was detected in miR-133b morphants compared to WT embryos (see Chapter 6, section 6.2.2.1 and Figure 85).

3.4 Overexpressing miR-133b

In order to assess whether overexpressing miR-133b has any effects on dopaminergic neurons through further repression of its target genes, a synthetic mimic of miR-133b was injected into the embryos. To validate the upregulation of miR-133b using this synthetic mimic, miRNA levels were assessed both spatially and temporally. Subsequently, to determine whether the upregulation of miR-133b has any negative effects on dopaminergic neurons, these neurons were counted after WISH for *th*.

3.4.1 Optimisation

3.4.1.1 Initial dosage optimisation

A synthetic mimic of miR-133b was injected into one-cell stage zebrafish embryos. The dosage was optimised by first injecting different concentrations of the mimic at the one cell stage and assessing toxicity. Overexpression of the mimic was assessed by qPCR. 1nl of each 10, 20, 40 and 60 μ M mimic was injected into one cell stage embryos. Both 10 and 20 μ M

doses were well tolerated by the embryos. Significantly increased death rates were observed in embryos injected with 40 or 60 μ M, therefore the highest tolerated dose, 20 μ M, was chosen for further experiments. The expression levels of miR-133b were assessed by qPCR from at 1, 2 and 3 days post fertilisation (Figure 34)

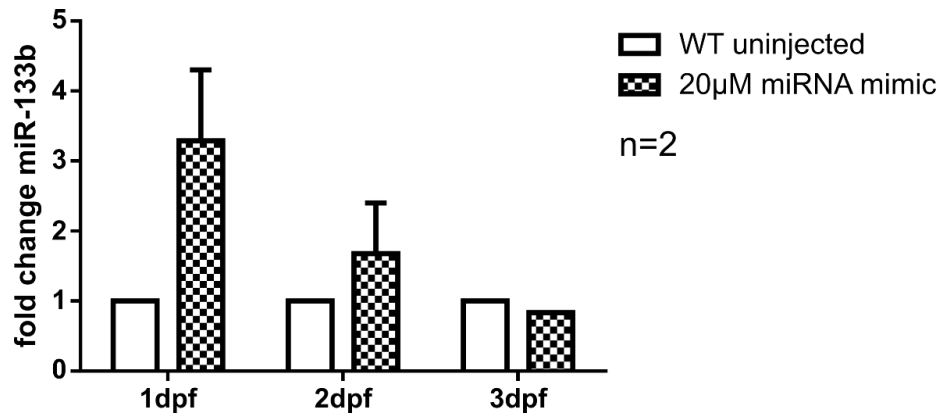


Figure 34. miR-133b levels after miRNA mimic injection. miR-133b mimic was injected into the yolk of one-cell stage embryos and the expression of miR-133b was assessed by qPCR at 1, 2 and 3dpf. Data are from two biological replicates. Error bars represent standard deviation.

Despite the large initial upregulation of miR-133b, just over 4 times the endogenous levels of miR-133b, the upregulation is reduced at 2dpf and no upregulation is observed at 3dpf. In order to combat this problem and to ensure increased levels of miR-133b in the brain, another dose of miR-133b mimic was injected into the ventricles at 1dpf.

3.4.1.2 Optimisation of ventricle-injection technique and dosage of mimic

To ensure that ventricle injections were successful and do not damage the embryo, a fluorescent construct which has been shown not to leak out of the ventricles was injected (Gutzman & Sive 2009); the embryos were imaged three hours later to check the injection had been successful. Figure 35 shows a 1dpf embryo with 70,000KDa FITC dextran injected into the ventricles, imaged 3 hours after injection. The ventricles are clearly defined from both the dorsal and lateral view. The survival rate of injected embryos up to 3dpf was close to 100%. These data show that ventricle injections were successful and did not cause damage to the embryo. In order to prevent leakage of the injected solution the embryos that were to be injected were mounted in 0.8% LMP agarose before injecting. The lack of movement of fluid around the injection site prevented leakage of the solution giving better overexpression of the miRNA.

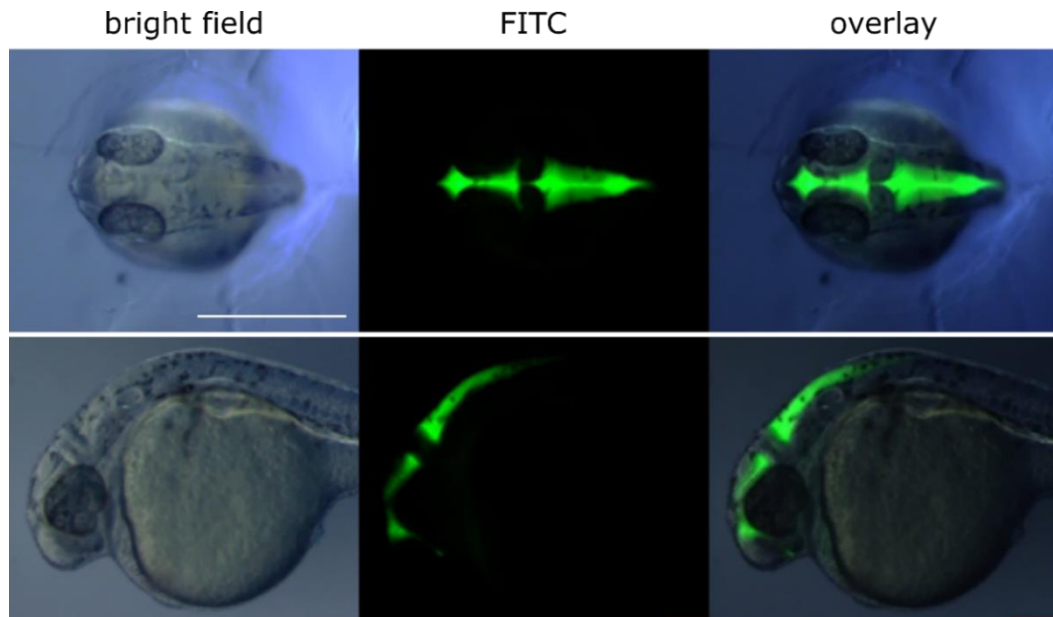


Figure 35. FITC dextran injections into zebrafish ventricles. 70000kDa FITC dextran was injected into the ventricles of a 1dpf zebrafish embryo. The injected embryos were imaged 3 hours post injection. The FITC-dextran clearly labels the ventricles in both the dorsal (top) and lateral (bottom) views. Scale bar = 500 μ m.

Next, dosage of the mimic to be injected into the ventricles at 1dpf was optimised. Doses of 1nl of 5, 10 and 20 μ M were tested. The lower two doses, 5 μ M and 10 μ M, were well tolerated, whereas death was increased in embryos injected with 20 μ M mimic. The higher tolerated dose of 10 μ M was used for ongoing experiments. The level of miR-133b was assessed at 1dpf, 1dpf + 3 hours after ventricle injection, 2dpf and 3dpf to quantify the increase in miR-133b levels. As shown in Figure 36, injection of the mimic into the ventricles on top of the initial injection allows the overexpression of miR-133b to persist at a high level until 2dpf. A 2fold increase of miR-133b is still present at 3dpf.

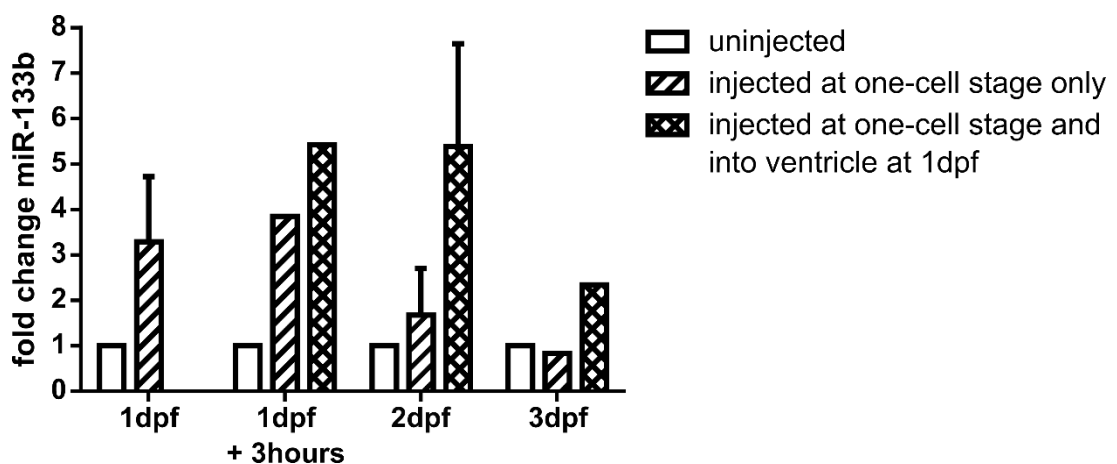


Figure 36. miR-133b levels after injection of miRNA mimic into ventricles. The levels of miR-133b after injection with miR-133b mimic was assessed by qPCR. Injection of miR-133b mimic into zebrafish embryos at both the one-cell stage and subsequently into the ventricles at 1dpf results in increased levels of miR-133b at 2dpf and 3dpf. 1dpf and 2dpf data are from two biological replicates and 1dpf + 3 hours and 3dpf data are from one biological replicate. Error bars represent standard deviation.

3.4.2 Results

3.4.2.1 Effect of miR-133b overexpression on dopaminergic neuron number

After optimisation of the injection technique and qPCR confirmation that the levels of miR-133b are increased after injection of the miR-133b mimic, the number of *th+* dopaminergic neurons at 2 and 3dpf was investigated. It was hypothesised that overexpression of miR-133b would cause further repression of target genes and result in a decrease in numbers of *th+* dopaminergic neurons; however no change in neuron number was observed (Figure 37).

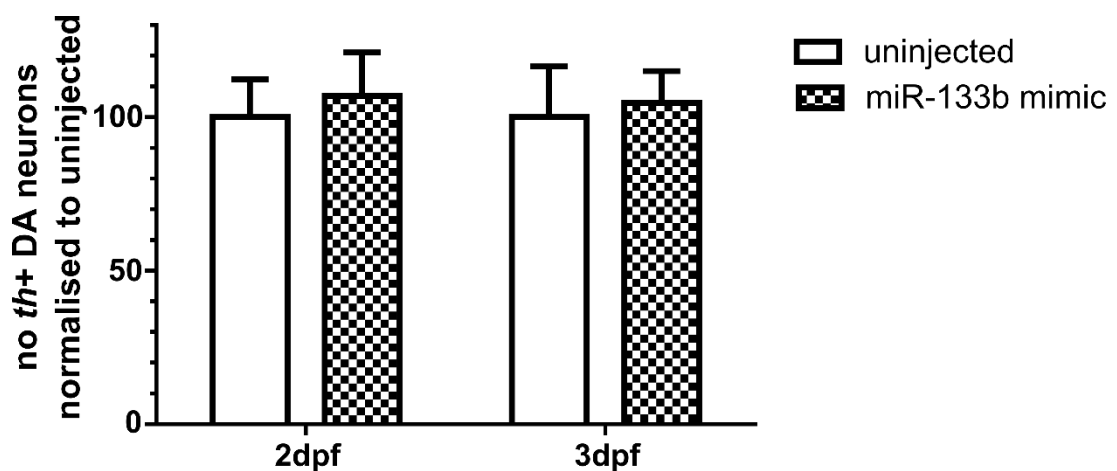


Figure 37. Number of *th+* dopaminergic neurons after miR-133b mimic injection. No change in *th+* dopaminergic neuron number is observed at 2 or 3dpf in embryos injected with miR-133b mimic. Data is from 1 biological replicate with neuron counts performed on 10 embryos per group. Error bars represent standard deviation. On axis labels DA = dopaminergic.

3.4.2.2 Localisation of miR-133b after injection of mimic

Although the total levels of miR-133b are increased at 1-3dpf, as detected by qPCR, this does not confirm spatial location of the miRNA. In order to visualise the location of miR-133b after mimic injection, WISH was performed for miR-133b at 1, 2 and 3dpf (Figure 38). From observing the spatial location of miR-133b after mimic injection, there is no obvious increase in miR-133b in the brain at any age. At 1dpf and 2dpf, slightly darker staining can be seen in the tail region. At 2dpf slightly darker staining can be seen in the head of injected embryos. At 3dpf no difference in staining levels is obvious. Although by qPCR an increase in miR-133b levels was observed, the localisation of the miRNA doesn't seem to be in the appropriate regions at an early enough age to cause further repression of the target genes.

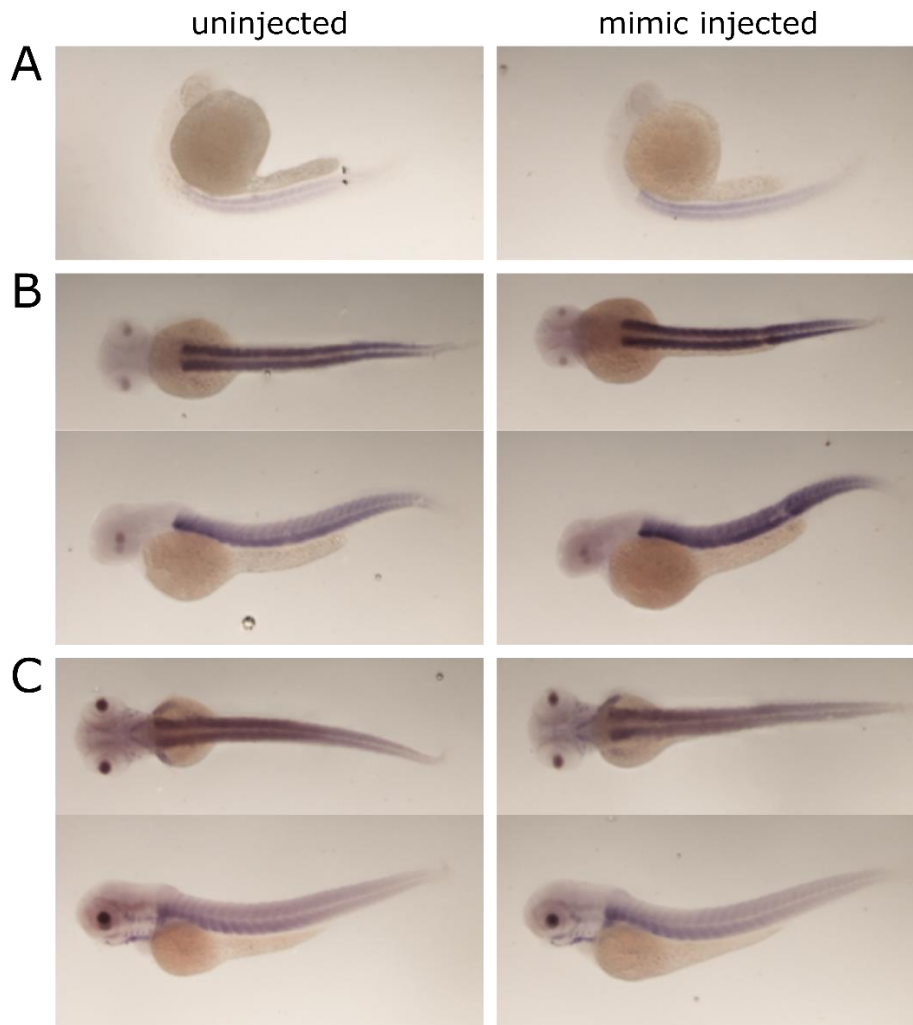


Figure 38. Localisation of miR-133b after miR-133b mimic injection. Localisation of miR-133b was assessed by WISH. The right panel shows embryos which are injected with 20 μ M mimic at the one-cell stage and 10 μ M mimic into the ventricles at 1dpf. The left panel shows uninjected embryos. **A** shows miR-133b staining at 1dpf. The staining intensity in the tail is slightly increased however only a very slight change in intensity can be seen in the head. **B** shows 2dpf embryos. In these embryos slightly darker staining can be seen in the head and tail regions. **C** shows a dorsal and lateral view of 3dpf embryo. No change in staining can be seen in these embryos.

3.5 Effect of miR-133b knockdown on *pitx3*/Pitx3

PITX3 has been identified as a target of miR-133b in humans and mice (Kim et al. 2007). Although the site is not predicted by the miRNA target prediction database TargetScanFish (Release 6.2, June 2012), the miRanda algorithm suggests that miR-133b does have binding site in the 3'UTR of zebrafish *pitx3* (as made available in the miR_Targets database at: http://mamsap.it.deakin.edu.au/~amitkuma/mirna_targetsnew/find_mirna.html (Kumar et al. 2012)). Moreover, research performed Rodriguez group strongly suggests that this interaction is conserved in zebrafish (Sanchez-Simon et al. 2010). To confirm their result and to assess the interaction in miR-133b morphant zebrafish, three methods were used to

determine whether miR-133b is able to regulate *pitx3*. These were: qPCR to assess *pitx3* mRNA levels, a reporter plasmid to elucidate whether the interaction is direct and to determine the binding site of miR-133b in the 3'UTR of *pitx3*, and western blotting to assess Pitx3 protein levels.

If the validation of an interaction using the reporter plasmid is successful it is possible to validate the binding site by directed mutation of the predicted binding site. To determine which region of the *pitx3* 3'UTR may be a potential binding site of miR-133b, alignment of the miR-133b binding site in human *PITX3* with the zebrafish *pitx3* 3'UTR was performed using Clustal Omega to identify a region similar to the validated binding sites in the 3'UTR of human in the zebrafish *pitx3* 3'UTR.

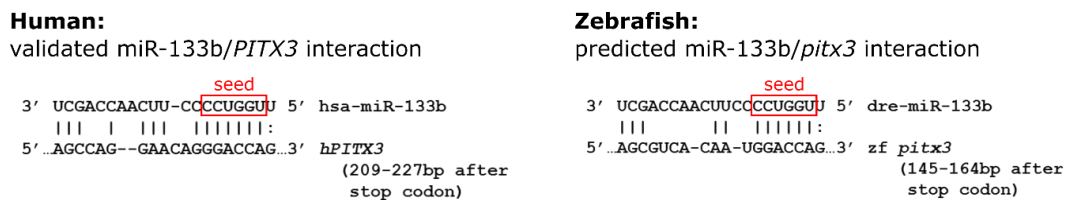


Figure 39. A potential miR-133b binding site in zebrafish *pitx3* 3'UTR. The left panel shows the validated interaction between human miR-133b and the 3'UTR of *PITX3* (Kim et al. 2007). The right panel shows a potential binding site for miR-133b in the 3'UTR of *pitx3* in zebrafish. The seed region of miR-133b is highlighted in both cases.

3.5.1 Optimisation

3.5.1.1 Validation of reporter plasmid method using control plasmid

Another method of determining direct targets of miRNA is to place a fluorescent reporter under the control of the 3'UTR of the gene of interest. This technique is described in detail by Mishima and colleagues who identified a number targets of miR-133 and miR-1 important for the regulation of sarcomeric actin organisation (Mishima et al. 2009).

To validate the reporter plasmid method, a control construct was tested. This dual reporter plasmid containing RFP under the control of a mock 3'UTR containing two perfect miR-133b binding sites and GFP with no 3'UTR as a control was kindly provided by Professor Giraldez. A plasmid map of this construct is shown in Figure 40A.

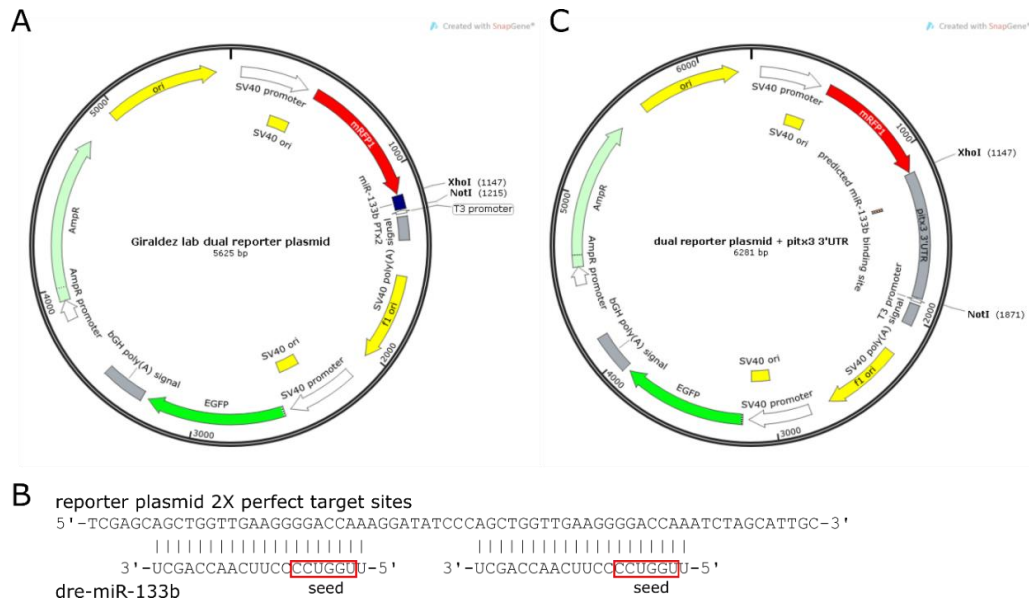


Figure 40. Dual reporter plasmid maps. **A** shows a map of the control plasmid containing 2 perfect target sites for miR-133b (miR-133b PTx2) downstream of RFP. **B** shows the sequence of this region and the target sites. **C** shows a map of the dual reporter plasmid with the pitx3 3'UTR downstream of RFP. GFP is not under the control of any 3'UTR and is included as a control.

The control plasmid was injected into one-cell stage zebrafish embryos. In some cells the plasmid will be incorporated into the genome. In these cells and descendants of these cells, GFP will be expressed freely as there are no regulatory sequences downstream of it. In miR-133b containing cells RFP will be repressed as miR-133b will bind to the binding sites present in the 3'UTR downstream of RFP. As these binding sites have perfect complementarity this repression is likely to be via mRNA cleavage. When miR-133b is knocked down by co-injection of the miR-133b MO, RFP will be freed from repression and therefore plasmid-containing cells will display both green and red fluorescence (as shown in Figure 41). To quantify the effect of repression of RFP by miR-133b, GFP and RFP fluorescence was measured in muscle fibres. As miR-133b is strongly expressed in muscle the repressive effect of miR-133b is evident in this tissue (Figure 41A). To quantify this data the ratio between GFP and RFP fluorescence intensity can be measured. GFP acts as a loading control and is expressed freely in all cells containing the plasmid. To do this GFP positive muscle fibres are identified, i.e. the muscle fibres which contain the reporter plasmid. In these cells the fluorescence intensity of both GFP and RFP is measured (Figure 41B).

As there is no difference between the no MO group and the control MO group for subsequent experiments using this technique, the control MO was not used. The increase in RFP/GFP fluorescence in the miR-133b MO injected group shows that this technique is working as expected.

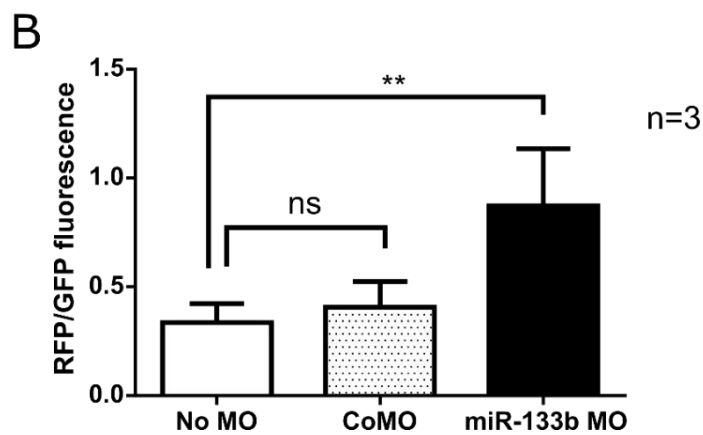
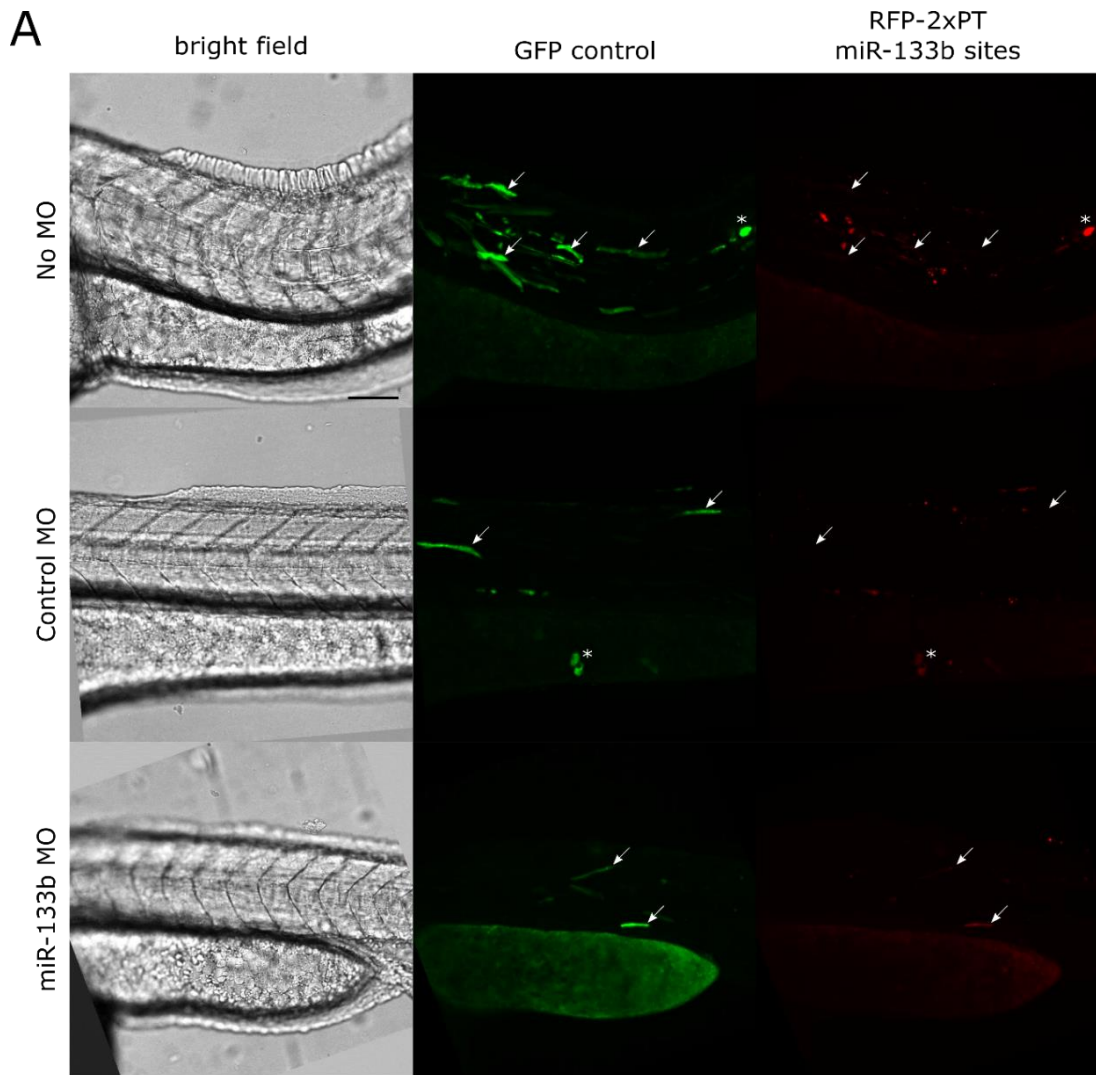


Figure 41. GFP and RFP fluorescence with control reporter plasmid. **A** White arrows indicate muscle fibres expressing the reporter plasmid. Asterisks indicate non-muscle cells. In the top two panels the muscle fibres which express GFP do not express any RFP. In the bottom panel where miR-133b is knocked down RFP repression is released and RFP can be detected in the muscle fibres which express the reporter plasmid. Scale bar = 100 μ m. **B** shows quantification of RFP and GFP expression, expressed as RFP/GFP fluorescence intensity in the muscle fibres. Scale bars represent standard deviation. Data are from three biological replicates. For each biological repeat images from 10 injected embryos were analysed. Data were analysed by one way ANOVA with Bonferroni post-tests. ** = $p < 0.001$.

3.5.1.2 Western blotting

Currently there are no commercially available antibodies designed to detect zebrafish Pitx3. However, one commercially available antibody was identified which was raised against a portion of human PITX3 with high homology to zebrafish Pitx3. This antibody was tested.

Morpholinos for pitx3

In order to test the specificity of antibodies for Pitx3, *pitx3* knockdowns were generated using MOs. Two MOs were designed for *pitx3*. Before purchasing the MOs, the sequence of the target was confirmed using direct sequencing to confirm that no SNPs are present which may prevent MO binding. A BLAST search of the MO sequence against the zebrafish genome was also performed to ensure specificity for *pitx3*. The target sites of these MOs are marked in Figure 42A. The first MO is a start site MO (SS MO) which is expected to prevent translation of Pitx3 but will not cause any change to the mRNA. The second MO is a splice blocker targeting the exon2-intron2 boundary (e2i2 MO). This is predicted to cause an exon skip of exon2. As the start site of Pitx3 is present in exon2 this would cause a complete loss of protein if exon2 was deleted. The effect of this MO can be assayed by RT-PCR. The primers used to assay this potential deletion are shown in Figure 42B. Figure 42C shows a RT-PCR gel analysing the effect of the e2i2 MO. Although there is a band at a lower weight than the WT transcript, indicating an exon skip transcript, the e2i2 MO does not cause complete loss of the wild type transcript; therefore this MO is unlikely to cause a complete loss of Pitx3 protein.

Each MO was injected at a range of concentrations to determine the highest tolerated dose of the MO. Either 2ng of the SS MO or 4ng of the e2i2 MO was injected into the embryos that were subsequently used for western blotting. These concentrations were chosen as the highest tolerated dose out of a range of 3 doses previously tested.

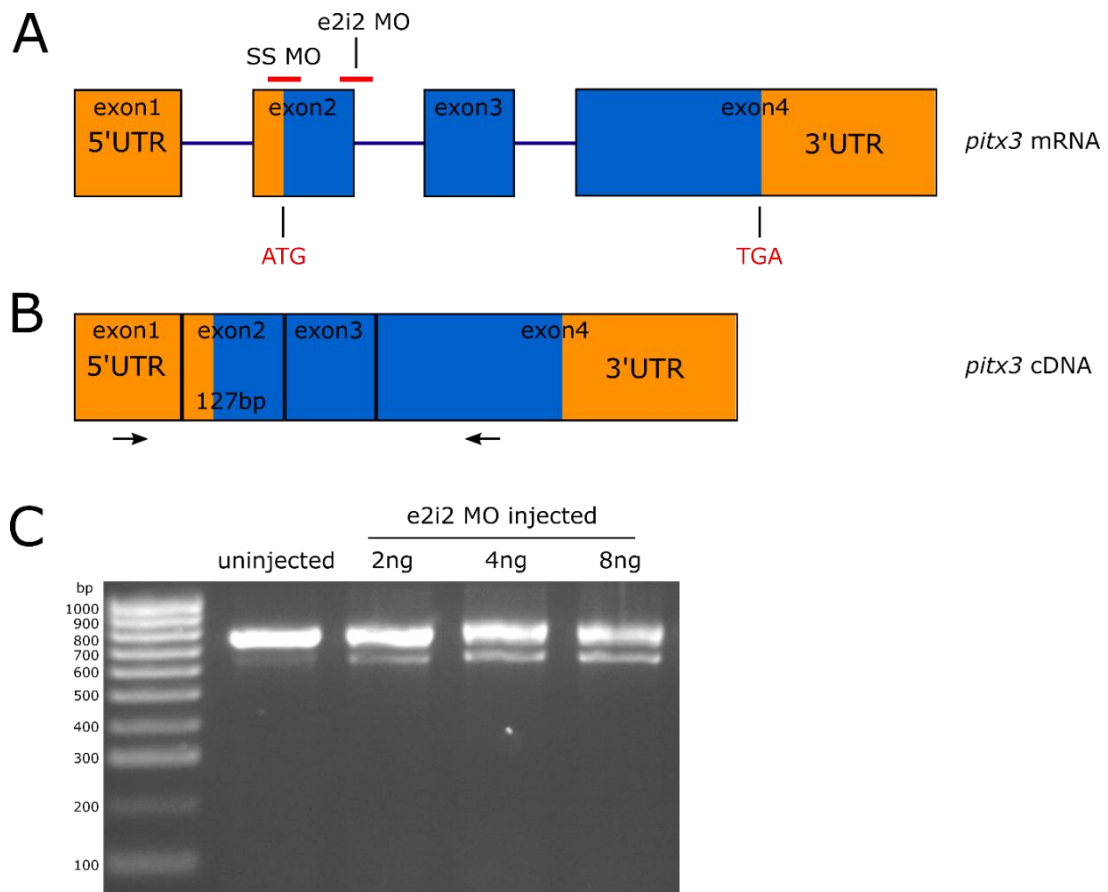


Figure 42. MOs targeting *pitx3*. **A** shows a schematic of un-spliced *pitx3* mRNA and the position of the start site MO (SS MO) and the exon1-intron2 splice blocking MO (e2i2 MO). The e2i2 MO is predicted to cause a deletion of exon2 (which contains the start site of *pitx3*). The SS MO should prevent translation of Pitx3 but does not alter the splicing of the mRNA. The location of the start and stop codons are noted. Orange represents UTR and blue represents the protein coding region. **B** shows the *pitx3* cDNA and the location of the primers used to assay the effect of e2i2 MO. **C** shows an RT-PCR gel analysing the effect of the e2i2 MO on the *pitx3* transcript.

Testing of a commercially available antibody for Pitx3

An antibody designed to human PITX3 with an epitope with 84% similarity to zebrafish, produced by Abcam, was identified. Although the exact epitope of this antibody is not known, it is within the N-terminal region of PITX3. This antibody was tested in zebrafish using the conditions recommended by the manufacturer. To determine whether this antibody can recognise zebrafish Pitx3 protein lysates from both WT embryos and embryos which had been injected with the SS MO, were used. If the antibody can recognise zebrafish Pitx3 a band at approximately 32kDa should be detectable in the WT samples but absent in the morphant samples.

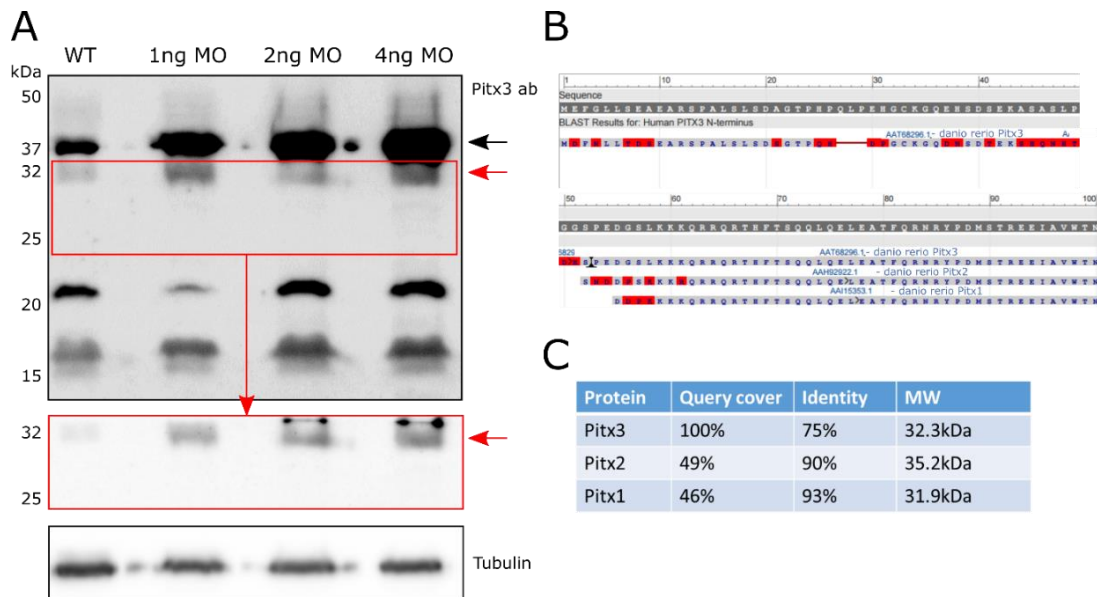


Figure 43. Testing of Abcam Pitx3 antibody. **A** shows the western blot using the Abcam antibody for Pitx3 on protein samples from WT and SS MO injected embryos. The region around 32kDa, the weight of zebrafish Pitx3, is highlighted in red and repeated below the main blot. Tubulin was used as a loading control. **B** shows a summary of the results of a BLAST search comparing the N-terminal region of human PITX3, where the epitope of this antibody is located, to the zebrafish proteome. The alignments of the top three results are shown. Grey amino acids are perfect matches and red amino acids are similar to corresponding amino acid in the human sequence. **C** shows a table summarising the top three results from this BLAST search. The molecular weights (MW) of these proteins are also shown.

As shown in Figure 43A although this antibody does detect a band at 32kDa (indicated by a red arrow) this is also present in samples from MO-injected embryos, thus this band is not Pitx3. Interestingly, there is a large band at 37kDa (indicated by a black arrow) which increases in intensity with MO injection. This suggests it is a protein which is upregulated when Pitx3 is knocked down. To investigate whether this antibody can recognise any other zebrafish proteins a BLAST (NCBI) search was performed comparing the N-terminal region of human PITX3 to the zebrafish proteome. The alignments of the top three results, Pitx3, Pitx2 and Pitx1, are shown in Figure 43B. These alignment results, and the molecular weights of these proteins are shown in Figure 43C. These results show that it is possible that the large band at 37kDa corresponds to Pitx2, which may be being upregulated to compensate for Pitx3 knockdown, and the band at 32kDa corresponds to Pitx1.

As this antibody does not appear to be specific to zebrafish Pitx3, a custom antibody for zebrafish Pitx3 was commissioned from Eurogentec (Seraing, Belgium).

Design and production of a custom Pitx3 antibody

Two 15-amino acid epitopes, unique to zebrafish Pitx3, assessed by local alignment against the zebrafish proteome, using BLAST (NCBI) were chosen. Pitx3 is a small protein with a large

homeodomain which is present in many other zebrafish proteins of similar sizes. The most unique region of zebrafish Pitx3 is at the N-terminal end. Peptides corresponding to aa15-30 and aa30-45 of Pitx3 were chosen as the epitopes to raise the antibodies against. The antibodies provided were rabbit polyclonal antibodies which had been affinity purified using the original epitope. In order to successfully use the custom antibody to quantify levels of zebrafish Pitx3, these antibodies first had to be carefully tested to validate their specificity for Pitx3. The two antibodies will be referred to as ab164, raised against a peptide corresponding to aa15-30 of zebrafish Pitx3 and ab165, raised against a peptide corresponding to aa30-45.

Characterisation of custom Pitx3 antibodies - determining optimal working conditions

To determine the optimal working conditions of these antibodies they were first tested at a range of antibody concentrations and subsequently different incubation times. From the initial optimisation experiment the more promising of the two antibodies was chosen to develop further.

Figure 44 shows the first optimisation experiment testing a range of antibody concentrations of both ab164 and ab165. From this initial experiment, antibody ab164 seemed the more promising candidate as a band could be identified at around 32kDa (indicated by an arrow in Figure 44A). All subsequent experiments were carried out with this antibody only. The chosen working concentration of the antibody for subsequent experiments was 1:100.

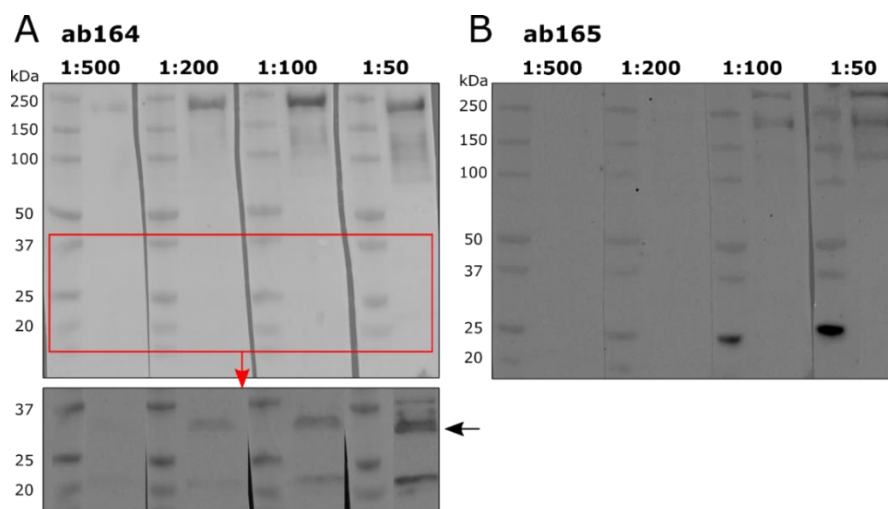


Figure 44. Initial testing of custom antibodies for Pitx3. A western blot was performed using a range of dilutions of the custom antibodies for Pitx3 to determine whether they are able to recognise this protein. Protein lysates were from de-yolked 3dpf zebrafish. **A** shows blots testing ab164 at a range of antibody concentrations. The bottom panel shows the lower portion of the membrane developed for longer to reveal weaker bands. The arrow indicates a band at the expected MW of Pitx3 (32kDa). **B** shows blots testing ab165 at a range of antibody concentrations. No further bands could be detected by developing the membrane for longer and no bands were detected at around 32kDa.

Next, the optimal incubation time of this antibody was tested. Incubating the antibody with the membrane overnight at 4°C produced a stronger and cleaner signal (Figure 45). A range of bands can be seen on this membrane close to 37kDa. To identify which of these bands is Pitx3 further testing of the antibody specificity was performed.

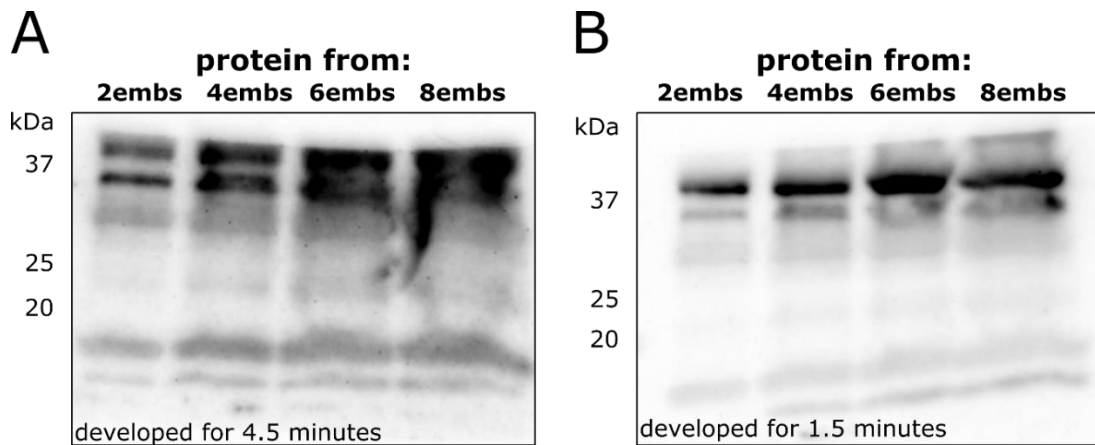


Figure 45. Optimisation of antibody incubation time. Membranes were incubated with ab164 for either 2 hours at room temperature or overnight at 4°C to determine optimum incubation conditions. A range of concentrations of protein were loaded on the gel. **A** shows a blot where ab164 is incubated with the membrane for 2 hours at room temperature. **B** shows a blot where ab164 is incubated with the membrane overnight at 4°C.

Characterisation of custom Pitx3 antibody ab164 – validating specificity for Pitx3

Once the optimal concentration and incubation time with this antibody had been established, the specificity of the signal was then tested. To do this, a range of control blots were performed and compared against the use of the Pitx3 antibody (ab164). These controls are, incubation of the membrane with: primary antibody only; blocked antibody (and subsequently secondary antibody), this control involved pre-incubation of the Pitx3 antibody with the peptide it was raised to; and, pre-immune serum. Pre-immune serum is serum taken from the rabbit before it was immunised with the Pitx3 peptide, therefore it will not contain any antibodies specific for zebrafish Pitx3. An appropriate concentration of the pre-immune serum was chosen by first performing a dot blot using a range of concentrations of the serum to determine which gave a similar level of signal to the primary antibody. Any bands present on these control blots are not specific to zebrafish Pitx3. These control blots are shown in (Figure 46A).

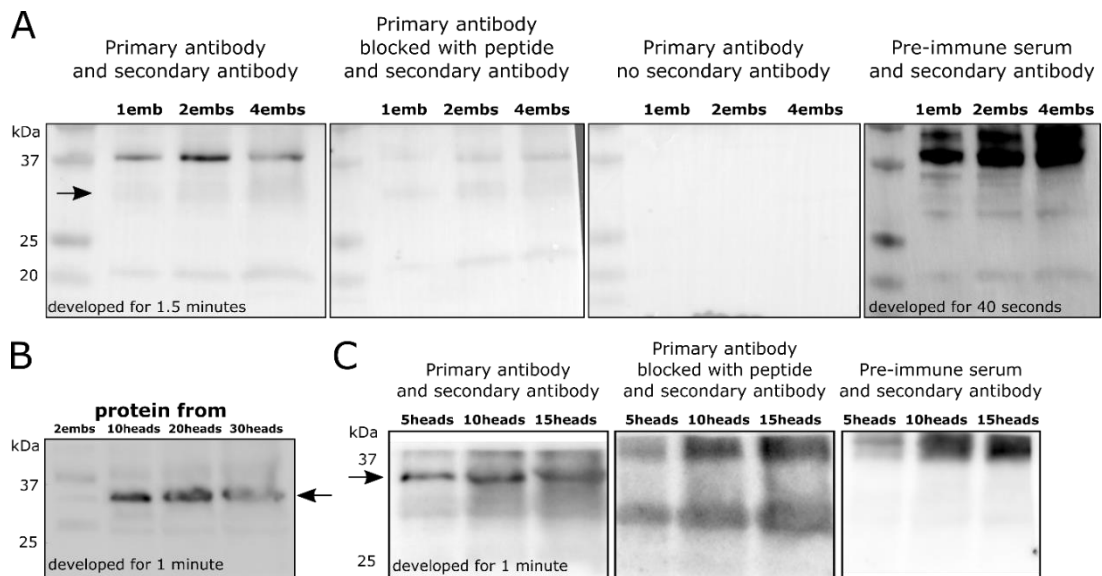


Figure 46. Antibody ab164 specifically detects a band at 32kDa. A range of controls were performed to determine the specificity of ab164 for zebrafish Pitx3. As Pitx3 is expressed in the brain of zebrafish embryos to enrich Pitx3 within the protein sample, protein lysates were collected from heads only (B and C). In all blots the arrow indicates a band at 32kDa which is thought to be Pitx3. This band can only be observed in blots which are probed with both primary and secondary antibody and not in the control blots indicating that ab164 specifically detects this band. A and C show images of a collection of membranes which have been probed with primary antibody and secondary antibody, blocked primary antibody and secondary, primary antibody only (A only) and pre-immune serum and secondary antibody. These optimisation experiments are designed to examine the specificity of the bands observed. B shows a blot where protein samples from whole embryos and heads only are compared. For the blots in A protein samples from whole embryos are used; in C protein samples from heads only are used.

The “no secondary” control and blocked antibody controls produced the expected results; no visible bands at all and vastly reduced intensity bands, respectively. However, in the pre-immune serum control it is still possible to see the band around 37kDa which was previously thought to be Pitx3. Under closer inspection of the staining it is possible to see that there is a faint band below the 37kDa marker, marked with an arrow (Figure 46A). As Pitx3 is a 32kDa protein it is likely that this band is Pitx3.

As Pitx3 is only expressed in the zebrafish brain, in order to enrich Pitx3 in the sample the western blot was performed with protein lysates from zebrafish heads only (Figure 46B). As expected, performing the western blot with protein from zebrafish heads only enriches the band at around 32kDa, indicated with an arrow, and reduces the intensity of the ‘non-specific’ band at around 37kDa seen in the whole embryo lysates. As the sample was changed the previous experiment using blocked antibody and pre-immune serum was repeated (Figure 46C). The concentration of the peptide used to block the primary antibody was also increased to ensure complete blocking of the antibody. As shown in Figure 46C the strong band, indicated by an arrow, in the first panel is not present in the blocked antibody panel.

However, the other non-specific bands are present. When the membrane is incubated with pre-immune serum rather than primary antibody, a large non-specific band is present above 37kDa; no other bands are clearly visible. These results are encouraging in that the indicated band at 32kDa is specific to the antibody and is likely to be Pitx3.

To further validate that the observed band is Pitx3, two MOs targeting Pitx3 were injected into one-cell stage embryos, and the embryos were collected at 3dpf. Protein was extracted from the heads of these embryos only. As both of these MOs cause the embryos to have slightly smaller heads, protein from a larger number of heads of injected embryos were loaded compared to wild type.

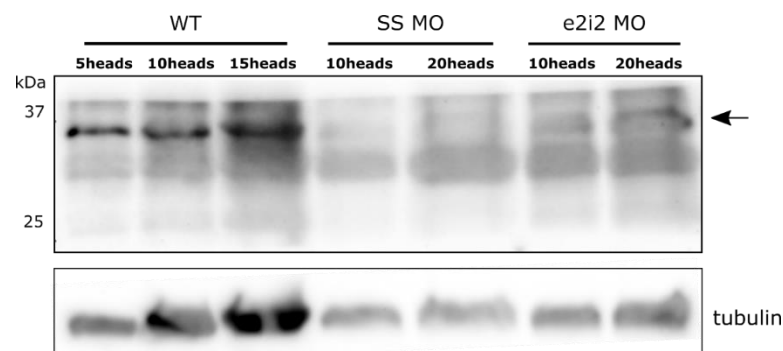


Figure 47. Antibody ab164 specifically detects zebrafish Pitx3. A western blot was performed using samples from WT embryos and *pitx3* MO injected (both the start site (SS) and exon2-intron2 (e2i2) MOs were used) embryos which are expected to have reduced levels of Pitx3 protein. This blot show that the band of interest (indicated by an arrow) is present in the WT samples but is not present in samples from SS MO injected embryos and is reduced in e2i2 MO injected embryos. This indicates that the band of interest at 32kDa is Pitx3. Tubulin was used a loading control.

The band of interest, indicated by an arrow, is not present in the SS MO samples and is reduced in the e2i2 MO samples (Figure 47B). These data show that this band is indeed Pitx3 validating that this antibody is suitable for measuring Pitx3 protein levels in protein lysates from zebrafish embryos. In this section the method for performing western blots using this antibody has been optimised, this method will be continued for all experiments using this antibody.

3.5.2 Results

3.5.2.1 Assessment of *pitx3* mRNA levels

Firstly, the effect of miR-133b knockdown on *pitx3* mRNA levels at 3dpf was assessed by qPCR (Figure 48). If miR-133b is able to downregulate *pitx3* through mRNA cleavage or degradation, an increase in *pitx3* mRNA level would be expected after knockdown of

miR-133b. These data show that there is no significant increase in the mRNA level, therefore if miR-133b is able to regulate *pitx3* in zebrafish this is by translational repression.

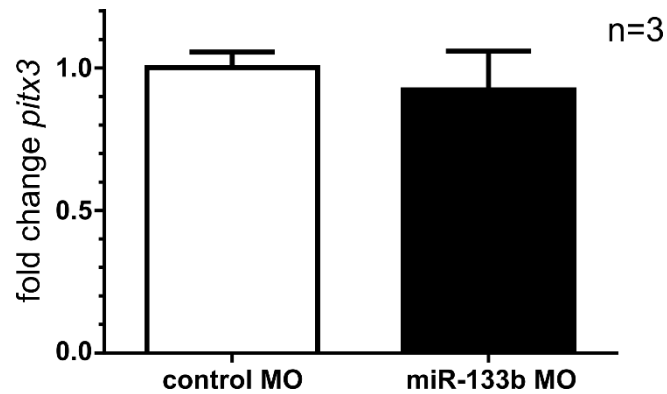


Figure 48. miR-133b knockdown does not increase *pitx3* mRNA levels at 3dpf. *pitx3* mRNA levels were assessed at 3dpf by qPCR. Knockdown of miR-133b has no effect of *pitx3* mRNA levels at 3dpf. Error bars represent standard deviation. Data are from three biological replicates.

3.5.2.2 Using a reporter plasmid to investigate the miR-133b-*pitx3* 3'UTR interaction

As expected, the RFP/GFP ratio with the *pitx3* reporter plasmid was similar to the control reporter plasmid when miR-133b is expressed at normal levels. This suggests that *pitx3* is under repression by its 3'UTR. However, in the miR-133b knockdown group there was no change between the RFP/GFP fluorescence intensity (Figure 12). This suggests that either miR-133b is not able to bind to the 3'UTR of *pitx3*, or that in these cells other miRNAs are also repressing *pitx3* and removal miR-133b is not enough to release *pitx3* from repression.

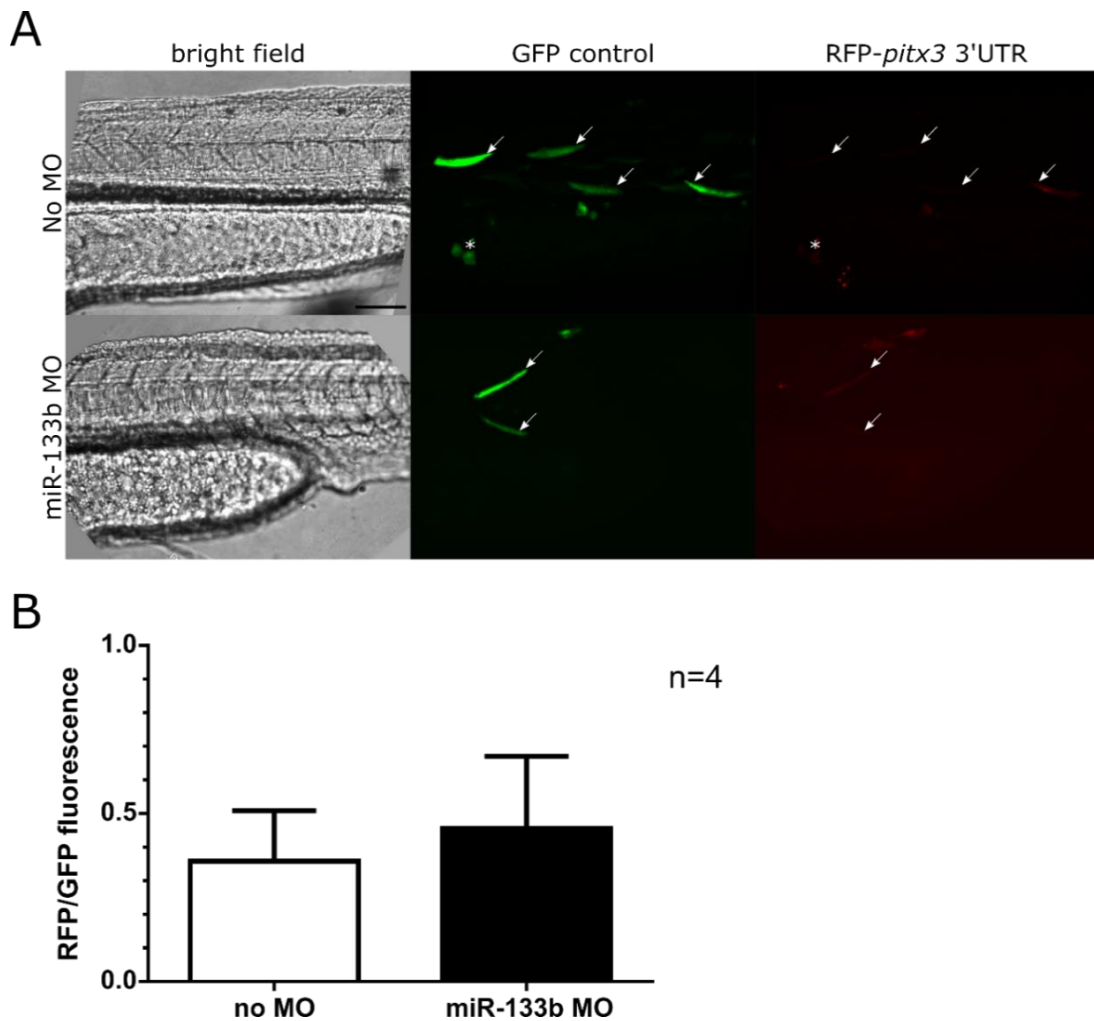


Figure 49. Assessment of miR-133b-pitx3 interaction using reporter plasmid. A reporter plasmid containing RFP under the control of the 3'UTR of *pitx3* was used to investigate the interaction of miR-133b and *pitx3*. RFP fluorescence did not increase in reporter plasmid containing cells after miR-133b knockdown. **A** White arrows indicate muscle fibres expressing the reporter plasmid. Asterisks indicate non-muscle cells. RFP is not expressed in muscle fibres containing the reporter plasmid in either group. Scale bar = 100µm. **B** shows quantification of RFP and GFP expression, expressed as RFP/GFP fluorescence intensity in the muscle fibres. Scale bars represent standard deviation. Data are from three biological replicates and analysed by an unpaired t-test with Welch's correction, $p > 0.05$.

3.5.2.3 Assessment of Pitx3 protein levels

As *pitx3* mRNA levels are not increased in miR-133b morphants and the reporter plasmid data were inconclusive, the protein levels of Pitx3 were measured to determine whether miR-133b is able to regulate *pitx3* at the translational level, the protein levels of Pitx3 were measured. Protein lysates were collected from the heads of wild type and miR-133b morphant embryos at 3dpf.

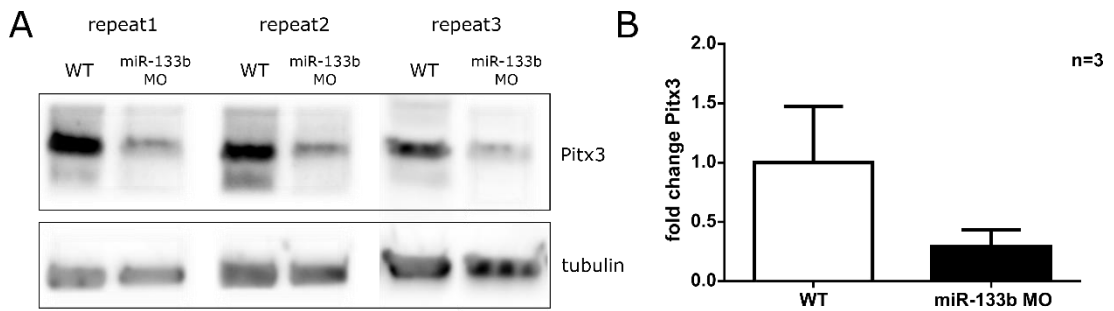


Figure 50. miR-133b knockdown does not increase Pitx3 protein levels at 3dpf. Western blotting was performed to investigate the protein levels of Pitx3 in miR-133b morphants and WT at 3dpf. A decrease in protein levels was observed however this was not significant. **A** shows the western blot where Pitx3 protein levels are compared between lysates from WT and miR-133b MO injected embryos. Tubulin was used as a loading control. **B** shows a quantification of this western blot. Pitx3 protein levels are normalised to tubulin levels. Data are from three biological replicates and analysed by an unpaired t-test with Welch's correction, $p > 0.05$.

Unexpectedly, this experiment shows that contrary to Pitx3 protein levels being increased in miR-133b morphant embryos they appear to be decreased. Although the decrease in Pitx3 protein levels is not significant there is clearly a trend in this direction. These data show that miR-133b knockdown does not result in an increase in Pitx3 protein levels at this age.

3.6 Effect of miR-133b knockdown on the proliferation of dopaminergic neurons

In order to assess whether the increase number of neurons in the diencephalic catecholaminergic cluster is due to increased proliferation, an EdU exposure and staining experiment was performed. EdU is a thymine analogue and, when available, proliferating cells will incorporate EdU into the DNA during S-phase. Any cell which proliferates after EdU exposure is performed will be labelled. At the desired time point, the embryos are fixed and EdU labelling can be visualised.

3.6.1 Optimisation

3.6.1.1 Determining time points to use for EdU analysis

To determine at which age the neurons in the diencephalic dopaminergic cluster are born, EdU was injected at a range of time points in the development of WT and miR-133b MO injected embryos. Embryos were fixed at 2dpf, as this is the earliest age where an increase in dopaminergic neurons has been detected. In this experiment the dopaminergic neurons were detected by IHC for TH or GFP (where the ETvmat2:GFP line was used).

As shown in Figure 51 In embryos injected with EdU at 18, 24 and 30hpf, no or very little co-localisation was seen between EdU and GFP. In the embryos injected at 12hpf, the GFP+ neurons were very close to the EdU labelled cells, however, not all cells are labelled indicating that the dopaminergic neurons proliferate before and around 12hpf.

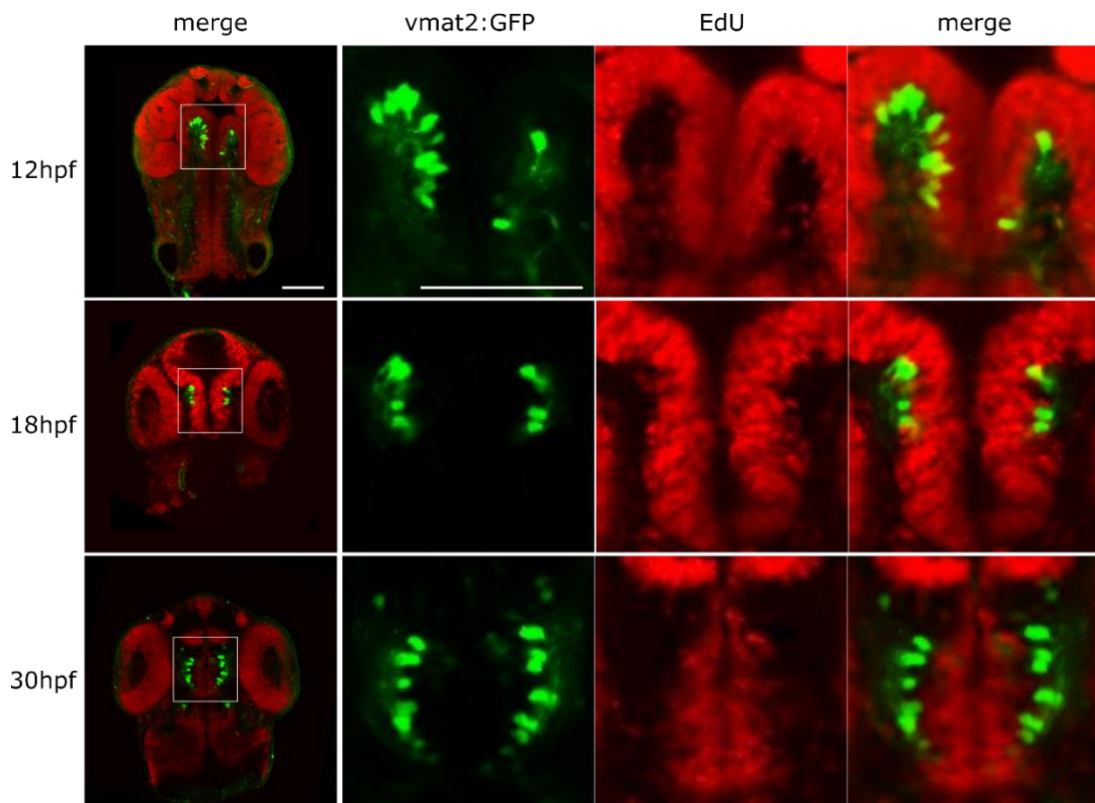


Figure 51. EdU incorporation into proliferating neurons. To determine at what age dopaminergic neurons proliferate EdU is injected into the yolk of zebrafish embryos at 12, 18 and 30hpf. Embryos are fixed at 48hpf. IHC to label GFP+ cells is performed alongside staining for EdU. Representative single slices of injected embryos are shown. Scale bar = 100 μ m.

In order to further investigate the time at which these neurons are born, embryos were injected with EdU at 6, 8, 10 and 12hpf. Figure 52 shows the localisation of TH+ dopaminergic neurons and EdU incorporation. As TH is only present in the cytoplasm and EdU labels the nucleus, no direct overlap in staining is seen. However it is easy to identify where the EdU labels the nucleus of a TH+ cell. In embryos injected at 6, 8 and 10hpf, all the TH+ neurons are labelled with EdU, showing that these neurons were born after the point when the EdU was injected. In the embryos which are injected at 12hpf, some TH+ neurons were labelled with EdU and others were not, suggesting that a number of neurons proliferate between 10 and 12 hours and some proliferate later.

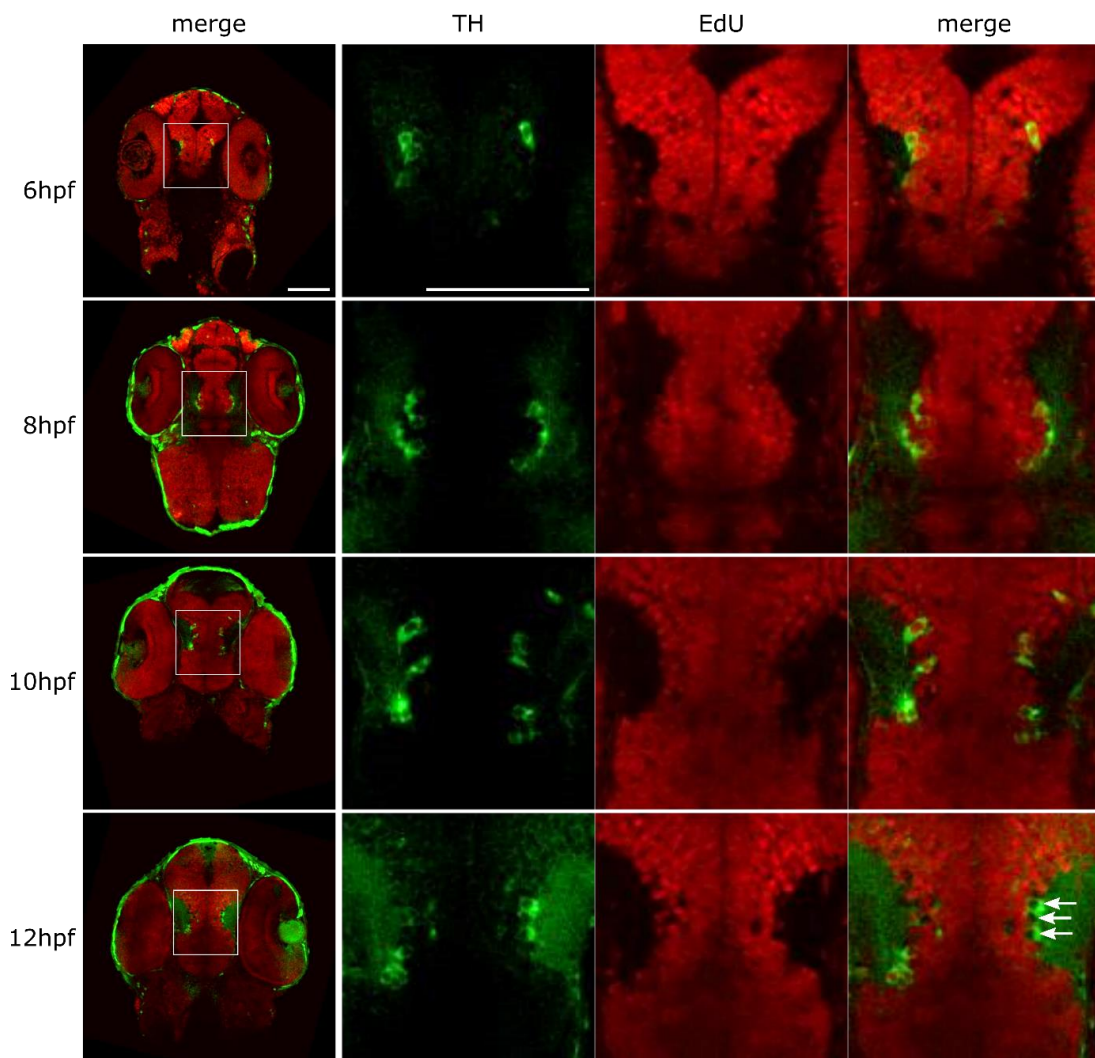


Figure 52. EdU incorporation into proliferating neurons in early development. To determine at what age dopaminergic neurons proliferate EdU is injected into the yolk of zebrafish embryos at 6, 8, 10 and 12hpf. Embryos are fixed at 48hpf. IHC to label TH+ cells is performed alongside staining for EdU. Representative single slices of injected embryos are shown. Arrows indicate TH+ cells which are not labelled by EdU, indicating these cells proliferated before EdU was injected. Scale bar = 100 μ m.

3.6.2 Results

3.6.2.1 Comparison of proliferation between 12-48hpf in WT and miR-133b morphants

EdU was injected into both WT and miR-133b MO injected embryos at the time points listed above. The staining in both groups was analysed in embryos injected at 12hpf to search for any differences in co-localisation of EdU and TH at these ages or if and drastic increase in proliferation is evident (Figure 53). In these images the increase in TH+ neurons in the miR-133b morphants is evident. In WT embryos it is possible to identify a small number of neurons that are TH+ but not stained by EdU. However, in the miR-133b morphants all TH+ are also labelled with EdU.

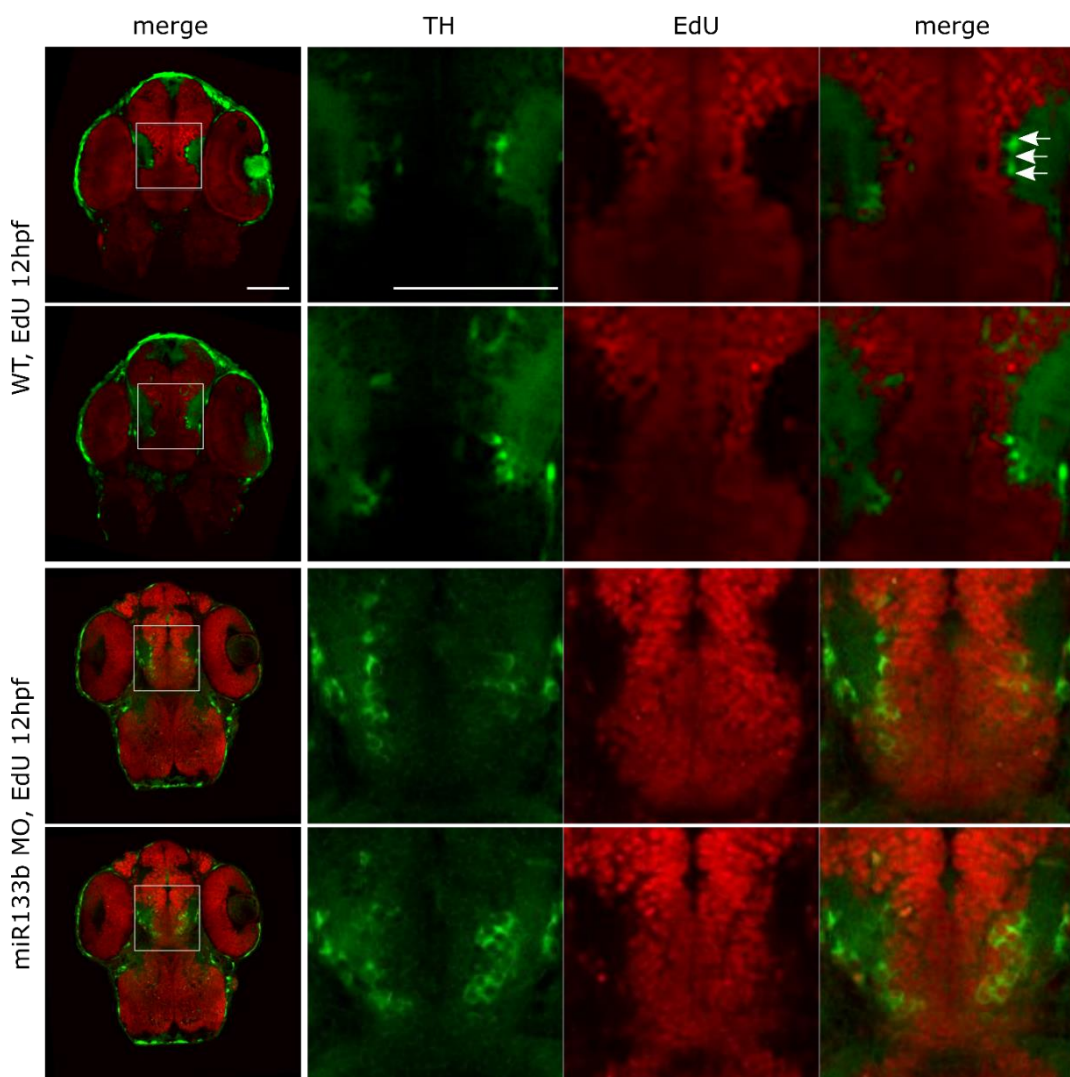


Figure 53. EdU and TH in WT and miR-133b morphants. To examine proliferation of dopaminergic neurons in miR-133b morphants and WTs EdU is injected at 12hpf. Injected embryos were fixed at 48hpf. IHC to label TH+ cells is performed alongside EdU staining. Arrows indicate TH+ cells which are not labelled by EdU, indicating these cells proliferated before 12hpf. Two slices from representative embryos are shown. Scale bar = 100 μ m.

3.6.2.2 Comparison of proliferation between 12-13hpf in WT and miR-133b morphants

To further investigate the proliferation at an age relevant to the proliferation of the TH+ neurons, EdU was injected at 12hpf then embryos were fixed 1 hour later. As TH is not detectable at this age, it was not possible to use this marker to identify which cells will become dopaminergic. A *wish* probe for *neurogenin1*, a marker of dopaminergic neural progenitors (Jeong et al. 2006) was tested. Although this probe worked well in older zebrafish embryos (Figure 54A), in the EdU injected embryos fixed at 13hpf, well defined fluorescence from this probe was not detectable and therefore it was not possible to identify neural progenitors. Also, as zebrafish embryos develop rapidly, even within the short EdU exposure time of 1 hour between 12 and 13hpf, a large number of cells were labelled (Figure 54B). Therefore, it was not possible to identify any increase in proliferation of an individual population of neurons.

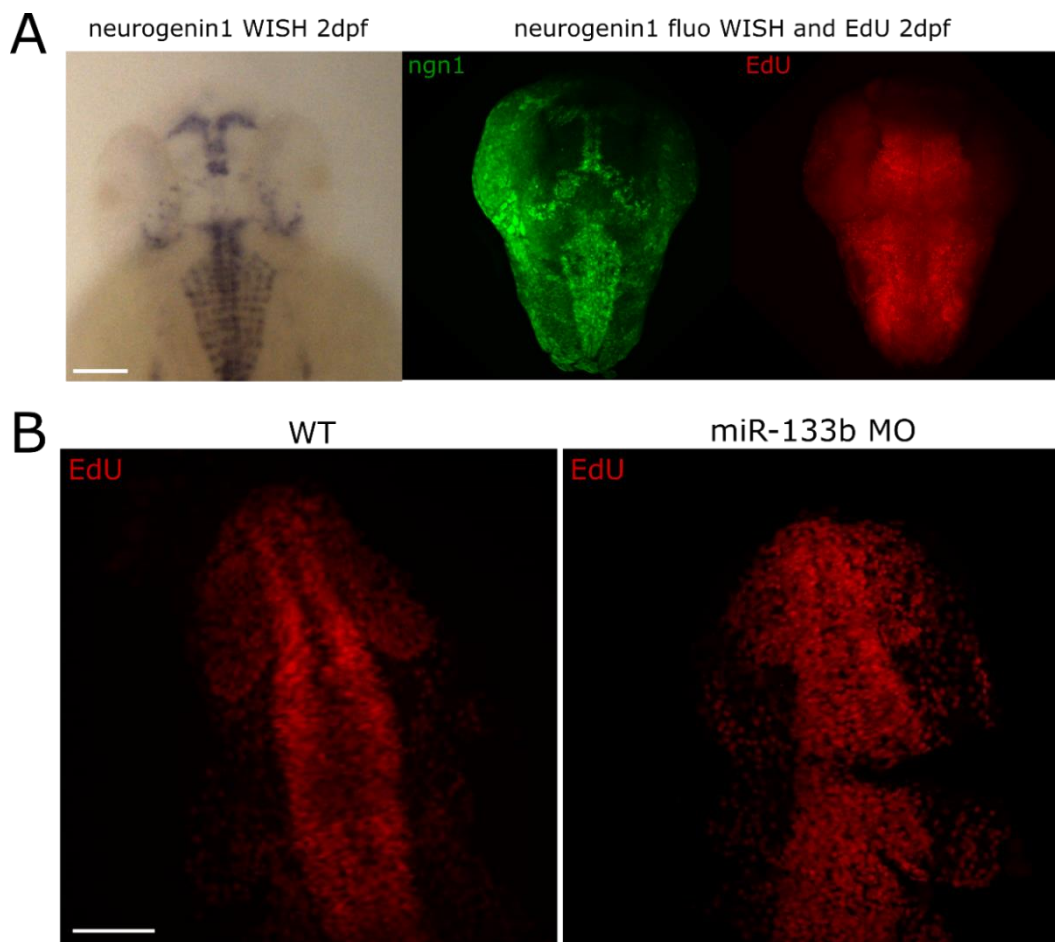


Figure 54. neurogenin1 WISH and EdU staining at 13hpf. A shows maximum projections image of a co-fluorescent WISH (for neurogenin1) and EdU staining experiment in 2dpf embryos. An image of a standard WISH experiment with the neurogenin1 probe is also shown for comparison. B shows maximum projections of EdU staining in 13hpf WT and miR-133b MO injected embryos. Scale bars = 100 μ m.

3.7 Discussion

This study aimed to investigate the effect of miR-133b on development and survival of dopaminergic neurons in zebrafish. It was hypothesised that through its proposed target *pitx3*, knockdown of miR-133b would increase the number of dopaminergic neurons and protect against both endogenous (i.e. genetic) and exogenous (i.e. toxic) deleterious effects on dopaminergic neuron survival.

Characterisation of miR-133b and pitx3 in zebrafish

In order for miR-133b to regulate *pitx3*, these genes must be co-expressed. miR-133b appears to have diffuse expression within the brain. This is in contrast to human and mice studies which found that miR-133b was specifically expressed in the midbrain (Kim et al. 2007). However, in this study expression was only analysed in adult samples, therefore it is possible that this spatial restriction only occurs later in life. Alternatively, this may reflect differences in neuron specification in zebrafish.

Although performing WISH for miR-133b and *pitx3* at 3dpf provides important information about the expression pattern of these genes and suggests that they are co-expressed in the zebrafish brain, it does not provide definitive proof that this is the case as the resolution of WISH images is not sufficient. Firstly, a control probe for miR-133b must be used to determine that the diffuse staining observed in the brain is specific for miR-133b rather than background staining. Secondly, in order to further investigate the co-expression of these genes a dual-fluorescence WISH could be performed. This experiment was attempted however was not successful. To increase the success of this experiment, sections of the zebrafish embryo brain could be made and WISH for miR-133b and *pitx3* performed on alternate sections. Alternatively, the custom antibody for Pitx3 developed in this study could be tested in IHC applications and subsequently combined with fluorescent WISH for miR-133b.

Finally, as EdU experiments suggest that the proliferation of dopaminergic neurons occurs very early in development, it would be interesting to investigate the expression of both miR-133b and *pitx3* at these early time points. The expression of *pitx3* was assessed by qPCR from 1-5dpf indicating it is detectable at 1dpf, however investigating the spatial expression pattern would be more informative.

Knockdown of miR-133b and effect of dopaminergic neurons in WTs

Prior to this study the effect of knockdown of miR-133b on the developing zebrafish embryo had not been investigated. Two previous publications have used MOs for miR-133b, however these were used to knockdown miR-133b in adult spinal cord injury only, or as a tool to investigate miR-133b targets in muscle. The chosen MO was able to produce a 60% knockdown of miR-133b at 3dpf and did not result in any obvious toxic off-target effects or significant deformity at the chosen dose.

Knockdown of miR-133b resulted in an increase of *th*+ dopaminergic neurons in WT embryos. This increase in dopaminergic neuron number is likely to be due to the increase in development of these neurons rather than an increase in their survival as one would not expect any death of these neurons to have occurred by 3dpf in WT embryos. Therefore it is likely that targets of miR-133b, which are increased upon knockdown of this miRNA, are involved in the development of dopaminergic neurons.

EdU exposures were performed to investigate whether the observed increase in the number dopaminergic neurons was through increased proliferation of neural progenitors. EdU was injected at a number of time points to identify a relevant age at which proliferation should be further studied. 12hpf was chosen as the most promising time point to study since some, but not all, TH+ dopaminergic neurons are labelled with EdU when EdU was injected in WTs at this age. This suggests that these neurons are beginning to proliferate during this stage of development.

Injection of EdU at 12hpf was also performed in miR-133b morphants. In the morphant embryos analysed, no EdU-negative TH+ cells could be identified. This suggests that TH+ neurons proliferate slightly later in the morphants, perhaps due to a mild developmental delay. Only a small number of embryos were examined in this experiment, therefore to confirm these findings a larger number of embryos would need to be imaged and analysed. As EdU is present in the embryos for 36 hours between 12hpf, when the EdU is injected, and 48hpf when the embryos are fixed, a large number of cells incorporate EdU. This means that it is very difficult to identify small increases in proliferation.

To further investigate the proliferation occurring at around 12hpf, EdU was injected at 12hpf then embryos were fixed 1 hour later. This experiment only labeled cells which are proliferating within this 1 hour time-frame. As TH is not detectable at this age it was not possible to identify neurons of interest using this marker. A WISH probe for *neurogenin1*, a

marker of dopaminergic neural progenitors (Jeong et al. 2006) was tested. Although this probe worked well in older zebrafish embryos, in the EdU injected embryos fixed at 13hpf, well defined fluorescence from this probe was not detectable. Therefore it was not possible to identify neural progenitors. As zebrafish embryos develop rapidly, a large number of cells were labelled in this experiment; therefore it was not possible to identify any increase in proliferation of an individual population of neurons.

In order to further investigate an increase in proliferation in the miR-133b morphants, WISH for *proliferating cell nuclear antigen (PCNA)* could be performed. *PCNA* is a marker of cell proliferation and can be used to identify proliferating cells at one particular time point. Alongside this, an antibody or fluorescent reporter line for *neurogenin1* (McGraw et al. 2008), or another marker of dopaminergic neural progenitors, could be used to identify and count the number of proliferating neural progenitors. Alternatively, if no increase in proliferation is detectable, it is possible that rather than more neurons being produced, a higher proportion of developing cells are differentiating to a dopaminergic phenotype. It would also be interesting to demonstrate whether the observed increase in neurons is exclusive to the *th+* dopaminergic neurons in the diencephalic dopaminergic cluster. If a neuron increase is present in other related neuronal populations this could help elucidate at which stage in development an increase in proliferation or differentiation is occurring.

Knockdown of miR-133b and effect of dopaminergic neurons in zebrafish models of PD

The *pink1*-deficient zebrafish model of PD has been previously shown to exhibit approximately a 20% decrease in dopaminergic neurons at 3dpf. It is unknown whether *pink1* deficiency results in death of dopaminergic neurons or whether development of these neurons is impaired. Although a panel of developmental markers was examined in *pink1*-deficient embryos, these were only assessed at 24hpf which is later than when the majority of dopaminergic neurons develop (Flinn et al. 2013).

If the decrease of dopaminergic neurons in *pink1*-deficient zebrafish is due to death of these neurons it is likely that the rescue effect of miR-133b knockdown is due to increased numbers of dopaminergic neurons developing initially. A small amount of neuronal death in the *pink1*-deficient miR-133b morphants would then result in the total number of dopaminergic neurons being similar to WT embryos at 3dpf. If the *pink1*-deficiency results in a developmental defect, miR-133b knockdown may ameliorate this developmental phenotype. This could be investigated by examining the expression of developmental

markers in early development. Investigations into the mechanism of dopaminergic neuron decrease in *pink1*-deficient embryos would help determine in what way miR-133b is protective to dopaminergic neurons, whether this is through increased development or increased survival. These studies would also help determine whether miR-133b knockdown may continue to be protective over the life of the zebrafish. By 18 months old *pink1*-deficient zebrafish demonstrate a 50% loss of dopaminergic neurons (Flinn et al. 2013). The effect of miR-133b on other features shown to be dysregulated in *pink1*-deficient zebrafish should also be examined. These include the effect on mitochondrial dysfunction and microglial count. As knockdown of *tigarb*, an inhibitor of glycolysis, was also shown to rescue dopaminergic neurons in *pink1*-deficient zebrafish (Flinn et al. 2013). Whether miR-133b is able to interact with the *tigarb* could also be investigated.

Knockdown of miR-133b was not able to rescue the neuronal loss caused by the exposure of the embryos to MPP+. MPP+ and *pink1* deficiency both result in inhibition of mitochondrial complex I (Flinn et al. 2013; Celardo et al. 2014). It has not yet been determined whether miR-133b knockdown has any effect on mitochondrial function. However, while *pink1* deficiency is chronic defect, MPP+ toxin exposure is an acute insult on the dopaminergic neurons. Therefore, even if miR-133b is able to exert its rescue effect in *pink1*-deficient zebrafish through increased mitochondrial resistance, this is not enough to provide resistance against MPP+. Realistically, rescue of the dopaminergic neuron loss caused by MPP+ exposure would have to be through prevention of this toxin entering the neurons, or increased clearance of this toxin. miR-133b knockdown does not appear to have the capacity to alter sensitivity to MPP+ in this way.

miR-133b morphants already display an increase in the number of dopaminergic neurons at the time of treatment with MPP+ (2dpf), however MPP+ treatment resulted in a similar number of dopaminergic neurons by 3dpf in both WTs and morphants, thus showing that more neurons are lost in morphants than in WT embryos. This shows that an increased number of dopaminergic neurons does not increase resistance to MPP+. MPP+ related neurotoxicity specifically effects dopaminergic neurons as this toxin is able to enter these neurons through *dat* (Hare et al. 2013). Although expression of *dat* in miR-133b morphants has not been tested directly, as expression *th* and *vmat2* are both increased through an increased number of neurons, it is likely that *dat* expression is also increased. Therefore rather than the increase in neurons being protective, the total amount of MPP+ entering the brain may be proportionate to the number of *dat*-expressing neurons. To test this hypothesis

the number of *dat*-expressing neurons could be counted in miR-133b morphants and HPLC could be utilised to determine the concentration of MPP+ present in the brains of both WT and miR-133b morphant embryos after treatment.

miR-133b overexpression experiments

No effect of miR-133b mimic injection was observed on the dopaminergic neuron number. Although an increase in expression was detected by qPCR, when the spatial expression of miR-133b was observed by WISH an increase in miR-133b expression in the brain was not evident. This may explain why no change in dopaminergic neuron number was observed. Injection of a construct that specifically results in miR-133b expression in the brain by using a neuron specific promoter would allow the study of the effects of this on neuron development. If a loss of dopaminergic neurons was observed using this approach, careful controls would have to be performed to ensure that this loss is not a non-specific toxic effect. For example, another unrelated miRNA, or a scrambled miR-133b sequence could be introduced in the same way and the effect compared.

Stable overexpressing lines could also be produced which induce overexpression of miR-133b in specific cell types, for example in neural progenitors. Using these lines, it would be able to assess the effect of overexpression of this miRNA specifically in developing neurons. Conditional overexpressing lines, for example using the Cre-LoxP system, could allow the effect of overexpression of this miRNA at different points in development and adulthood to be studied. The effect of miR-133b overexpression could be compared with conditional knockdowns of predicted targets of miR-133b. This would help determine what proportion of any observed phenotype is through a single target or whether a network of targets is involved.

Effect of miR-133b on Pitx3

The increase in dopaminergic neuron number in miR-133b morphants was hypothesised to be due to de-repression of *pitx3*. Unexpectedly, an increase of neither *pitx3* mRNA nor protein levels could be detected in miR-133b morphants.

As miRNAs more commonly direct translational repression of their targets, the lack of an increase of *pitx3* mRNA levels after miR-133b knockdown was expected. This finding is similar to that of Kim and colleagues; they showed that neither overexpression nor inhibition of miR-133b in embryonic stem cell cultures resulted in a change in *Pitx3* mRNA levels. Protein levels were shown to be altered in these cells (Kim et al. 2007). However, conversely, the Rodriguez

group were able to identify an increase in *pitx3* mRNA levels after miR-133b downregulation in zebrafish embryos. To elicit a downregulation of miR-133b exogenous *pitx3* 3'UTR was injected into the zebrafish embryos. This was shown to act as a "sponge" for miR-133b and free miR-133b levels were decreased (Barreto-Valer et al. 2012; Sanchez-Simon et al. 2010). This group did not assess the protein levels of Pitx3.

While optimisation of an antibody for Pitx3 was in progress, a reporter plasmid which contained RFP under the control of the *pitx3* 3'UTR was used to determine whether miR-133b was able to regulate RFP through binding sites in the 3'UTR. No change in RFP fluorescence was detected after miR-133b knockdown and RFP appeared repressed in both WT and miR-133b morphant embryos. This suggests that repressive forces are acting on RFP through the *pitx3* 3'UTR even in the absence of miR-133b. This does not confirm that miR-133b cannot repress *pitx3*, rather, it indicates that there are other repressive forces acting on *pitx3* in muscle tissue. This is not wholly unexpected as *pitx3* is not naturally expressed in muscle tissue and therefore there may be factors that prevent it being expressed here. Other miRNAs with predicted binding sites in the 3'UTR of *pitx3* are miR-187, miR-145, miR-192, miR-135 and miR-204 (TargetScanFish, release 6.2). Little work has been performed to investigate the expression and function of these miRNAs in zebrafish, however miR-135 is suggested to have expression in zebrafish muscle (Wienholds & Kloosterman 2005). Therefore this is a possible candidate for causing the observed repression of RFP through the *pitx3* 3'UTR in zebrafish muscle.

To determine whether miR-133b is able to bind the *pitx3* 3'UTR this reporter plasmid experiment should be performed in a tissue where no other repressive forces are acting on *pitx3*. Unfortunately, expression of the reporter plasmid was not detected in the brain. Consequently, it was not possible determine whether miR-133b is able to repress *pitx3* in cells where it these genes are naturally expressed. To drive the expression of the reporter plasmid in relevant tissues, the *pitx3* promoter could be used in place of the SV40 promoter, thus allowing analysis of the miR-133b-*pitx3* 3'UTR interaction in relevant cells.

In this study the reporter plasmid method was not able to deliver conclusive results about the interaction of miR-133b and the *pitx3* 3'UTR. If it had been successful this method has the potential ability to determine the specific binding site of a miRNA within the 3'UTR. The effect of mutagenesis of potential binding sites in the 3'UTR allows the researcher to investigate where the miRNA of interest binds to the 3'UTR. Had this experiment been successful and a miR-133b binding site in the 3'UTR of *pitx3* validated, the next step of this

study would have been to design a target protector MO to specifically block the interaction of miR-133b and *pitx3*. This would help determine whether the dopaminergic phenotype observed in miR-133b morphants is specific to this interaction. This experimental process is described in detail by Staton & Giraldez (2011).

To examine levels of Pitx3 protein, a custom designed Pitx3 antibody was commissioned and subsequently carefully optimised to ensure specificity for zebrafish Pitx3. Unexpectedly, at 3dpf the Pitx3 protein levels appear to be decreased in miR-133b morphants. The observed decrease is not significant however it does show that Pitx3 protein levels are not increased in morphants at 3dpf.

These data are puzzling as previous work in zebrafish suggests that miR-133b is able to regulate *pitx3* in zebrafish (Barreto-Valer et al. 2012; Sanchez-Simon et al. 2010). These studies only assessed the effect at 24 and 48hpf and protein levels of Pitx3 were not investigated. A region specific effect of miR-133b on *pitx3* was also shown. In all regions studied, repression of miR-133b, resulting from treatment with cocaine, was evident at both 24 and 48hpf. In the brain, *pitx3* mRNA levels were increased at both time points. However, in whole embryos and peripheral body, *pitx3* mRNA levels were increased at 24hpf but decreased at 48hpf. The effect of this on downstream targets of Pitx3, including *th* and *dat*, was also determined. The detection of brain-specific factors, such as *pitx3* and markers of dopaminergic neurons, in the peripheral body of zebrafish by this study suggests contamination of these samples (Barreto-Valer et al. 2012). In the present study, neither *th* nor *pitx3* could be detected in the peripheral body of 3dpf zebrafish by WISH.

A more recent study by the same group also demonstrated a bi-phasic effect of treatment with cocaine on expression of *th*, *dat* and *nurr1* (*pitx3* was not examined in this study). They showed that treatment with cocaine results in increased expression of these factors at 24hpf and a subsequently downregulation at 48hpf (Barreto-Valer et al. 2013). These data suggest either a compensatory effect is stimulated by the initial increase of these markers. Alternatively, death of dopaminergic neurons may be induced treatment of cocaine by 48hpf, thus resulting in decrease of these markers. Cocaine has shown to induce neuron death in other model systems (Poon et al. 2007).

It is possible that if there is an interaction between miR-133b and *pitx3*, this occurs at an early age only and subsequently a compensatory mechanism to normalise Pitx3 levels is activated. Examination of other transcription factors which are involved in dopaminergic

neuron development such as *nurr1* and *lmx1b* should be examined. Kim and colleagues have previously showed that the expression of *nurr1* was increased by overexpression of miR-133b, potentially to compensate for the decrease in Pitx3 protein levels (Kim et al. 2007).

Interestingly, a miR-133b binding site is predicted to be present in the 3'UTR of *pitx3* paralogue *pitx2*; however this has not been functionally validated. The Pitx3 and Pitx2 proteins are very similar, differing only in the N-terminal region. In mice a functional redundancy between *Pitx3* and *Pitx2* has been identified in muscle development (L'Honoré et al. 2007). The expression of Pitx2 has also been detected in the developing mouse midbrain and is required for terminal differentiation of neurons in the subthalamic nucleus and midbrain (Martin et al. 2004). In zebrafish, although the effect of Pitx2 on dopaminergic neuron development has not been studied, expression of *pitx2* the developing diencephalon has been observed (Liu & Semina 2012). It is possible that in zebrafish Pitx2 may be involved in development of dopaminergic neurons, therefore the effect of miR-133b knockdown may be through regulation of this gene rather than *pitx3*. Alternatively, upregulation of Pitx2 by miR-133b may result in the downregulation of Pitx3 protein levels observed and the neuronal phenotype is elicited through an alternate mechanism.

Future work

The mechanism of the observed increase in dopaminergic neuron number in miR-133b morphants is unknown and therefore future work must aim to elucidate this mechanism. The unexpected finding that neither *pitx3* mRNA nor protein levels are elevated at 3dpf in miR-133b morphants suggests that this mechanism may be Pitx3-independent.

Data from EdU experiments show that the population of *th+* dopaminergic neurons begin to develop very early (10-12hpf). Therefore, it is possible that an interaction between *pitx3* and miR-133b is more crucial earlier in development. As discussed above it is possible that an early upregulation of Pitx3 leads to the observed increase in dopaminergic neurons and also initiates another regulatory mechanism to normalise its expression. This may be why no increase in Pitx3 mRNA or protein levels is observed at 3dpf. An assessment of Pitx3 mRNA and protein levels should be repeated at younger ages to assess whether this interaction is only present at an early age. If an increase in Pitx3 protein levels are detectable at earlier time points, the effect on negative regulators of *pitx3* should be explored.

Alternatively, other targets of miR-133b may be responsible for the increase in dopaminergic neurons. There are a small number of targets of miR-133b which have been previously

validated in zebrafish, of these the majority are involved in muscle development (Mishima et al. 2009). Another validated target of miR-133b in zebrafish is *mps1*, a regulator of blastemal proliferation (Yin et al. 2008). However, there are a large number of interesting targets of miR-133b which have been validated in mice and humans. Although these have not yet been examined in zebrafish, bioinformatics analyses predict that an interaction is likely. A selection of these targets are listed in Table 17 with a description of how upregulation of these targets may be beneficial in PD.

Table 17. Potential targets of miR-133b of interest in Parkinson's disease.

Target	Tissue used for validation	Relevance to PD	References
Fibroblast growth factor receptor 1	Gastric cancer cell lines	Activation of the fibroblast growth factor receptor is able to protect dopaminergic neurons against toxic insults in a toxin-induced rat model of PD	(Wen et al. 2013; Claus et al. 2004; Sleeman et al. 2012)
Insulin-like growth factor 1 receptor	Adipose tissue-derived stem cells and osteosarcoma cell lines	Activated IGF1R signalling may be neuroprotective. Decreased IGF1R signalling in PD brain.	(Ning et al. 2010; Tong et al. 2010; Xu et al. 2009; Zhao et al. 2013)
GLI family zinc finger 1	Human gastric cancer cells and cell lines	Neuronal expression of Gli1 is protective in a toxin-induced rat model of PD	(Suwelack et al. 2004; Zhao et al. 2014)
Glutathione-S-transferase pi	HeLa cells	Mutations in this gene appear in a higher rate in PD patients with pesticide exposure suggesting its involvement in detoxification.	(Patron et al. 2012; Liu et al. 2013)
MCL-1	Osteosarcoma cell lines and adenocarcinoma cell lines	Anti-apoptotic factor, mitochondrial pro-survival factor. Parkin helps maintain levels of MCL-1. Loss of parkin leads to a loss of MCL-1 sensitising cells to oxidative stress.	(Crawford et al. 2009; Zhao et al. 2013; Ekholm-Reed et al. 2013)

Despite the exact mechanism being unclear, this study shows that miR-133b plays a role in dopaminergic neuron development and survival. Intriguingly, this was not observed in miR-133b knockout mice. In this model the dopaminergic neurons were unaffected (Heyer et al. 2012). It is possible that there are differences in dopaminergic neuron development in mice, as conditional knockout mouse models of PD-genes fail to accurately model dopaminergic neuron loss (reviewed by Blesa & Przedborski (2014)). Models of genetic PD in zebrafish, however, are able to model dopaminergic neuron loss (Flinn et al. 2009; Flinn et al. 2013).

Other neuronal populations should also be examined to determine whether miR-133b knockdown results in a specific increase in dopaminergic neurons or whether other neuronal populations are also affected by miR-133b. This work would help elucidate a mechanism for neuronal increase. Lineage tracing analysis could be combined with these experiments to determine at what stage in development an increase in proliferation occurs. Understanding the effects of miR-133b knockdown on other neural populations would also help determine whether miR-133b has a specific enough effect to be used as a therapeutic target without causing unwanted side effects.

Finally, a stable mutant line with miR-133b knockout could be generated to validate the results seen in this study. The reliability of MO-based experiments has recently been criticised (Kok et al. 2015). This study shows a rescue effect, and therefore this is unlikely to be due to off-target toxic effects that are associated with MOs, such as neural apoptosis. However, validation of this data using a stable mutant line is still required. As miR-133b has been shown to have important roles elsewhere, for example in muscle development, limitation of this knockdown to relevant regions of the brain may be beneficial.

Once a stable mutant line or a line possessing a tissue specific knockdown of miR-133b is generated, it would also be possible to cross this line with a number of other zebrafish lines which demonstrate dopaminergic neuron loss. Currently, dopaminergic neuron loss has only been validated in the *pink1*^{-/-} and *gba1*^{-/-} mutant lines (Flinn et al. 2013; Keatinge et al. 2015), however with the rapid development of CRISPR/Cas9 genome editing technology new zebrafish models of PD are continually being generated. Using these lines the effect of miR-133b deficiency in later development and in adulthood could also be studied and would help confirm miR-133b as a therapeutic target for PD.

Chapter 4. Investigating the interaction between miR-205 and *Irrk2* in zebrafish

Contents

Chapter 4. Investigating the interaction between miR-205 and <i>lrrk2</i> in zebrafish	132
4.1 Introduction	134
Lrrk2 and Parkinson's disease	134
miR-205 is a regulator of <i>lrrk2</i>	136
Zebrafish <i>lrrk2</i>	137
Functions of miR-205	138
4.2 Characterisation of miR-205 and <i>lrrk2</i>	138
4.2.1 Optimisation	138
4.2.1.1 WISH probe for <i>lrrk2</i>	138
4.2.2 Results	139
4.2.2.1 miR-205 sequence is conserved in zebrafish	139
4.2.2.2 Expression and localisation of miR-205	140
4.2.2.3 Expression and localisation of <i>lrrk2</i>	140
4.3 Knockdown of miR-205 and effect on dopaminergic neurons	141
4.3.1 Optimisation	141
4.3.1.1 Dosage optimisation of MO and validation of knockdown	141
4.3.2 Results	142
4.3.2.1 Effect of miR-205 knockdown on dopaminergic neurons	142
4.4 Effect of miR-205 knockdown on <i>lrrk2</i>/<i>Lrrk2</i>.....	143
4.4.1 Optimisation	144
4.4.1.1 Western blotting	144
Morpholinos for <i>lrrk2</i>	144
Testing of a commercially available antibody for <i>lrrk2</i>	146
Design of a custom antibody for <i>lrrk2</i>	148
4.4.2 Results	148
4.4.2.1 Assessment of <i>lrrk2</i> mRNA levels.....	148
4.4.2.2 Assessment of <i>Lrrk2</i> protein levels	149
4.5 Discussion.....	150
Characterisation of miR-205 and <i>lrrk2</i> in zebrafish	150
Knockdown of miR-205 and effect on dopaminergic neurons	151
Effect of miR-205 knockdown on <i>lrrk2</i> / <i>Lrrk2</i>	153
Future work for investigation of miR-205 and <i>Lrrk2</i> in zebrafish	154

4.1 Introduction

Lrrk2 and Parkinson's disease

LRRK2 is a very large, highly conserved protein with many functional domains. Human *LRRK2* consists of 51 exons which encode a 286kDa protein. LRRK2 belongs to the ROCO family of proteins, which typically contain a Ras-like G-domain (ROC), a C-terminal of ROC (COR) domain and a kinase domain (Gilsbach & Kortholt 2014). The domain structure of human LRRK2 is shown in Figure 55.

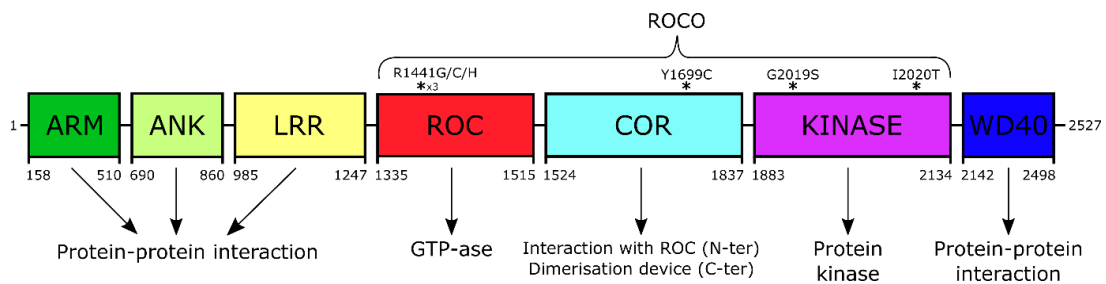


Figure 55. *Lrrk2* domain structure, domain functions and mutations associated with PD. Figure adapted with permission from Sheng et al. (2010).

Although the definitive function of LRRK2 is unclear, distinct functions have been associated with each of the domains of LRRK2. The armadillo repeat (ARM), ankyrin repeat (ANK), leucine rich repeat (LRR) and WD40 domains are all associated with protein-protein interactions (Mills et al. 2014). The ROC domain is a GTPase and the associated COR domain is able to interact with the ROC domain and functions as a dimerisation device. Most GTPases are activated by G-protein activation proteins (GAPs) (Bernards & Settleman 2004). However, there have been few reports of GAPs specific for LRRK2 suggesting activation by a different mechanism (Gilsbach & Kortholt 2014). Monomeric LRRK2 has a much slower GTP hydrolysis rate than dimeric LRRK2, this suggests that the LRRK2 GTPase is activated by dimerisation (Gotthardt et al. 2008). GTP binding has been shown to regulate kinase activity in LRRK2 (Biosa et al. 2013). The kinase domain is a serine/threonine specific protein kinase. It is activated, like most protein kinases, by autophosphorylation (Li et al. 2010).

In 2002, a study of a large Japanese family found that a novel locus (12p11.2-q13.1) segregated with autosomal dominant PD (Funayama et al. 2002), this was named the PARK8 locus. In 2004, *LRRK2* was identified as the gene which contained missense mutations which segregated with the PARK8 locus and were associated with PD (Paisán-Ruíz et al. 2004; Zimprich et al. 2004). These studies confirmed the association of mutations in *LRRK2* with PD in two families in North America and five families in the UK and Spain (Paisán-Ruíz et al. 2004; Zimprich et al. 2004).

Mutations in *LRRK2* are the most common cause of familial and sporadic PD (Li et al. 2014). A large number of mutations have been identified in *LRRK2*, six of these been shown to be pathogenic, these are shown in Figure 55. In familial cases, PD associated with these mutations is inherited in an autosomal dominant fashion and results in “classical” Parkinsonism (Haugarvoll & Wszolek 2009). These mutations are all present within the enzymatic ROC, COR or kinase domains of *LRRK2*.

The most common and most well studied of these mutations is the G2019S mutation. This mutation is responsible for 5-6% of familial cases and 1-2% sporadic cases of PD in those of Caucasian origin. It has been shown to have a penetrance of approximately 75% at the age of 79 years (Kumari & Tan 2009). This mutation increases the catalytic rate of the enzyme, leading to a toxic increase in kinase activity (West et al. 2005). The other mutations have also been associated with increased kinase activity, however this increase is much more variable than the consistent increase shown with the G2019S mutation. This variation may be due to the different substrates used and different data collection methods by the different studies (Esteves et al. 2014).

There is a mutational “hotspot” at R1441. Three different mutations at this site, R1441G/H/C, have been associated with PD. These mutations and the Y1699C mutation in the COR domain are thought to reduce GTP-hydrolysis, resulting in an increase in GTP-bound *LRRK2*. It has been speculated that this may result in increased activation of kinase activity (West et al. 2007).

Mutations in *LRRK2* are also commonly identified in sporadic PD patients and are responsible for 1-5% of all sporadic cases of the disease (Kumari & Tan 2009). A GWAS has also identified risk variants upstream of *LRRK2* which may play a role in transcriptional regulation of the gene (Satake et al. 2009).

LRRK2 is expressed in most organs, with particularly high levels in the kidney and lung (Paisán-Ruiz et al. 2004). Expression within the brain is diffuse, with relatively low expression in dopaminergic neurons of the *substantia nigra* and ventral tegmentum. *LRRK2* is detected at higher levels in the striatum, cortex, cerebellum and hippocampus (Esteves et al. 2014). Within cells, *LRRK2* is associated with many intracellular membrane structures. These include: endosomes, lysosomes, the outer mitochondrial membrane, endoplasmic reticulum and lipid rafts. The membrane association of *LRRK2* is thought to alter its biochemical function, with membrane-associated *LRRK2* having greater kinase activity (Berger et al.

2010). The unique and varied intracellular location of LRRK2 is likely to reflect its involvement in a number of cellular pathways, including: Wnt signalling, vesicular trafficking, cytoskeletal function, mitochondrial function, protein synthesis, autophagy and regulation of neurite outgrowth (Esteves et al. 2014).

The mechanism by which mutations in LRRK2 result in PD is unclear, however as most pathogenic mutations have been shown to alter enzymatic activity it is thought to be a toxic gain of function mechanism. To support this, LRRK2 knockout models rarely mimic Parkinson's pathology. LRRK2 knockout mice do not display any loss of dopaminergic neurons or change in dopamine dynamics (Hinkle et al. 2012), however they do display a motor phenotype. Kinase activity was originally thought to be required for the toxic effects of LRRK2 (Greggio et al. 2006) as kinase inhibitors and mutation of autophosphorylation sites can rescue the neurite outgrowth phenotype of neurons containing mutant LRRK2 (Esteves et al. 2014). However, more recent data using techniques to measure LRRK2 level and detect toxicity at single-cell resolution suggest that the toxic activity of LRRK2 depends on the relative level of LRRK2 and presence of α -synuclein rather than a specific increase in kinase activity (Skibinski et al. 2014).

miR-205 is a regulator of Lrrk2

miR-205 has been identified as a key regulator of LRRK2 (Cho et al. 2013). A two-fold increase in LRRK2 was observed in the frontal cortex of sporadic PD and PDD (PD with dementia) patients compared to non-pathological controls (NPCs). *LRRK2* mRNA levels, however, were not altered, thus suggesting altered post-transcriptional regulation of *LRRK2* in patient brains. A number of miRNAs have predicted binding sites in the *LRRK2* 3'UTR. As the miR-205 binding site is highly conserved among vertebrates the authors studied the expression levels of miR-205. A significant decrease of miR-205, but not other miRNAs which are also predicted to target *LRRK2*, was detected in the frontal cortex of PD and PDD patients compared to NPCs. When correlated, the expression levels of miR-205 and LRRK2 protein levels revealed an inverse correlation. The interaction of miR-205 with *LRRK2* was then confirmed by a luciferase assay. In HEK293T cells transfection of pre-miR-205 resulted in a 60% decrease of LRRK2 levels.

To further investigate the expression and interaction between miR-205 and LRRK2 a rodent model was used. Similarly to the findings from human brain samples, in the mouse brain an inverse correlation between miR-205 expression and LRRK2 protein levels was also observed. miR-205 demonstrated the highest expression in dopaminergic neurons in the mouse

midbrain. This is where LRRK2 protein levels are at their lowest. Over the course of aging (1 month-18 months of age) miR-205 expression levels appear to increase while LRRK2 protein levels decrease; *Lrrk2* mRNA levels remain stable.

The therapeutic potential of miR-205 was also examined in this study. Neurons were derived from transgenic mice which overexpress the R1441G mutant form of LRRK2; these displayed a shortened neurite phenotype. This neurite defect was rescued by overexpression of miR-205 and exacerbated by inhibition of miR-205. These data show that miR-205 has the potential to be a therapeutic target in PD by reducing the load of toxic LRRK2 protein.

The decrease in miR-205 sporadic PD brain suggests that it may be used as a biomarker. The mechanism of the decrease in miR-205 expression is unknown, but the authors suggest that this may be pathogenic. Discovery of regulators of miR-205 expression may help uncover pathogenic mechanisms in PD.

Zebrafish *Lrrk2*

Zebrafish possess one orthologue of *lrrk2* on chromosome 25. Overall, the zebrafish *Lrrk2* protein has 47% similarity with human LRRK2, however there is higher homology within some of the discrete domains. The kinase domain has the highest homology of 71% similarity to the human LRRK2 kinase domain (Figure 56). Similarly to humans, rat and mouse, zebrafish *lrrk2* expression is ubiquitous within the brain. In embryos *lrrk2* expression is limited to the brain and in adult zebrafish *lrrk2* mRNA was also detected in the gut, muscle and ovaries (Sheng et al. 2010). Functions of zebrafish *Lrrk2* have not yet been confirmed.

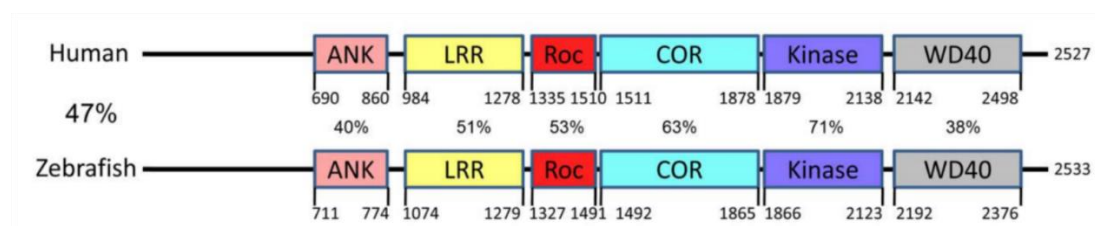


Figure 56. Conservation of amino acid sequences and functional domains of LRRK2 between human and zebrafish. This figure shows that human and zebrafish share an overall homology of amino acids of 47%. Homologies between the individual functional domains vary with the highest homology being in the kinase domain of this protein. ANK = ankyrin repeats domain, LRR = leucine rich repeats domain, Roc = Ras-like G-domain, COR = C-terminal of ROC domain. Figure reproduced from Sheng et al. (2010).

Functions of miR-205

Despite the above described role of miR-205 in the brain, miR-205 is mainly expressed in epithelial tissues. In mice, miR-205 is strongly expressed in the skin and is detectable in squamous stratified epithelial derived organs, including the stomach, pancreas, uterus and bladder (Farmer et al. 2013). In adult mice miR-205 is also detectable in the brain (Cho et al. 2013). miR-205 has been shown to be a regulate epithelial to mesenchyme transition (EMT) through ZEB1 and SIP1/ZEB2. Downregulation of miR-205 (and members of the miR-200 family) was shown to initiate EMT by releasing their targets from repression. EMT is important for tissue remodelling in embryogenesis and also plays a role in tumour metastasis (Gregory et al. 2008).

Due to its involvement in metastatic pathways miR-205 has been implicated in a number of cancers and is thought to have a tumour suppressor function. It has been shown to be downregulated in gastric cancer, prostate cancer, bladder cancer and head and neck squamous cell carcinomas (Gandellini et al. 2009; Yin et al. 2014; Childs et al. 2009; Wiklund et al. 2011). In breast cancer patients decreased miR-205 expression was associated with shorter disease free intervals and overall survival times (Markou et al. 2014).

The aim of this study is to determine whether the interaction between miR-205 and *lrrk2* is conserved in zebrafish, and whether knockdown of miR-205 has a neurotoxic effect on dopaminergic neurons through an increase in Lrrk2 protein levels.

4.2 Characterisation of miR-205 and *lrrk2*

To determine whether it is possible for miR-205 and *lrrk2* to interact the spatial and temporal expression was investigated by WISH at 3dpf, and qPCR from 1-5dpf, respectively.

4.2.1 Optimisation

4.2.1.1 WISH probe for *lrrk2*

Lrrk2 is a very large gene containing 51 exons. Firstly, a probe previously used by another group which investigated the expression pattern of zebrafish *lrrk2* was tested (Sheng et al. 2010). This probe was designed to target the region of mRNA which encodes the WD40 domain. When this probe was tested staining took over 5 days to develop. This suggests that this probe did not have optimal annealing properties. Within this staining period a similar staining pattern also developed when the sense probe was used. This suggests that the staining seen with the antisense probe may not be specific to *lrrk2*. Another probe was designed to the region of the mRNA encoding the ROC domain of Lrrk2.

Figure 57 shows the approximate locations of the forward and reverse primers used to generate a PCR product from which the WISH probe was transcribed. To allow both a sense and antisense probe to be transcribed the forward and reverse primers were tagged with the SP6 and T7 promoter sequences, respectively. WISH using the antisense probe transcribed from this PCR produced staining which developed within 2 hours. Within the same time scale, WISH performed with the sense control probe did not produce any staining, therefore indicating that staining produced with the antisense probe is specific for *lrrk2*.

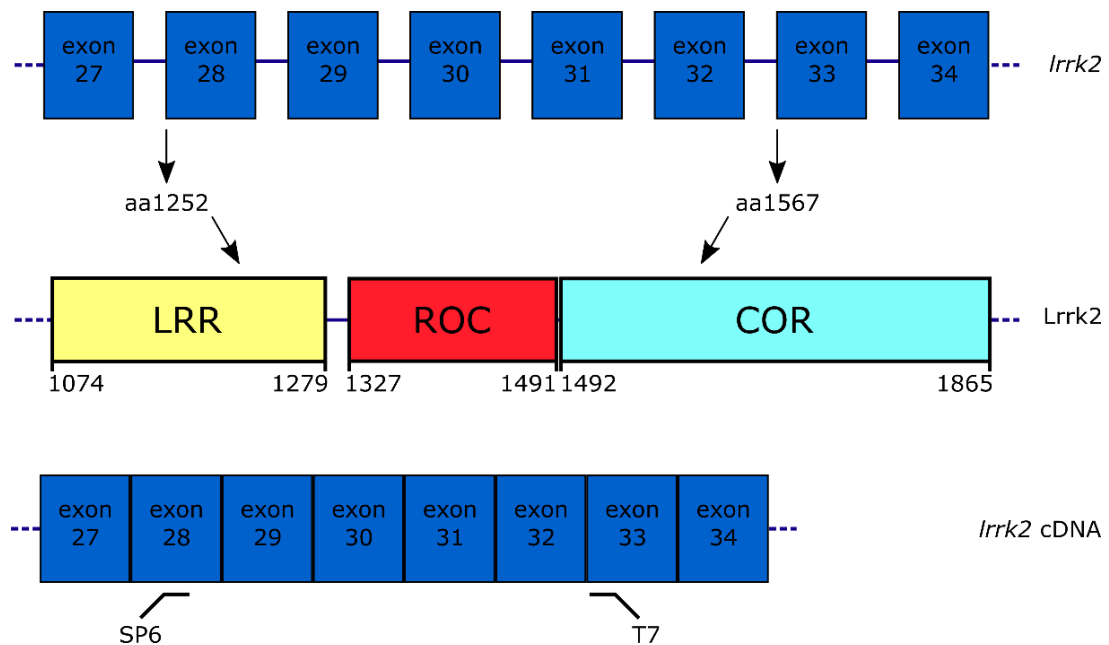


Figure 57. Design of a WISH probe for *lrrk2*. The top panel shows a schematic of exons 27-34 of the *lrrk2* gene. The first amino acid encoded by both exons 28 and 33 is labelled and how this matches up to the domain structure of Lrrk2 protein is shown. The bottom panel shows the location of the primers used to generate a PCR product from which the WISH probe is transcribed. LRR = leucine rich repeats domain, ROC = Ras-like G-Domain, COR = C-terminal of ROC domain.

4.2.2 Results

4.2.2.1 miR-205 sequence is conserved in zebrafish

miR-205 is highly conserved across a wide range of species (miR-Base and Ensembl). There is good homology between the human and zebrafish miR-205 sequences. Figure 58A shows the alignment of the whole miR-205 exon between humans and zebrafish. Over the whole exon there is an 78% similarity over 100% of the zebrafish sequence (the human sequence is 21bp longer). The mature miRNA sequence of zebrafish miR-205 is 100% homologous to both human and mouse miR-205 (Figure 58B).

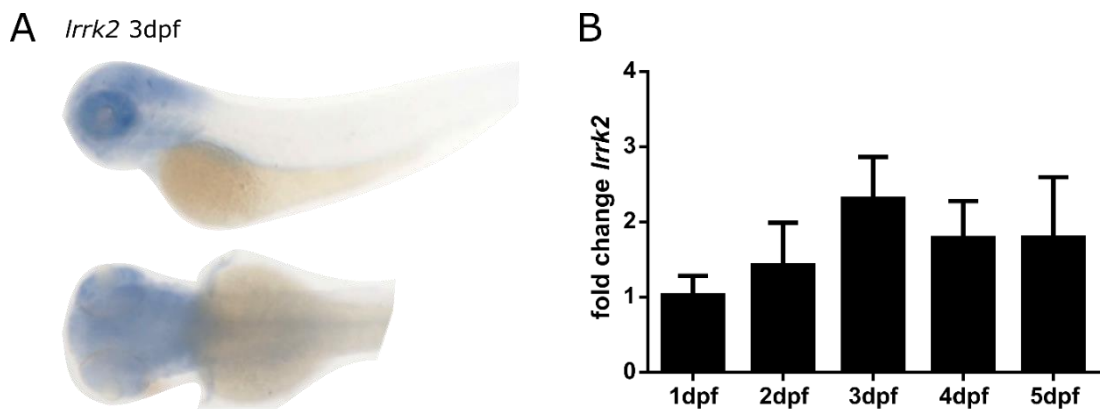


Figure 60. Expression and localisation of *Irrk2*. **A** shows the spatial expression pattern of *Irrk2* as determined by WISH, at 3dpf. The sense control probe for *Irrk2* did not show any staining indicating that the staining shown above is specific to *Irrk2*. **B** shows the relative temporal expression of *Irrk2* from 1-5dpf, as determined by qPCR. Error bars represent standard deviation.

4.3 Knockdown of miR-205 and effect on dopaminergic neurons

In order to study the role of miR-205 in the development of dopaminergic neurons a MO was used to generate a transient knockdown of this miRNA. Once a knockdown had been validated the number of dopaminergic neurons present in both control MO injected and miR-205 morphants was determined.

4.3.1 Optimisation

4.3.1.1 Dosage optimisation of MO and validation of knockdown

MOs can be used to knockdown miRNAs as well as protein coding genes. For miR-205 a MO targeting the overlapping loop region of the pri-miRNA was used (see Materials and Methods Figure 12 on page 50). This MO was previously used by (Kloosterman et al. 2007) who tested a number of MOs targeting different regions of the miR-205 pri-miRNA transcript. The knockdown of the miR-205 was visualised by WISH and quantified by qPCR.

To determine the optimal dose of the miR-205 MO it was injected at three different doses into one-cell stage embryos. A control MO was also injected to control for death and deformity attributable to the injection process and presence of MO. The three doses of MO were injected, these were: 2.5ng, 5ng or 7.5ng MO. The toxicity was assessed visually and by counting death rates. The miR-205 MO was very well tolerated and none of the groups displayed any deformity or increase in death rate above the WTs (5-10% death). As the MO

was well tolerated all doses the middle dose, 5ng, was chosen as the working concentration for subsequent experiments. The efficacy of MO at 3dpf was assessed by qPCR. The qPCR data show that a near-complete knockdown was achieved with this MO (Figure 61).

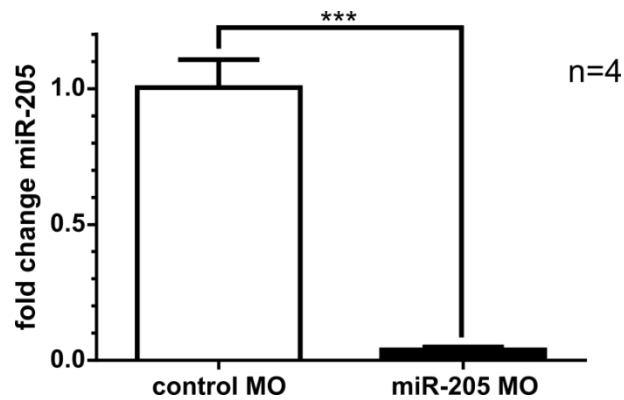


Figure 61. Knockdown of miR-205 using MO. miR-205 levels were quantified at 3dpf by qPCR. Injection of miR-205 MO results in a 95% decrease in miR-205 levels at 3dpf. The data shown are from experiments using the chosen dose of MO, that is, injection of 5ng of miR-205 MO. miR-133b was used as a reference gene. Error bars represent standard deviation. Data are from 4 biological replicates and are analysed by an unpaired t-test with Welch's correction, *** = $p < 0.001$.

4.3.2 Results

4.3.2.1 Effect of miR-205 knockdown on dopaminergic neurons

Two methods were used to assess the effect of miR-205 knockdown on dopaminergic neurons. Firstly, the mRNA levels of *th* were assessed by qPCR. As shown in Figure 62 knockdown of miR-205 does not cause any change in *th* mRNA levels at 3dpf.

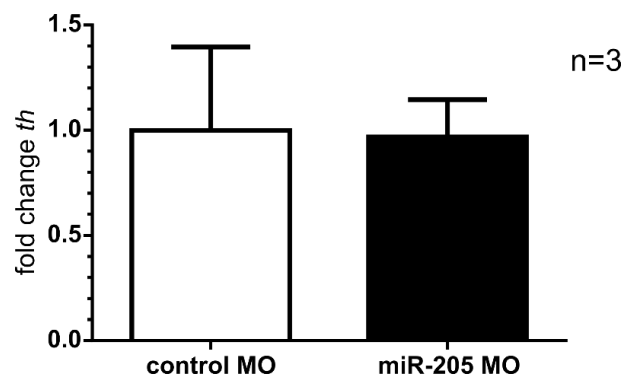


Figure 62. miR-205 knockdown has no effect on *th* mRNA levels at 3dpf. *th* mRNA levels were assessed at 3dpf by qPCR. There is no change in *th* mRNA levels after knockdown of miR-205. *ef1a* was used as a reference gene. These data are from 3 biological replicates. Data is analysed by an unpaired t-test with Welch's correction, $p > 0.05$.

To further investigate the effect of miR-205 knockdown on dopaminergic neurons the number of *th+* dopaminergic neurons were counted after WISH for *th* was performed. This experiment revealed a slight but significant decrease in the number of *th+* dopaminergic neurons in the miR-205 morphants compared to the control MO injected embryos (Figure 63).

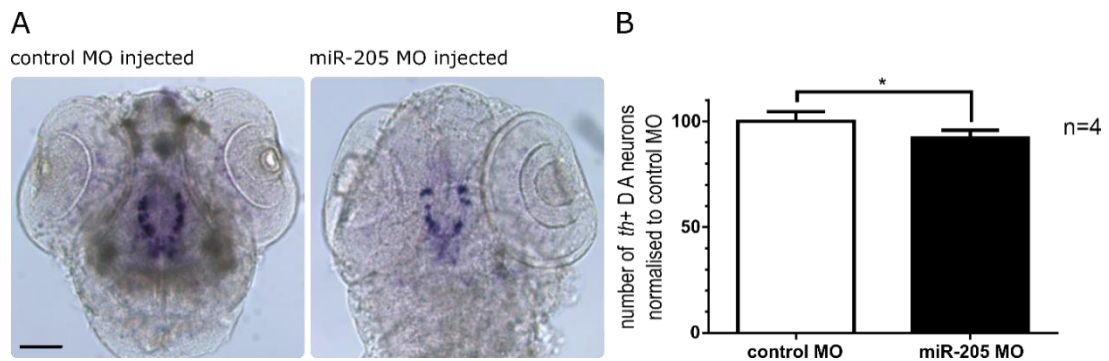


Figure 63. miR-205 knockdown results in a small decrease in *th+* dopaminergic neurons at 3dpf. A shows a representative image of the *th+* dopaminergic neurons in both control MO and miR-205 MO injected embryos. Scale bar = 100 μ m. B shows the quantified number of *th+* dopaminergic neurons normalised to WT control MO injected. A slight but significant decrease of 8% is observed in miR-205 MO injected embryos. Error bars represent standard deviation. These data are from four biological replicates. In each biological replicate the number of dopaminergic neurons is counted in 20 embryos and the average taken. Data are analysed with an unpaired t-test with Welch's correction. * = $p < 0.05$. On axis labels, DA = dopaminergic.

4.4 Effect of miR-205 knockdown on *lrrk2/Lrrk2*

LRRK2 has been validated as a target of miR-205 in humans and mice (Cho et al. 2013). Both TargetScanFish (Release 6.2, June 2012) and the miRanda algorithm predict the presence of a miR-205 binding site in the 3'UTR of *lrrk2*. Figure 64 shows the predicted binding site in the 3'UTR of zebrafish *lrrk2*. To investigate the effect of miR-205 knockdown on *lrrk2*, mRNA levels were measured by qPCR and *Lrrk2* protein levels were quantified using western blotting.

Human and Mouse:

validated miR-205/*LRRK2* interaction

```

3'   gucUGAGGCCACCUUACUUCu 5'   hsa-miR-205
      :|||  || | |||||
5'   ...auagCUCGUGU-GUAUGAAGGa...3'   hLRRK2
                                      (103-123bp after
                                      stop codon)

3'   gucUGAGGCCACCU-UACUUCu 5'   mmu-miR-205
      :|||  || | |||||
5'   ...aaagUUCAUAUGUAUAUGAAGGa...3'   mLRRK2
                                      (159-191bp after
                                      stop codon)

```

Zebrafish:

predicted miR-205/*lrrk2* interaction

```

3'   gucUGAGGCCACCUUACUUCu 5'   dre-miR-205
      :  : || |||||
5'   uguGAGAUUGU-GAAUGAAGGc 3'   zf lrrk2
                                      (953-972bp after
                                      stop codon)

```

Figure 64. Validated and predicted binding sites for miR-205 in *lrrk2* 3'UTR. The left panel shows the validated interactions between human and mouse miR-205 and the 3'UTR of *LRRK2* (Cho et al. 2013). The right panel shows a potential binding site for miR-205 in the 3'UTR of *lrrk2* in zebrafish. The seed region of miR-205 is highlighted in both cases.

4.4.1 Optimisation

4.4.1.1 Western blotting

Currently there are no commercially available antibodies designed to specifically detect zebrafish Lrrk2. However, the human and zebrafish Lrrk2 proteins are approximately 50% homologous (Figure 56), therefore a search was performed to identify an antibody with an epitope which has a high homology to zebrafish Lrrk2.

Morpholinos for Lrrk2

In order to test the specificity of antibodies for Lrrk2, *lrrk2* knockdowns were generated using MOs. The chosen MOs were selected from a publication studying deletion of the WD40 domain of Lrrk2 in zebrafish (Ren et al. 2011). The first MO targets the boundary of intron 38 and exon 39, this in the region of the gene that encodes part of the kinase domain; it will be referred to as kinase MO. The second MO targets the boundary of exon 44 and intron 44, the region of the gene which encodes part of the WD40 domain; it will be referred to as WD40 MO. Before purchasing the MOs, the sequence of the target was confirmed using direct sequencing to confirm that no SNPs are present which may prevent MO binding. A BLAST search of the MO sequence against the zebrafish genome was also performed to ensure specificity for *lrrk2*.

The MOs were tested at two different doses, 8ng and 10ng. As these MOs were only being used for generating morphants from which protein could be collected the any toxic effects of these MOs were largely ignored as long as the embryo developed sufficiently for protein collection to be possible. The 10ng dose of the kinase MO was discarded as the majority of these embryos did not survive until 3dpf, those that did were grossly deformed and it was not possible to collect protein. At 3dpf RNA was collected from the morphants and uninjected embryos to assess the modification of *lrrk2* by RT-PCR. A complete loss of the WT *lrrk2* transcript was seen with the kinase MO and approximately a 50% loss with the WD40 MO (Figure 65).

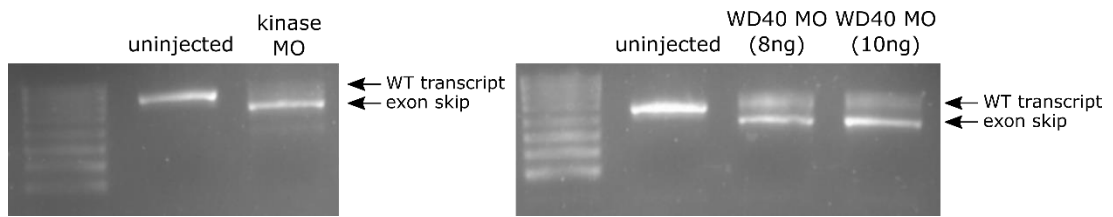


Figure 65. RT-PCR analysis of the effect of the *lrrk2* MOs. This figure shows the assessment of the effect of both the kinase and WD40 MOs by RT-PCR. Arrows indicate the WT transcript and the shorter transcript, thought to be an exon skip, present in the MO injected samples

These MOs both cause deletions of all or part of the exon they target and then a premature stop codon, this was confirmed by direct sequencing. The kinase MO causes an exon skip, exon 39 is deleted (113bp). This causes a frame shift and a premature stop codon resulting in a truncated protein 72kDa smaller than full length *Lrrk2*. The WD40 MO causes a 98bp deletion corresponding to the second half of exon 44; this may be due to activation of a cryptic splice site. This also results in a frame shift and a premature stop codon thus generating a truncated protein 39.6kDa smaller than full length *Lrrk2*. This is shown in Figure 66. These MOs will be used to assess the specificity of any *Lrrk2* antibodies tested.

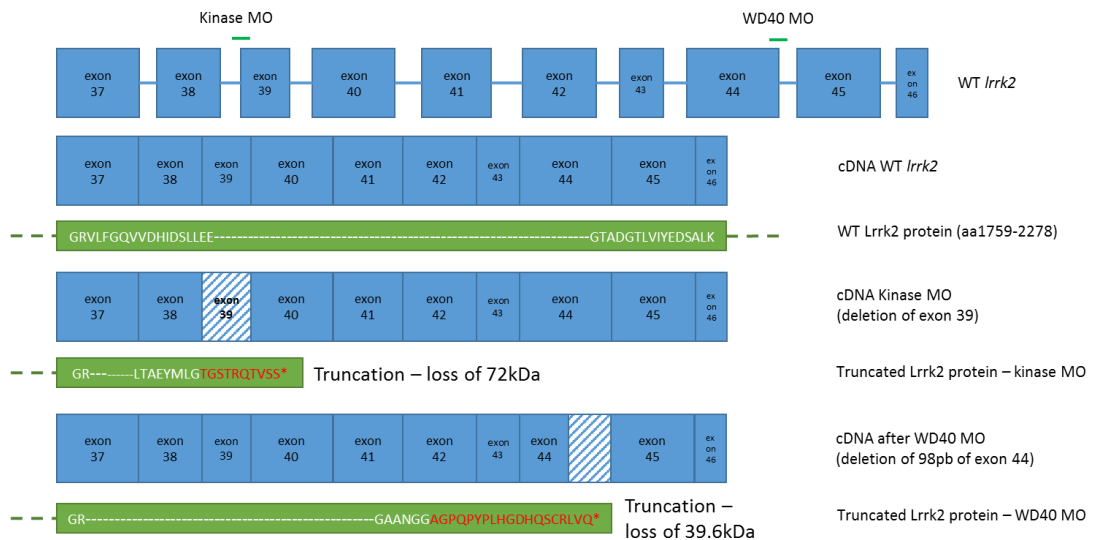


Figure 66. Effect of *lrrk2* MOs on the *lrrk2* transcript. This figure shows the exon structure of WT zebrafish *Lrrk2* and the effect of the kinase and WD40 MOs on this. The kinase MO results in a deletion of exon 39 which generates a frameshift and subsequent premature stop codon, resulting in loss of 72kDa of *Lrrk2*. The WD40 MO results in a deletion of the second half of exon 44, presumably by activation of a cryptic splice site. This also causes a frame shift and premature stop codon resulting in loss of 39.6kDa of *Lrrk2*.

Testing of a commercially available antibody for Lrrk2

Davies and colleagues, tested a range of anti-LRRK2 monoclonal antibodies (Davies et al. 2013). The antibody recommended by this study was chosen for testing in zebrafish. This antibody was raised to a synthetic peptide corresponding to amino acids 970-2527 of human LRRK2. It was shown to react with the C-terminal end of human LRRK2 (aa1326-end). This region has a 55% identity with zebrafish Lrrk2 and 77% positive matches. When a BLAST search is performed to compare this amino acid sequence against the zebrafish proteome, the next closest match after Lrrk2 only has 30% similarity over 23% of the sequence. This suggests that this antibody will not recognise any other proteins other than Lrrk2.

Lrrk2 is a large protein with a molecular weight of 280kDa therefore the western blotting protocol was optimised for large proteins. Modifications of the protocol included: using a low percentage acrylamide gel (7.5% resolving gel and 4% stacking gel), reducing the percentage of methanol in the transfer buffer to 5% and transferring the blot over night at 90mA.

The antibody was first tested using protein lysates from whole, deyolked 3dpf embryos and protein lysates from fibroblasts were used as a positive control. Tubulin was used as a loading control. Figure 67 shows that there is a clear band at the correct weight, 280kDa, in the fibroblast sample, however a band at this weight is not present in zebrafish samples; instead a clear band is present just below 150kDa. It is possible that this could be a C terminal fragment of Lrrk2.

To ensure that the antibody is functioning within its linear range and is therefore can be used to quantify protein levels, a range of protein concentrations were loaded onto the gel and the protein levels were quantified using densitometry. The relative levels of Lrrk2 and Tubulin from 10, 20 and 30 embryos are very similar, but differ in the 40 embryo lane, where Tubulin levels appear to level off. This is likely due to overloading of the gel and saturation of the Tubulin antibody. The levels of "Lrrk2" protein were normalised to the Tubulin loading control. For 10-30 embryos the values are very close to 1 showing that the level of protein is accurately corrected by the loading control and the antibodies were working within their linear range. For subsequent experiments protein from approximately 20 embryos was loaded onto the gel.

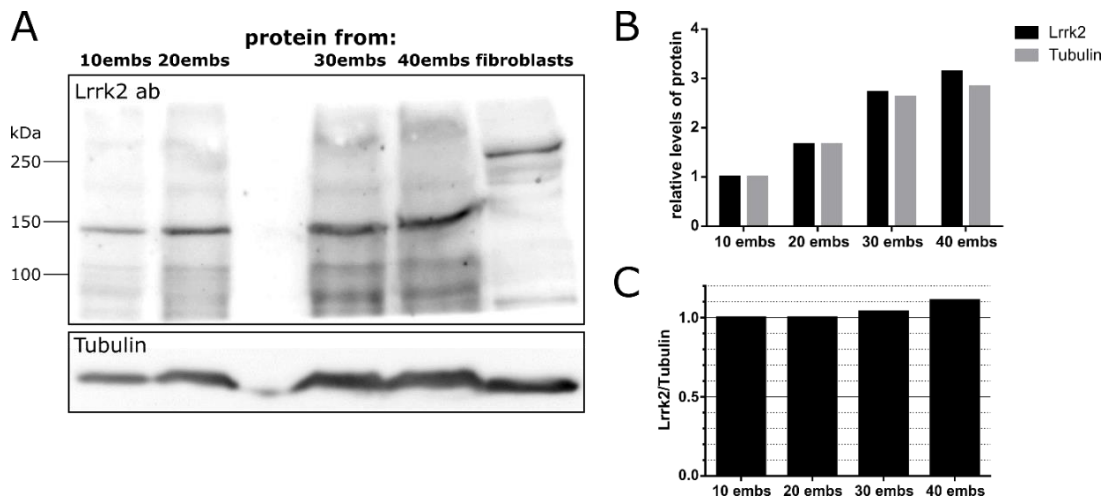


Figure 67. Initial testing of Lrrk2 antibody. A shows a blot testing the antibody on protein from zebrafish embryos at a range of concentrations and from fibroblasts as a positive control. In fibroblasts a band just above 250kDa can be seen. As Lrrk2 (in humans and zebrafish) is a 280kDa protein this band is very likely to be LRRK2. In the lanes loaded with zebrafish protein a band of this weight is not visible, however a clear band and approximately 150kDa is visible. It is possible that this could be a fragment of Lrrk2. B shows a quantification of the “Lrrk2” and Tubulin bands. The relative levels of Lrrk2 and Tubulin from 10, 20 and 30 embryos are very similar, but differ in the 40 embryo lane. C shows the “Lrrk2” protein levels normalised to the loading control.

To determine whether the band observed 150kDa is a fragment of Lrrk2, two MOs were used to knockdown Lrrk2. If the band at 150kDa is indeed Lrrk2 then injection of the kinase MO or WD40 MO injection would cause the band to be present at a lower weight as part of the protein has been deleted, or the antibody would not be able to bind to the truncated protein as a sufficient proportion of the epitope is no longer present. Protein was collected from MO injected and WT embryos at 3dpf, a western blot was performed using these samples to test the specificity of the antibody.

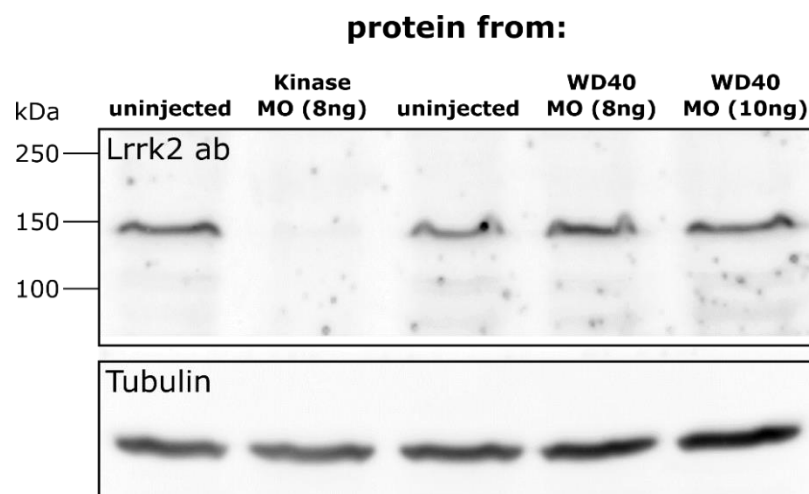


Figure 68. Investigating the specificity of the Lrrk2 antibody using MOs. This figure shows the western blot with samples from un.injected and MO injected embryos. No band can be detected in kinase MO injected embryos. Tubulin was used a loading control.

The western blot using protein from both WT and *lrrk2* morphant embryos is shown in Figure 68. There is no visible band at 150kDa in the embryos injected with the kinase MO. This suggests that a sufficiently large portion of the protein is missing in these morphants that the antibody is unable to recognise this band. This indicates that this band at 150kDa is likely to be a fragment of Lrrk2. Unexpectedly, injection with WD40 MO does not have any visible effect on this band. This suggests that the truncation of Lrrk2 caused by this MO is not large enough to disrupt antibody binding, however if this is the case a bandshift should be visible as the truncation results in a loss of 39.6kDa. The reason why a band shift is undetectable is unclear. One explanation could be that the truncated protein was not translated due to nonsense mediated decay of the mutated transcript and the residual full length is translated at a higher rate to compensate.

Design of a custom antibody for Lrrk2

To complement the use of the commercially available antibody described above a custom antibody for zebrafish Lrrk2 was commissioned from Eurogentec (Seraing, Belgium). Two 15-amino acid epitopes, unique to zebrafish Lrrk2, assessed by local alignment against the zebrafish proteome, using BLAST (NCBI) were chosen.

The first peptide to which a custom antibody will be raised corresponds to amino acids 1656-1671 of zebrafish Lrrk2. This is within the COR domain of the protein. The second peptide corresponds to amino acids 2076-2091, this is towards the end of the kinase domain of Lrrk2. These peptides either have partial (80%) or total homology with human LRRK2, therefore they may also be useful in cell culture applications. The antibodies generated will be rabbit polyclonal antibodies. These antibodies provided by Eurogentec are affinity purified against the peptide they were raised to enrich for antibodies specific to Lrrk2.

4.4.2 Results

4.4.2.1 Assessment of *lrrk2* mRNA levels

Firstly, the effect of miR-205 knockdown on *lrrk2* mRNA levels was determined by qPCR. If miR-205 is able to regulate *lrrk2* by mRNA cleavage and degradation, knockdown of miR-205 would result in an increase in *lrrk2* mRNA. No change in *lrrk2* mRNA level was observed (Figure 69), therefore if miR-205 is able target *lrrk2* in zebrafish this is by translational repression.

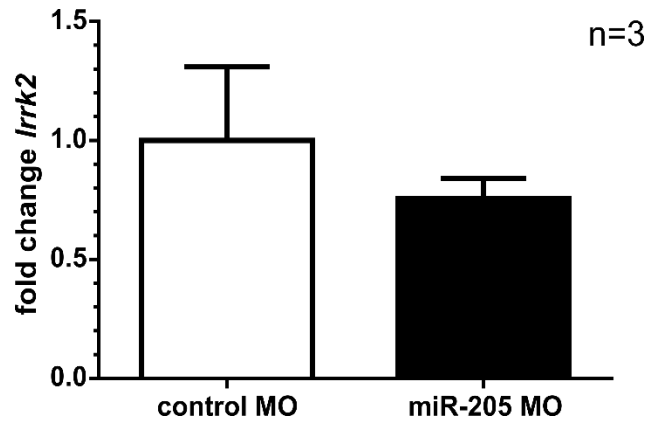


Figure 69. miR-205 knockdown has no effect on *lrrk2* mRNA levels at 3dpf. *lrrk2* mRNA levels were assessed by qPCR. Error bars represent standard deviation. Data are from three biological replicates and are analysed by an unpaired t-test with Welch's correction, $p > 0.05$.

4.4.2.2 Assessment of *Lrrk2* protein levels

Next, it was investigated whether miR-205 can repress the translation of *Lrrk2*. *Lrrk2* protein levels were quantified using western blotting in embryos injected with either the control MO or miR-205 MO

Although the optimisation data for the commercially available antibody do not definitively prove that this antibody is indeed detecting *Lrrk2*, no other antibodies were available, therefore this antibody was used generate preliminary data regarding the ability of miR-205 to regulate *lrrk2* at the translational level. Protein was collected from 3dpf embryos which had been injected with either miR-205 MO or with the control MO. These samples were run on a western blot to assess levels of *Lrrk2* protein (Figure 70).

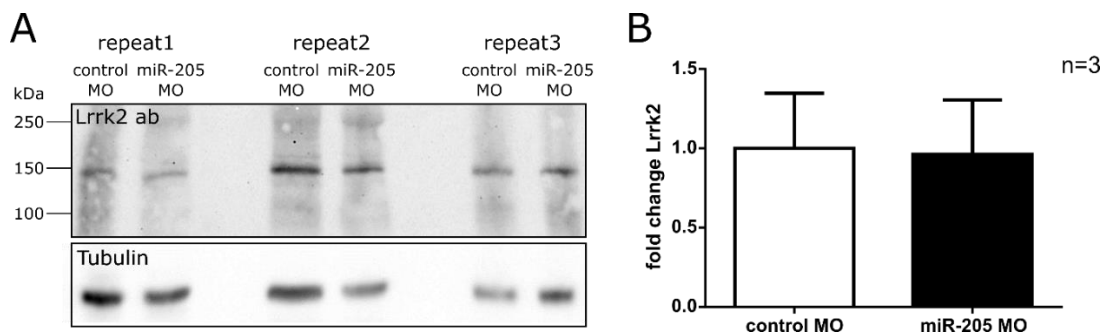


Figure 70. miR-205 knockdown has no effect on *Lrrk2* protein levels at 3dpf. **A** shows the western blot where *Lrrk2* protein levels are compared between lysates from control MO and miR-205 MO injected embryos. Tubulin was used as a loading control. **B** shows a quantification of this western blot. *Lrrk2* protein levels are normalised to tubulin levels. Data are from three biological replicates and analysed by an unpaired t-test with Welch's correction, $p > 0.05$.

Figure 70 shows that, using this antibody, there is no detectable change in the band at 150kDa in miR-205 morphants. This may indicate that miR-205 is unable to regulate Lrrk2 protein levels in zebrafish. Due to the concerns regarding the specificity of this antibody for Lrrk2 another antibody must be used to confirm this result. The custom antibody will be optimised and used to repeat this experiment in the future.

4.5 Discussion

This study aimed to investigate the effect of miR-205 on the development of dopaminergic neurons. The hypothesis was that knockdown of miR-205 would result in an increase in Lrrk2 protein levels which would result in neurotoxicity. The present study is the first to attempt to elucidate a function of miR-205 in zebrafish.

Characterisation of miR-205 and lrrk2 in zebrafish

miR-205 is conserved in a wide variety of species. The mature miRNA sequence is 100% homologous to human and mouse miR-205, thus indicating that the function of miR-205 is conserved in zebrafish.

The observed expression pattern of miR-205 is similar to that determined by a group which investigated a large number of miRNAs as part of a large scale study assessing the differences in vertebrate miRNA expression where strong staining in the epidermis around the pharyngeal arches is observed (Ason et al. 2006). The present study also detects diffuse staining in the brain of the zebrafish and within the intersegmental cells in the zebrafish tail. A sense control probe should also be used to determine that the expression pattern observed is specific to miR-205 rather than non-specific background staining.

In developing mice, miR-205 expression was detected in the skin, and squamous stratified epithelium derived organs such as the stomach, pancreas and bladder. No expression was observed in the developing mouse brain (Farmer et al. 2013). Expression of miR-205 has been confirmed in the brain of 1 month old mice. It was detectable in the mouse cortex, hippocampus, midbrain, striatum and cerebellum with the highest expression in the midbrain (Cho et al. 2013).

To ensure that observed staining for miR-205 in the head of the zebrafish is not solely attributable to staining in the skin, WISH should be performed on sections to confirm that miR-205 is indeed expressed in the developing zebrafish brain. Investigation of the expression of miR-205 in the brains of adult zebrafish would also be interesting to determine whether regions of the brain containing the dopaminergic neurons exhibit a higher level of

expression of miR-205 than other regions, as is seen in brains of both humans and mice (Cho et al. 2013).

Zebrafish *Lrrk2* was observed to have ubiquitous expression within the brain at 3dpf. This is in agreement with other studies (Sheng et al. 2010). In adult zebrafish Sheng and colleagues were able to detect *Lrrk2* expression in the brain, muscle, gut and ovary. Using their own custom *Lrrk2* antibody, full length *Lrrk2* protein was detected in the adult zebrafish brain by western blot.

To date, only two studies have been published on the function of zebrafish *Lrrk2* (Sheng et al. 2010; Ren et al. 2011). These studies represent a dichotomy in the literature over the effect of deletion of the WD40 domain of zebrafish *Lrrk2*.

Sheng and colleagues report that knockdown of *Lrrk2* through use of start site MOs to block translation results in severe embryonic lethality and developmental abnormalities. The defects described are very similar to the standard toxic and off targets effects often caused by MOs through p53 activation. These include gross neuronal apoptosis and developmental delay (Robu et al. 2007). To allow further study of the function of *Lrrk2*, a MO was used that introduces a stop codon before the WD40 domain. They showed that truncation of zebrafish *Lrrk2* resulted in loss of *th+* neurons, disorganisation of axon tracts, increased apoptosis within the brain and a locomotion defect. They also demonstrated that these defects could be, at least partially, rescued by overexpression of either human or zebrafish full length *Lrrk2* (Sheng et al. 2010). Another group studying the function of *Lrrk2* in zebrafish, however, were unable to replicate these findings. Ren and colleagues used the same MOs and validated the deletion of the WD40 domain however were not able to reproduce the results seen by Sheng and colleagues. No neuronal loss or locomotion defect could be detected (Ren et al. 2011).

The protein homology and expression of *Lrrk2* suggests a conserved role in zebrafish. However, the data presented by the two studies above highlight the need for additional studies to be performed to elucidate the role of *Lrrk2* in zebrafish. Furthermore, overexpression models containing WT and mutated *Lrrk2* may be more relevant for the study of the role of *Lrrk2* in PD.

Knockdown of miR-205 and effect on dopaminergic neurons

Prior to this study the effect of knockdown of miR-205 had not been investigated in zebrafish. Another group had previously used miR-205 MOs however this was purely to demonstrate the effects of designing the MO to different regions of the pri-miRNA (Kloosterman et al.

2007). This previous validation of a miR-205 MO was utilised by this study; the non-overlapping loop MO was used for knockdown of miR-205. MO optimisation was successful and a near complete knockdown of miR-205 was achieved without any noticeable deformities or increase in death rate of injected embryos.

The effect of miR-205 knockdown on dopaminergic neurons was investigated, and a small but significant decrease in dopaminergic neuron number was observed. Despite this result reaching significant an 8% decrease only equates to 2 fewer neurons, as WT embryos have approximately 20-25 *th+* dopaminergic neurons in Wulliman-Rink groups 1, 2, 4 and 5. Therefore it is unlikely that this is a meaningful defect at this age, however it may indicate the beginnings of increased susceptibility of these neurons to a toxic load of Lrrk2. To determine whether miR-205 causes a meaningful decrease in *th+* dopaminergic neurons these must be counted at later time points. As knockdown by MO is transient, to do this a stable miR-205 knockout line could be generated.

The neurotoxic effect of overexpression of WT LRRK2 is disputed. While increase in LRRK2 activity has been suggested to be a risk factor for PD (Cho et al. 2013; Satake et al. 2009) a number of studies have failed to identify any neurotoxic effects of upregulation of WT LRRK2 alone (Cho et al. 2013; Parisiadou et al. 2009; Lin et al. 2009).

Cho and colleagues saw that although de-repression of mutant LRRK2 in neuron culture by inhibition of miRNA-205 resulted in reduced neurite out-growth, inhibition of miR-205 in non-transgenic neurons, thus resulting in an increased load of WT LRRK2 did not result in any neurotoxic effects. These results are in agreement with a study from the same group where a direct, rather than miR-205 mediated, upregulation of WT and G2019S LRRK2 was investigated (Parisiadou et al. 2009). In an *in vivo* mouse model it has similarly been demonstrated that upregulation of LRRK2 alone did not cause neurodegeneration. However, the upregulation of WT LRRK2 exacerbated progression of neuropathological abnormalities developed in mice harbouring the A53T α -synuclein mutation (Lin et al. 2009).

The studies discussed above were all performed in mice. It is possible that, in mice, there are differences the susceptibility of dopaminergic neurons to toxic effects as classical knockout mouse models of PD also fail to accurately model dopaminergic neuron loss (reviewed by Blesa & Przedborski (2014)). Models of genetic PD in zebrafish, however, are able to model dopaminergic neuron loss (Flinn et al. 2009; Flinn et al. 2013). Therefore it is possible that

upregulation of LRRK2 in zebrafish may have a more damaging effect of dopaminergic neurons.

In a human cell culture model of PD (dopaminergic neurons differentiated from iPSCs) it was shown that LRRK2 protein levels were a strong predictor of cell death. This was shown to be independent of kinase activity of LRRK2. However in the absence of α -synuclein the toxicity of increased LRRK2 levels was reduced (Skibinski et al. 2014). Although the effect on neuronal survival were not investigated, zebrafish which were induced to transiently overexpress either WT or G2019S-mutant-LRRK2 (a human construct) displayed a similar impairment in protein clearance suggesting that this defect is more dependent on expression levels than the specific LRRK2 mutation (Lichtenberg et al. 2011). In drosophila the effect of overexpression of WT LRRK2 is disputed. Two studies have shown that overexpression of WT LRRK2, either systemically or in dopaminergic neurons only, results in a dopaminergic neuron loss, albeit in a less severe manner than expression of G2019S-mutant-LRRK2 (Liu et al. 2008; Venderova et al. 2009). However this finding was not replicated in a third study which showed that expression of three Parkinson's-related LRRK2 alleles resulted in neuronal loss however expression of WT LRRK2 did not (Ng et al. 2009).

Zebrafish do not possess an orthologue of α -synuclein (Milanese et al. 2012). Therefore the effects of LRRK2 will be interesting to study in zebrafish as this model allows the study of toxicity independent of α -synuclein to be studied. Interestingly, α -synuclein knockout mice are resistant to MPTP toxicity (Dauer et al. 2002). Zebrafish, despite being α -synuclein deficient are not resistant to this toxin (Bretaud et al. 2004; the present study). This suggests that either, this toxin induces neurotoxicity in a different manner in zebrafish, or, other genes are present in zebrafish which compensate for the lack of α -synuclein.

*Effect of miR-205 knockdown on *lrrk2/Lrrk2**

It has previously been shown that miR-205 regulates *LRRK2* in mice and humans through a binding site in the 3'UTR of *LRRK2*. This repression was shown to be due to translational repression rather than through transcript degradation, therefore it was expected that no change in mRNA level of *lrrk2* in miR-205 morphants was observed. To determine whether a change in *Lrrk2* protein levels was detectable western blots were performed. The anti-*Lrrk2* antibody used did not detect any change in protein levels however the specificity of the antibody used for *Lrrk2* has not been conclusively validated.

Two custom anti-Lrrk2 antibodies specific for zebrafish have been commissioned and will be used to repeat this experiment in the future. Before these antibodies are used for experimental applications the optimal working conditions of these antibodies must be determined and the specificity of these antibodies for Lrrk2 must be validated. To do this a similar protocol will be followed as for the Pitx3 custom antibody, this is described in Chapter 3 section 3.5.1.2.

As expression of mouse miR-205 is not detectable in the brain until 1 month it may be possible that the miR-205-*lrrk2* interaction is not meaningful in zebrafish until later in development. To ensure that data suggesting that the interaction is not present in zebrafish is not false-negative, these interaction experiments should be carried out in relevant tissue at a range of ages. As knockdown using MOs is transient, to do this a miR-205 inhibitor, mimic or a stable knockout line could be used.

Future work for investigation of miR-205 and Lrrk2 in zebrafish

Firstly, the presence of an interaction between miR-205 and *lrrk2* in zebrafish must be validated. The strategy for achieving this is discussed above. Once this interaction is validated the functional consequences may be examined in more detail.

As discussed in the previous sections further work to determine whether miR-205 has true expression in the brain should be performed. In mice the expression of miR-205 in the brain gradually increases from 1 month to 18 months, this correlates with the decrease in LRRK2 protein levels (Cho et al. 2013). Once an antibody has been validated for zebrafish Lrrk2 these experiments could be replicated to provide indirect evidence of an interaction and show that the expression of both miR-205 and Lrrk2 is relevant over the life of the zebrafish.

The loss of dopaminergic neurons must be investigated in more detail to determine whether this observed effect is specific or a toxic effect of the injected MO. To do this a stable miR-205 knockout line could be generated to assess the effects of this knockdown over a longer period. In mice knockout of miR-205 resulted in partially-penetrant postnatal lethality (Farmer et al. 2013). These mice exhibit skin defects. Although the internal organs which exhibited miR-205 appeared morphologically normal, the authors speculate that the lethality may be due to a digestive dysfunction. It would be interesting to investigate whether miR-205 plays the same developmental role in zebrafish. If premature death due to non-neuronal related phenotypes was observed a conditional knockout of miR-205 in brain tissue could be utilised to study the specific neuronal effects of this miRNA.

As Cho and colleagues suggest, miR-205 has potential as a therapeutic target in PD, however the beneficial effects of miR-205 overexpression have only been studied in cell culture models (Cho et al. 2013). It would be beneficial to study this in an *in vivo* model which displays neurotoxicity related to LRRK2 overexpression or mutation. As there is minimal evidence of neurodegeneration in murine models expressing WT or mutated *LRRK2* (Li et al. 2009) new models which are able to demonstrate the neurotoxicity of mutant LRRK2 (or overexpression of WT LRRK2) are needed. In the Bandmann lab the CRISPR/Cas9 system is currently being utilised to generate a point mutation in zebrafish *lrrk2* corresponding to the G2019S mutation. Once developed, characterisation of this line will help add to the body of knowledge of the effect of this mutation, specifically the α -synuclein-independent effects of this mutation. If a neurotoxic effect is seen with this model, miR-205 overexpression can be tested to determine whether this modulation of expression levels of the mutated *Lrrk2* is able to ameliorate the phenotype.

Chapter 5. miR-155 and the role of neuroinflammation in neurodegeneration

Contents

Chapter 5. miR-155 and the role of neuroinflammation in neurodegeneration	156
5.1 Introduction	158
Inflammation in Parkinson's disease	158
The involvement of miR-155 in inflammation and immunity.....	158
miR-155 and neurodegenerative disease	160
5.2 Expression levels of miR-155 in PD zebrafish models.....	161
5.2.1 Optimisation	162
5.2.1.1 Testing miRNA qPCR reference genes	162
5.2.1.2 Validation of using the QuantiFluor™ RNA system to control for loading ..	163
5.2.2 Results	164
5.2.2.1 miR-155 expression levels in <i>gba1</i> mutant zebrafish	164
5.2.2.2 Spatial expression of miR-155 in <i>gba1</i> mutant larvae	165
5.2.2.3 miR-155 expression levels in <i>pink1</i> and <i>parkin</i> deficient zebrafish	165
5.3 Expression of downstream markers of miR-155 in GD zebrafish	166
5.3.1 Optimisation	166
5.3.1.1 Identification of suitable markers.....	166
5.3.2 Results	167
5.3.2.1 Expression of TNF α and IL8 orthologues in <i>gba1</i> mutants	167
5.4 Using the CRISPR/Cas9 system to create a miR-155 KO zebrafish line	168
5.4.1 Design and testing of CRISPR/Cas9 targets sites in miR-155	169
5.4.2 Raising miR-155 CRISPR injected zebrafish and line management.....	173
5.5 Discussion.....	174
miR-155 expression in zebrafish models of PD and Gaucher's disease.....	174
Expression of relevant inflammatory markers in <i>gba1</i> mutant zebrafish	175
Generation of a miR-155 knockout line and future work.....	176
Summary	177

5.1 Introduction

Inflammation in Parkinson's disease

Inflammation in the brain is a common contributor in neurodegenerative diseases (Amor et al. 2014). In post-mortem studies of PD patient brains, activated microglia and increased concentrations of pro-inflammatory cytokines have been identified within the *substantia nigra* (McGeer et al. 1988; Boka et al. 1994). These data show that there is an increase in inflammatory processes in the brain of PD sufferers, however they do not determine whether this effect is causative or a consequence of neuronal cell death. It has been shown that neuromelanin, which is released from dying dopaminergic neurons, is able to elicit an immune response (Wilms et al. 2003). *In vivo* studies in PD patients and studies in animal models of disease can help elucidate the role of inflammation in PD. An increase of pro-inflammatory cytokines has been detected in patient serum and cerebrospinal fluid (CSF) (Dobbs et al. 1999; Mogi et al. 1994), showing that these changes are taking place during the course of disease. Genetic studies of risk factors for PD and epidemiological studies also support the role of inflammation. Mutations in a number of genes involved in inflammation are associated with increased risk of PD, while a decreased risk of PD has been associated with use of ibuprofen (a non-steroidal anti-inflammatory drug), reviewed by Hirsch & Hunot (2009).

Many of the inflammatory changes observed in PD patients can be identified in animal models of PD. In a mouse model of PD it was shown that microglial activation caused by injections of MPTP preceded neuronal loss. Furthermore, the inhibition of microglial activation mitigates the damage to neurons (Wu et al. 2002). To further support the role of inflammation as a causative mechanism of neuronal loss in PD, directly inducing an episode of neuronal inflammation in rodent brains by exposure to bacterial lipopolysaccharide (LPS), a potent activator of both peripheral immune cells and glial cells, results in a specific loss of dopaminergic neurons reminiscent of PD (Dutta et al. 2008).

The involvement of miR-155 in inflammation and immunity

miRNAs have been implicated in inflammation, including critical roles in inflammation in the CNS mediated by microglia (Su et al. 2015). Perhaps the best studied of these miRNAs is miR-155.

Before the discovery of miRNAs the primary transcript of miR-155 was known as *bic* (B-cell integration cluster). This was characterised as a gene that was activated in B-cell lymphomas by a promoter insertion upstream of this gene at a common retroviral integration site. It was

later discovered that pre-miR-155 is encoded within *bic*, this gene is now more commonly referred to as the miR-155 host gene. miR-155 is highly conserved in all jawed vertebrates. Jawless vertebrates utilise an alternative system for receptor diversification, thus suggesting that miR-155 developed alongside the beginnings of antigen receptors (Vigorito et al. 2013).

Figure 71A shows the alignment of pre-miR-155 sequences from humans, mice, chickens, *Xenopus tropicalis*, zebrafish and *Ciona intestinalis*. *C. intestinalis* is the most primitive species which contains miR-155. Although it does not contain a well-developed adaptive immune system as is present in jawed vertebrates it is thought to contain core elements of rearranging antigen receptors (Kasahara et al. 2004). This alignment shows that the mature sequence of miR-155 (but not miR-155*) is highly conserved in all of these species and the seed sequence, the major determinant of target specificity, is 100% conserved. Figure 71B shows a relationship tree based on the alignment in Figure 71A.

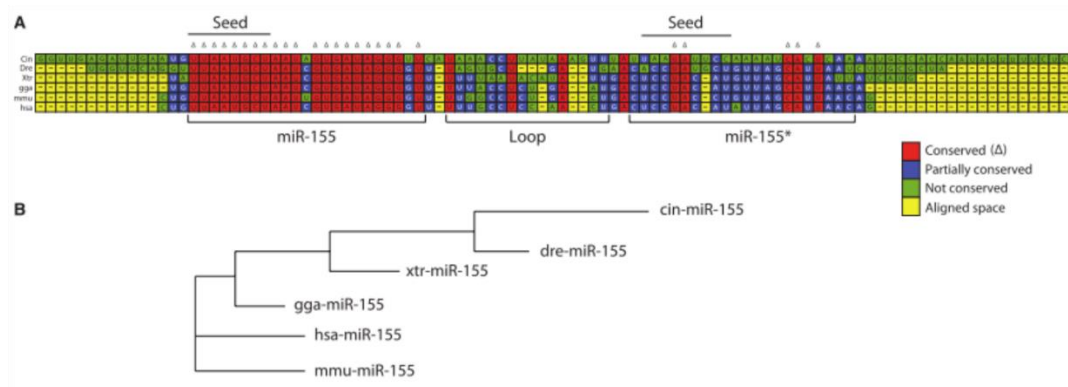


Figure 71. Conservation of miR-155 across species. Reproduced with permission from Vigorito et al. (2013).

miR-155 is a typical multifunctional miRNA which is involved in haematopoiesis, B-cell and T-cell regulation, immunity and inflammatory process (Faraoni et al. 2009). It was also one of the first miRNAs to be considered “oncogenic” after it was shown that overexpression of miR-155 in B-cells in mice leads to B-cell lymphoma (Costinean et al. 2006).

miR-155 is upregulated in activated T and B-cells and is thought to play an important role in their development and function (Rodriguez et al. 2007). In miR-155 deficient mice, both T-cell dependent and independent functions are impaired. miR-155 deficient mice have reduced number and size of germinal centres, the outcome of germinal centres is also impaired resulting in decreased production of high-affinity antibody and reduced number of memory

B-cells (Thai et al. 2007). After infection with *Salmonella* mice containing miR-155 deficient B-cells also demonstrate reduced production of IgM and IgG antibodies (Vigorito et al. 2013).

T-cells are also influenced by miR-155 expression. Overexpression of miR-155 in CD4⁺ T cells drove Th1 cell proliferation (Banerjee et al. 2010) while miR-155 deficient mice have a reduced number of both Th1 and Th17 cells (O'Connell et al. 2010). Th17 cells are involved in mediation of chronic autoimmune inflammation (Langrish et al. 2005), these data therefore suggest the miR-155 is important for T-cell mediated immunity and autoimmune responses. This is further evidenced by the finding that miR-155 deficient mice are highly resistant to experimental autoimmune encephalitis (EAE) and autoimmune arthritis (Blüml et al. 2011; O'Connell et al. 2010).

Pro-inflammatory stimuli, such as LPS, and inflammatory mediators, such as TNF α are able to upregulate miR-155 expression in a number of immune cells, including macrophages and microglia (Cardoso et al. 2012; O'Connell et al. 2007). In microglia, the resident immune cells of the CNS, miR-155 has been shown to be activated by p53 and push microglia towards a pro-inflammatory phenotype through suppression of the anti-inflammatory transcription factor c-Maf (Su et al. 2013).

Other notable targets of miR-155 which mediate its pro-inflammatory function include suppressor of cytokine signalling-1 (SOCS1) and src homology 2 domain-containing inositol-5-phosphatase 1 (SHIP1) (O'Connell et al. 2009; Wang et al. 2010). These genes are negative regulators of the immune response through inhibition of JAK-STAT signalling and mediation of proteosomal degradation of key elements of pro-inflammatory pathways (SOCS1), and suppression of the P13K pathway through negative regulation of Akt (SHIP1).

miR-155 and neurodegenerative disease

Inflammation in the brain is associated with many neurodegenerative disorders and brain injury. As discussed above microglia are the resident immune cells of the brain, their function is regulated by miR-155 thus suggesting this miRNA may play an important role in mediating inflammatory responses in neurodegenerative disease.

Studies in patients have shown that miR-155 is upregulated in tissue from patients suffering from both multiple sclerosis and MND (Junker et al. 2009; Butovsky et al. 2015). Increases in the expression of this miRNA is also seen in animal models of neurodegenerative disease, including rodent models of Alzheimer's Disease, multiple sclerosis and MND (Guedes et al. 2014; Butovsky et al. 2015; Murugaiyan & Beynon 2011) and other animal models which

exhibit neuroinflammation through alcohol consumption (Lippai et al. 2013) or through infection with the Japanese Encephalitis Virus (Thounaojam et al. 2014). Knockdown of miR-155 has also been shown to be neuroprotective. Loss of miR-155 ameliorated disease severity in both SOD1 mutant mice (a model of MND) and in EAE (a model of multiple sclerosis) showing that it plays a key role in the pathogenesis of these diseases (Butovsky et al. 2015; Murugaiyan & Beynon 2011).

The aim of this study is to assess whether miR-155 is involved in inflammation in zebrafish models of PD. Expression of miR-155 will be investigated in two models of early onset PD, that is, *pink1*- and *parkin*-deficient zebrafish, and a third model which demonstrates *gba1*-deficiency.

In humans, mutations in *GBA* are the most common risk factor for PD (Neumann et al. 2009), whilst homozygous mutations in this gene cause Gaucher's disease, a lysosomal storage disorder. Gaucher's disease patients exhibit a wide range of symptoms of varying severity. A key feature of Gaucher's disease which is thought to underlie the multi-systemic features of this disease is the accumulation of Gaucher's cells. These are glycolipid-engorged macrophages, which accumulate in many organs including the brain (Baris et al. 2014). It is thought that these pathological macrophages are the source of increased inflammatory markers observed in Gaucher's disease patients (Panicker et al. 2014). Moreover, neuroinflammation is thought to be a contributing feature to the neurodegeneration in neuronopathic forms of Gaucher's disease. Progressive microglial activation and increases in inflammatory markers in the brain of mouse models of neuronopathic Gaucher's disease correlate with neuron loss (Vitner et al. 2012; Farfel-Becker et al. 2011).

Glial activation is a common feature in both Parkinson's and Gaucher's disease brain (Ginns et al. 2014), and increased levels of inflammatory markers have been identified in PD patients carrying *GBA* mutations (Chahine et al. 2013) suggesting neuroinflammation is a common feature of these diseases. miR-155 has not yet been implicated in the pathology of either Parkinson's or Gaucher's disease.

5.2 Expression levels of miR-155 in PD zebrafish models

In order to investigate the expression of miR-155 by qPCR a suitable reference gene first had to be determined. In previous chapters, qPCR for miRNA was only performed to validate specific changes in miRNA expression caused by injection of a MO or miRNA mimic. For these experiments an unrelated miRNA, which was not expected to be altered by this specific

MO/mimic, was used as a reference gene. In this chapter, this method cannot be used as it is possible that a large number of miRNAs may have altered expression in the genetic models of PD utilised in this study. Therefore, a miRNA reference gene must be chosen with care to ensure its stability in the models being used.

5.2.1 Optimisation

5.2.1.1 Testing miRNA qPCR reference genes

In order to choose a small number of miRNAs for testing as potential reference genes a literature search was performed to investigate what miRNAs have been used as reference genes by other groups performing qPCR, specifically using the taqman miRNA assays, for miRNAs in zebrafish. The most commonly used reference gene was U6 small RNA. Unexpectedly, very few publications provided evidence that the miRNA they used as a reference gene has stable expression in the range of samples being investigated.

Applied Biosystems do not produce a taqman miRNA assay specific for zebrafish U6, however it is possible to order custom assays, therefore a U6 assay was ordered. Another miRNA of interest is miR-24. This miRNA has already been used in-house as a reference gene for human PD samples (Mandal 2014). The zebrafish miR-24 sequence is 100% homologous to the human sequence. The stability of miR-24 and U6 snRNA were assessed in a range of RNA samples from zebrafish brain. To ensure accurate levels of RNA loaded into the reverse transcription reaction the QuantiFluor™ RNA system (Promega) and the Qubit® fluorometer (Life Technologies) were used. Firstly, the efficiency of the primers was assessed. Both assays had an efficiency of close to 100%. The samples used to test the stability of these small RNAs, all from zebrafish brain, were: 6 WT samples (of varying ages), 2 *pink1*^{-/-} samples, 2 *gba1*^{+/-} and 2 *gba1*^{-/-} samples. The Ct values for U6 were highly variable in this range of samples, thus showing it is unsuitable for use as a reference gene (Figure 72A). miR-24 is much more stable in this range of samples (Figure 72B and C). miR-24 demonstrated stable expression in samples from wild type and *pink1*^{-/-} brains, however the expression was not stable in *gba1* mutant zebrafish brains. This shows that this miRNA is unsuitable for use as a reference gene in this range of samples.

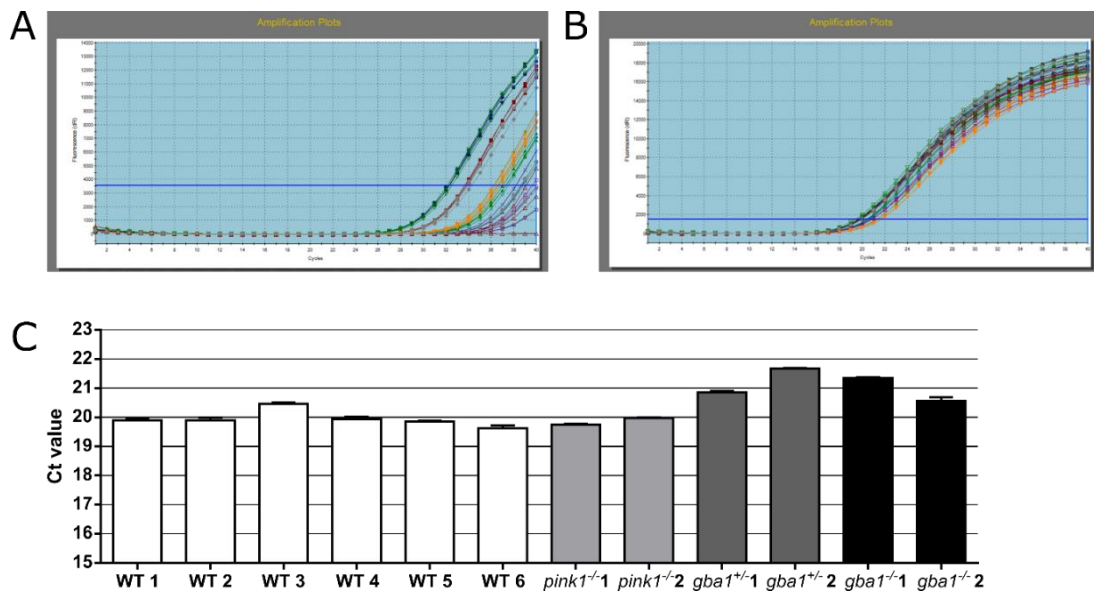


Figure 72. Stability of zebrafish U6 snRNA and miR-24 in a range of samples. A and B show the amplification plots of U6 and miR-24, respectively. The amplification plot for U6 shows that the Ct vary dramatically in this range of samples and are very high. This indicates that U6 is not a suitable reference gene for these samples. The amplification plot for miR-24 show that the Ct values are much more similar. C shows the Ct values for each of the 12 groups tested. miR-24 expression levels are stable in samples from wild types and pink^{-/-} zebrafish brains with a Ct value of close to 20. However miR-24 is not stable in gba1 mutant zebrafish brains who show a higher Ct value.

5.2.1.2 Validation of using the QuantiFluor™ RNA system to control for loading

As a suitable reference gene was not identified, use of the QuantiFluor™ RNA system to accurately measure RNA levels was investigated to determine whether this system could be used to control for loading rather than using a reference gene. To do this two of WT samples and *gba1* mutant samples used for the previous experiments were used to repeat the entire process, from RNA quantification to qPCR, to assess the similarity of the results. These results were expressed as a fold change compared to the average of the WT expression levels. As shown in Figure 73, the two replicates match very closely with the fold change differing by no more than 0.2. For subsequent experiments miRNA expression analysis will be performed using the QuantiFluor™ RNA system to accurately measure RNA levels so exactly 100ng can be loaded into the reverse transcription reaction. As this is not a standard protocol due care will be taken to ensure the loading is as accurate as possible and small fold changes will be treated with caution.

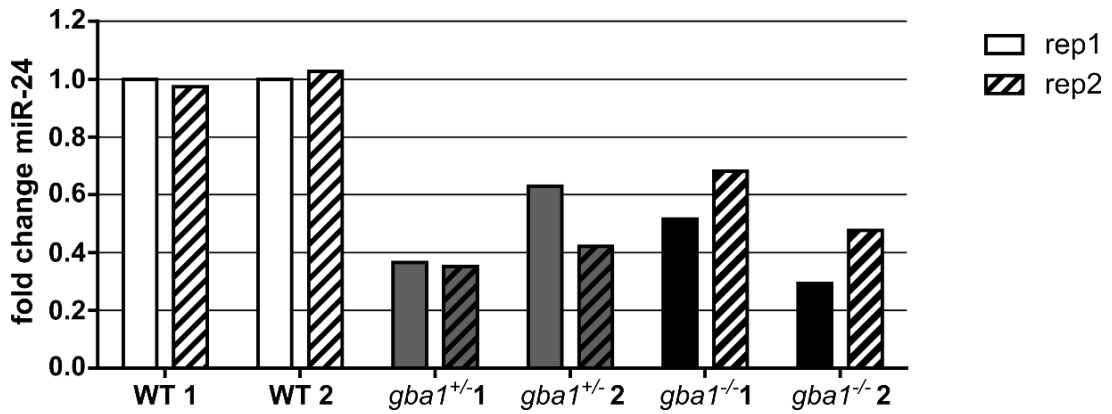


Figure 73. Reliability of qPCR results using accurate RNA quantification. These data show the similarity of the results from two separate replicates performed with the same samples. In each experiment the results are expressed as fold change from the average of the WT samples. The variation between the two replicates is minimal; the fold change differs by no more than 0.2.

5.2.2 Results

5.2.2.1 miR-155 expression levels in *gba1* mutant zebrafish

As discussed above inflammation is a major feature of Gaucher's disease. The expression levels of miR-155 were examined in whole *gba1* mutant larvae and 3 month old brains (Figure 74). In larvae a 2 fold increase in miR-155 levels was observed in the *gba1*^{-/-} compared to WT. This indicates that inflammation is being driven from a very early age in *gba1*-deficient zebrafish. At the 3 month time point there is a striking 5 fold increase in *gba1*^{-/-} compared to WT. 3 months of age is the end-stage of disease in the *gba1*^{-/-} zebrafish. There is no change in miR-155 expression levels in *gba1*^{+/-} brains at this age.

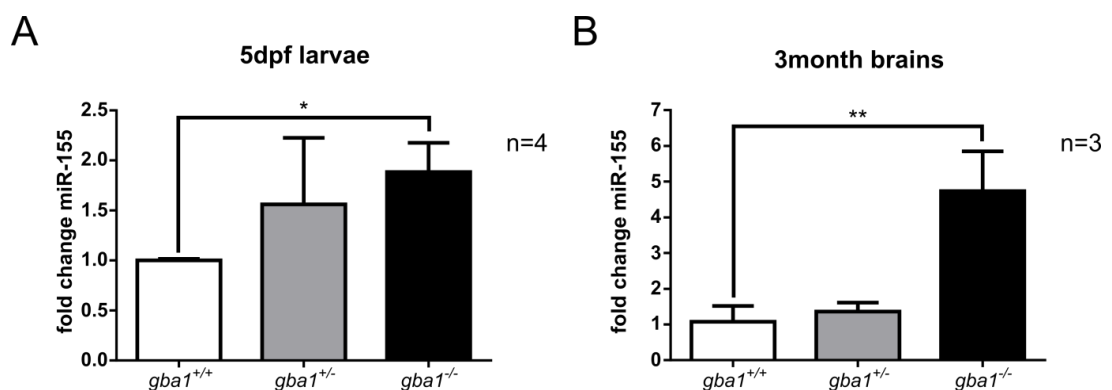


Figure 74. miR-155 expression levels are increased in *gba1* mutant brains and larvae. miR-155 levels are analysed by qPCR. A shows miR-155 expression in 5dpf larvae. B shows miR-155 expression in 3month old brains. Error bars represent standard deviation. Data were analysed by one-way ANOVA with Bonferroni post-tests. * = $p < 0.05$, ** = $p < 0.01$.

5.2.2.2 Spatial expression of miR-155 in *gba1* mutant larvae

To determine if the upregulation of miR-155 indicated by qPCR is driven by overexpression in a particular organ or whether this expression is diffuse within the embryo WISH was performed using an LNA probe for miR-155. The spatial expression pattern of miR-155 in 5dpf *gba1* mutant zebrafish is shown in Figure 75.

In *gba1*^{+/+} (WT) larvae miR-155 does not appear to be spatially restricted and displays diffuse expression within the brain and trunk of the larvae. In *gba1*^{+/-} larvae this staining pattern and intensity was very similar to the WT larvae. In *gba1*^{-/-} larvae the staining intensity appears to be darker over the whole larvae, indicating that the increased expression of miR-155 is systemic rather than specific to a particular organ.

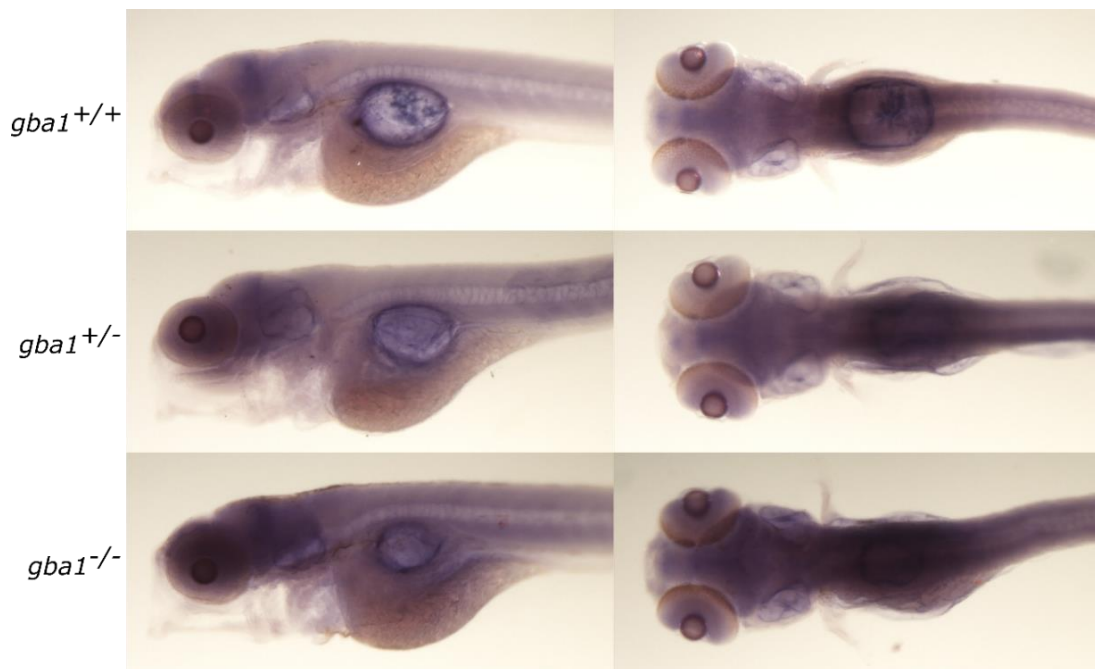


Figure 75. Spatial expression of miR-155 in *gba1* mutants. WISH for miR-155 was performed in *gba* genotypes to determine spatial expression of this miRNA.

5.2.2.3 miR-155 expression levels in *pink1* and *parkin* deficient zebrafish

miR-155 expression was then assessed in zebrafish models of early onset PD, in both adult brain and in 5dpf larvae. No change in miR-155 expression can be detected in 5dpf larvae or aged brains of *pink1*^{-/-} or *parkin*^{-/-} zebrafish. Brains were from 2.5 year old *pink1*^{-/-} and WT siblings or 1.5 year old *parkin*^{-/-} and WT siblings. Although there is a very slight increase in

both *pink1*^{-/-} and *parkin*^{-/-} 5dpf larvae this is not significant. The expression data is highly variable in the aged brains.

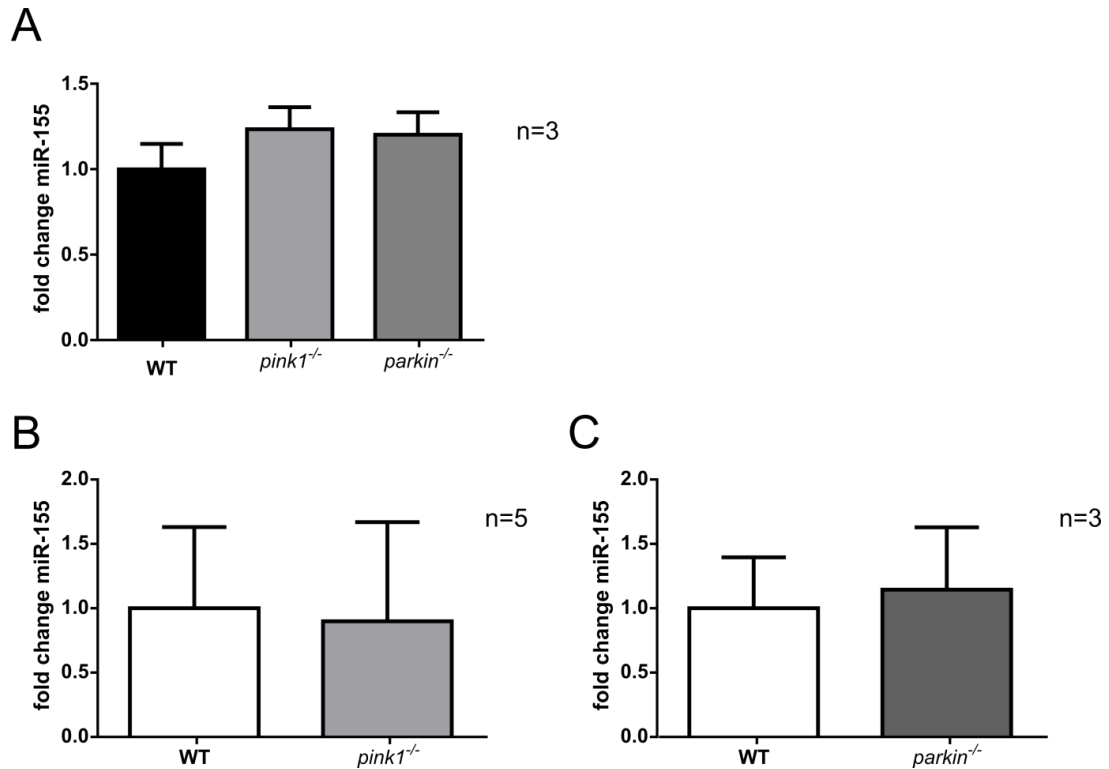


Figure 76. miR-155 expression is not altered in PD zebrafish larvae and adult brains. miR-155 expression was assessed by qPCR. **A** shows the expression data for WT, *pink1*^{-/-} and *parkin*^{-/-} 5dpf larvae. Data are analysed by one-way ANOVA with Bonferroni post-tests, $p > 0.05$. **B** shows expression data for WT and *pink1*^{-/-} 2.5 year old brains and **C** shows expression data from WT and *parkin*^{-/-} 1.5 year old brain. Error bars represent standard deviation. Data in **B** and **C** are analysed by an unpaired t-test with Welch's correction, $p > 0.05$.

5.3 Expression of downstream markers of miR-155 in GD zebrafish

5.3.1 Optimisation

5.3.1.1 Identification of suitable markers

To determine whether the observed increase in miR-155 expression in *gba1*^{-/-} zebrafish also has an effect on downstream markers of inflammation relevant to Gaucher's disease and PD a literature search was carried out to identify suitable markers. Three publications describing gene expression changes in PD patients with and without *GBA* mutations (Chahine et al. 2013), in Gaucher's disease patient serum (Barak et al. 1999) and in the brain of a mouse model of Gaucher's disease (Vitner et al. 2012) were studied to generate a short list of inflammatory markers that are increased.

Table 18. Inflammatory markers increased in GD patients, *gba1* deficient mouse brains and PD patients with GBA mutations.

Inflammatory marker	Increased in	reference
Interleukin-8 (IL-8)	PD patients with <i>GBA</i> mutations (blood plasma)	(Chahine et al. 2013)
Monocyte chemoattractant protein-1 (MCP-1)	PD patients with <i>GBA</i> mutations (blood plasma)	(Chahine et al. 2013)
interleukin-1 receptor antagonist (IL-1RA)	Gaucher's disease patient serum	(Barak et al. 1999)
Soluble interleukin-2 receptor (sIL-2R)	Gaucher's disease patient serum	(Barak et al. 1999)
Interleukin-1 beta (IL-1 β)	Gaucher's disease patient serum and brain of a <i>Gba</i> -deficient mouse	(Barak et al. 1999; Vitner et al. 2012)
Tumour necrosis factor- α (TNF α)	Gaucher's disease patient serum and brain of a <i>Gba</i> -deficient mouse	(Barak et al. 1999; Vitner et al. 2012)
Tumour necrosis factor- α receptor (TNF α -r)	Brain of a <i>Gba</i> -deficient mouse	(Vitner et al. 2012)
Macrophage colony stimulating factor (M-CSF)	Brain of a <i>Gba</i> -deficient mouse	(Vitner et al. 2012)
Transforming growth factor β (TGF β)	Brain of a <i>Gba</i> -deficient mouse	(Vitner et al. 2012)

From the short-list shown in Table 18, IL-8 and TNF α were chosen as markers of interest as these have also previously been shown to be regulated by miR-155 (Min et al. 2014; Pathak et al. 2015; Lippai et al. 2013).

5.3.2 Results

5.3.2.1 Expression of TNF α and IL8 orthologues in *gba1* mutants

Zebrafish possess two orthologues of both TNF α (*tnfa* and *tnfb*) and IL-8 (CXCL8-I1 and CXCL8-I2). For both genes both orthologues are thought to be functional (Bates et al. 2007; de Oliveira et al. 2013). qPCR was performed for these markers to assess their expression level in 5dpf larvae and 3 month brains of *gba1*^{+/+} and *gba1*^{-/-} zebrafish. In the 5dpf larvae

there is a trend towards an increase in expression in three out of the four markers. Although none of these markers reach significance individually the overall effect of *gba1* deficiency on these markers is significant ($p=0.0353$). In 3 month old brains both orthologues of *IL-8* and *tnfb* show a substantial 15- to 20-fold increase (Figure 77C). A two-fold increase of *tnfa* is observed however this is not significant.

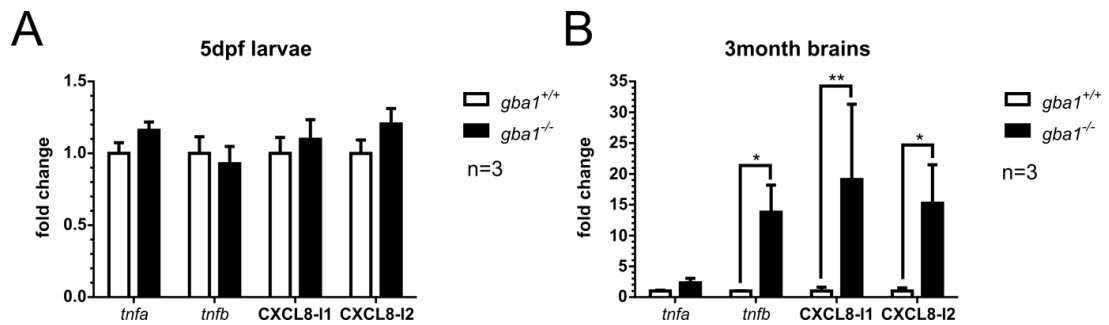


Figure 77. Expression of inflammatory markers in *gba1* mutant brains and larvae. mRNA levels of zebrafish orthologues of inflammatory markers TNF α (*tnfa* and *tnfb*) and IL8 (CXCL8-I1 and CXCL8-I2) were assessed by qPCR. **A** shows expression of inflammatory markers in 5dpf larvae. Although none of the markers reach significance individually the overall effect of *gba1*-deficiency on these markers is significant ($p=0.0353$). **B** shows expression of inflammatory markers in 3 month brains. *tnfb*, CXCL8-I1 and CXCL8-I2 have significantly increased expression at this age. Error bars represent standard deviation. Data are from 3 biological replicates and are analysed by two-way ANOVA with Bonferroni post-tests. * = $p<0.05$, ** = $p<0.01$.

5.4 Using the CRISPR/Cas9 system to create a miR-155 KO zebrafish line

In order to generate a stable mutant line deficient for miR-155 the CRISPR/Cas9 system was utilised. This system is present in bacteria as a prokaryotic immune system. Fragments of DNA from invading viruses are stored by the bacteria and spliced into a region of the bacterial genome containing clustered regularly interspaced short palindromic repeats or CRISPRs. When this region is transcribed, the guide-RNA can then be used to guide CRISPR-associated (Cas) nucleases to the viral DNA and cleave it, thus preventing replication of the virus (Bhaya et al. 2011).

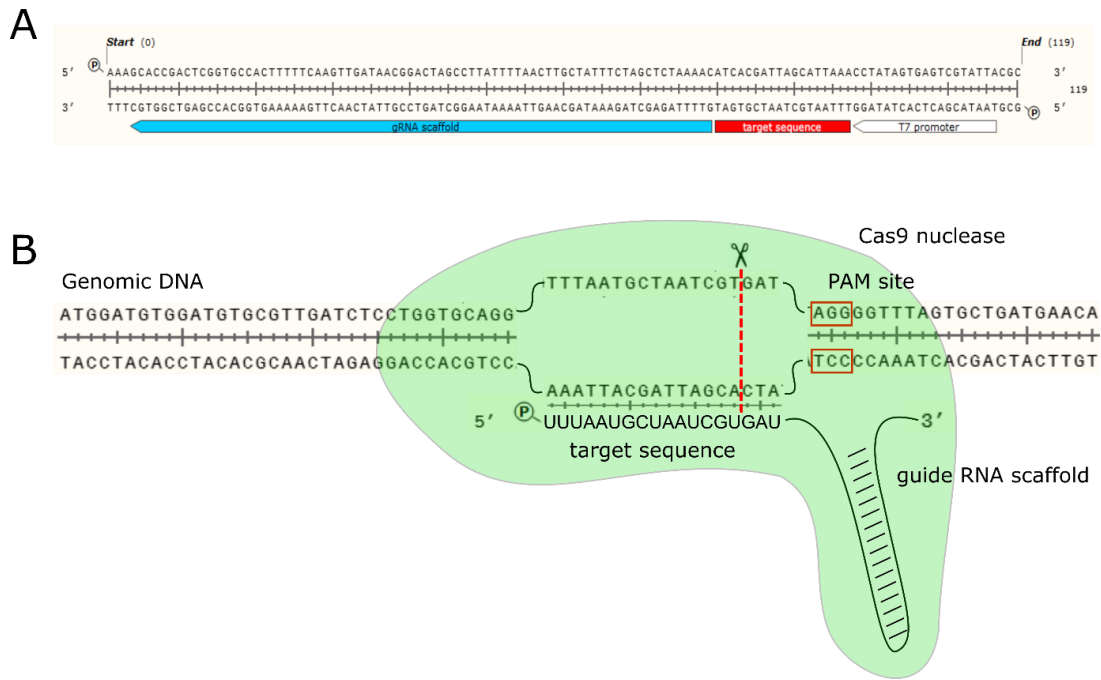


Figure 78. CRISPR/Cas9 gene editing system. *A* shows the design of an ultramer, from which the guide RNA can be transcribed. *B* shows the guide RNA recruiting the cas9 nuclease to the CRISPR site.

The potential of this system was realised in 2012 (Hale et al. 2013); since then the development of the CRISPR/Cas9 system for gene-specific editing has gained momentum and is now a popular tool in many model organisms (Varshney et al. 2015; Wang et al. 2013; Hou & Zhang 2013). To generate site specific mutations a user-designed target sequence is placed between a T7 promoter and a guide RNA scaffold sequence (Figure 78A). When transcribed the target sequence binds to the genomic DNA and the guide RNA scaffold recruits Cas9 nuclease to the CRISPR site within the gene of interest (Figure 78B). Cas9 will cleave the DNA 3 bases upstream of the PAM site (NGG). Mutations can then be generated due to error prone repair, homology directed repair (for example if another fragment of DNA is co-injected), or large (targeted) deletions can be generated if two CRISPR sites are cut simultaneously.

5.4.1 Design and testing of CRISPR/Cas9 targets sites in miR-155

To allow mutations caused by the CRISPR/Cas9 system to be easily identified PAM sites close to large restriction sites such as *Mwo1* and *Bs1* are preferable. These are optimal sites to use for CRISPR as they are large and therefore relatively easy to disrupt. *Mwo1* site is GCNNNNNNNGC and the *Bs1* site is CCNNNNNNNCC. *Bs1* sites naturally contain PAM sites which gRNAs can be targeted to. miR-155 contains a number of *Bs1* and *Mwo1* sites which

can be used as CRISPR targets. Four gRNAs were designed to such sites. The aim was to either generate a large deletion removing the miR-155 coding sequence entirely or to cause a disruption within the miR-155 coding sequence. Figure 79 shows these sites and where the CRISPR cuts the DNA.

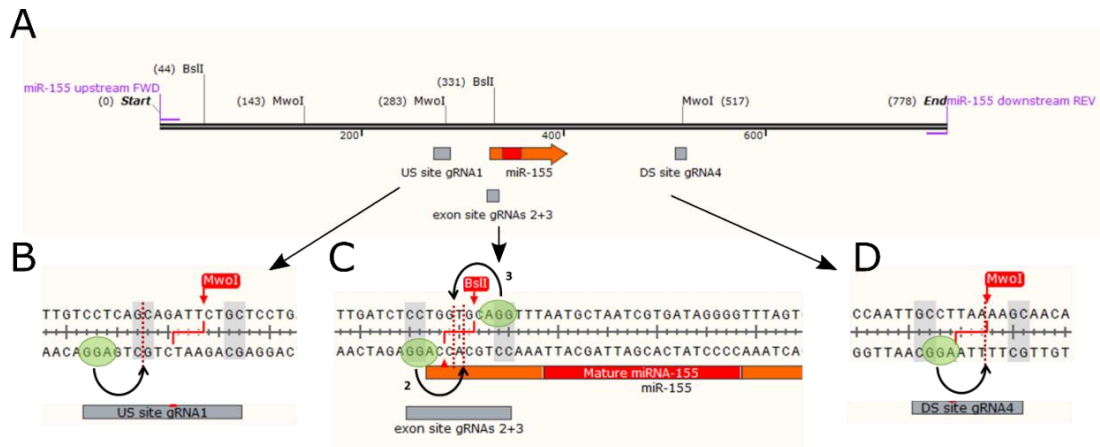


Figure 79. CRISPR sites in miR-155 region. This figure shows CRISPR sites present within and in the region around miR-155. A shows an overview of the miR-155 region with the miR-155 exon shown in orange and CRISPR sites marked. All Bsl1 and Mwo1 restriction sites are also labelled. B-D show the individual sites in detail. The restriction site is shaded on the DNA and its cut site labelled with a red line. The PAM site is circled in green with an arrow and dotted line marking the site where Cas9 will cut the DNA. US = upstream, DS = downstream.

The gRNAs listed above were injected into one-cell stage zebrafish embryos in pairs. The injected pairs were: gRNA1+4, gRNA2+4, gRNA3+4 and gRNA2+3. To test the efficacy of the injected CRISPRs DNA was extracted from four embryos from each injected group. PCR was performed to amplify the region of interest. This was run on an analytical gel to determine whether any large deletions had been created. As shown in Figure 80A, no large deletions were detected after injection of these pairs of gRNAs. As no large deletions were detectable, it was determined whether gRNAs 2 or 3 had induced any mutations. To do this the PCR product from embryos injected with this pair of gRNAs was digested with *Bsl1*. If the *Bsl1* site is disrupted in the injected embryos a 734bp fragment would be expected. Figure 80B shows the fragments after digest with *Bsl1*. A very faint band the size of the undigested fragment is detectable in the gRNA injected samples suggesting the *Bsl1* site present at the beginning of the miR-155 exon is disrupted in some cells. As the cut site for gRNAs 2 and 3 are within the exon of miR-155 mutations caused by this CRISPR may disrupt the transcription, processing or mature sequence of miR-155.

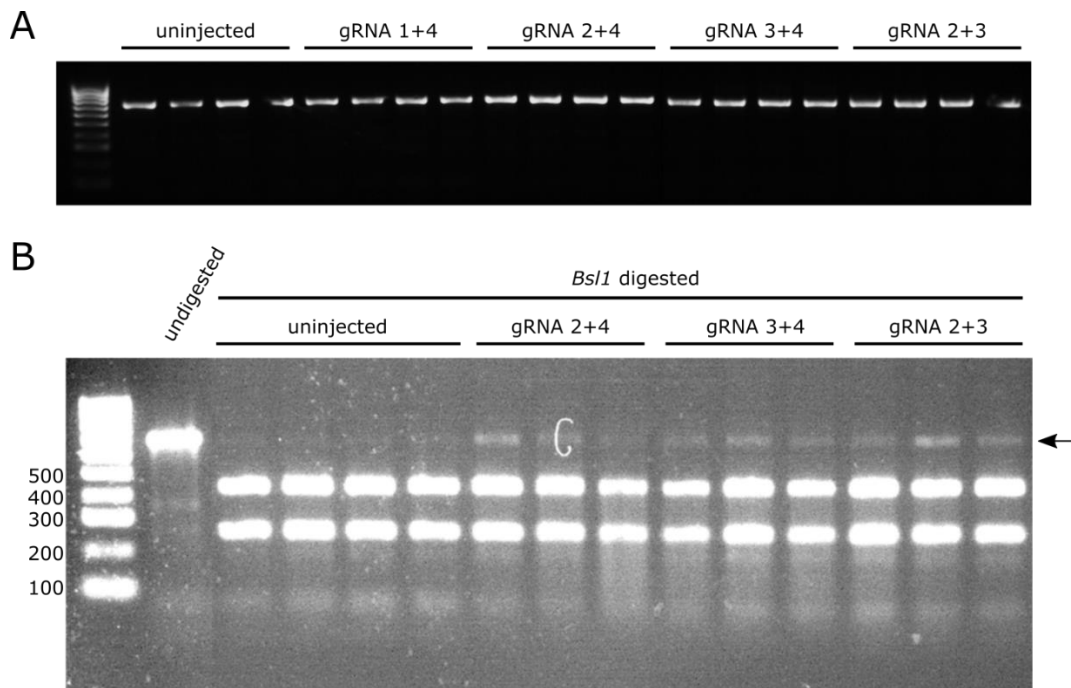


Figure 80. Analysis of efficacy of miR-155 CRISPRs. The efficacy of miR-155 CRISPRs was analysed by PCR (to screen for large deletions/insertions) and restriction digest to screen for disruption of restriction sites by small mutations. **A** shows an analytical gel showing the PCR products generated from uninjected embryos and embryos injected with each of the 4 pairs of gRNAs. No large deletions or insertions are detected. **B** shows an analytical gel of the PCR products from embryos injected with gRNA2 and/or 3 digested by *Bsl1*. In uninjected embryos the expected fragments can be seen (44bp and 287bp and 447bp). In the injected embryos a faint band at ~734bp (marked with an arrow) can be seen. This suggests that the *Bsl1* restriction site is disrupted in some cells.

To determine what mutations are caused by disruption of CRISPR sites 2 or 3 the products generated by the original PCR were cloned into the *TOPO*[®] vector. This method allows the individual products to be separated so they can be analysed individually. 90 colonies were analysed and it was assessed whether any of these fragments were mutated by PCR and digestion with *Bsl1*. No mutated products were detected. This shows that although the undigested fragment was detected in the first experiment these CRISPRs are not efficacious and very few mutations are created.

Although there are no other suitable CRISPR target sites within *Mwo1* or *Bsl1* restriction sites, there are other target sites which can be assayed using different restriction enzymes. A site within the mature miR-155 sequence was found. This site is within an *Hpy188III* (TCNNGA) restriction site. A gRNA (gRNA5) was designed to recruit Cas9 to this site. As the site is within the mature miR-155 sequence it is likely that miR-155 function will be disrupted by this CRISPR, even if only small mutations are made. Figure 81A shows the location of the gRNA5 target site within the miR-155 coding region. After injection of gRNA5 embryos were collected at 24hpf to extract DNA. PCR was performed to amplify this region and the efficacy

of the CRISPR was assessed by digestion with *Hpy188III*. This CRISPR appears to have a high efficacy as the digested products are virtually undetectable in gRNA5 injected embryos (Figure 81B). This shows that in almost all cells the *Hpy188III* restriction site present within the miR-155 exon is disrupted and therefore this DNA fragment cannot be digested.

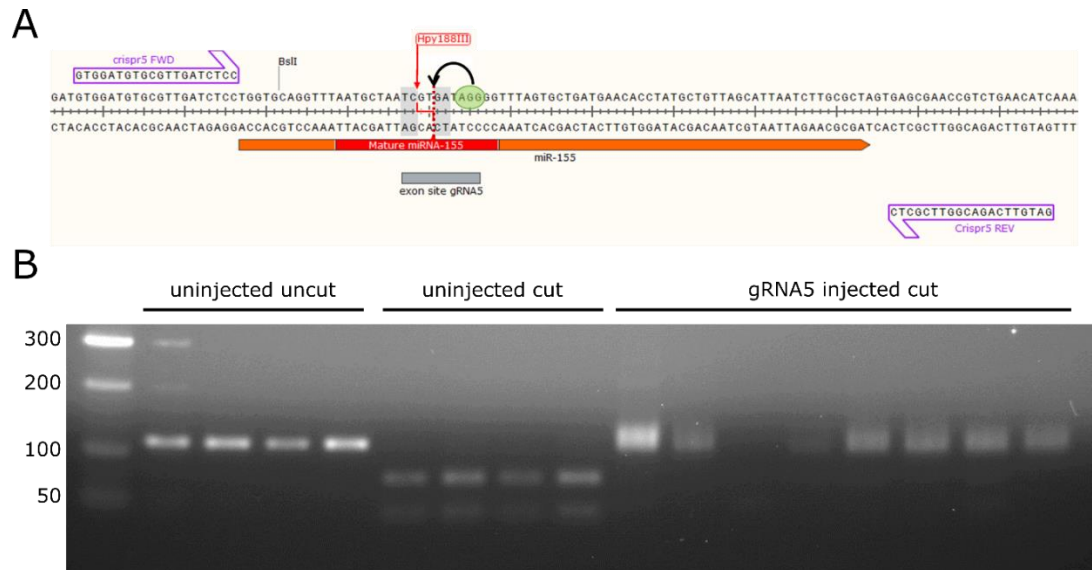


Figure 81. Design and efficacy of miR-155 gRNA5. A shows the miR-155 exon, the primers which will be used to amplify it and the location of the target site for gRNA5. The *Hpy188III* restriction site is shaded on the DNA and its cut site labelled with a red line. The PAM site is circled in green with an arrow and dotted line marking the site where Cas9 will cut the DNA. B shows an analytical gel showing the uncut product (120bp) and fragments from the digest with *Hpy188III* in uninjected and gRNA5 injected embryos.

In order to examine individual mutations caused by this CRISPR, *TOPO[®] TA* cloning was performed and 30 samples were sent for direct sequencing. Table 19 shows a selection of the mutations that are generated by injection of gRNA5 and Cas9 protein. These mutations are likely to disrupt the function of miR-155 as a large part of the mature sequence is deleted or there is an insertion the will likely disrupt the correct processing of the pri-miRNA.

Table 19. Mutations caused by miR-155 CRISPR5. Mature miRNA sequence is shown in red.

	Sequence	mutation
WT	GTGGATGTGCGTTGATCTCCTGGTGCAGGTTT AATGCTAATCGTGATAGGGG TTTA GTGCTGATGAACACCTATGCTGTTAGCATTAATCTTGCCTAGTGAGCGAACCGTC TGAACATC	-
1	NNNNNTGTGCGTTGNTCNCCTGGT----- GGGG TTTA GTGCTGANNANCACCT	24bp del
2	GTGCGTTGATCTCCTGGTGCAGGTTTAATGCT AAT - [+24bp] - GATAGGGG TTTA GTGC Insertion: [CGGGNTAGTGCTGGGGTTAGGG]	9bp del + 24bp ins
3	NNNNATGTGCGTTGNTNCCTGGTGCAGGTTT AATGCT ----- -----GANNAACACNTATGCTGTNAGCATTAATCTTGCCTAGTGAGCGAANCCTC TGAAC	23bp del
4	NNNNNNNTGCGTTGATCTCCTNGTGCAGGTTT AATGC [+8bp] TGATAGGGG TTTA GTGCTGANNANNCCT Insertion: [AGGCTTAA]	6bp del + 8bp ins
5	NNNNNGTGTGCGTTGATCTCCTGGTNCAGGTTT AATGCTAATCG - GATAGGGG TTTA GTGCTGATGAACACCNTAGCTGTTAGCATTAATCTTGCCTAGTGAGCGAACCGTC TGAA Insertion: [CGGGNGGTTTAGTAGGGGGTTTAGTGCTA]	1dp del + 27bp ins

5.4.2 Raising miR-155 CRISPR injected zebrafish and line management

Embryos which were injected with gRNA5 were raised. When they reach breeding age individual zebrafish will be out-crossed to a WT zebrafish. DNA will be extracted from a selection of embryos from each pairing. This will be examined by PCR and subsequent digestion with to *Hpy188III* to determine whether they carry a mutation in miR-155. If any of these embryos carry a mutation this would indicate that the parent is a founder as it carries mutations for miR-155 in its germ line. Embryos from such founders will be raised, this is the F1 generation. When the F1 zebrafish are large enough for fin clipping to be performed, the mutation each carries will be determined by PCR and direct sequencing of the PCR product. The F1 zebrafish will be heterozygous for an individual mutation in the miR-155 gene. These zebrafish only carry one type of mutation for this gene; however each individual F1 zebrafish

is likely to carry a different mutation. The zebrafish carrying the largest or most easily detectable mutations will be kept to ensure time and cost-effective screening for mutations in the future. If any zebrafish of opposite sexes carry the same or very similar mutation they may be mated together to produce progeny which are either WT, heterozygous (for either mutation) or compound homozygous in the F2 generation. If this is not possible, for example if founders are only of one sex, the F1 zebrafish with the selected mutations will be out crossed again to produce the F2 generation. The F2 generation can then be in-crossed to generate homozygous mutants.

5.5 Discussion

The aim of this study was to investigate the involvement of miR-155 and inflammation in the pathology of *pink1*-, *parkin*- and *gba1*- deficient zebrafish. To do this miR-155 expression levels and the expression of relevant inflammatory markers regulated by miR-155 were assessed. A miR-155 knockout zebrafish line was also generated using the CRISPR/Cas9 system.

miR-155 expression in zebrafish models of PD and Gaucher's disease

In 3 month old *gba1*^{-/-} brains a significant 5-fold increase in miR-155 was detected. At this age these zebrafish are close to the end of their life. Gaucher cells are present within the ventricles and the cerebellum of *gba1*^{-/-} zebrafish and an increased microglial infiltration of the brain has been detected at this age. These microglial cells have retracted processes, indicating they are activated (Keatinge et al. 2015). These data show that inflammatory pathology is present in 3 month old *gba1*^{-/-} zebrafish. To further investigate the role miR-155 in aged *gba1*^{-/-} brains, WISH could be performed on sections to examine the localisation of this miRNA within the brain. This would determine whether miR-155 is primarily expressed in the Gaucher cells or activated microglia. The proximity of miR-155-expressing cells to the affected dopaminergic neurons could also be determined.

The expression of miR-155 in *gba1* mutants was also assessed in whole 5dpf larvae. In larvae a significant 2 fold increase in miR-155 expression was detected in *gba1*^{-/-}. When assessed by WISH miR-155 expression appeared to be increased systemically rather than originating from a specific organ. These data suggest that inflammation is an important feature of Gaucher's disease pathology from an early age. At 5dpf a significant change in microglial morphology was also detected (Keatinge et al. 2015) thus providing more evidence for an inflammatory phenotype in *gba1*^{-/-} larvae.

To determine when an increase in miR-155 expression is first detectable in the brain and whether this precedes neuronal loss more time points need to be examined to quantify both miR-155 expression levels and correlate this with the number dopaminergic neurons.

No change in miR-155 expression levels could be detected in 5dpf larvae or aged brains from *pink1*- or *parkin*- deficient zebrafish. As PD is a heterogeneous disease with many causative factors, it is possible that some subtypes of PD have more inflammatory involvement than others. Therefore, although miR-155 upregulation is not detected in *pink1*- and *parkin*-deficient zebrafish models it is possible this miRNA may be important other forms of the disease. To test this in zebrafish the MPP+ toxin-induced Parkinson's model could be used. As miR-155 has not previously been associated with PD it would be interesting to examine the expression levels of miR-155 in a range of murine models and in human post mortem brain and peripheral tissues from patients to determine whether this miRNA is elevated.

Expression of relevant inflammatory markers in gba1 mutant zebrafish

IL-8 and TNF α were chosen as relevant inflammatory markers to study in *gba1* mutant zebrafish. IL-8 has been shown to be increased in the blood plasma of PD patients carrying *GBA* mutations (Chahine et al. 2013) and TNF α is increased in the serum of Gaucher's disease patients and in the brains of a *Gba1*-deficient mouse (Barak et al. 1999; Vitner et al. 2012). These inflammatory markers have also been shown to be downstream of miR-155. Two groups studying ulcerative colitis showed that IL-8 can be positively regulated by miR-155 through repression of its direct targets SOCS1 and FOXO3a (Min et al. 2014; Pathak et al. 2015). Inflammation in alcohol fed mice has also been shown also regulated by miR-155, which is induced in a TLR-4-dependent manner. Chronic exposure of WT mice to ethanol leads to an increase of a number of inflammatory markers, including TNF α , in the cerebellum. NF- κ B was also activated in these mice. In miR-155 deficient mice, chronic alcohol exposure does not increase the expression of TNF α suggesting that miR-155 drives the increase in expression of these inflammatory marker through activation of the NF- κ B (Lippai et al. 2013).

In the brains of 3 month old *gba1*^{-/-} zebrafish large significant increases in three out of the four markers was observed. For *tnfa* a smaller non-significant 2 fold increase was detected. In 5dpf larvae the overall effect of the *gba1*^{-/-} genotype confers significant effect on the expression of inflammatory markers. This result is encouraging and supports the notion that inflammation precedes the neurodegenerative phenotype in these zebrafish. However the observed changes are not sufficient to assume that these inflammatory markers are truly increased at this age. To further validate these findings analysis of protein levels is necessary.

Generation of a miR-155 knockout line and future work

The CRISPR/Cas9 system was used to generate mutations in miR-155. Analysis of the mutations in the F0 generation identified a number mutations which are likely to completely remove miR-155 function (i.e. the mature miRNA sequence is deleted). At the time of writing (August 2015) this colony is in the F0 generation. As discussed in section 5.4.2, these zebrafish need to be outcrossed and founders identified to raise zebrafish from which a colony of miR-155 knockout zebrafish can be produced. Once established the miR-155 knockout line may be crossed with the *gba1*^{-/-} line to determine whether loss of miR-155 is protective and can increase health and longevity of these zebrafish through prevention or modulation of inflammatory pathways.

By 3 months of age *gba1*^{-/-} display a marked increase in chitotriosidase activity. The activity of this enzyme is commonly used as a biomarker to monitor disease in Gaucher Disease patients. Chitotriosidase is mainly produced by activated macrophages and epithelial cells and therefore is indicative of the inflammatory involvement of Gaucher's disease. Other inflammatory phenotypes of the *gba1*^{-/-} zebrafish are the increased infiltration of microglial cells in the brain and the presence of Gaucher cells in the brain and other organs.

Further work that could be performed on this project is increased investigation of the inflammatory phenotype in *gba1*^{-/-} zebrafish. Experiments which could be performed are further examination of microglial activation at a range of time points. The protein levels of a range of inflammatory markers could be assessed and microglial production of reactive oxygen or nitrogen species could be analysed. Reactive oxygen species in the brain are known to contribute to neurotoxicity (Block et al. 2007). miR-155 has previously been shown to drive nitric oxide production of microglia through its target SOCS1 (Cardoso et al. 2012). RNA-sequencing on WT microglia compared to microglia from *gba1*^{-/-} could be performed to identify altered expression patterns. This could be used to determine important downstream targets of miR-155 if compared to microglia from miR-155 deficient zebrafish. An assessment of the numbers of microglial cells in the brain should also be performed a range of ages to determine when an increase is first detectable and whether this precedes neuronal loss. The effect of genetic miR-155 inactivation on these key phenotypes could be then examined.

To investigate the wider effect of miR-155 in Gaucher's disease pathology, the effect of miR-155 knockout on mitochondrial function, number of dopaminergic neurons and the movement phenotype of the *gba1*^{-/-} zebrafish could be assessed.

No change in miR-155 expression was seen in the *gba1^{+/-}* brains at 3 months. As heterozygous mutations in *gba1* are a common risk factor for PD it would be interesting to assess the miR-155 expression in *gba1^{+/-}* zebrafish at a much older time point when they may begin to develop a parkinsonian phenotype. The movement and neurodegenerative of aged *gba1^{+/-}* should also be characterised. If any phenotype is present this is relevant to PD pathology and miR-155 knockdown could be performed to determine whether this ameliorates any observed phenotype.

Finally, a miR-155 overexpressing line could be generated and subsequently crossed with Parkinson's and Gaucher's zebrafish models to determine whether miR-155 upregulation results in increased inflammation and if so, whether this results in the predicted exacerbation of dopaminergic cell loss.

Summary

This study provides the first evidence of miR-155 involvement in Gaucher's disease and demonstrates that this miRNA is upregulated in *gba1*-deficient zebrafish before the presence of a neurodegenerative phenotype. The inflammatory phenotype observed in these zebrafish must also be characterised further to determine whether this precedes, or even drives, the neurodegeneration observed.

Chapter 6. Developing a high throughput imaging system for zebrafish larval brains

Contents

Chapter 6. Developing a high throughput imaging system for zebrafish larval brains ... 178

6.1 Introduction	180
6.2 Using the <i>ETvmat2:GFP</i> neuronal reporter line to study dopaminergic neurons ..	183
6.2.1 Optimisation	183
6.2.1.1 Validation of GFP expression in <i>th+</i> neurons.....	183
6.2.1.2 Development of a method to image and analyse dopaminergic neurons in the <i>ETvmat2:GFP</i> reporter line	185
6.2.2 Results	187
6.2.2.1 Validation of the <i>ETvmat2:GFP</i> reporter line to count dopaminergic neurons	187
6.3 Development of a high throughput orientation and imaging system for assessment of dopaminergic neuron number in zebrafish embryos	192
6.3.1 Optimisation	193
6.3.1.1 Generation of a 3D printed mould to allow high throughput orientation of zebrafish embryos.....	193
6.3.1.2 Testing imaging systems to accurately measure dopaminergic neuron number in high throughput manner.....	195
6.3.2 Results	199
6.3.2.1 Validation of high throughput imaging process.....	199
6.4 Discussion.....	201
Using the <i>ETvmat2:GFP</i> reporter line to measure dopaminergic neuron number	201
Development of a high throughput imaging process	204
Future prospects for phenotypic drug screening using the described method ..	207

6.1 Introduction

Zebrafish are an ideal model organism for use in phenotypic drug discovery. The embryos develop rapidly, allowing the study of effects of drugs and toxins at a whole system level. Their small size allows for efficient handling in 96-well plates, which are commonly used for drug screening and are compatible with automated liquid handling machinery. The large number of progeny ensures enough embryos are easily available for high throughput studies and their transparent nature also means they are highly suitable for imaging. Ease of genetic manipulation allows the creation of transgenic fluorescent reporter lines which provide easily quantifiable read outs that can be used for high throughput screening. Examples of this include a screen performed by McGown and colleagues (2013), aiming to identify compounds able to reduce stress in the interneurons in a *sod1*-mutant zebrafish. For this screen a transgenic zebrafish containing dsRED under the control of the *Hsp70* promoter was utilised. Under increased oxidative stress dsRED fluorescence increases thus allowing the authors to quantify changes in the oxidative stress response exhibited after treatment (McGown et al. 2013). In another screen, a transgenic line with GFP-tagged neutrophils was used to identify compounds able to modulate resolution of inflammation after fin injury (Robertson et al. 2014). Use of this transgenic line allowed the authors to score the number of neutrophils remaining at the site of injury 12 hours post injury. These are just two examples of drug screens which utilise the tools available enabling zebrafish to be a powerful model organism for use in high throughput screens which use imaging as a read out.

Compared to traditional target-driven drug discovery, where on average it takes 12-15 years for a drug to enter the clinic, phenotypic drug discovery has the potential to significantly reduce the time taken for a promising drug to enter human trials and eventually clinical use. Typical pipelines and approximate timings for both target-driven drug discovery and phenotype-driven drug discovery are shown in Figure 82. With target-driven drug discovery a large number of initially promising compounds fail upon animal testing due to bioavailability and toxicity issues, thus resulting in a large amount of wasted time and resources. These problems are largely eliminated by usage of animal models in the initial drug discovery phase as the effects of the drug in the environment of a whole organism can be analysed, thus allowing an assessment of bioavailability, toxicity and efficacy to be made in the earliest stages of drug testing (Bowman & Zon 2010).

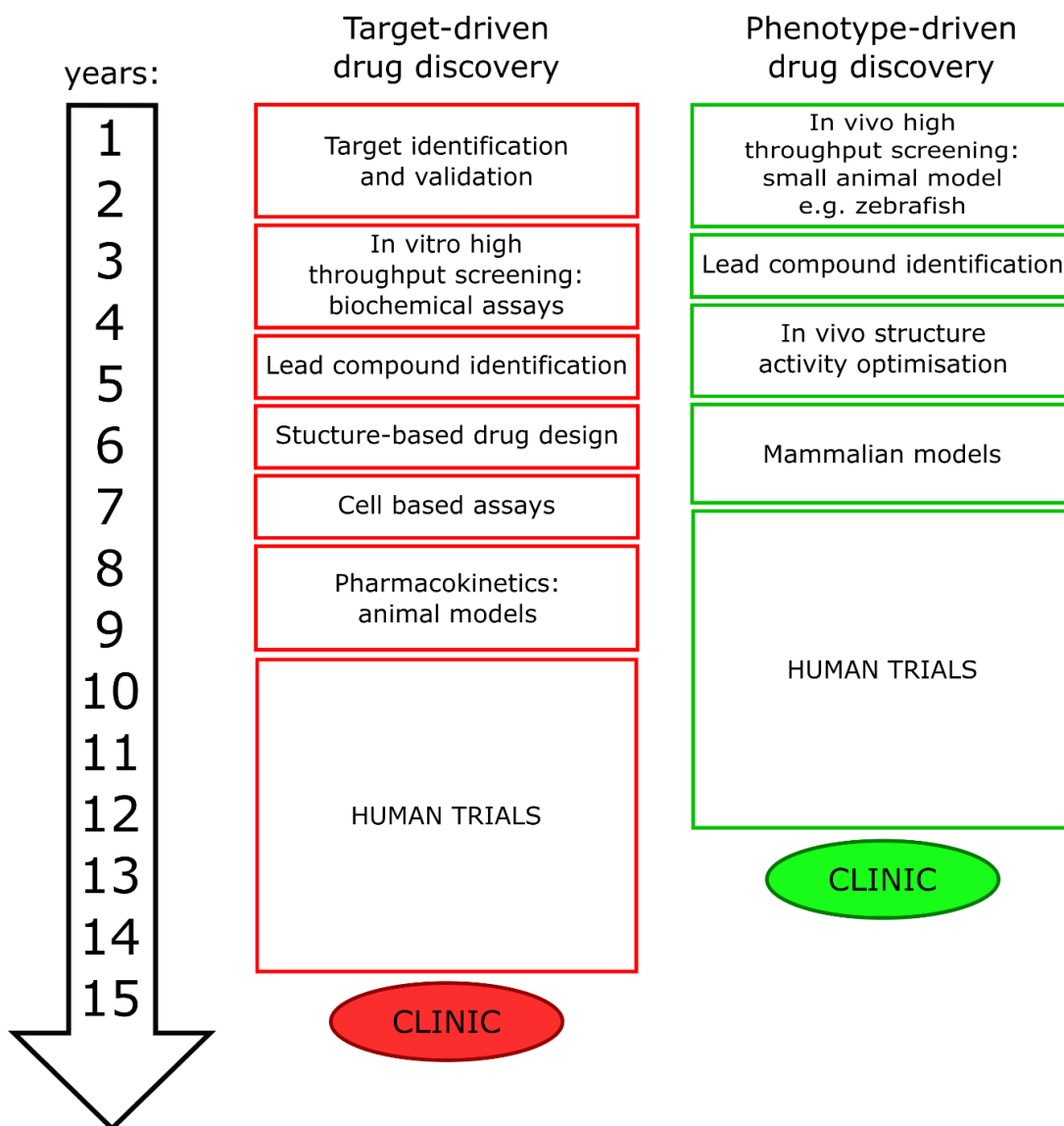


Figure 82. Comparison of strategies for drug discovery. This flow diagram illustrates the typical pipeline of both target-driven drug discovery and phenotype-driven drug discovery. Adapted with permission from Bowman & Zon (2010).

As there are currently no disease modifying treatments available for PD, research into developing such drugs is of critical importance. In order to identify compounds of interest drug screening platforms must be available with read outs which are relevant to the disease process. Likewise, a similar process could be used to identify toxins that contribute to PD pathology. Only a small proportion of PD diagnoses are attributable to a known cause (de Lau & Breteler 2006). Although a large number of genetic risk factors have been identified by GWAS, the overall heritability of PD is only estimated at approximately 27% (Keller et al. 2012). It is clear that there are unidentified genetic and environmental factors which increase the risk of developing PD. Thus, a toxin screen to identify potential modifiers of dopaminergic

neuron survival would be extremely valuable to help uncover other mechanisms which infer increased risk for PD.

In the field of PD research, study of the survival of dopaminergic neurons is key. A method for counting dopaminergic neurons in zebrafish using WISH for *th* has previously been established and is described in detail in section 2.15.1 (page 70). One limitation of using WISH for *th* and subsequently counting the neurons as a drug screening tool is that it is a very labour intensive protocol. Robots are available to automate and therefore increase the throughput of the WISH process; however, post-WISH, the embryos need to be mounted dorsally and the neurons manually counted. Another limitation is unintentional bias and inconsistency in counting. It is possible to blind the researcher to the individual samples which are being counted; however, some treatments, such as MPP+ or particular MOs, produce a remarkably different appearance in the embryo morphology, making the treatment condition apparent. Despite these limitations, in 2012 a study was published that screened the effect of 5000 compounds on the development and survival of dopaminergic neurons. To do this, IHC for TH was performed post-drug treatment and subsequently the fluorescence was assessed using confocal microscopy (Sun et al. 2012). This study shows that it is indeed possible to perform a drug screen using methods that stain the neurons of interest and perform manual imaging to assess the effects of the compounds on the staining. However, this is an extremely time consuming and expensive process. To develop more time and cost effective methods for studying the effects of small molecules on dopaminergic neuron development and survival, alternative methods to measure dopaminergic neuron number and screen large numbers of embryos must be established. Fluorescent reporter lines which label cells of interest are a useful tool that remove the need for manual staining techniques, allowing for more cost effective visualisation of the region of interest.

Although there are currently no reporter lines which specifically label only the *th*+ dopaminergic neurons, a fluorescent reporter line is available which expresses GFP in monoaminergic neurons (Wen et al. 2008). The production of this transgenic line used enhancer trap technology to insert the transgene (GFP linked to the zebrafish *gata2* minimal promoter) into the second intron of *vmat2*. *Vmat2*, vesicular monoamine transporter 2, is responsible for transport of monoaminergic neurotransmitters from the cytosol to the synapse. The insertion of GFP into the *vmat2* intronic region allows GFP to be expressed in *vmat2* containing neurons as it is placed under control of the *vmat2* enhancer. The authors verified that the expression pattern of GFP recapitulates that of *vmat2*, including expression

in the *th*+ neurons of the ventral diencephalon. They discuss that this line may be a useful tool for drug studies relevant to PD in the future. This transgenic reporter line is referred to as the *ETvmat2:GFP* reporter line.

The first aim of this section of my thesis was to develop a method to use the *ETvmat2:GFP* reporter line for study of the dopaminergic neuron cluster. As discussed above, using WISH to stain the dopaminergic neurons is a time-consuming process, and therefore use of a fluorescent reporter line to measure the number of dopaminergic neurons would be beneficial as it is possible to image live embryos and visualise the diencephalic catecholaminergic cluster. This prevents the need to fix embryos at the desired time point and perform WISH, thus reducing sample processing time greatly and increasing capacity for high throughput analysis. The second aim of this section is to use the *ETvmat2:GFP* reporter line to generate a high throughput imaging process, from which analyses of dopaminergic neurons can be made, and subsequently be used as a read-out for a phenotypic drug screen.

6.2 Using the *ETvmat2:GFP* neuronal reporter line to study dopaminergic neurons

6.2.1 Optimisation

6.2.1.1 Validation of GFP expression in *th*+ neurons

To successfully use the *ETvmat2:GFP* reporter line to replace neuron counting experiments it must first be determined whether this reporter line accurately labels the *th*+ dopaminergic neurons. To do this, a dual WISH-IHC was performed to label *th* and GFP-positive neurons simultaneously.

Figure 83A shows the brain of a 3dpf zebrafish embryo and the neuronal groups labelled by the *ETvmat2:GFP* reporter line. As well as the diencephalic catecholaminergic cluster, which contains the neurons which are detected using WISH for *th*, other GFP positive neuronal groups include: the raphe nuclei, and hypothalamic, pretectal and telencephalic neuron populations. Figure 83B shows the diencephalic catecholaminergic cluster in more detail and indicates co-localisation of GFP and *th*. These data show that this reporter line can indeed be used to study this neuronal group.

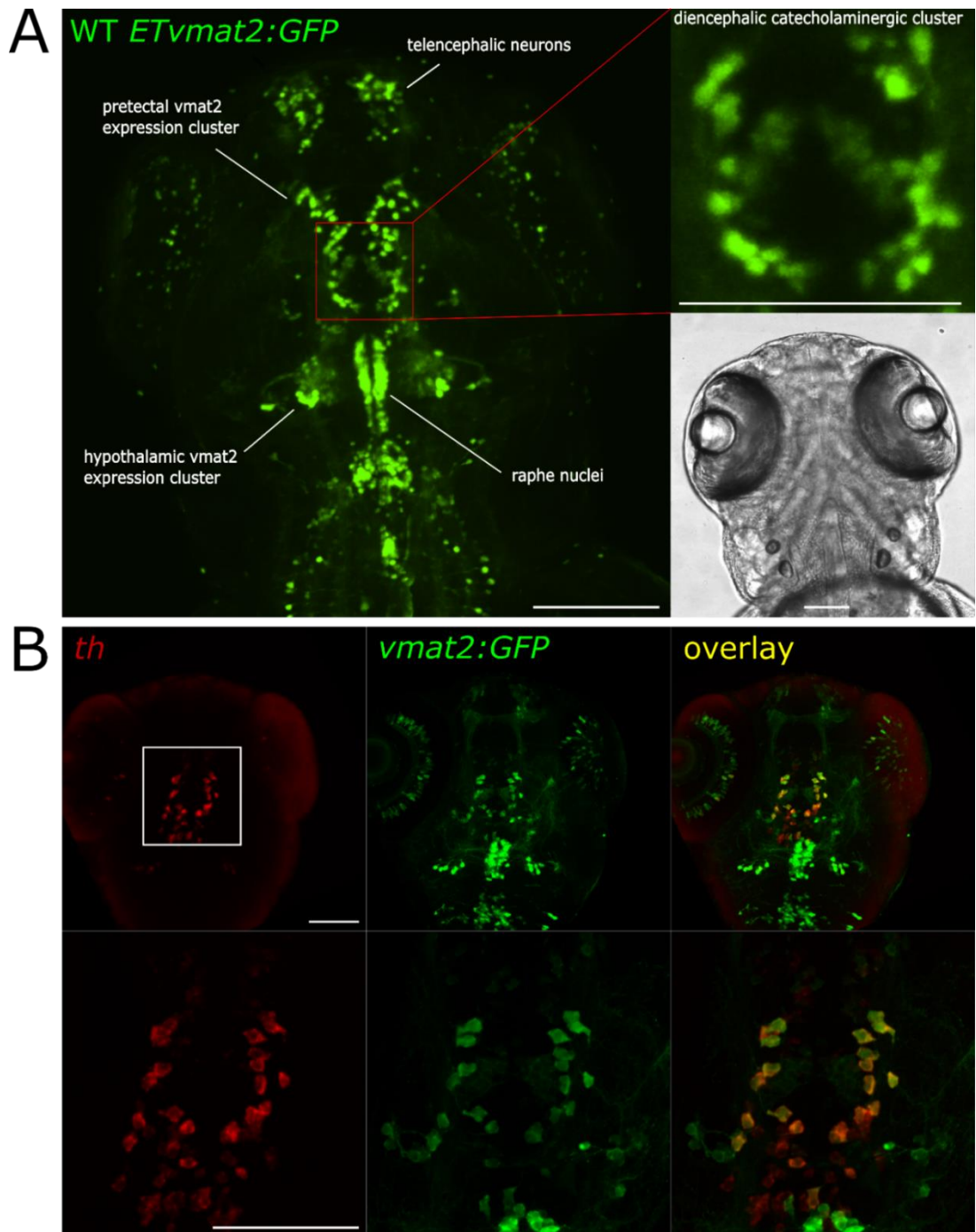


Figure 83. Neuronal groups labelled by the *ETvmat2:GFP* reporter line. A shows neuronal groups labelled by the *ETvmat2:GFP* reporter line. **B** shows co-localisation of *th* positive neurons and GFP labelled neurons in the *ETvmat2:GFP* reporter line. Scale bar = 100 μ m

6.2.1.2 Development of a method to image and analyse dopaminergic neurons in the *ETvmat2:GFP* reporter line

To utilise the *ETvmat2:GFP* reporter line to analyse dopaminergic neuron number, a method was developed which aimed to use total fluorescence intensity of the diencephalic catecholaminergic cluster as an indication of dopaminergic neuron number. Total fluorescence intensity takes into account the fluorescence intensity of the GFP positive pixels and the number of GFP positive pixels. As zebrafish which contain the *ETvmat2:GFP* transgene express GFP in the dopaminergic neurons the hypothesis behind this method was that, in embryos with more dopaminergic neurons more pixels will be GFP positive therefore the total fluorescence intensity reading will be increased.

To ensure that copy number of the transgene did not obscure any otherwise quantifiable changes in fluorescence, the WT *ETvmat2:GFP* zebrafish, which are either homozygous or heterozygous for the transgene, were outcrossed to WTs for all experiments. These zebrafish will be referred to as *ETvmat2:GFP*;WT. This ensured that all GFP positive zebrafish were heterozygous for the transgene. Using a mixed population of homozygous and heterozygous embryos, as would be generated from an incross, would allow copy numbers to differ between embryos. At 24hpf the embryos were screened to select for GFP-positive embryos.

To image the *ETvmat2:GFP*;WT embryos, at 3dpf the embryos were anaesthetised in tricaine and mounted on a glass coverslip in 1% LMP agarose. To ensure the best orientation of the embryo to allow capture of a high quality image of the developing brain, the embryo was held in the dorsal position using fine forceps or a mounted needle as the agarose had set. Images were captured using the 10x objective on an UltraViewVoX spinning-disk confocal microscope (PerkinElmer Life and Analytical Sciences). A z-stack encompassing the entire fluorescent portion of the zebrafish brain with 3µm slices was generated for each embryo.

To quantitatively measure the fluorescence levels of the diencephalic catecholaminergic cluster an image analysis process was developed using ImageJ (Figure 84). Each image was rotated and cropped (136.54µm x 136.54µm) around the diencephalic catecholaminergic cluster. A substack was created which included only slices containing the diencephalic catecholaminergic cluster in order to exclude neurons from other groups. A maximum intensity projection of this substack was generated; this is where the maximum fluorescence intensity reading for each pixel in the specified stack is recorded and projected onto the final image. In order to analyse the images, the total fluorescence intensity above a determined threshold was measured in the maximum projection image; shown in Figure 84.

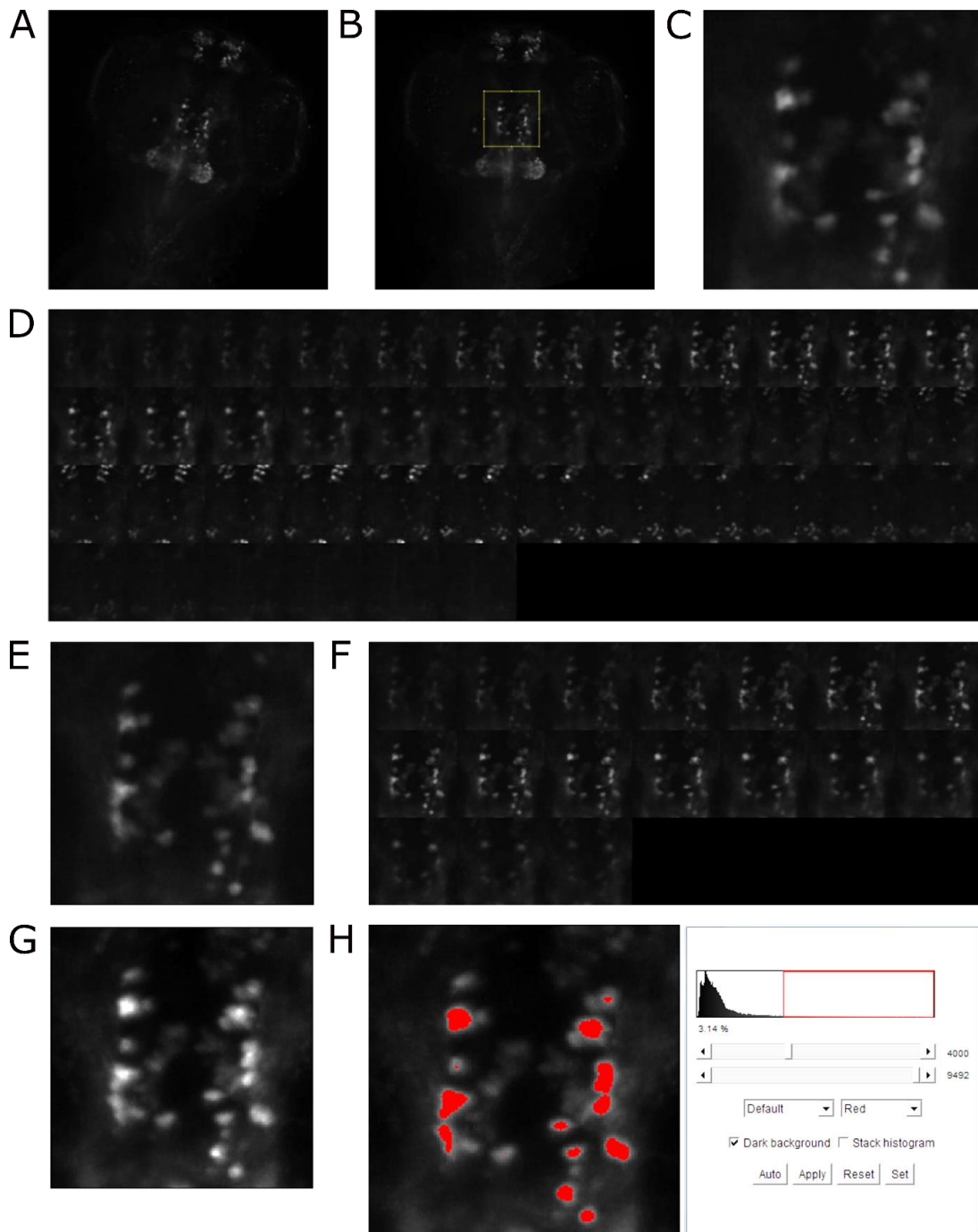


Figure 84. Image analysis process with ETvmat2:GFP embryos. *A* shows the whole image taken on the spinning disk microscope. *B* shows this image rotated and a box drawn around the region of interest. *C* shows the cropped image which only contains the diencephalic catecholaminergic cluster which we are interested in. *D* shows a montage of all the slices present in this cropped image. *E* shows a substack (slices 3-19) of the same image; this only contains slices that show the neuronal group of interest. *F* shows a montage of the slices present in the substack. *G* shows the maximum projection image of the substack. *H* shows how the total fluorescence intensity (no of pixels reaching threshold value multiplied by the mean intensity of the selected area) of the maximum projection image is acquired.

To determine the most suitable threshold, a range of thresholds were tested. The threshold function in ImageJ allows the user to set the threshold value and view which regions of the image are above this threshold value. By viewing the regions of the image captured by a range of thresholds, it was determined that a threshold of 4000 accurately captures the majority of the neurons of interest. If the value is set much higher than 4000, only the central regions of the brighter neurons are included and some fainter neurons which would be included in a manual neuron count are excluded. If the threshold is set much lower than 4000, some background noise reaches the threshold value. This is shown in Figure 84H where the red masking highlights the areas captured by this threshold; the unmasked image is shown in Figure 84G. As there was no significant variation between the background noise level of the images between individual embryos or experiments, this threshold value was used for all subsequent experiments. The number of overexposed pixels and number of captured pixels was also monitored; if any particular image had more than 15% overexposed pixels it was excluded. Likewise, if less than 200 pixels are above the threshold then this image was also excluded.

To validate the suitability of *ETvmat2:GFP* reporter line and the image analysis method described above, results using this method were compared to previously established data sets where dopaminergic neurons were manually counted using after WISH for *th*. If able to replicate previous results, this technique has the potential to remove researcher bias as the process may be automated rather than relying on manual counting of neurons.

6.2.2 Results

6.2.2.1 Validation of the *ETvmat2:GFP* reporter line to count dopaminergic neurons

To validate the use of the *ETvmat2:GFP* reporter line and the image analysis method, three experimental groups which have previously been shown to have altered dopaminergic neuron numbers were used. These are: miR-133b morphants, treatment with MPP+ and *pink1* deficiency. The first of these groups, miR-133b morphants, demonstrate an increase in dopaminergic neuron number; this is shown in Chapter 3 section 3.3.2.1. Secondly, treatment with MPP+ results in a loss of dopaminergic neurons. Finally, *pink1* deficiency results in a more moderate decrease in dopaminergic neurons. *ETvmat2:GFP* zebrafish were previously crossed with *pink1*^{-/-} zebrafish to generate zebrafish which express this transgene on a *pink1*^{-/-} background. To generate embryos for image analysis, these zebrafish are outcrossed to *pink1*^{-/-} zebrafish which do not possess the *ETvmat2:GFP* transgene. Resulting progeny were screened for fluorescence prior to confocal microscopy.

miR-133b morphants demonstrate a 20% increase in *th*+ dopaminergic neuron number compared to WT as measured by manual neuron counting after WISH for *th* (Figure 85A). To determine whether this result could be replicated using the *ETvmat2:GFP* reporter line, miR-133b MO injections were performed in the *ETvmat2:GFP*;WT embryos. For each biological replicate ten embryos from each group were mounted and imaged at 3dpf. The total fluorescence intensity was measured using the image analysis method described above. For each biological replicate the total fluorescence intensity is normalised to the average of the WT. Measuring fluorescence intensity in morphants compared to WT also detects a significant increase of approximately 40% (Figure 85). This is a larger increase than is detectable in neuron number seen by counting *th*+ dopaminergic neurons after staining by WISH. This may be due to the increased expression levels of dopaminergic markers as well as the increased number of neurons. These data show that an increase in dopaminergic neuron number can be detected by measuring fluorescence intensity measurements in the *ETvmat2:GFP* reporter line.

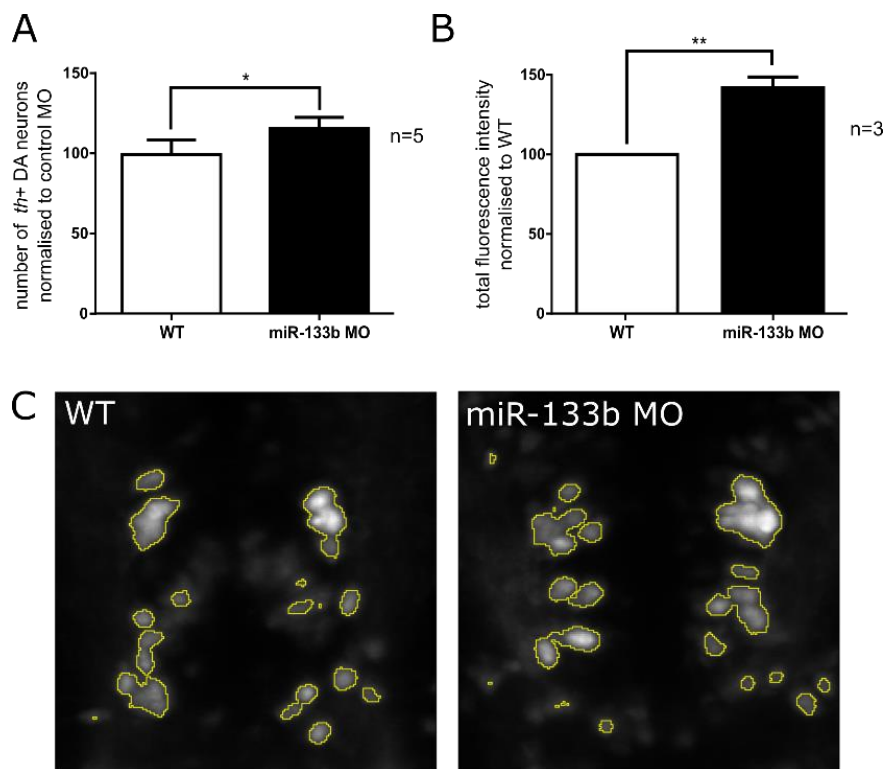


Figure 85. *th*+ dopaminergic neuron counts and fluorescence intensity in WT and miR-133b morphants. **A** shows previous data collected by counting the number of neurons labelled after WISH for *th*. In miR-133b MO injected embryos there is a 20% increase in *th*+ dopaminergic neuron number. **B** shows the total fluorescence intensity measurements of the same population of neurons. In miR-133b MO injected embryos there is a 40% increase in fluorescence intensity compared to WT. Data are from three biological replicates with a minimum of 10 images are analysed per biological replicate and the average taken. **C** shows a representative maximum projection image from each WT and miR-133b MO injected embryos. The yellow bounded areas are the regions which reach the set threshold and will be included in the image analysis. Error bars represent standard deviation. Both data sets analysed using an unpaired t-test with Welch's correction, * = $p < 0.05$, ** = $p < 0.01$. On axis DA = dopaminergic.

It was also important to determine whether this method is also able to detect a decrease in dopaminergic neurons. For this experiment, embryos were treated with a high dose of MPP+; 6mM MPP+ was added to E3 medium at 1dpf and replaced at 2dpf. Neurons were counted at 3dpf. This high dose of MPP+ causes approximately a 60% decrease in *th*+ dopaminergic neurons, as measured by neuron counting using WISH for *th* (neuron counting was performed by Rebecca Wilcock, Figure 86A). Similarly, when *ETvmat2:GFP*;WT embryos are treated with this dose of MPP+ a 60% decrease in fluorescence intensity is also detected (Figure 86B). When the percentage changes in the measurements of dopaminergic neuron number collected by these two different methods are compared by a two-way ANOVA there is no significant difference between these two data sets. This shows that this method can be used to accurately measure large decreases in dopaminergic neuron number.

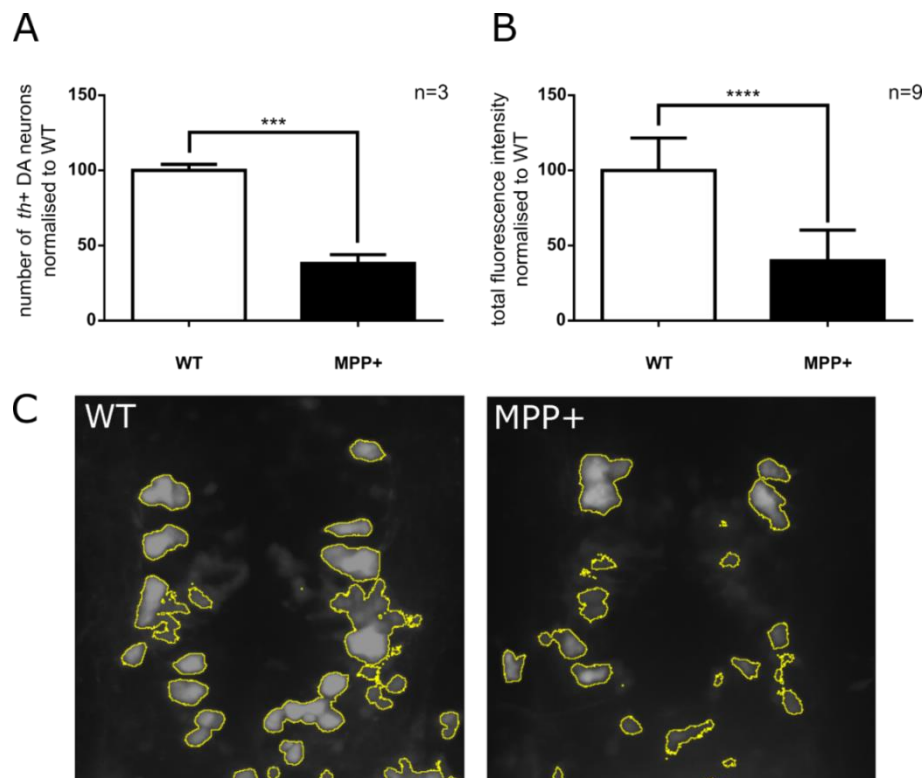


Figure 86. *th*+ dopaminergic neuron counts and fluorescence intensity in WT and MPP+ treated embryos. **A** shows previous data collected by counting the number of neurons labelled after WISH for *th* data is from 3 biological repeats with 10 zebrafish per group per experiment. These data were collected by Rebecca Wilcock. **B** shows fluorescence intensity after MPP+ treatment. Data is from 1 biological repeat with 9 embryos per group. Both data sets show a 60% decrease in fluorescence intensity after treatment with MPP+. **C** shows a representative maximum projection image from each WT and MPP+ treated embryos. The yellow bounded areas are the regions which reach the set threshold and will be included in the image analysis. Error bars represent standard deviation. Both data sets analysed by an unpaired t-test with Welch's correction, *** = $p < 0.001$, **** = $p < 0.0001$. On axis DA = dopaminergic.

Finally, in order to determine whether more subtle decreases in dopaminergic neuron number can be detected, *ETvmat2:GFP* zebrafish raised on a *pink1*^{-/-} background were analysed and compared to *ETvmat2:GFP* with a WT background. *pink1* deficiency causes a more moderate decrease of around 25% of dopaminergic neurons at 3dpf (Flinn et al. 2013). The fluorescence intensity method was unable to detect a decrease in the *pink1*^{-/-} zebrafish compared to WT (Figure 87A). Generation of a maximum projection image may have masked some neurons which are in the same XY plane but different Z position. Therefore, an alternative method for analysing the images was tested to determine whether it could be more accurate in determining the number of neurons present. To achieve this, the total fluorescence intensity above a threshold of 4000 was calculated for each individual slice in the substack (Figure 84I). The sum of the total fluorescence intensity from each slice was calculated. This method was slightly more sensitive; the mean change in fluorescence intensity was an 8% decrease in *pink1*^{-/-} compared to WT. However, this decrease does not represent the known decrease of dopaminergic neurons and is not significant (Figure 87B).

As fluorescence intensity methods were unable to detect any change, we tested whether it is possible to accurately count neurons using images generated using the *ETvmat2:GFP* reporter line. To count neurons the substack image was opened in ImageJ. To identify neurons and count individual neurons, each slice of the stack was examined and the centre of each neuron was marked using the “point picker” tool. This tool allows the researcher to mark a particular point with a cross. Figure 87C shows a representative slices from *ETvmat2:GFP* embryos on a WT and *pink1*^{-/-} background which have the neurons present marked. Once the whole stack has been examined for neurons the “point picker” tool generates a report which includes the coordinates of the points marked and allows the researcher to count the number of marks made. To reduce researcher bias counting the neurons in these images was performed whilst blinded to genotype.

Neuron counting was able to detect a 25% decrease in neuron number. These data are not statistically significant. However, this experiment is only pilot data with an n of 2, therefore these data have weak statistical power (Figure 87C and D). As these data replicate the 25% decrease in dopaminergic neuron observed by neuron counting after WISH for *th* this shows that the images generated from the *ETvmat2:GFP* line have sufficient resolution that individual neurons can be accurately identified.

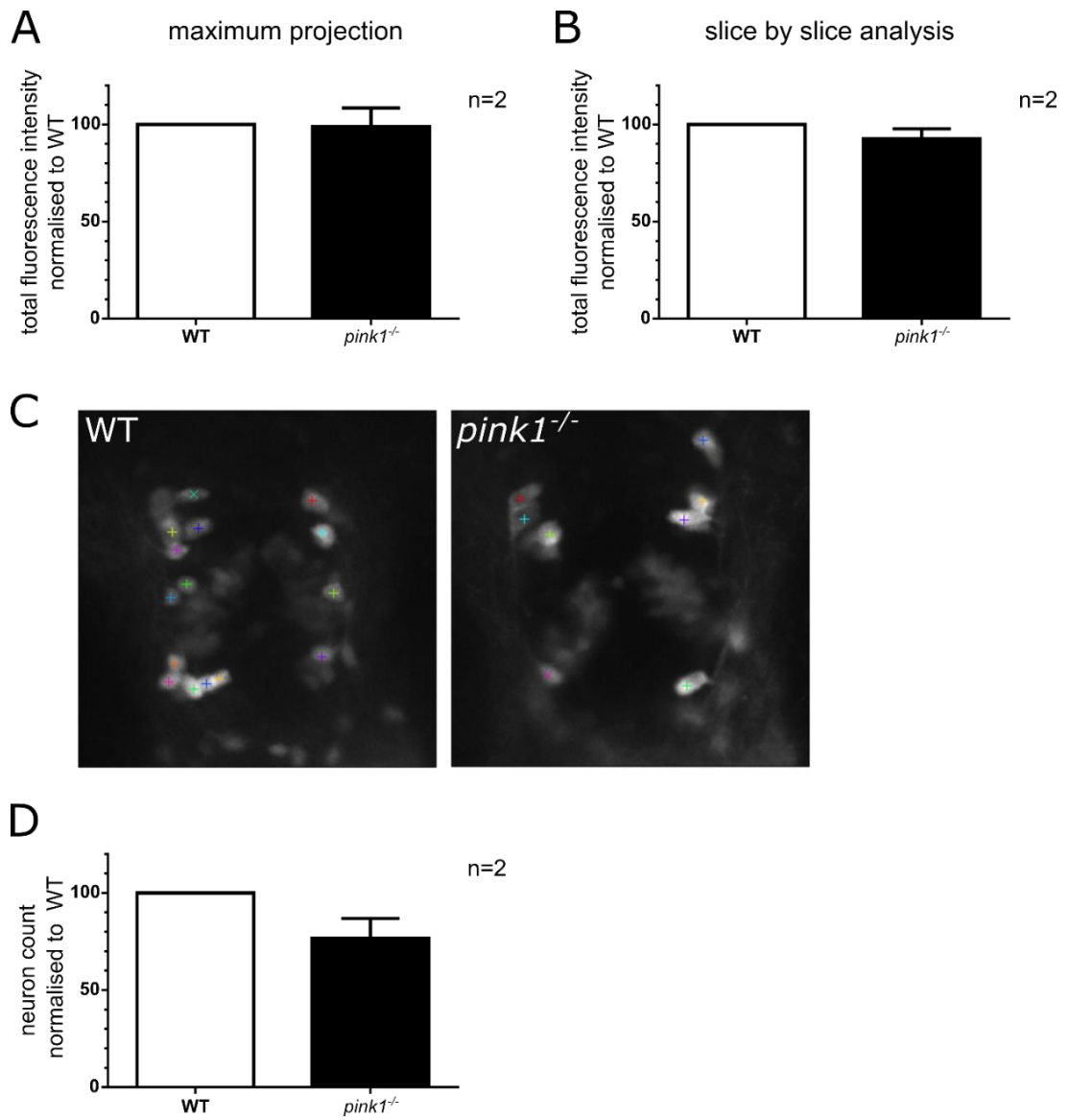


Figure 87. Image analysis methods with WT and $pink1^{-/-}$ embryos. **A** and **B** show the fluorescence intensity analyses, using the maximum projection image and the substack image respectively. **C** shows an example slice and point picking of individual neurons from a WT and $pink1^{-/-}$ substack. **D** shows the normalised neuron count from WT and $pink1^{-/-}$. Around a 25% decrease in neuron number is detectable. Data are from two biological replicates. A minimum of 10 images are analysed per biological replicate and the average taken. Error bars represent standard deviation.

6.3 Development of a high throughput orientation and imaging system for assessment of dopaminergic neuron number in zebrafish embryos

In the previous section it was demonstrated that it is possible to use the *ETvmat2:GFP* reporter line to measure dopaminergic neuron number. This is progress toward a high throughput screen through time-savings inherent to using a reporter line rather than performing WISH. However, one major limitation of this system that would prevent a high throughput screen being performed is the need for manual orientation of the zebrafish embryos. In order to capture high quality images of the zebrafish larval brain, the embryos must be carefully orientated into a dorsal position. The data in the previous section were collected by manually mounting each embryo onto a cover slip in 1% LMP agarose. This process is time consuming as the embryo must be held in the correct orientation until the agarose has set. In this section, the generation and testing of a mould which improves the speed of orientation of embryos and therefore allows high throughput imaging will be presented as a step towards automating the process of analysing dopaminergic neuron numbers.

A need for tools to allow high throughput orientation of zebrafish embryos was also recognised by Jens Westhoff and colleagues. This group is interested in the development of the zebrafish larval kidney and identification of compounds which may affect this process (Westhoff et al. 2013). The need to carefully orientate zebrafish for imaging of the brain is similarly required for visualisation of internal organs such as the kidney. To increase the accuracy and speed of orientation of zebrafish embryos, the authors designed and generated a mould which allows the generation of agarose wells within a 96-well plate. Zebrafish embryos could be accurately orientated in these wells allowing generation of standardised views of the developing kidney. Use of this tool to quickly and consistently orient the zebrafish embryos allowed the authors to develop an automated imaging platform. This method was used to perform a pilot toxin screen which was able to identify morphological changes caused by nephrotoxic compounds in a fluorescent reporter line which labels the developing kidney (Westhoff et al. 2013). As the authors discuss, this system may be easily adapted for analysis of other organ systems, including the developing brain.

The aim of this section of my thesis is to develop a high throughput imaging system to study changes in dopaminergic neuron number using the *ETvmat2:GFP* reporter line with the view of performing a phenotypic drug screen in the future. This project shares many similarities with the aims of the study performed by Westhoff and colleagues. In their study, the imaging

pipeline could only be used to score gross morphological changes. However, for this study a more subtle read out must be detectable. For this reason optimisations to the imaging protocol must be performed to develop this pipeline further; these will be discussed in this chapter.

6.3.1 Optimisation

6.3.1.1 Generation of a 3D printed mould to allow high throughput orientation of zebrafish embryos

The original mould described by Jens Westhoff and colleagues was produced by CNC milling from brass; this is a relatively expensive and specialised technique. To improve dissemination of the mould to allow other researchers to benefit the same group generated a second version of the mould by 3D printing on a standard desktop 3D printer (Wittbrodt et al. 2014), thus making the mould reproducible in Sheffield. This mould comprises of 8 strips of 12 pins which slot into a base plate. The pins are cuboid and tapered at the end. The tip of the pin has a very fine point of 0.1mm width; this allows the production of deep V-shaped agarose wells which are able to accurately hold zebrafish embryos in the desired orientation. Figure 88 shows the mould, how wells are generated in a 96 well plate, and how embryos are mounted into these wells.

Following the protocol described by Wittbrodt and colleagues, 100µl of molten 1% agarose was added to each well and was left to cool in the wells of the 96-well plate for a two minutes before the mould was added. The mould was left inside the 96-well plate for 15 minutes until the agarose set before being carefully removed. Anaesthetised zebrafish embryos were added to each well in up to 150µl of E3 medium using a cut 200µl pipette tip. Prior cutting of the pipette tip widens the tip and helps to prevent damage to the embryos. Embryos were then carefully manipulated into the correct orientation within the well using a mounted needle. A small number of embryos fell into the well in the correct orientation of their own accord; however the majority required gentle orientation. This process was considerably more time and cost effective than individual mounting of embryos. By individual mounting each embryo took approximately 2 minutes to mount, a total of 48 minutes for 24 embryos; using the mould it was possible to orient 24 embryos in approximately 5 minutes.

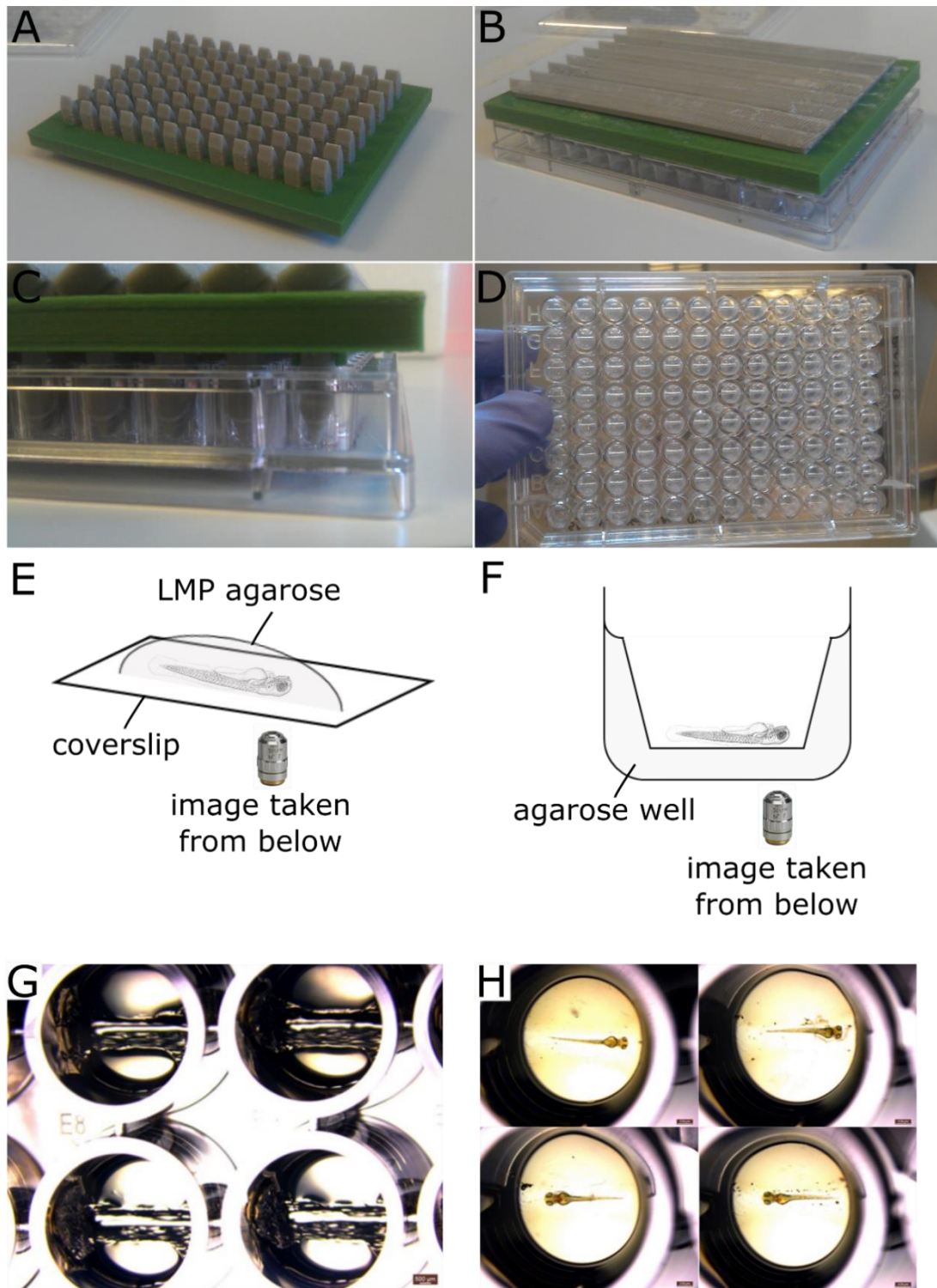


Figure 88. Using a 3D printed mould for zebrafish orientation for imaging. A-D show the mould, the mould inside a clear 96-well plate and a view of the wells made in the agarose by the mould. E shows the mounting method for individual embryos where the embryos are held in the dorsal position in a bubble of LMP agarose on top of a thin glass coverslip. F shows how embryos are mounted in the wells created by the mould, the steep sides of the well hold the embryo in the dorsal position once they have been manipulated into the well using a mounted needle. G and H show close up images of the wells and embryos mounted within the well taken from above on a dissecting microscope.

6.3.1.2 Testing imaging systems to accurately measure dopaminergic neuron number in high throughput manner

Two different imaging systems were tested to determine the best method of capturing fluorescent images of the zebrafish larval brains in a high throughput manner. These were, the IN Cell Analyzer 2000 (GE Healthcare Life Sciences) high throughput fluorescent microscope and UltraViewVoX spinning-disk confocal microscope (PerkinElmer Life and Analytical Sciences).

The IN Cell Analyzer 2000 is a high content imaging system. It is commonly used for live and fixed cell culture imaging and has also been successfully used for rapid zebrafish screening to identify embryos containing a fluorescent transgene (Alex McGown, personal correspondence). This system combines the advantages of a high power fluorescent microscope with those of an automated plate reader, thus allowing a large number of samples to be processed quickly and high quality images produced. Other advantages of this system include the ability to control the environment of the microscope chamber, allowing long time-lapses to be performed. The IN Cell Analyzer system also uses IN Cell Investigator software which allows the user to develop an analysis routine to select regions of interest and perform analyses in an objective manner.

The UltraViewVoX spinning-disk confocal microscope is also commonly used in house for acquiring images for time-lapse microscopy and other experiments which require automation (Gray et al. 2011; Wilkinson et al. 2012). Confocal imaging allows capture of higher resolution images of discrete optical sections in a thick sample compared to standard wide-field microscopy as any out-of-focus signal is eliminated by the pin hole. However, the time taken to generate an image using confocal microscopy is hugely increased compared to wide-field microscopy as the thin laser beam scans the sample sequentially rather than illuminating the whole sample simultaneously. Also, long exposure times are often required as the increased resolution reduces the signal intensity. Spinning-disk confocal microscopy uses a number moving pin-holes, allowing an array of laser beam to scan the image simultaneously thus using the multiplex principle to increase image capture time. The UltraViewVoX spinning-disk system also possesses a movable stage which can accept microtitre plates. The controlling software, Volocity, allows the user to pre-set to a number of X, Y and Z positions to allow directed imaging of the region of interest.

Firstly, the IN Cell Analyzer 2000 was tested for this application. In order to capture the zebrafish brain in enough detail, the 20x objective was used. As the head of the embryo was

not in exactly the same position in every well, a grid of 9, slightly overlapping, fields of view were used to ensure that images of the head were captured. To ensure the head was captured in focus in each well a standard initial focus point can be set. As the sample is not in the same z-position in each well, due to variation in the well depth and position of the embryo within the well, the microscope then was set to use a large adaptive software autofocus system to identify the region of interest in the region around this pre-set focal point. The software generally selected the bright raphe nuclei to focus on. As the diencephalic catecholaminergic cluster is slightly ventral to the raphe nuclei the z-range was set accordingly. Figure 89 shows the location of these fields of view and example images captured using this process.

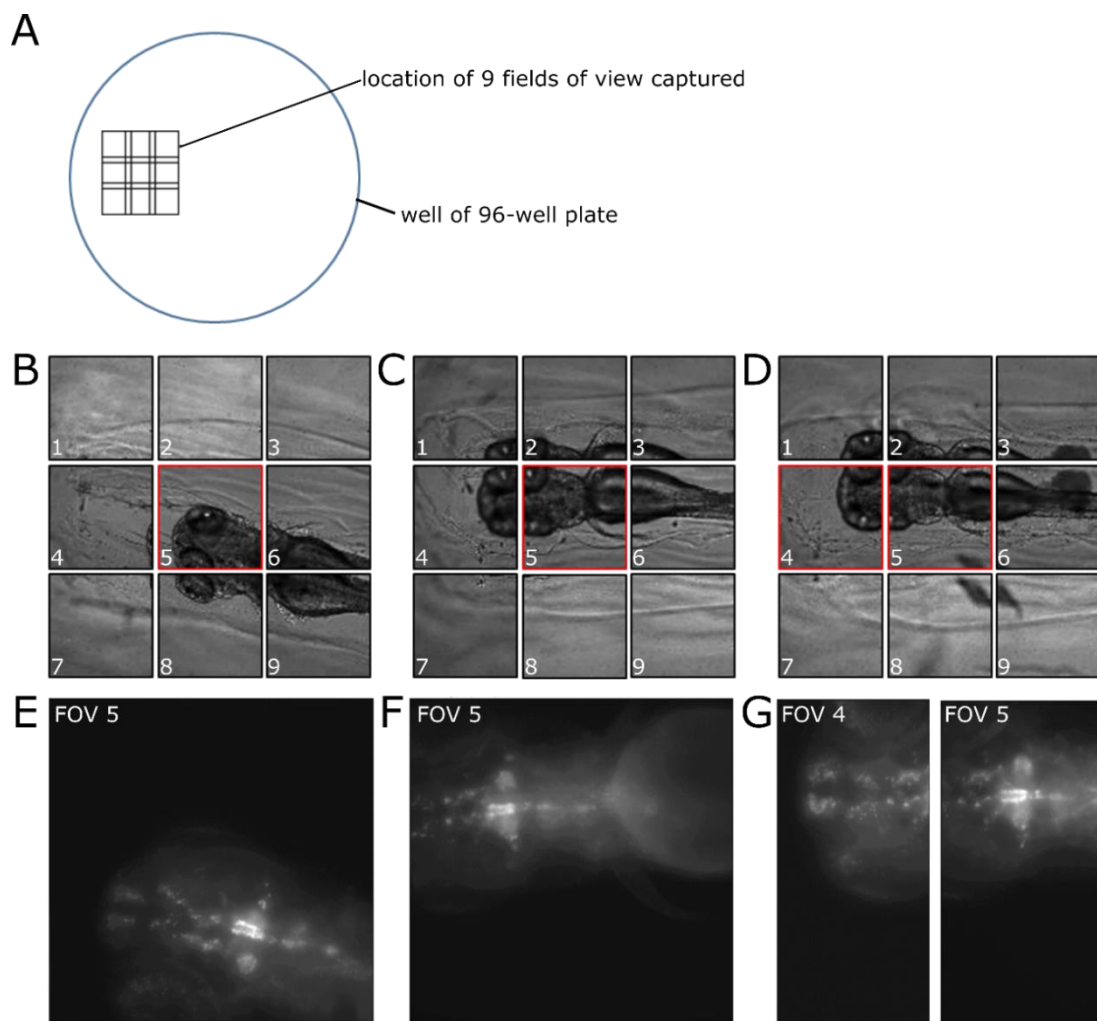


Figure 89. Testing high throughput imaging of zebrafish embryos using the IN Cell Analyzer 2000. A shows the set up of the well to capture 9 overlapping fields of view (FOV) to ensure that the head of the embryo is captured. B-D shows the brightfield images captured of three example embryos. The FOV of interest, i.e. that captures the region of the brain of interest, is highlighted in red. Sometimes more than one FOV captures the region of interest due to the overlap (D,G). E-G show the fluorescent image captured in the FOV(s) of interest. The images shown are maximum projections of the stack taken.

When tested on a plate containing 12 embryos the head of the zebrafish embryo was present in one of the 9 fields of view in all cases. The focus set up also ensured that the region of interest was in focus in all images captured. This demonstrates that it is possible to image the brain of zebrafish embryos mounted into a 96-well plate using the IN Cell Analyzer 2000. Advantages of this system include the ability to save the imaging program. This minimised researcher input in the imaging stage as the plate can be inserted and imaging begun. However, this system has some major disadvantages. As 9 fields of view must be used to ensure that the head of each zebrafish is captured and a large z-stack is performed to ensure the region of interest is captured, the imaging process is very slow. This also results in a very large number of images that need to be manually processed to select the images which contain the region of interest.

This system took approximately 45 minutes to image 6 wells of the plate. If a full plate were to be run this would take approximately 12 hours. As the end goal for this project is to use this process for drug or toxin screening this is not practical. Firstly, realistically one plate per day could be processed which is a severe limitation to the high throughput nature of the screen. Secondly, as live zebrafish will be used for this screen, the long imaging time may also introduce biological variation through either differences in exposure time to drugs/toxins or continued neuronal development over the course of the experiment. For these reasons the IN Cell Analyser 2000 is not suitable for this experiment.

Secondly, the UltraViewVoX spinning-disk confocal microscope was tested. This microscope was previously used to acquire images of the individually mounted zebrafish (shown in section 6.2.1.2 on page 185), thus showing it is capable of producing high quality images from which the number of neurons in the diencephalic catecholaminergic cluster can be quantified. Using the stage on this microscope it was possible to pre-set the X, Y and Z positions in each well before setting the system to take images at all of these points. This process required much more initial user input, but dramatically reduced the total time of the imaging process and increases accuracy as all images included the region of interest and were in focus. On this microscope it was recommended that the outside wells of the plate are not used to avoid any damage to the objective while moving between wells, leaving 60 usable wells on the plate. It was possible to pre-set all the points in around 30 minutes. Once the imaging started the microscope took 45-60 minutes to image the whole plate, depending on the exposure time and number of slices in the stack. To ensure the region of interest was captured in each well, a range of approximately 120µm was set to be included in the stack

with 2 μ m z slices. This was a larger region than was typically used for individually imaged embryos, but it allowed for any slight movement of the plate as it was moved between wells. This imaging system was used for all subsequent experiments.

To improve the image quality Greiner μ Clear 96 well plates, designed specifically for imaging purposes, were used. These plates have black walls and an optical-quality base allowing better imaging of the subject inside the well. To further increase the clarity of the acquired images the composition of the mounting media was optimised. When imaging individually mounted embryos, the embryo was pressed directly against the cover slip with the agarose bubble over the top to hold the embryo in place (Figure 88E). This meant there was less medium between the objective and the region to be imaged; and therefore, minimal distortion and a higher resolution image. When imaging the embryos loaded into the wells, there was a small amount of agarose between the embryo and the base of the plate which varied slightly between wells (Figure 88F). To ensure as high image quality as possible the material composing the well should be as transparent as possible. For this reason a range of materials were tested. These were: silicone, and a variety of concentrations of both standard and LMP agarose.

Sylgard[®] 184 Silicone Elastomer (Dow Corning) was combined as a base and curing agent at a ratio of 10:1 (weight:weight). This was incubated at room temperature for 48 hours to set in a 96 well plate using the mould. Although this product has a high optical quality, removal of the mould resulted in damage to a high proportion of the wells, making it unsuitable for using for this purpose.

Figure 90 shows a comparison between images taken from individually mounted embryos (Figure 90A) and embryos mounted in wells made from a range of concentrations of standard and LMP agarose (Figure 90D and E). An overview of the wells made with standard and LMP agarose is shown in Figure 90B and C respectively. Towards the lower concentrations of both standard and LMP agarose the wells become less defined, the embryos sit higher within these well and were held less securely. The lowest concentrations tested were not used as they failed to make defined wells. The images of embryos mounted in LMP agarose wells are clearer than with standard agarose. A concentration of 1.6% LMP agarose was taken forward to future experiments as it was the lowest concentration of LMP agarose which gave the highest quality images.

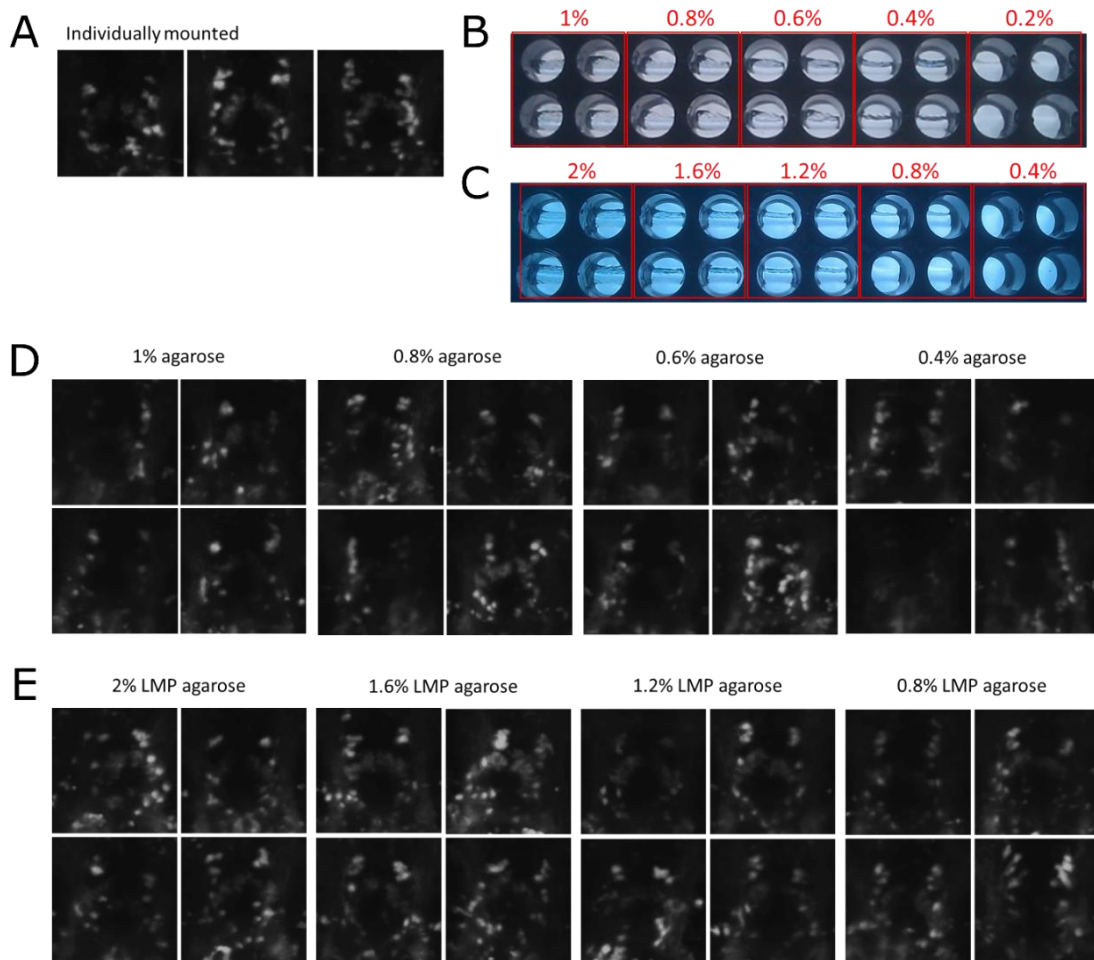


Figure 90. Testing different concentrations of agarose to make wells. *A*, *D* and *E* are maximum projection images of the diencephalic catecholaminergic cluster. *A* shows an example of images taken from individually mounted embryos for comparison. *D* and *E* show images taken of embryos mounted in wells made of different concentrations of standard and LMP agarose respectively. *B* and *C* show an overview of the wells made with standard and LMP agarose respectively.

6.3.2 Results

6.3.2.1 Validation of high throughput imaging process

To validate whether the image quality and reliability of the images taken using this method were sufficient to replicate results obtained with individually mounted embryos, the MPP+ treatment was repeated. Two biological replicates of this experiment were performed with 10 embryos per group. The variation between the two experiments was larger than expected. In the first replicate there is only a small and non-significant decrease in total fluorescence intensity in the MPP+ treated group (Figure 91A). However, in the second replicate the results are very similar to what was seen with individually mounted embryos. To determine whether the variation between these results and previous results are due to image quality issues or due to variation in the MPP+ treatment, the number of neurons

present in each image were counted. This was performed whilst blinded to treatment group of each image.

Although images obtained using the mould did not have the same resolution as images from individually mounted embryos, it was still possible to identify the individual neurons in these images. However the variation in the resolution of the images was noticeable. This is likely to be due to variation in the depth of the well; in some wells the embryo is further from the objective than in others. This is likely to introduce some of the variation in fluorescence intensity readings in the results shown below. The neuron counting results are shown in Figure 91B. These data show a statistically significant decrease in neuron number in both replicates. However, this decrease is not as large as in previous MPP+ treatment experiment where a 60% decrease in neuron number was observed (Figure 86). These results show that whilst the fluorescence intensity measurements are not as robust using this imaging system it is still possible to detect significant changes in dopaminergic neuron number by performing neuron counting on images captured in this way. With the ongoing development of a software to automatically count neurons in this region, it is likely that this system can be used to generate robust and reproducible data sets in the near future.

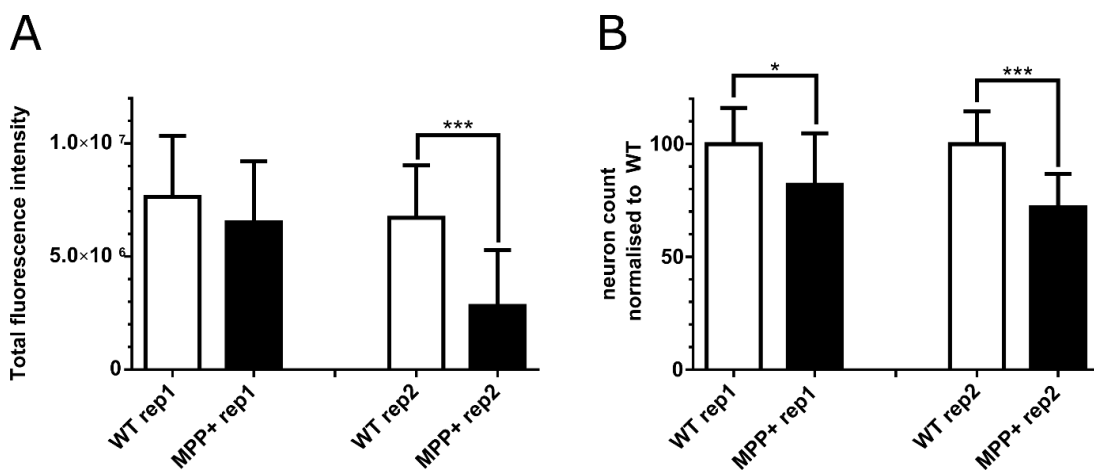


Figure 91. Fluorescence intensity measurements using new mounting and imaging technique. *A* shows data analysed by measurement of the total fluorescence intensity and *B* shows data analysed by neuron counting of the same images. Error bars represent standard deviation. 10 embryos were imaged per group, data was analysed using an unpaired t-test with Welch's correction, * = $p < 0.05$ and *** = $p < 0.001$.

6.4 Discussion

The aims of this chapter were to develop a method by which the *ETvmat2:GFP* reporter line can be used to replace traditional neuron counting experiments and to develop a high throughput image analysis system allowing the first method to be implemented as the read out of a phenotypic drug screen. Data in this chapter validate the use of the *ETvmat2:GFP* reporter line for dopaminergic neuron counting, and progress has been made towards developing a high throughput imaging system. This system may, in the future, be used to perform a phenotypic drug or toxin screen to identify compounds that modify the number of dopaminergic neurons using the measurement methods developed with the *ETvmat2:GFP* reporter line as a read out.

Using the ETvmat2:GFP reporter line to measure dopaminergic neuron number

In this study it has been demonstrated that the *ETvmat2:GFP* reporter line labels the *th+* dopaminergic neurons and can be used to measure the number of dopaminergic neurons in the diencephalic catecholaminergic cluster. Compared to using WISH to identify dopaminergic neurons for manual counting, using this fluorescent reporter line to measure number of dopaminergic neurons allows for a large time saving as these embryos may be used live at 3dpf and do not require additional staining protocols. Although WISH is a powerful tool for determining expression patterns, the protocol is labour intensive and there is potential for error due to the inadvertent mixing of groups as there are many wash steps. Simplification of any protocol is always desirable as it reduces the number of stages at which errors can be made and therefore increases efficiency and accuracy of the experiment. Decreasing the process time of the experiment also increases the efficiency of the experiment as it allows a greater number of samples that can be processed in a given period.

The staining intensity using WISH can also be quite variable. Variation in the bleaching and permeabilisation of embryos, differences in the length of time the embryos are present in stain solution and clearing solution, may all affect the staining intensity and clarity. If the staining intensities or clarity of the staining varies between groups or experiments this may introduce error in neuron counting, and a number of samples may need to be excluded if neuron counting is not possible. When using a fluorescent reporter line, as long as care is taken to ensure all groups carry the same number of copies of the transgene, the fluorescence intensity is less likely to vary considerably between individuals. However, care must always be taken to ensure groups are treated as similarly as possible.

One disadvantage of using a fluorescent reporter line, however, is that as the zebrafish must be imaged live; therefore these experiments have a fixed time in which they must be performed. This decreases the flexibility of the experimental process and increases the reliance on availability of equipment.

For experiments described in this chapter, care was taken to ensure that only embryos which were heterozygous for the *ETvmat2:GFP* transgene were included in experiments. To do this, our colony of *ETvmat2:GFP* which is a mix of zebrafish which are heterozygous and homozygous for this gene were outcrossed to WTs then GFP positive embryos were selected at 24hpf. This adds another manual step in the process. In order to use this line for high throughput analyses, a colony of zebrafish which are exclusively homozygous for the transgene could be created. Progeny from an incross or outcross of this colony would all be homozygous or heterozygous, respectively, thus ensuring the copy number of the transgene remains equal and removing the requirement for manual sorting of the embryos.

The first method developed to detect changes in neuron number in the diencephalic catecholaminergic cluster using the *ETvmat2:GFP* reporter line involved measuring the total fluorescence intensity of a maximum projection image of this region. This method is desirable as it is easily automated using standard image analysis software ImageJ and avoids subjective manual counting of neurons which may introduce researcher bias. This method was able to detect large changes in dopaminergic neuron number. The large 60% decrease detected by neuron counting after MPP+ treatment was accurately replicated by measurement of fluorescence intensity (Figure 86). There was no significant difference in the percentage change detected by either method. It has been previously established by the researchers who generated the *ETvmat2:GFP* reporter line that the GFP labelled neurons corresponding to *th+* neurons are sensitive to MPP+ treatment (Wen et al. 2008). However, the present study is the first to develop a method that can accurately quantify this decrease in neuron number using the *ETvmat2:GFP* reporter line.

In miR-133b morphants that display a 20% increase in dopaminergic neurons, as detected by traditional neuron counting, the increase in neuron number as measured by total fluorescence intensity was over estimated; an increase of 40% was identified using this method (Figure 85). The total fluorescence intensity is calculated by multiplying the area above threshold by the mean fluorescence intensity of this region. It is possible that the large increase calculated by this measurement is due to the increased expression levels of dopaminergic markers as well as the increased number of neurons. As shown in Figure 28 in

Chapter 3 (page 95), miR-133b knockdown resulted in a 40% increase in *th* expression at 3dpf as assessed by qPCR; although this change is not significant there is a strong trend. Therefore *vmat2* may also be upregulated in miR-133b morphants. For GFP expression to be influenced by increased *vmat2* expression in the *ETvmat2:GFP* reporter line, increased activation of the enhancer must be the cause of *vmat2* upregulation. To determine the individual involvement of the two components making up the total fluorescence intensity reading these two readings were plotted individually.

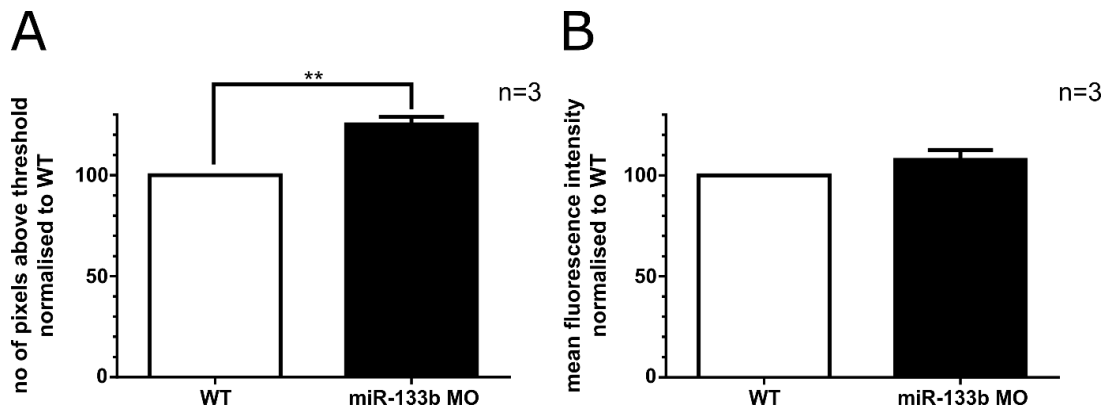


Figure 92. Contribution of area and intensity to total fluorescence intensity reading in WT and miR-133b morphants. The contribution of the two factors making up the total fluorescence intensity reading are plotted individually in this graph. **A** shows the area reaching the threshold in WT and miR-133b morphants. There is a 25% increase in area above the threshold in the morphants. **B** shows the mean fluorescence intensity of the area above the threshold, there is a slight but non-significant increase in mean fluorescence intensity in the morphants. Data are from three biological replicates. Error bars represent standard deviation. Data are analysed by an unpaired t-test with Welch's correction, ** = $p < 0.01$.

As shown in Figure 92, an increase in both area above the threshold (measured as a number of pixels) and mean fluorescence intensity is present in the morphants. The increase in area above the threshold in the morphants (25%) more accurately recapitulates the increase in number of neurons calculated by neuron counting (20%). Although the increase in mean fluorescence intensity does not reach significance alone, it does contribute a portion of the variation in total fluorescence intensity (area above threshold multiplied by mean fluorescence intensity). Although it may be possible for an increase in Pitx3 to be driving increased activity of the *vmat2* enhancer due to the Pitx3 binding site present here (Hwang et al. 2009), the direct regulation of Pitx3 by miR-133b has not been confirmed in this study.

More subtle changes in dopaminergic neuron number were not detectable by measuring total fluorescence intensity. However, it was possible to accurately measure these differences using the *ETvmat2:GFP* reporter line by counting neurons using the substack image. These data show that the images taken using this reporter line are of sufficient quality to precisely identify individual neurons (Figure 87).

Neuron counting is a more sensitive method as, unlike measurement of total fluorescence intensity in this region which measures any pixels which reach the set threshold value, it is possible to discriminate the sub-populations of dopaminergic neurons. For changes in neuron number relevant to PD, the population of dopaminergic neurons with ascending projections are important. These neurons are analogous to the neurons of the *substantia nigra* in humans. In the developing zebrafish brain the dopaminergic neurons which belong to Wulliman-Rink groups 1, 2, 4 and 5 are those neurons with ascending projections into the sub-pallium (analogous to the human striatum). For this reason, only neurons from these groups are counted in neuron counting experiments.

When performing neuron counting post-WISH the whole head is mounted. Any distinct morphological changes, such as small head induced by the treatment conditions or genotype can be easily recognised and potentially introduce researcher bias. Using images of a small region of the brain to count neurons, such as those processed from images of the *ETvmat2:GFP* reporter line, provides less distinguishing features between treatment groups. This may reduce researcher bias despite still relying on subjective neuron counting.

In order to automate the image analysis process further, a collaboration with Professor Alex Frangi in the Department of Mechanical Engineering in Sheffield was established. His group are developing software that can automatically, and therefore objectively, count the neurons in the diencephalic dopaminergic cluster. At first this software was being developed using images from WISH for *th*; however, it is currently being adapted for use with images of the *ETvmat2:GFP* reporter line. This software will be a powerful tool for us to use in our research as it will eliminate researcher bias from our neuron counts and also speed up the process of image analysis considerably.

Development of a high throughput imaging process

The future direction of this project is to generate a high throughput imaging process which in conjunction with the *ETvmat2:GFP* reporter line may be used to perform a phenotypic drug or toxin screen.

One limitation of imaging studies that require standardised views of the zebrafish embryo is the lack of tools that allow consistent and quick mounting of zebrafish. For the initial experiments performed using the *ETvmat2:GFP* reporter line the embryos were individually mounted in 1% agarose; a time consuming process. Recently, a tool was developed by Westhoff and colleagues which enables quicker mounting of zebrafish for imaging studies.

The same group published a second version of the tool which was generated by 3D printing (Wittbrodt et al. 2014), enabling the reproduction of this tool in Sheffield. The second part of this chapter consisted of preliminary work to develop a high throughput mounting and imaging system using this tool.

Use of the tool to generate wells in a 96-well plate able to hold zebrafish embryos in the desired position drastically reduced the amount of time spent mounting and imaging embryos. Two imaging systems were tested to assess the quality of images captured from zebrafish mounted in this way. The UltraViewVoX spinning-disk confocal microscope was chosen as the most suitable system for imaging these embryos. This system is compatible with imaging in microtitre plates and allows the user to pre-set the X, Y and Z position for each well before allowing the system to image each well. Although this requires more user input, it ensures that the region of interest is captured in every well. The overall image acquisition speed of this microscope was also much faster than the other system tested. As the embryos are imaged live, reduced imaging time is extremely important to reduce variation between the first and last embryos to be imaged. The UltraViewVoX spinning-disk confocal microscope was also used to capture images of individually mounted zebrafish in the initial development of use of the *ETvmat2:GFP* reporter line showing that is able to capture high quality images that can be used to measure dopaminergic neuron number.

One limitation of using the UltraViewVoX spinning-disk confocal microscope is that the outer wells of the 96 well plate cannot be used for automated imaging. This is to reduce the risk of damage to the objective. If the outer wells are used it is possible the objective may come into contact with the stage as it moves around the plate. This leaves 60 usable wells per plate. Another limitation is that as this is an inverted microscope, the embryo must be imaged through the base of the plate and a small amount of agarose that comprises the well, this is depicted in Figure 88F (page 194). The depth of the well and the position of the embryo within the well are slightly variable, resulting in quality differences between the images captured. To reduce the variability caused by this optical quality plates were used and material composing the well was optimised to ensure it was transparent as possible and consistent wells could be produced.

The quality of the images generated using this mounting and imaging system was tested using WT and MPP+ treated embryos. Using individually mounted embryos, a 60% decrease in fluorescence intensity was measured after MPP+ treatment. Using a measurement of fluorescence intensity a 15% decrease was measured in replicate1, this was not significant,

and a 60% decrease was measured in replicate2, $p < 0.001$. The variation between the biological repeats is unexpected, further experiments must be performed to determine whether this variation is inherent of this technique or whether the result from the first experiment is anomalous. The variation within the groups (images of 10 embryos was taken and analysed per group) is also very high. The standard deviation of these groups was compared to the standard deviation of WT and MPP+ treated embryos imaged after individual mounting. To ensure these standard deviations are comparable the standard deviation was taken from groups with contain the same number of data points. The standard deviation of the measurement normalised to the average of the WT value was used. This comparison is shown in Figure 93.

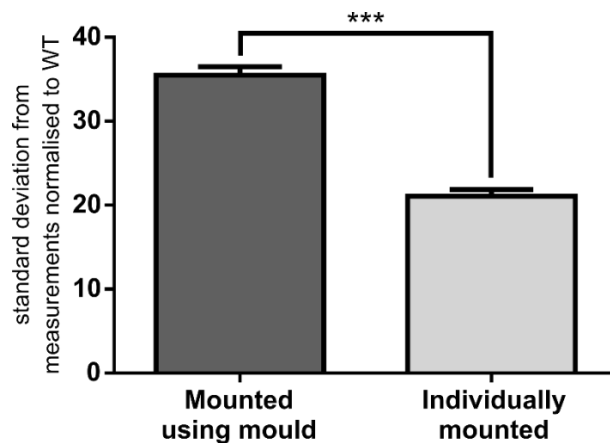


Figure 93. Comparison of standard deviation from image analysis data from mould mounted and individually mounted zebrafish embryos. This graph shows the variation in the fluorescence intensity values calculated from images captured from embryos mounted within the mould ($n=4$) is significantly higher than the variation in the fluorescence intensity values calculated from images captured from individually mounted embryos ($n=2$). To ensure the standard deviations presented here are comparable, the standard deviations used were calculated from WT and MPP+ treated groups where the fluorescence intensity measurement were normalised to the average of the WT value. The same number of embryos were analysed per group. Error bars represent standard deviation. These data are analysed by an unpaired t-test with Welch's correction, *** = $p < 0.001$.

This shows that the fluorescence intensity measurements within groups taken from images of embryos mounted within the mould are significantly more variable than individually mounted embryos. This is likely to be due to the variability in the depth of the well and the position of the embryo within the well as mentioned above. These data show that the images taken with mould-mounted embryos are not consistent enough to enable this measurement to be used. As the neuron counting has already been established as the more robust read out from these images it was important to determine whether the image quality of embryos imaged within the mould is sufficient for neuron counting. It was possible to identify and count individual neurons using these images and significant differences in the neuron

number between the WT and MPP+ treated groups where detectable. While these decreases are not as large as expected further work needs to be performed to determine whether this is an inherent shortcoming of image quality and whether data generated in future experiments is reliable and reproducible. Images generated using embryos mounted within the mould must be tested with the software being developed by Professor Alex Frangi and Bo Dong.

An upright (non-inverted) fluorescence microscope may be capable of generating higher quality images as the issue of distortion is caused by imaging through the base of the plate and well. Although no upright microscopes which can capture images of a high enough quality are currently available within the department, these may become available in the future. Another possibility which may allow capture of higher quality images while maintaining high throughput mounting and imaging techniques is to investigate the development of a microtitre plate which has similar shaped wells to the ones produced using this mould. This would remove the need for using agarose or other medium within the well and therefore may increase optical clarity of the captured images.

Future prospects for phenotypic drug screening using the described method

The present study aimed to develop methods which allow for a more time and cost effective analysis of dopaminergic neurons which may be applied to a high throughput screen. To do this the use of the *ETvmat2:GFP* reporter line was combined with the use of a mould for quick and accurate orientation of zebrafish allowing a standardised view of the zebrafish embryo to be captured.

Until now, the barrier preventing us from performing such a screen has been a technical one. Manual staining of the dopaminergic neurons by WISH followed by neuron counting is preventatively time consuming and would only allow a very small number of compounds to be tested. Despite this, a previous study has been performed that assessed the effects of over 5000 compounds on the development and survival of dopaminergic neurons using IHC for TH and subsequent manual imaging of these embryos (Sun et al. 2012). Although this study was successful in identifying compounds which had previously unknown neurotoxic effects on dopaminergic neurons, this model for performing drug screens is highly time consuming and not economically viable for most laboratories to perform. As discussed above, using a combination of the reporter line and the mould for mounting embryos allows for a large time saving thus hugely increasing the potential for processing large numbers of samples in a time and cost effective manner. The 96-well plate format of the mould increases

compatibility with liquid handling machinery that is commonly used for high throughput compound screens. In this section, the features of the drug screen which may be performed using the method described in this chapter will be discussed and compared to other similar drug screens.

For reasons previously discussed, zebrafish are a popular model organism for use in drug screens. To increase the number of compounds it is possible to screen, these studies are designed to have very simple read outs, such as a change in fluorescence which is present in a large area, and often do not require manual manipulation to generate the images needed. A study by McGown and colleagues used fluorescence from embryo homogenates as the read out. Using this simple read out, the authors were able to screen 2000 compounds from the spectrum library. Using their highly automated set up it was possible for an individual to screen approximately 250 compounds per day (McGown et al. 2013 and personal correspondence). Screens which require more complex read outs are often limited to smaller number of compounds. The group which originally designed the mould used in this study were able to perform a pilot drug screen examining the effects of 7 different compounds at 5 different doses on a number of morphological features of the developing kidney (Westhoff et al. 2013). This drug screening pipeline used by this group is easily modifiable for a number of readouts, such as the readout described in this study.

Fully automated systems are much more amenable for high content screening and larger numbers of compounds can be tested. Technologies are continually being developed to allow a larger proportion of the steps in the drug screening process to be automated. One such study screened 640 compounds to identify modulators of the acute-immune response in transgenic zebrafish which express GFP in neuromasts and RFP in granulocytes. The authors developed a method to chemically injure the zebrafish thus removing the need to manually injure the embryos. The chemical insult and drug treatment were performed with a liquid handling system before the embryos were imaged using a high content microscope. The images were analysed using custom developed software which allowed measurement of granulocyte presence around the injured neuromasts (Wittmann et al. 2012).

The phenotypic drug screen we hope to be able to perform in the future shares many commonalities with the studies mentioned. Primarily the use of fluorescent reporter lines is key. The orientation technique developed by Westhoff and colleagues will be used. However, unlike their screen where the gross morphology of the developing kidney is scored, our proposed screen will have a quantitative read out indicating change in neuron number in a

specific region of the brain. Similar to the study performed by Wittmann and colleagues, this read out will be generated by custom developed software. Similar to the screens described by Westhoff and Wittmann, another benefit using the imaging method described in this chapter is that any toxic or off target effects can be identified in the same screen as an image of the whole head is captured, and therefore any toxic compounds can be identified quickly and easily and removed from analysis. A potential pipeline for this drug screen is shown in Figure 94.

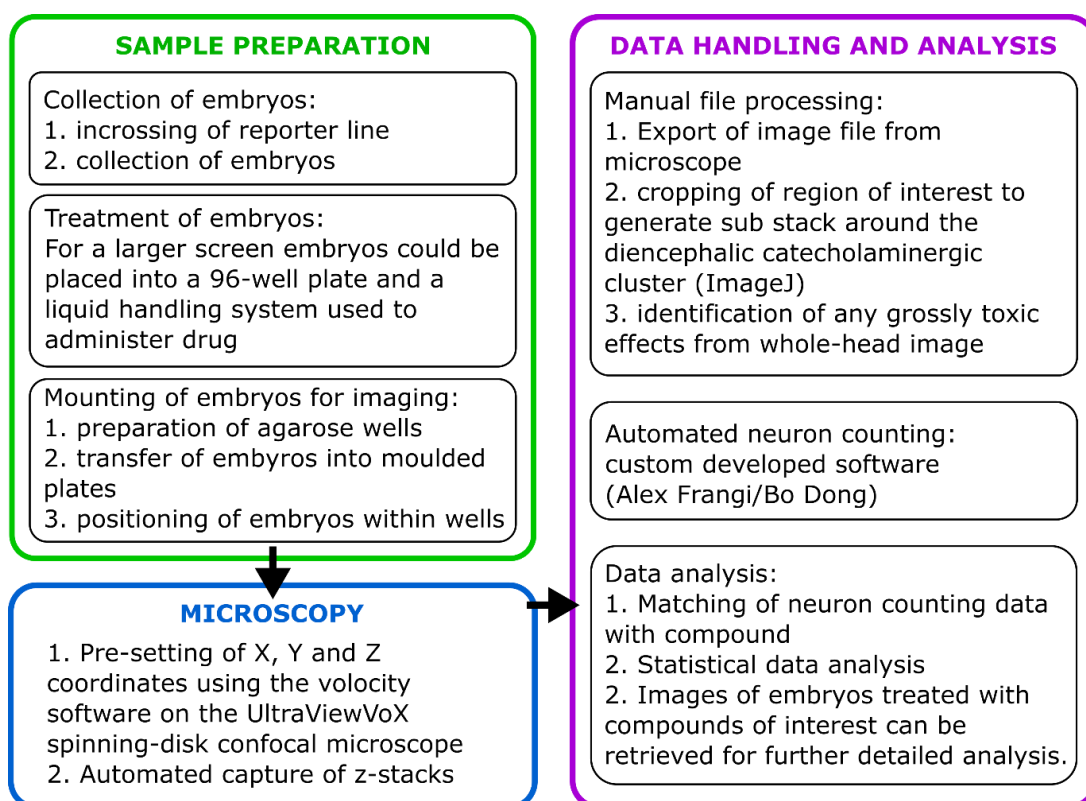


Figure 94. Potential drug screening pipeline.

With the advances described in this chapter and further development of the image analysis technique and the automated neuron counting software, it is plausible to assume that it will soon be possible to undertake a PD-orientated phenotypic drug or toxin screen in our group in the near future.

Chapter 7. General Discussion

Contents

Chapter 7. General Discussion.....	210
7.1 Overview	212
7.2 Main limitations	212
7.3 Neuroinflammation and PD	215
7.4 miRNA involvement in neurodegeneration and therapeutic potential.....	216
7.5 Concluding remarks	220

7.1 Overview

The first aim of this thesis was to investigate the function of three miRNAs, which may be relevant to PD, in zebrafish. These miRNAs were chosen as a single, well conserved orthologue of these miRNAs and their relevant target genes are present in zebrafish. The first two chapters investigated whether modulation of miR-133b and miR-205 expression resulted in a change in dopaminergic neuron number through altered regulation of their targets *pitx3* and *Irrk2*. As hypothesised, knockdown of miR-133b resulted in an increase in dopaminergic neuron number. However, this study was not able to elucidate the mechanism for through which this occurs. Neither *pitx3* nor *Irrk2* were confirmed as direct targets of miR-133b or miR-205 in zebrafish. The third chapter investigated the involvement of miR-155 in three zebrafish models of neurodegeneration. No change in miR-155 was observed in zebrafish models of *pink1*- or *parkin*-deficiency, however an increase in miR-155 was observed in a zebrafish model of Gaucher's disease. This is the first study which has implicated miR-155 in the pathogenesis of Gaucher's disease.

The second aim of this study was to develop an imaging system which would allow high throughput screening of the zebrafish larval brain. This project was successful in validating use of the *ETvmat2:GFP* reporter line as an alternative method for measuring dopaminergic neuron number. Progress has been made towards developing an imaging system, however further work needs to be performed to validate the quality of the images captured.

The results of each individual study and suggested future work is discussed in the respective chapters. In this chapter the overall findings and limitations of this study will be discussed.

7.2 Main limitations

The main limitation of this study is that all work was carried out in zebrafish. Although this model organism confers many advantages for the study of human diseases, not least their practical simplicity and low cost, they are less closely related to humans than rodents or primates. In order to draw conclusions from animal models of disease there must be evolutionary conservation of the involved biological processes. More than 90% of human genes have a recognisable orthologue in mice, while in zebrafish the percentage of conserved genes is closer to 70% (Chinwalla et al. 2002; Howe et al. 2013). Despite the fact that zebrafish are more distantly related to humans than rodents, zebrafish models of PD have shown promise in modelling neurodegeneration while the majority of mouse models have failed to demonstrate neurodegeneration (Blesa & Przedborski 2014; Flinn et al. 2013). However, the more recently developed rat models are a promising mammalian model of PD.

Although the zebrafish CNS has a similar overall organisation to the human brain there are many structural differences. Of particular relevance to PD research are the dopaminergic neurons. In mammals the ascending dopaminergic neurons are present in the midbrain, whereas in zebrafish they are present in the forebrain. However, the ventral telencephalon (subpallium) and the posterior tuberculum and their containing neurons display many similarities to the human nigrostriatal system (Xi, Noble, et al. 2011; Rink & Wullimann 2001). Although the factors involved in development of the ascending dopaminergic system in zebrafish is not as well studied as the development of the human system, many transcription factors involved in this process are thought to have conserved roles in zebrafish (Filippi et al. 2007). To validate that PD-causing mutations in zebrafish accurately model neurodegeneration, the effect of these developmental factors must be studied to ensure that any decrease in dopaminergic neurons observed is due to degeneration of neurons, rather than a developmental phenotype.

A major difference between zebrafish and humans which may impact research into mechanisms of neurodegeneration is that zebrafish have a high regenerative capacity and are able to regenerate many tissues which humans cannot. Neural stem cells and neurogenesis has been detected in the zebrafish brain. Although neurogenesis does occur in adult human brains the zebrafish brain has higher proliferative potential (Schmidt et al. 2013). This feature of zebrafish does present some advantages as research may be undertaken allowing a deeper understanding of the mechanisms behind regeneration, with the aim of stimulating similar regeneration in human tissues. However, for modelling neurodegenerative diseases, such regeneration is a disadvantage as neuron loss may stimulate regenerative pathways thus obscuring pathogenic changes.

Another feature of the zebrafish to consider is that approximately 20% of human genes have multiple orthologues in zebrafish (Postlethwait et al. 2004). This is due to a large genome duplication event in teleost ancestry which has resulted in functional redundancy for many genes (Postlethwait 2000; Prince & Pickett 2002). The majority of the genes directly investigated in this study are thought to have only one orthologue in zebrafish. However, wider pathways involved in pathogenesis may be affected by multiple copies of a gene, thus complicating investigation of these affected pathways.

For the above reasons findings in zebrafish models would benefit from validation in mammalian animal models or in human cell culture. Previously, the effect of modulating miR-205 and miR-133b have been studied in cell culture models. The effect of knockdown of

miR-205 has been studied in primary neurons derived from transgenic mice expressing mutant LRRK2; in these cells knockdown of miR-205 exacerbated the neurite outgrowth defect through increasing the load of mutant LRRK2 (Cho et al. 2013). The effect of miR-133b knockdown was also examined in mouse embryonic stem cells; an increase in expression of dopaminergic markers *TH* and *DAT* was observed after miR-133b knockdown (Kim et al. 2007). However, a miR-133b knockout mouse did not display any neuronal phenotype (Heyer et al. 2012). This is unexpected, however may reflect differences in dopaminergic neuron vulnerability in mice. The present study represents the first to uncover an effect of miR-133b knockdown at a system level. However, in light of the mouse knockout data the effect observed in this study must be reproduced in another animal model to ensure this is not a teleost-specific effect. Study of the effect of these miRNAs in rat models may be more appropriate than studies in mice.

Although human cell culture models are not able to represent a whole system, study of these miRNAs in human cells will be important to validate that the effects of these miRNAs are relevant in a human model system. In human patient fibroblasts, neither miR-133b nor miR-205 were detectable (Mandal 2014). However, as both of these miRNAs are thought to be expressed specifically in midbrain neurons, iPSCs differentiated to a dopaminergic phenotype may be a suitable model to study the effect of knockdown of these miRNAs.

Zebrafish larvae are highly suited to phenotypic drug screening. One of the advantages of zebrafish for drug screening is their permeability, allowing drugs to be placed into the medium surrounding the larvae. However, limitations to consider when using this system for drug discovery for neurodegenerative disorders include the differences in the blood brain barrier (BBB). One of the major obstacles limiting development of drugs to treat brain disorders is that less than 2% of small molecules are able to cross the BBB (Pardridge 2005). In zebrafish the BBB is thought to mature between 3dpf and 10dpf. Fleming and colleagues used 5-10dpf zebrafish to examine penetration of the BBB by a number of compounds which are either known to be penetrant or excluded from the brain in mammals. Although the BBB had not fully matured in these larvae, differences in concentration, which increased with age, were observed between the trunk and head for molecules which are known to be excluded from the brain in mammals (Fleming et al. 2013). These data suggest that although the BBB is not fully formed, non-penetrant compounds will have, at least, a reduced bioavailability in the brain. Therefore when performing compound screens in zebrafish further analysis of compounds of interest must be performed to show that these can indeed penetrate the BBB.

Another important limitation of this study is the method used to generate knockdowns. MOs were used to generate a knockdown of both miR-133b and miR-205. Findings with MOs should be validated with a stable mutant, especially as recent studies have identified differences between MO-induced knockdown and stable mutant lines (Kok et al. 2015; Rossi et al. 2015). MOs may also result in off-target effects (Robu et al. 2007). While these are unlikely to have resulted in the increase of dopaminergic neurons observed after miR-133b knockdown, the mild decrease in dopaminergic neurons after miR-205 knockdown may have been due to developmental delay or non-specific apoptosis. Therefore longer term studies with a stable mutant are required to validate this.

7.3 Neuroinflammation and PD

It is currently unclear whether neuroinflammation is a primary or secondary feature of PD, however attenuation of this inflammatory response has been shown to have beneficial effects in animal models (Wu et al. 2002). While moderately activated microglia play a homeostatic and protective role in the brain by removing dying cells and releasing trophic factors such as BDNF, fully activated microglia release inflammatory cytokines and reactive oxygen species. The *substantia nigra* may be more vulnerable than other regions to oxidative damage due to increased content of oxidisable species, including dopamine and neuromelanin, and reduced anti-oxidant capacity (Block et al. 2007). Oxidative stress is known as a key pathogenic factor in PD however this is usually studied in the context of mitochondrial dysfunction (Celardo et al. 2014). Activated microglia, as well as increased levels of inflammatory cytokines, have been identified in the *substantia nigra* and other affected brain regions of PD patients (Imamura et al. 2003). Breaking the neuroinflammatory cycle by attenuation of oxidant producing enzymes in MPTP-induced mouse models of PD have been shown to ameliorate neuron loss and protein oxidation (Choi et al. 2005; Wu et al. 2003).

One of the aims of this study was to investigate the involvement of miR-155, a pro-inflammatory miRNA which modulates microglial activation, in PD pathology. In this study miR-155 was not found to be upregulated in either 5dpf larvae or adult brains of *pink1*- or *parkin*-deficient zebrafish. This suggests that miR-155 may not play a role in the pathogenesis of *pink1* and *parkin* related PD. This does not, however, prove that inflammation is not important in the pathogenesis of PD. Inflammation may be driven through different mechanisms that do not involve miR-155, miR-155 may be more relevant in other genetic forms or sporadic cases of PD, or zebrafish may be more resistant to

inflammation as a result of mutations in *pink1* and *parkin*. Previously *pink1*-deficient zebrafish have been shown to have an increased number of microglia. However inhibition of PU-1 to, prevent microglial maturation, did not result in rescue of dopaminergic neuron number (Flinn et al. 2013).

The expression of miR-155 was also examined in *gba1*-deficient zebrafish. Although no change in miR-155 was observed in zebrafish carrying one mutant copy of *gba1*, increases in miR-155 were observed in both the larvae and adult brain of homozygous mutant zebrafish. The contribution of neuroinflammation to neuronal cell death in Gaucher's disease has previously been investigated (Vitner et al. 2012), however this is the first study to implicate miR-155 in Gaucher's disease. The early upregulation of miR-155 is intriguing as this upregulation occurs before any neuronal loss is observed. This suggests that inflammation may be an early feature of Gaucher's disease which precedes neurodegeneration. The oldest heterozygote zebrafish studied were 3 months old. It is possible that any inflammatory phenotype in these zebrafish may manifest much later and therefore older zebrafish should be studied to investigate this.

Microglial activation has been associated with many other neurodegenerative disorders, including MND, Huntington's disease, Alzheimer's disease and multiple sclerosis (Pavese et al. 2006; Schlachetzki & Hüll 2009; Brettschneider et al. 2012; Giunti et al. 2014). This suggests that neuroinflammation may provide a link between these disorders. As neurodegeneration appears to result in excessive inflammation which in turn results in further neuronal toxicity and cell death, breaking this cycle by inhibition of microglial activation and release of inflammatory factors may be a valuable therapeutic strategy.

7.4 miRNA involvement in neurodegeneration and therapeutic potential

miRNAs are implicated in a large number of biological processes and expression changes of miRNAs have been implicated in many human diseases (Esteller 2011). The Human microRNA Disease Database lists miRNA associations with human diseases (this is accessible at: <http://210.73.221.6/hmdd> (Lu et al. 2008)). There are also reported cases where mutations in either a single miRNA or miRNA binding site have been shown to be causative of a disease. For example, deletion of an intragenic region containing miR-361 results in Choroideraemia (van Bokhoven et al. 1994), and two point mutations identified in the 3'UTR of *REEP1* have been associated with autosomal dominant form hereditary spastic paraplegia (Beetz et al. 2008; Züchner et al. 2006). Other such mutations are reviewed by Meola et al. (2009).

Approximately 70% of miRNAs are expressed in the CNS (Cao et al. 2006). As previously discussed, deletion of *dicer* in neuronal populations results in the death of many neuronal populations (Kim et al. 2007; Schaefer et al. 2007; Huang et al. 2010). These data show that miRNAs are required for development and survival of many neuronal groups, therefore disruption of the miRNA network may contribute to neurodegeneration. In many neurodegenerative disorders there is a clear gene dosage effect which contributes to pathology. For example, duplication or triplication of the *SNCA*-containing locus is causative of PD (Singleton et al. 2003). Similarly, duplication of the amyloid precursor protein encoding gene (*APP*) results in early onset Alzheimer's disease (Rovelet-Lecrux et al. 2006). Moreover, in PD altered levels of both α -synuclein and LRRK2 have been detected in sporadic cases of PD (Chiba-Falek et al. 2006; Cho et al. 2013). As such dosage effects are apparent in neurodegenerative disorders it is conceivable that dysregulation of miRNAs that negatively regulate these genes may contribute to disease pathology. Even if this cannot be proven, the miRNAs which target these genes may be overexpressed as a therapy to reduce the toxic load of these proteins.

Huntington's disease is caused by a CAG repeat expansion in *huntingtin* (*htt*) resulting in an expanded polyglutamine stretch which is prone to misfolding and aggregation. miR-196a has been shown to indirectly alter the expression of *htt* and has been suggested as a therapy to reduce the toxic load of the mutant HTT protein. Overexpression of miR-196a ameliorates the phenotype of a transgenic mouse model of Huntington's disease and was able to reduce the number of protein aggregates in human iPSCs differentiated to neurons (Cheng et al. 2013). This demonstrates the therapeutic potential of this miRNA for Huntington's disease.

Inhibition of miR-155 has been shown to be protective in animal models of both multiple sclerosis and MND (Butovsky et al. 2015; Murugaiyan & Beynon 2011). Th1 and Th17 T-helper cells are involved in several autoimmune diseases including multiple sclerosis. Genetic ablation of miR-155 in the EAE mouse model of multiple sclerosis resulted in reduced Th1 and Th17 responses and reduced inflammation in the CNS (Murugaiyan & Beynon 2011). In a SOD1 mouse model of MND, loss of miR-155 normalised the abnormal and pro-inflammatory molecular signature associated with microglia in SOD1 mice. miR-155 deficient SOD1 mice demonstrated a delayed onset of symptoms and increased life-span (Butovsky et al. 2015). In both the EAE mouse model and the SOD1 model of MND, inhibition of miR-155 after the onset of symptoms was also effective at reducing symptoms or extending the life-span of the animal to some degree. As increased inflammation and microglial activation have

been implicated in a number of neurodegenerative diseases (as discussed above) it is tempting to hypothesise that the protective effects of silencing this miRNA will extend to other neurodegenerative diseases.

Development of miRNAs for therapeutics is still in its early stages, however new potential miRNA therapeutic targets are continuously being discovered and enter preclinical development, particularly in the field of cancer. There are two different strategies for miRNA-based therapeutics. Firstly, miRNA mimics can be used to downregulate specific target genes. Secondly, anti-miRNAs may be used to release specific targets from repression. Currently, there are two miRNA-based therapies in clinical trials. These are an antagonist for miR-122 for treatment of hepatitis C and a miR-34 replacement therapy for a variety of cancers (Janssen et al. 2013; Agostini & Knight 2014). miR-122 is highly expressed in the liver and appears to stabilise the hepatitis C virus by protecting it from the host innate immune response (Shimakami et al. 2012). This therapy is currently yielding promising results in phase 2 clinical trials; no adverse effects were observed in healthy volunteers in phase 1 (Janssen et al. 2013). The members of the miR-34 family have key roles as tumour suppressors in many cancers with targets including *BCL2*, *CDK4* and *MET*. Suppression of targets by miR-34 arrests the cell cycle and induces apoptosis (Agostini & Knight 2014). A miR-34 replacement therapy, MRX34, is currently in phase 1 clinical trials. There are also a number of miRNA therapies in preclinical development for diseases including cancer, cardiovascular disease and insulin resistance. A selection of these are summarised in Table 20.

Table 20. Selected miRNA therapies currently in development. Reproduced with permission from Li & Rana (2014)

MicroRNA	Oligonucleotide format	Indications	Companies	Developmental stage
miR-122	LNA-modified antisense inhibitor	HCV infection	Santaris Pharma	Phase II
miR-122	GalNAc-conjugated antisense inhibitor	HCV infection	Regulus Therapeutics	Phase I
miR-34	miRNA mimic replacement	Liver cancer or metastasized cancer involving liver	miRNA Therapeutics	Phase I
Let-7	miRNA mimic replacement	Cancer (details undisclosed)	miRNA Therapeutics	Preclinical
miR-21	2'-F and 2'-MOE bicyclic sugar modified antisense inhibitor	Cancer, fibrosis	Regulus Therapeutics	Preclinical
miR-208	Antisense inhibitor	Heart failure, cardiometabolic disease	miRagen/Servier	Preclinical
miR-195 (miR-15 family)	Antisense inhibitor	Post-myocardial infarction remodelling	miRagen/Servier	Preclinical
miR-221	Antisense inhibitor	Hepatocellular carcinoma	Regulus Therapeutics	Preclinical
miR-103/105	Antisense inhibitor	Insulin resistance	Regulus Therapeutics	Preclinical
miR-10b	Antisense inhibitor	Glioblastoma	Regulus Therapeutics	Preclinical

2'-F, 2'-fluoro; 2'-MOE, 2'-O-methoxyethyl; GalNAc, N-acetylgalactosamine; HCV, hepatitis C virus; LNA, locked nucleic acid; miRNA, microRNA.

There are still, however, many challenges facing the development of miRNA therapies, particularly for neurodegenerative disorders. The main obstacle, as with all therapies for brain diseases, is the issue of delivery to the brain. Many strategies to aid delivery of miRNA based therapies are being developed; progress in delivery strategies is reviewed by Zhang et al. (2013). One promising strategy for delivery of miRNA therapeutics to the brain are exosomes; these are naturally occurring nanovesicles which transport mRNA and proteins. Alvarez-Erviti and colleagues showed that exosomes purified from dendritic cells from a particular animal did not result in an immune response when injected intravenously to the brain of the same animal. These exosomes were able to deliver siRNA to the brain of mice (Alvarez-Erviti et al. 2011). It has been suggested that miRNAs may be an active therapeutic element in some herbal medicines, after plant miRNAs were identified in human tissue after ingestion of such medication (Sala-Cirtog et al. 2015). Although the functional effects of these miRNAs are yet to be validated, study of the delivery of these plant miRNAs may present new strategies for encapsulation of known therapeutic miRNAs.

Another important feature of miRNA-based therapies which can be both an advantage and a limitation is the large number of potential targets of each miRNA. For the promising anti-cancer miR-34 based therapy, inhibition of a large number of targets is beneficial and a network of potentially oncogenic genes is repressed. For other potential therapies, however,

researchers must be aware of the wide range of targets that each miRNA may have and ensure that modulation of these targets does not result in unwanted side effects.

Despite the challenges that remain for the development of miRNA therapies for neurodegenerative disorders, the rapidly advancing field of miRNA research may uncover new directions for potential therapies. This is not only possible by identifying miRNAs that may be directly useful as therapeutic targets but also by elucidating novel cellular mechanisms involved in pathogenesis through miRNA research.

7.5 Concluding remarks

One of the main aims of this study was to investigate miRNAs which may have therapeutic potential. Although further investigation is required to validate the findings presented in this thesis, these data suggest that knockdown of miR-133b may be beneficial by increasing development or survival of dopaminergic neurons. The observation that miR-155 expression levels are increased in *gba1* mutant zebrafish suggest that inhibition of this miRNA may modulate the inflammatory phenotype demonstrated in these mutants. Further investigation into the action of miRNAs may uncover pathways that may be therapeutically modified to provide a beneficial effect for PD patients or may validate the miRNA itself as a potential therapeutic target. Finally, study of these miRNAs in a model organism such as zebrafish allows for system level analysis of their effects. Therefore it is possible to identify both beneficial effects and any unexpected targets of these miRNAs.

Bibliography

- Aarsland, D. et al., 2007. Neuropsychiatric symptoms in patients with Parkinson's disease and dementia: frequency, profile and associated care giver stress. *Journal of neurology, neurosurgery, and psychiatry*, 78(1), pp.36–42.
- Agostini, M. & Knight, R. a, 2014. miR-34: from bench to bedside. *Oncotarget*, 5(4), pp.872–81.
- Akundi, R.S. et al., 2011. Increased mitochondrial calcium sensitivity and abnormal expression of innate immunity genes precede dopaminergic defects in Pink1-deficient mice. *PLoS ONE*, 6(1).
- Alexandrov, P.N. et al., 2012. MicroRNA (miRNA) speciation in Alzheimer's disease (AD) cerebrospinal fluid (CSF) and extracellular fluid (ECF). *International Journal of Biochemistry and Molecular Biology*, 3(4), pp.365–373.
- Alvarez-Erviti, L. et al., 2011. Delivery of siRNA to the mouse brain by systemic injection of targeted exosomes. *Nature biotechnology*, 29(4), pp.341–345.
- Alvarez-Erviti, L. et al., 2013. Influence of microRNA deregulation on chaperone-mediated autophagy and α -synuclein pathology in Parkinson's disease. *Cell death & disease*, 4(3), p.e545.
- Ambros, V. et al., 2003. A uniform system for microRNA annotation. *RNA (New York, N.Y.)*, 9(3), pp.277–279.
- Amor, S. et al., 2014. Inflammation in neurodegenerative diseases - an update. *Immunology*, 142(2), pp.151–166.
- Anichtchik, O. et al., 2008. Loss of PINK1 Function Affects Development and Results in Neurodegeneration in Zebrafish. , 28(33), pp.8199–8207.
- Ardayfio, P. et al., 2009. Genetic Model for Striatum-Dependent Cognitive Symptoms in. , 31(3), pp.406–412.
- Askenasy, J.J. & Yahr, M.D., 1990. Parkinsonian tremor loses its alternating aspect during non-REM sleep and is inhibited by REM sleep. *Journal of neurology, neurosurgery, and psychiatry*, 53(9), pp.749–753.
- Ason, B. et al., 2006. Differences in vertebrate microRNA expression. *Proceedings of the National Academy of Sciences of the United States of America*, 103(39), pp.14385–14389.
- Auer, T.O. & Del Bene, F., 2014. CRISPR/Cas9 and TALEN-mediated knock-in approaches in zebrafish. *Methods*, 69(2), pp.142–150.
- Babin, P.J., Goizet, C. & Raldúa, D., 2014. Zebrafish models of human motor neuron diseases: Advantages and limitations. *Progress in Neurobiology*, 118, pp.36–58.
- Bai, Q. et al., 2007. Generation of a transgenic zebrafish model of Tauopathy using a novel promoter element derived from the zebrafish *eno2* gene. *Nucleic Acids Research*, 35(19), pp.6501–6516.
- Bandmann, O. & Burton, E. a, 2010. Genetic zebrafish models of neurodegenerative diseases. *Neurobiology of disease*, 40(1), pp.58–65.
- Banerjee, A. et al., 2010. Micro-RNA-155 inhibits IFN-gamma signaling in CD4+ T cells. *European journal of immunology*, 40(1), pp.225–231.
- Barak, V. et al., 1999. Cytokines in Gaucher's disease. *European Cytokine Network*, 10(2),

pp.205–210.

- Baris, H.N., Cohen, I.J. & Mistry, P.K., 2014. Gaucher disease: the metabolic defect, pathophysiology, phenotypes and natural history. *Pediatric endocrinology reviews : PER*, 12 Suppl 1, pp.72–81.
- Barreto-Valer, K. et al., 2012. Modulation by cocaine of dopamine receptors through miRNA-133b in zebrafish embryos. *PLoS one*, 7(12), p.e52701.
- Barreto-Valer, K., López-Bellido, R. & Rodríguez, R.E., 2013. Cocaine modulates the expression of transcription factors related to the dopaminergic system in zebrafish. *Neuroscience*, 231, pp.258–71.
- Bates, J.M. et al., 2007. Intestinal Alkaline Phosphatase Detoxifies Lipopolysaccharide and Prevents Inflammation in Zebrafish in Response to the Gut Microbiota. *Cell Host and Microbe*, 2(6), pp.371–382.
- Beetz, C. et al., 2008. REEP1 mutation spectrum and genotype/phenotype correlation in hereditary spastic paraplegia type 31. *Brain*, 131(4), pp.1078–1086.
- Berg, D. et al., 2013. Changing the research criteria for the diagnosis of Parkinson's disease: Obstacles and opportunities. *The Lancet Neurology*, 12(5), pp.514–524.
- Berger, Z., Smith, K.A. & Lavoie, M.J., 2010. Membrane localization of LRRK2 is associated with increased formation of the highly active Lrrk2 dimer and changes in its phosphorylation. *Biochemistry*, 49(26), pp.5511–5523.
- Bernards, A. & Settleman, J., 2004. GAP control: Regulating the regulators of small GTPases. *Trends in Cell Biology*, 14(7), pp.377–385.
- Bhaya, D., Davison, M. & Barrangou, R., 2011. CRISPR-Cas Systems in Bacteria and Archaea: Versatile Small RNAs for Adaptive Defense and Regulation. *Annual Review of Genetics*, 45(1), pp.273–297.
- Lo Bianco, C. et al., 2002. alpha -Synucleinopathy and selective dopaminergic neuron loss in a rat lentiviral-based model of Parkinson's disease. *Proceedings of the National Academy of Sciences of the United States of America*, 99(16), pp.10813–10818.
- Biosa, A. et al., 2013. GTPase activity regulates kinase activity and cellular phenotypes of parkinson's disease-associated LRRK2. *Human Molecular Genetics*, 22(6), pp.1140–1156.
- Bird, A., 2002. DNA methylation patterns and epigenetic memory DNA methylation patterns and epigenetic memory. *Genes & Development*, pp.6–21.
- Bird, A., 2007. Perceptions of epigenetics. *Nature*, 447(7143), pp.396–8.
- Blesa, J. & Przedborski, S., 2014. Parkinson ' s disease : animal models and dopaminergic cell vulnerability. , 8(December), pp.1–12.
- Block, M.L., Zecca, L. & Hong, J.-S., 2007. Microglia-mediated neurotoxicity: uncovering the molecular mechanisms. *Nature reviews. Neuroscience*, 8(1), pp.57–69.
- Blüml, S. et al., 2011. Essential role of microRNA-155 in the pathogenesis of autoimmune arthritis in mice. *Arthritis and Rheumatism*, 63(5), pp.1281–1288.
- Boka, G. et al., 1994. Immunocytochemical analysis of tumor necrosis factor and its receptors in Parkinson's disease. *Neuroscience letters*, 172(1-2), pp.151–154.
- van Bokhoven, H. et al., 1994. Mutation spectrum in the CHM gene of Danish and Swedish choroideremia patients. *Human molecular genetics*, 3(7), pp.1047–1051.
- Bonifati, V. et al., 2005. Early-onset parkinsonism associated with PINK1 mutations:

- Frequency, genotypes, and phenotypes. *Neurology*, 65(1), pp.87–95.
- Bonifati, V. et al., 2003. Mutations in the DJ-1 gene associated with autosomal recessive early-onset parkinsonism. *Science (New York, N.Y.)*, 299(5604), pp.256–259.
- Bové, J. & Perier, C., 2012. Neurotoxin-based models of Parkinson's disease. *Neuroscience*, 211, pp.51–76.
- Bowman, T. V. & Zon, L.I., 2010. Swimming into the future of drug discovery: In vivo chemical screens in zebrafish. *ACS Chemical Biology*, 5(2), pp.159–161.
- Braak, H. et al., 2003. Staging of brain pathology related to sporadic Parkinson's disease. *Neurobiology of Aging*, 24(2), pp.197–211.
- Breese, G.R. & Traylor, 1972. Developmental characteristics of brain catecholamines and tyrosine hydroxylase in the rat: effects of 6-hydroxydopamine. *British Journal of Pharmacology*, 44(2), pp.210–222.
- Bretau, S., Lee, S. & Guo, S., 2004. Sensitivity of zebrafish to environmental toxins implicated in Parkinson's disease. *Neurotoxicology and Teratology*, 26(6 SPEC. ISS.), pp.857–864.
- Brettschneider, J. et al., 2012. Microglial activation correlates with disease progression and upper motor neuron clinical symptoms in amyotrophic lateral sclerosis. *PLoS ONE*, 7(6).
- Brooks, J. et al., 2009. Parkin and PINK1 mutations in early-onset Parkinson's disease: comprehensive screening in publicly available cases and control. *Journal of medical genetics*, 46(6), pp.375–381.
- Broom, L. et al., 2011. Neuroprotection by the selective iNOS inhibitor GW274150 in a model of Parkinson disease. *Free Radical Biology and Medicine*, 50(5), pp.633–640.
- Butovsky, O. et al., 2015. Targeting miR-155 restores abnormal microglia and attenuates disease in SOD1 mice. *Annals of Neurology*, 77, pp.75–99.
- Byers, B. et al., 2011. SNCA triplication parkinson's patient's iPSC-Derived DA neurons accumulate α -Synuclein and are susceptible to oxidative stress. *PLoS ONE*, 6(11).
- Cammaerts, S. et al., 2015. Genetic variants in microRNA genes: impact on microRNA expression, function, and disease. *Frontiers in Genetics*, 6(May), pp.1–12.
- Cao, X. et al., 2006. Noncoding RNAs in the mammalian central nervous system. *Annual review of neuroscience*, 29, pp.77–103.
- Cardoso, A.L. et al., 2012. miR-155 modulates microglia-mediated immune response by down-regulating SOCS-1 and promoting cytokine and nitric oxide production. *Immunology*, 135(1), pp.73–88.
- Castillo, S.O. et al., 1998. Dopamine biosynthesis is selectively abolished in substantia nigra/ventral tegmental area but not in hypothalamic neurons in mice with targeted disruption of the Nurr1 gene. *Molecular and cellular neurosciences*, 11(1-2), pp.36–46.
- Celardo, I., Martins, L.M. & Gandhi, S., 2014. Unravelling mitochondrial pathways to Parkinson's disease. *British Journal of Pharmacology*, 171(8), pp.1943–1957.
- Chahine, L.M. et al., 2013. Clinical and Biochemical Differences in Patients Having Parkinson Disease With vs Without GBA Mutations. *JAMA Neurology*, 70(7), p.852.
- Chartier-Harlin, M.C. et al., 2011. Translation initiator EIF4G1 mutations in familial parkinson disease. *American Journal of Human Genetics*, 89(3), pp.398–406.
- Chartier-Harlin, M.C. et al., 2004. α -synuclein locus duplication as a cause of familial Parkinson's disease. *Lancet*, 364(9440), pp.1167–1169.

- Chen, X. et al., 2014. MiR-133b regulates bladder cancer cell proliferation and apoptosis by targeting Bcl-w and Akt1. , pp.1–11.
- Cheng, P.H. et al., 2013. MiR-196a ameliorates phenotypes of huntington disease in cell, transgenic mouse, and induced pluripotent stem cell models. *American Journal of Human Genetics*, 93(2), pp.306–312.
- Chiba-Falek, O., Lopez, G.J. & Nussbaum, R.L., 2006. Levels of alpha-synuclein mRNA in sporadic Parkinson disease patients. *Movement Disorders*, 21(10), pp.1703–1708.
- Childs, G. et al., 2009. Low-level expression of microRNAs let-7d and miR-205 are prognostic markers of head and neck squamous cell carcinoma. *The American journal of pathology*, 174(3), pp.736–745.
- Chinwalla, A.T. et al., 2002. Initial sequencing and comparative analysis of the mouse genome. *Nature*, 420(6915), pp.520–562.
- Cho, H.J. et al., 2013. MicroRNA-205 regulates the expression of Parkinson's disease-related leucine-rich repeat kinase 2 protein. *Human molecular genetics*, 22(3), pp.608–20.
- Choi, D.-K. et al., 2005. Ablation of the inflammatory enzyme myeloperoxidase mitigates features of Parkinson's disease in mice. *The Journal of neuroscience : the official journal of the Society for Neuroscience*, 25(28), pp.6594–6600.
- Chung, S. et al., 2009. Wnt1-Imx1a Forms a Novel Autoregulatory Loop and Controls Midbrain Dopaminergic Differentiation Synergistically with the SHH-FoxA2 Pathway. *Cell Stem Cell*, 5(6), pp.646–658.
- Clark, J. et al., 2012. Pgc-1 α overexpression downregulates Pitx3 and increases susceptibility to MPTP toxicity associated with decreased Bdnf. *PLoS one*, 7(11), p.e48925.
- Claus, P. et al., 2004. Expression of the fibroblast growth factor-2 isoforms and the FGF receptor 1-4 transcripts in the rat model system of Parkinson's disease. *Neuroscience Letters*, 360(3), pp.117–120.
- Da Costa, M.M.J. et al., 2014. A new zebrafish model produced by TILLING of SOD1-related amyotrophic lateral sclerosis replicates key features of the disease and represents a tool for in vivo therapeutic screening. *Disease Models & Mechanisms*, 7(1), pp.73–81.
- Costinean, S. et al., 2006. Pre-B cell proliferation and lymphoblastic leukemia/high-grade lymphoma in E(mu)-miR155 transgenic mice. *Proceedings of the National Academy of Sciences of the United States of America*, 103(18), pp.7024–7029.
- Cracknell, R., 2010. The ageing population. *Population Ageing-A Threat to the Welfare State?*, p.2010.
- Crawford, M. et al., 2009. MicroRNA 133B targets pro-survival molecules MCL-1 and BCL2L2 in lung cancer. *Biochemical and Biophysical Research Communications*, 388(3), pp.483–489.
- Dächsel, J.C. et al., 2007. Identification of potential protein interactors of Lrrk2. *Parkinsonism & Related Disorders*, 13(7), pp.382–385.
- Daher, J.P.L. et al., 2014. Abrogation of α -synuclein-mediated dopaminergic neurodegeneration in LRRK2-deficient rats. *Proceedings of the National Academy of Sciences of the United States of America*, 111(25), pp.9289–94.
- Dai, E. et al., 2014. EpimiR: a database of curated mutual regulation between miRNAs and epigenetic modifications. *Database : the journal of biological databases and curation*, 2014, p.bau023.
- Dauer, W. et al., 2002. Resistance of alpha -synuclein null mice to the parkinsonian

- neurotoxin MPTP. *Proceedings of the National Academy of Sciences of the United States of America*, 99(22), pp.14524–14529.
- Dave, K.D. et al., 2014. Phenotypic characterization of recessive gene knockout rat models of Parkinson's disease. *Neurobiol. Dis.*, 70, pp.190–203.
- Davies, P. et al., 2013. Comprehensive characterization and optimization of anti-LRRK2 (leucine-rich repeat kinase 2) monoclonal antibodies. *The Biochemical journal*, 453(1), pp.101–113.
- Davis, T.H. et al., 2008. Conditional loss of Dicer disrupts cellular and tissue morphogenesis in the cortex and hippocampus. *The Journal of neuroscience : the official journal of the Society for Neuroscience*, 28(17), pp.4322–4330.
- Decressac, M. et al., 2012. Progressive neurodegenerative and behavioural changes induced by AAV-mediated overexpression of α -synuclein in midbrain dopamine neurons. *Neurobiology of Disease*, 45(3), pp.939–953.
- Dehay, B. et al., 2015. Targeting α -synuclein for treatment of Parkinson's disease : mechanistic and therapeutic considerations. , pp.855–866.
- Devine, M.J. et al., 2011. Parkinson's disease and α -synuclein expression. *Movement Disorders*, 26(12), pp.2160–2168.
- Dobbs, R.J. et al., 1999. Association of circulating TNF-alpha and IL-6 with ageing and parkinsonism. *Acta neurologica Scandinavica*, 100(1), pp.34–41.
- Dodson, M.W. & Guo, M., 2007. Pink1, Parkin, DJ-1 and mitochondrial dysfunction in Parkinson's disease. *Current Opinion in Neurobiology*, 17(3), pp.331–337.
- Dorsey, E.R. et al., 2007. Projected number of people with Parkinson disease in the most populous nations, 2005 through 2030. *Neurology*, 68(5), pp.384–386.
- Doxakis, E., 2010. Post-transcriptional regulation of alpha-synuclein expression by mir-7 and mir-153. *The Journal of biological chemistry*, 285(17), pp.12726–34.
- Duan, F. et al., 2013. miR-133b, a muscle-specific microRNA, is a novel prognostic marker that participates in the progression of human colorectal cancer via regulation of CXCR4 expression. *Molecular cancer*, 12, p.164.
- Dutta, G., Zhang, P. & Liu, B., 2008. The lipopolysaccharide Parkinson's disease animal model: mechanistic studies and drug discovery. *Fundamental & clinical pharmacology*, 22(5), pp.453–464.
- Ebersbach, G. et al., 2006. Scales in Parkinson's disease. In *Journal of Neurology*.
- Eisen, J.S. & Smith, J.C., 2008. Controlling morpholino experiments: don't stop making antisense. *Development (Cambridge, England)*, 135(10), pp.1735–43.
- Eiyama, A. & Okamoto, K., 2015. PINK1/Parkin-mediated mitophagy in mammalian cells. *Curr Opin Cell Biol*, 33C, pp.95–101.
- Ekholm-Reed, S. et al., 2013. Parkin-dependent degradation of the F-box protein Fbw7 β promotes neuronal survival in response to oxidative stress by stabilizing Mcl-1. *Molecular and cellular biology*, 33(18), pp.3627–43.
- Eslamboli, A. et al., 2007. Long-term consequences of human alpha-synuclein overexpression in the primate ventral midbrain. *Brain*, 130(3), pp.799–815.
- Esteller, M., 2011. Non-coding RNAs in human disease. *Nature Reviews Genetics*, 12(12), pp.861–874.
- Esteves, A.R., Swerdlow, R.H. & Cardoso, S.M., 2014. LRRK2, a puzzling protein: Insights into

- Parkinson's disease pathogenesis. *Experimental Neurology*, 261, pp.206–216.
- Fabbri, M. et al., 2007. MicroRNA-29 family reverts aberrant methylation in lung cancer by targeting DNA methyltransferases 3A and 3B. *Proceedings of the National Academy of Sciences of the United States of America*, 104(40), pp.15805–15810.
- Faraoni, I. et al., 2009. miR-155 gene: A typical multifunctional microRNA. *Biochimica et Biophysica Acta - Molecular Basis of Disease*, 1792(6), pp.497–505.
- Farfel-Becker, T. et al., 2011. Spatial and temporal correlation between neuron loss and neuroinflammation in a mouse model of neuronopathic Gaucher disease. *Human Molecular Genetics*, 20(7), pp.1375–1386.
- Farmer, D.T. et al., 2013. Partially Penetrant Postnatal Lethality of an Epithelial Specific MicroRNA in a Mouse Knockout. *PLoS one*, 8(10), p.e76634.
- Feil, S., Valtcheva, N. & Feil, R., 2009. Inducible cre mice. *Methods in Molecular Biology*, 530, pp.343–363.
- Feng, C.-W. et al., 2014. Effects of 6-Hydroxydopamine Exposure on Motor Activity and Biochemical Expression in Zebrafish (*Danio Rerio*) Larvae. *Zebrafish*, 11(3), pp.227–239.
- Fett, M.E. et al., 2010. Parkin is protective against proteotoxic stress in a transgenic zebrafish model. *PLoS ONE*, 5(7).
- Filippi, A. et al., 2007. Expression and function of nr4a2, lmx1b, and pitx3 in zebrafish dopaminergic and noradrenergic neuronal development. *BMC developmental biology*, 7, p.135.
- Fineberg, N. a et al., 2013. The size, burden and cost of disorders of the brain in the UK. *Journal of psychopharmacology (Oxford, England)*, 27(9), pp.761–70.
- Fleming, A., Diekmann, H. & Goldsmith, P., 2013. Functional Characterisation of the Maturation of the Blood-Brain Barrier in Larval Zebrafish. *PLoS ONE*, 8(10), pp.1–12.
- Flinn, L. et al., 2009. Complex I deficiency and dopaminergic neuronal cell loss in parkin-deficient zebrafish (*Danio rerio*). *Brain : a journal of neurology*, 132(Pt 6), pp.1613–23.
- Flinn, L.J. et al., 2013. TigarB causes mitochondrial dysfunction and neuronal loss in PINK1 deficiency. *Annals of neurology*, 74(6), pp.837–47.
- Di Fonzo, A. et al., 2005. A frequent LRRK2 gene mutation associated with autosomal dominant Parkinson's disease. *Lancet*, 365(9457), pp.412–415.
- Di Fonzo, A. et al., 2007. ATP13A2 missense mutations in juvenile parkinsonism and young onset Parkinson disease. *Neurology*, 68(19), pp.1557–1562.
- Friedman, J.H., 2013. Parkinson disease psychosis: Update. *Behavioural Neurology*, 27(4), pp.469–477.
- Funayama, M. et al., 2002. A new locus for Parkinson's disease (PARK8) maps to chromosome 12p11.2-q13.1. *Annals of Neurology*, 51(3), pp.296–301.
- Funayama, M. et al., 2015. CHCHD2 mutations in autosomal dominant late-onset Parkinson's disease: a genome-wide linkage and sequencing study. *The Lancet Neurology*, 14(3), pp.274–282.
- Gandellini, P. et al., 2009. MiR-205 exerts tumor-suppressive functions in human prostate through down-regulation of protein kinase C?? *Cancer Research*, 69(6), pp.2287–2295.
- Gan-Or, Z. et al., 2013. The p.L302P mutation in the lysosomal enzyme gene SMPD1 is a risk factor for Parkinson disease. *Neurology*, 80(17), pp.1606–1610.

- Gantier, M.P. et al., 2011. Analysis of microRNA turnover in mammalian cells following Dicer1 ablation. *Nucleic Acids Research*, 39(13), pp.5692–5703.
- Gapp, K. et al., 2014. Implication of sperm RNAs in transgenerational inheritance of the effects of early trauma in mice. *Nature neuroscience*, 17(5), pp.667–9.
- Gaughwin, P.M. et al., 2011. Hsa-miR-34b is a plasma-stable microRNA that is elevated in pre-manifest Huntington's disease. *Human molecular genetics*, 20(11), pp.2225–37.
- Gehrke, S. et al., 2010. Pathogenic LRRK2 negatively regulates microRNA-mediated translational repression. *Nature*, 466(7306), pp.637–41.
- Gilsbach, B.K. & Kortholt, A., 2014. Structural biology of the LRRK2 GTPase and kinase domains: implications for regulation. *Frontiers in molecular neuroscience*, 7(May), p.32.
- Ginns, E.I. et al., 2014. Neuroinflammation and α -synuclein accumulation in response to glucocerebrosidase deficiency are accompanied by synaptic dysfunction. *Molecular genetics and metabolism*, 111(2), pp.152–62.
- Gispert, S. et al., 2009. Parkinson phenotype in aged PINK1-deficient mice is accompanied by progressive mitochondrial dysfunction in absence of neurodegeneration. *PLoS ONE*, 4(6).
- Giunti, D. et al., 2014. Can we switch microglia's phenotype to foster neuroprotection? Focus on multiple sclerosis. *Immunology*, 141(3), pp.328–339.
- Goetz, C.G. et al., 2007. Movement disorder society-sponsored revision of the unified Parkinson's disease rating scale (MDS-UPDRS): Process, format, and clinimetric testing plan. *Movement Disorders*, 22(1), pp.41–47.
- Goodall, E.F. et al., 2013. Neuronal dark matter: the emerging role of microRNAs in neurodegeneration. *Frontiers in cellular neuroscience*, 7(October), p.178.
- Gotthardt, K. et al., 2008. Structure of the Roc-COR domain tandem of *C. tepidum*, a prokaryotic homologue of the human LRRK2 Parkinson kinase. *The EMBO journal*, 27(17), p.2352.
- Gray, C. et al., 2011. Simultaneous intravital imaging of macrophage and neutrophil behaviour during inflammation using a novel transgenic zebrafish. *Thrombosis and Haemostasis*, 105(5), pp.811–819.
- Greene, J.C. et al., 2003. Mitochondrial pathology and apoptotic muscle degeneration in *Drosophila parkin* mutants. *Proceedings of the National Academy of Sciences of the United States of America*, 100(7), pp.4078–4083.
- Greggio, E. et al., 2006. Kinase activity is required for the toxic effects of mutant LRRK2/dardarin. *Neurobiology of Disease*, 23(2), pp.329–341.
- Gregory, P. a et al., 2008. The miR-200 family and miR-205 regulate epithelial to mesenchymal transition by targeting ZEB1 and SIP1. *Nature cell biology*, 10(5), pp.593–601.
- Grishok, A., Tabara, H. & Mello, C.C., 2000. Genetic requirements for inheritance of RNAi in *C. elegans*. *Science (New York, N.Y.)*, 287(5462), pp.2494–2497.
- Guedes, J.R. et al., 2014. Early miR-155 upregulation contributes to neuroinflammation in Alzheimer's disease triple transgenic mouse model. *Human molecular genetics*, 23(23), pp.6286–6301.
- Gui, Y. et al., 2012. A novel synonymous SNP in PITX3 is associated with Parkinson's disease in a Chinese population. *Swiss Medical Weekly*, 142(MARCH), pp.2–6.
- Guo, L. et al., 2014. The role of microRNA-133b and its target gene FSCN1 in gastric cancer. ,

pp.1–12.

- Gurtan, A.M. & Sharp, P.A., 2013. The Role of miRNAs in Regulating Gene Expression Networks. *Journal of Molecular Biology*, 425(19), pp.3582–3600.
- Gutzman, J.H. & Sive, H., 2009. Zebrafish brain ventricle injection. *Journal of visualized experiments : JoVE*, (26).
- Hale, C.R. et al., 2013. function with the Cas RAMP module complex to cleave RNAs. , 45(3), pp.292–302.
- Hallett, P.J. et al., 2015. Successful Function of Autologous iPSC-Derived Dopamine Neurons following Transplantation in a Non-Human Primate Model of Parkinson's Disease. *Cell Stem Cell*, 16(3), pp.269–274.
- Halliday, G.M. & McCann, H., 2010. The progression of pathology in Parkinson's disease. *Annals of the New York Academy of Sciences*, 1184, pp.188–195.
- Halpern, M.E. et al., 2008. Gal4/UAS transgenic tools and their application to zebrafish. *Zebrafish*, 5(2), pp.97–110.
- Han, F. et al., 2015. Human induced pluripotent stem cell-derived neurons improve motor asymmetry in a 6-hydroxydopamine-induced rat model of Parkinson's disease. *Cytotherapy*, 17(5), pp.665–679.
- Hans, S. et al., 2009. Temporally-controlled site-specific recombination in zebrafish. *PLoS one*, 4(2), p.e4640.
- Haramati, S. et al., 2010. miRNA malfunction causes spinal motor neuron disease. *Proceedings of the National Academy of Sciences*, 107(29), pp.13111–13116.
- Hare, D.J. et al., 2013. Metallobiology of 1-methyl-4-phenyl-1,2,3,6-tetrahydropyridine neurotoxicity. *Metallomics : integrated biometal science*, 5(2), pp.91–109.
- Hartfield, E.M. et al., 2014. Physiological characterisation of human iPS-derived dopaminergic neurons. *PLoS ONE*, 9(2).
- Haugarvoll, K. & Wszolek, Z.K., 2009. Clinical features of LRRK2 parkinsonism. *Parkinsonism and Related Disorders*, 15(SUPPL. 3).
- He, L. & Hannon, G.J., 2004. MicroRNAs: small RNAs with a big role in gene regulation. *Nature reviews. Genetics*, 5(7), pp.522–531.
- Healy, D.G. et al., 2008. Phenotype, genotype, and worldwide genetic penetrance of LRRK2-associated Parkinson's disease: a case-control study. *The Lancet Neurology*, 7(7), pp.583–590.
- Hébert, S.S. et al., 2010. Genetic ablation of dicer in adult forebrain neurons results in abnormal tau hyperphosphorylation and neurodegeneration. *Human Molecular Genetics*, 19(20), pp.3959–3969.
- Hely, M.A. et al., 2008. The Sydney Multicenter Study of Parkinson's disease: The inevitability of dementia at 20 years. *Movement Disorders*, 23(6), pp.837–844.
- Henshall, T.L. et al., 2009. Selective neuronal requirement for huntingtin in the developing zebrafish. *Human Molecular Genetics*, 18(24), pp.4830–4842.
- Herzig, M.C. et al., 2011. LRRK2 protein levels are determined by kinase function and are crucial for kidney and lung homeostasis in mice. *Human molecular genetics*, 20(21), pp.4209–23.
- Heyer, M.P. et al., 2012. Normal midbrain dopaminergic neuron development and function in miR-133b mutant mice. *The Journal of neuroscience : the official journal of the Society*

- for *Neuroscience*, 32(32), pp.10887–94.
- Hinkle, K.M. et al., 2012. LRRK2 knockout mice have an intact dopaminergic system but display alterations in exploratory and motor co-ordination behaviors. *Molecular Neurodegeneration*, 7(1), p.25.
- Hirsch, E.C. & Hunot, S., 2009. Neuroinflammation in Parkinson's disease: a target for neuroprotection? *Review Literature And Arts Of The Americas*, 8(April), pp.382–97.
- Hobson, P., Gallacher, J. & Meara, J., 2005. Cross-sectional survey of Parkinson's disease and parkinsonism in a rural area of the United Kingdom. *Movement Disorders*, 20(8), pp.995–998.
- Höglinger, G.U. et al., 2007. The pRb/E2F cell-cycle pathway mediates cell death in Parkinson's disease. *Proceedings of the National Academy of Sciences of the United States of America*, 104(9), pp.3585–3590.
- Hou, Z. & Zhang, Y., 2013. Efficient genome engineering in human pluripotent stem cells using Cas9 from *Neisseria meningitidis*. *Proceedings of the*
- Howe, K. et al., 2013. The zebrafish reference genome sequence and its relationship to the human genome. *Nature*, 496(7446), pp.498–503.
- Hsu, S.-D. et al., 2014. miRTarBase update 2014: an information resource for experimentally validated miRNA-target interactions. *Nucleic Acids Research*, 42(D1), pp.D78–D85.
- Huang, T. et al., 2010. Wnt1-cre-mediated conditional loss of Dicer results in malformation of the midbrain and cerebellum and failure of neural crest and dopaminergic differentiation in mice. *Journal of molecular cell biology*, 2(3), pp.152–63.
- Hughes, A.J. et al., 1993. A clinicopathologic study of 100 cases of Parkinson's disease. *Archives of neurology*, 50(2), pp.140–148.
- Hughes, A.J. et al., 1992. Accuracy of clinical diagnosis of idiopathic Parkinson's disease: a clinico-pathological study of 100 cases. *Journal of neurology, neurosurgery, and psychiatry*, 55(3), pp.181–184.
- Hwang, D.Y. et al., 2003. Selective loss of dopaminergic neurons in the substantia nigra of Pitx3-deficient aphakia mice. *Molecular Brain Research*, 114(2), pp.123–131.
- Hwang, D.-Y. et al., 2009. Vesicular monoamine transporter 2 and dopamine transporter are molecular targets of Pitx3 in the ventral midbrain dopamine neurons. *Journal of Neurochemistry*, 111(5), pp.1202–1212.
- Imai, Y. et al., 2001. An unfolded putative transmembrane polypeptide, which can lead to endoplasmic reticulum stress, is a substrate of Parkin. *Cell*, 105(7), pp.891–902.
- Imamura, K. et al., 2003. Distribution of major histocompatibility complex class II-positive microglia and cytokine profile of Parkinson's disease brains. *Acta Neuropathologica*, 106(6), pp.518–526.
- Ishizawa, T. et al., 2003. Colocalization of tau and alpha-synuclein epitopes in Lewy bodies. *Journal of neuropathology and experimental neurology*, 62(4), pp.389–397.
- Jacobs, B.M., 2014. Stemming the hype: what can we learn from iPSC models of Parkinson's disease and how can we learn it? *Journal of Parkinson's disease*, 4(1), pp.15–27.
- Jacobs, F.M.J. et al., 2009. Pitx3 potentiates Nurr1 in dopamine neuron terminal differentiation through release of SMRT-mediated repression. *Development (Cambridge, England)*, 136, pp.531–540.
- Jacobs, F.M.J. et al., 2011. Retinoic acid-dependent and -independent gene-regulatory pathways of Pitx3 in meso-diencephalic dopaminergic neurons. *Development*, 138(23),

pp.5213–5222.

- Jankovic, J., 2008. Parkinson's disease: clinical features and diagnosis. *Journal of neurology, neurosurgery, and psychiatry*, 79(4), pp.368–376.
- Janssen, H.L. a et al., 2013. Treatment of HCV infection by targeting microRNA. *The New England journal of medicine*, 368(18), pp.1685–94.
- Javitch, J.A. et al., 1985. Parkinsonism-inducing neurotoxin, N-methyl-4-phenyl-1,2,3,6 - tetrahydropyridine: uptake of the metabolite N-methyl-4-phenylpyridine by dopamine neurons explains selective toxicity. *Proceedings of the National Academy of Sciences of the United States of America*, 82(7), pp.2173–2177.
- Jenuwein, T. & Allis, C.D., 2001. Translating the histone code. *Science (New York, N.Y.)*, 293(5532), pp.1074–1080.
- Jeong, J.-Y. et al., 2006. Neurogenin1 is a determinant of zebrafish basal forebrain dopaminergic neurons and is regulated by the conserved zinc finger protein *Tof/Fezl*. *Proceedings of the National Academy of Sciences of the United States of America*, 103, pp.5143–5148.
- Jiang, H. et al., 2012. Parkin controls dopamine utilization in human midbrain dopaminergic neurons derived from induced pluripotent stem cells. *Nature Communications*, 3, p.668.
- Jiménez-Jiménez, F.J. et al., 2014. PITX3 and Risk for Parkinson's Disease: A Systematic Review and Meta-Analysis. *European Neurology*.
- Johnson, R. et al., 2008. A microRNA-based gene dysregulation pathway in Huntington's disease. *Neurobiology of disease*, 29(3), pp.438–45.
- Jones, P. a., 2012. Functions of DNA methylation: islands, start sites, gene bodies and beyond. *Nature Reviews Genetics*, 13(7), pp.484–492.
- Junker, A. et al., 2009. MicroRNA profiling of multiple sclerosis lesions identifies modulators of the regulatory protein CD47. *Brain*, 132(12), pp.3342–3352.
- Junn, E. et al., 2009. Repression of alpha-synuclein expression and toxicity by microRNA-7. *Proceedings of the National Academy of Sciences of the United States of America*, 106(31), pp.13052–7.
- Kalia, L. V & Lang, A.E., 2015. Parkinson's disease. *The Lancet*, 6736(14), pp.1–17.
- Kasahara, M., Suzuki, T. & Du Pasquier, L., 2004. On the origins of the adaptive immune system: Novel insights from invertebrates and cold-blooded vertebrates. *Trends in Immunology*, 25(2), pp.105–111.
- Kawakami, K. et al., 2004. A transposon-mediated gene trap approach identifies developmentally regulated genes in zebrafish. *Developmental Cell*, 7(1), pp.133–144.
- Keatinge, M. et al., 2015. Glucocerebrosidase 1 deficient *Danio rerio* mirror key pathological aspects of human Gaucher disease and provide evidence of early microglial activation preceding alpha-synuclein-independent neuronal cell death. *Human molecular genetics*.
- Keller, M.F. et al., 2012. Using genome-wide complex trait analysis to quantify “missing heritability” in Parkinson's disease. *Human Molecular Genetics*, 21(22), pp.4996–5009.
- Kettleborough, R.N.W. et al., 2013. A systematic genome-wide analysis of zebrafish protein-coding gene function. *Nature*, 496(7446), pp.494–7.
- Khoo, T.K. et al., 2013. The spectrum of nonmotor symptoms in early Parkinson disease. *Neurology*, 80(3), pp.276–281.

- Kilarski, L.L. et al., 2012. Systematic Review and UK-Based Study of PARK2 (parkin), PINK1, PARK7 (DJ-1) and LRRK2 in early-onset Parkinson's disease. *Movement Disorders*, 27(12), pp.1522–1529.
- Kim, J. et al., 2007. A MicroRNA feedback circuit in midbrain dopamine neurons. *Science (New York, N.Y.)*, 317(5842), pp.1220–4.
- Kim, Y., 2015. Extracellular microRNAs as Biomarkers in Human Disease. , pp.51–57.
- Kitada, T., Tong, Y., et al., 2009. Absence of nigral degeneration in aged parkin/DJ-1/PINK1 triple knockout mice. *Journal of Neurochemistry*, 111(3), pp.696–702.
- Kitada, T., Pisani, A., et al., 2009. Impaired dopamine release and synaptic plasticity in the striatum of Parkin^{-/-} mice. *Journal of Neurochemistry*, 110(2), pp.613–621.
- Kitada, T. et al., 1998. *Mutations in the parkin gene cause autosomal recessive juvenile parkinsonism.*
- Kloosterman, W.P. et al., 2007. Targeted inhibition of miRNA maturation with morpholinos reveals a role for miR-375 in pancreatic islet development. *PLoS biology*, 5(8), p.e203.
- Kok, F.O. et al., 2015. Reverse Genetic Screening Reveals Poor Correlation between Morpholino-Induced and Mutant Phenotypes in Zebrafish. *Developmental Cell*, 32(1), pp.97–108.
- Konstantoulas, C.J., Parmar, M. & Li, M., 2010. FoxP1 promotes midbrain identity in embryonic stem cell-derived dopamine neurons by regulating Pitx3. *Journal of Neurochemistry*, 113(4), pp.836–847.
- Kozomara, A. & Griffiths-Jones, S., 2014. MiRBase: Annotating high confidence microRNAs using deep sequencing data. *Nucleic Acids Research*, 42(D1).
- Kumar, A. et al., 2012. MiRNA_Targets: A database for miRNA target predictions in coding and non-coding regions of mRNAs. *Genomics*, 100(6), pp.352–356.
- Kumari, U. & Tan, E.K., 2009. LRRK2 in Parkinson's disease: genetic and clinical studies from patients. *The FEBS journal*, 276(22), pp.6455–6463.
- L'Honoré, A. et al., 2007. Sequential expression and redundancy of Pitx2 and Pitx3 genes during muscle development. *Developmental Biology*, 307(2), pp.421–433.
- Lang, A.E. et al., 2006. Deep brain stimulation: Preoperative issues. *Movement Disorders*, 21(SUPPL. 14).
- Langrish, C.L. et al., 2005. IL-23 drives a pathogenic T cell population that induces autoimmune inflammation. *The Journal of experimental medicine*, 201(2), pp.233–240.
- Langston, J.W. et al., 1983. Chronic Parkinsonism in humans due to a product of meperidine-analog synthesis. *Science (New York, N.Y.)*, 219(4587), pp.979–980.
- de Lau, L.M.L. & Breteler, M.M.B., 2006. Epidemiology of Parkinson's disease. *The Lancet. Neurology*, 5(June), pp.525–535.
- Lau, N.C. et al., 2001. An abundant class of tiny RNAs with probable regulatory roles in *Caenorhabditis elegans*. *Science (New York, N.Y.)*, 294(5543), pp.858–862.
- Lebel, M. et al., 2001. Pitx3 activates mouse tyrosine hydroxylase promoter via a high-affinity binding site. *Journal of Neurochemistry*, 77, pp.558–567.
- Lee, B.D. et al., 2010. Inhibitors of leucine-rich repeat kinase-2 protect against models of Parkinson's disease. *Nature medicine*, 16(9), pp.998–1000.
- Lee, R.C. & Ambros, V., 2001. An extensive class of small RNAs in *Caenorhabditis elegans*. *Science (New York, N.Y.)*, 294(5543), pp.862–864.

- Lee, Y.B. et al., 2013. Hexanucleotide repeats in ALS/FTD form length-dependent RNA Foci, sequester RNA binding proteins, and are neurotoxic. *Cell Reports*, 5(5), pp.1178–1186.
- Lewis, B.P. et al., 2003. Prediction of Mammalian MicroRNA Targets. *Cell*, 115(7), pp.787–798.
- Li, J.-Q., Tan, L. & Yu, J.-T., 2014. The role of the LRRK2 gene in Parkinsonism. *Molecular Neurodegeneration*, 9(1), p.47.
- Li, X. et al., 2010. Reevaluation of phosphorylation sites in the parkinson disease-associated leucine-rich repeat kinase 2. *Journal of Biological Chemistry*, 285(38), pp.29569–29576.
- Li, Y. et al., 2009. Mutant LRRK2(R1441G) BAC transgenic mice recapitulate cardinal features of Parkinson's disease. *Nature neuroscience*, 12(7), pp.826–828.
- Li, Z. & Rana, T.M., 2014. Therapeutic targeting of microRNAs: current status and future challenges. *Nature Reviews Drug Discovery*, 13(8), pp.622–638.
- Lichtenberg, M. et al., 2011. The Parkinson's disease protein LRRK2 impairs proteasome substrate clearance without affecting proteasome catalytic activity. *Cell death & disease*, 2(8), p.e196.
- Lieschke, G.J. & Currie, P.D., 2007. Animal models of human disease: zebrafish swim into view. *Nature reviews. Genetics*, 8(5), pp.353–367.
- Lill, C.M. et al., 2012. Comprehensive research synopsis and systematic meta-analyses in Parkinson's disease genetics: The PDGene database. *PLoS genetics*, 8(3), p.e1002548.
- Lin, X. et al., 2012. Conditional Expression of Parkinson's Disease-Related Mutant α -Synuclein in the Midbrain Dopaminergic Neurons Causes Progressive Neurodegeneration and Degradation of Transcription Factor Nuclear Receptor Related 1. *Journal of Neuroscience*, 32(27), pp.9248–9264.
- Lin, X. et al., 2009. Leucine-Rich Repeat Kinase 2 Regulates the Progression of Neuropathology Induced by Parkinson's-Disease-Related Mutant α -synuclein. *Neuron*, 64(6), pp.807–827.
- Lippai, D. et al., 2013. Chronic alcohol-induced microRNA-155 contributes to neuroinflammation in a TLR4-dependent manner in mice. *PLoS one*, 8(8), p.e70945.
- Liu, H. et al., 2012. Decreased NURR1 and PITX3 gene expression in Chinese patients with Parkinson's disease. *European journal of neurology : the official journal of the European Federation of Neurological Societies*, 19(6), pp.870–5.
- Liu, N. et al., 2012. The microRNA miR-34 modulates ageing and neurodegeneration in Drosophila. *Nature*, 482(7386), pp.519–23.
- Liu, X. et al., 2013. Pesticide-induced gene mutations and parkinson disease risk: A meta-analysis. *Genetic Testing and Molecular Biomarkers*, 17(11), pp.826–832.
- Liu, Y. & Semina, E. V., 2012. PITX2 deficiency results in abnormal ocular and craniofacial development in zebrafish. *PLoS ONE*, 7(1), pp.1–9.
- Liu, Z. et al., 2008. A Drosophila model for LRRK2-linked parkinsonism. *Proceedings of the National Academy of Sciences of the United States of America*, 105(7), pp.2693–2698.
- Löw, K. & Aebischer, P., 2012. Use of viral vectors to create animal models for Parkinson's disease. *Neurobiology of Disease*, 48(2), pp.189–201.
- Lu, M. et al., 2008. An Analysis of Human MicroRNA and Disease Associations M. Isalan, ed. *PLoS ONE*, 3(10), p.e3420.
- Lu, X. et al., 2009. Bacterial artificial chromosome transgenic mice expressing a truncated

- mutant parkin exhibit age-dependent hypokinetic motor deficits, dopaminergic neuron degeneration, and accumulation of proteinase K-resistant alpha-synuclein. *The Journal of neuroscience : the official journal of the Society for Neuroscience*, 29(7), pp.1962–1976.
- Lücking, C.B. et al., 2000. Association between early-onset Parkinson's disease and mutations in the parkin gene. *The New England journal of medicine*, 342(21), pp.1560–1567.
- Mandal, A., 2014. *Mitochondrial Dysfunction and Biomarkers in Parkinson's Disease*. University of Sheffield.
- Manning-Bog, A.B. et al., 2002. The herbicide paraquat causes up-regulation and aggregation of ??-synuclein in mice: Paraquat and ??-synuclein. *Journal of Biological Chemistry*, 277(3), pp.1641–1644.
- Marco, A., Ninova, M. & Griffiths-Jones, S., 2013. Multiple products from microRNA transcripts. *Biochemical Society transactions*, 41(4), pp.850–4.
- Markou, A. et al., 2014. Prognostic significance of metastasis-related microRNAs in early breast cancer patients with a long follow-up. *Clinical Chemistry*, 60(1), pp.197–205.
- Marras, C. & Lang, a., 2012. Parkinson's disease subtypes: lost in translation? *Journal of Neurology, Neurosurgery & Psychiatry*, pp.409–415.
- Martí, E. et al., 2010. A myriad of miRNA variants in control and Huntington's disease brain regions detected by massively parallel sequencing. *Nucleic acids research*, 38(20), pp.7219–35.
- Martin, D.M. et al., 2004. PITX2 is required for normal development of neurons in the mouse subthalamic nucleus and midbrain. *Developmental Biology*, 267(1), pp.93–108.
- Massano, J. & Bhatia, K.P., 2012. Clinical approach to Parkinson's disease: Features, diagnosis, and principles of management. *Cold Spring Harbor Perspectives in Medicine*, 2(6), pp.1–15.
- Matsui, H. et al., 2009. A chemical neurotoxin, MPTP induces Parkinson's disease like phenotype, movement disorders and persistent loss of dopamine neurons in medaka fish. *Neuroscience Research*, 65(3), pp.263–271.
- Matsui, H., Taniguchi, Y., et al., 2010. Loss of PINK1 in medaka fish (*Oryzias latipes*) causes late-onset decrease in spontaneous movement. *Neuroscience Research*, 66(2), pp.151–161.
- Matsui, H. et al., 2013. PINK1 and parkin complementarily protect dopaminergic neurons in vertebrates. *Human Molecular Genetics*, 22(12), pp.2423–2434.
- Matsui, H., Ito, H., et al., 2010. Proteasome inhibition in medaka brain induces the features of Parkinson's disease. *Journal of Neurochemistry*, 115(1), pp.178–187.
- Mazzulli, J.R. et al., 2011. Gaucher disease glucocerebrosidase and α -synuclein form a bidirectional pathogenic loop in synucleinopathies. *Cell*, 146(1), pp.37–52.
- McCormack, A.L. et al., 2005. Role of oxidative stress in paraquat-induced dopaminergic cell degeneration. *Journal of Neurochemistry*, 93(4), pp.1030–1037.
- McCoy, M.K. & Cookson, M.R., 2011. DJ-1 regulation of mitochondrial function and autophagy through oxidative stress. *Autophagy*, 7(5), pp.531–532.
- McGeer, P.L. et al., 1988. Reactive microglia are positive for HLA-DR in the substantia nigra of Parkinson's and Alzheimer's disease brains. *Neurology*, 38(8), pp.1285–1291.
- McGown, A. et al., 2013. Early interneuron dysfunction in ALS: Insights from a mutant sod1 zebrafish model. *Annals of Neurology*, 73(2), pp.246–258.

- McGraw, H.F., Nechiporuk, A. & Raible, D.W., 2008. Zebrafish Dorsal Root Ganglia Neural Precursor Cells Adopt a Glial Fate in the Absence of Neurogenin1. *Journal of Neuroscience*, 28(47), pp.12558–12569.
- McLoughlin, H.S. et al., 2012. Dicer is required for proliferation, viability, migration and differentiation in corticoneurogenesis. *Neuroscience*, 223, pp.285–295.
- McNaught, K.S.P. et al., 2004. Systemic exposure to proteasome inhibitors causes a progressive model of Parkinson's disease. *Annals of Neurology*, 56(1), pp.149–162.
- Medina-Martinez, O., Shah, R. & Jamrich, M., 2009. Pitx3 controls multiple aspects of lens development. *Developmental Dynamics*, 238(9), pp.2193–2201.
- Meola, N., Gennarino, V.A. & Banfi, S., 2009. microRNAs and genetic diseases. *PathoGenetics*, 2(1), p.7.
- Milanese, C. et al., 2012. Hypokinesia and reduced dopamine levels in zebrafish lacking β - and γ 1-synucleins. *Journal of Biological Chemistry*, 287(5), pp.2971–2983.
- Miller, D.B. & O'Callaghan, J.P., 2015. Biomarkers of Parkinson's disease: Present and future. *Metabolism*, 64(3), pp.S40–S46.
- Mills, R.D. et al., 2014. Prediction of the Repeat Domain Structures and Impact of Parkinsonism-Associated Variations on Structure and Function of all Functional Domains of Leucine-Rich Repeat Kinase 2 (LRRK2). *Human Mutation*, 35(4), pp.395–412.
- Min, M. et al., 2014. MicroRNA-155 is involved in the pathogenesis of ulcerative colitis by targeting FOXO3a. *Inflammatory bowel diseases*, 20(4), pp.652–9.
- Miñones-Moyano, E. et al., 2011. MicroRNA profiling of Parkinson's disease brains identifies early downregulation of miR-34b/c which modulate mitochondrial function. *Human molecular genetics*, 20(15), pp.3067–78.
- Mishima, Y. et al., 2009. Zebrafish miR-1 and miR-133 shape muscle gene expression and regulate sarcomeric actin organization. *Genes & development*, 23(5), pp.619–32.
- Miura, E. et al., 2014. VPS35 dysfunction impairs lysosomal degradation of α -synuclein and exacerbates neurotoxicity in a Drosophila model of Parkinson's disease. *Neurobiology of disease*.
- Mizuno, H. et al., 2011. α -Synuclein Transgenic Drosophila As a Model of Parkinson's Disease and Related Synucleinopathies. *Parkinson's Disease*, 2011, pp.1–7.
- Mogi, M. et al., 1994. Tumor necrosis factor- α (TNF- α) increases both in the brain and in the cerebrospinal fluid from parkinsonian patients. *Neuroscience letters*, 165(1-2), pp.208–210.
- Mortiboys, H. et al., 2008. Mitochondrial function and morphology are impaired in parkin-mutant fibroblasts. *Annals of neurology*, 64(5), pp.555–65.
- Mortiboys, H. et al., 2010. Mitochondrial impairment in patients with Parkinson disease with the G2019S mutation in LRRK2. *Neurology*, 75(22), pp.2017–20.
- Mortiboys, H., Aasly, J. & Bandmann, O., 2013. Ursocholic acid rescues mitochondrial function in common forms of familial Parkinson's disease. *Brain : a journal of neurology*, pp.1–13.
- Van Den Munckhof, P. et al., 2006. Striatal neuroadaptation and rescue of locomotor deficit by L-dopa in aphakia mice, a model of Parkinson's disease. *Journal of Neurochemistry*, 96(1), pp.160–170.
- Murase, S. & McKay, R.D., 2006. A specific survival response in dopamine neurons at most

- risk in Parkinson's disease. *The Journal of neuroscience : the official journal of the Society for Neuroscience*, 26(38), pp.9750–9760.
- Murugaiyan, G. & Beynon, V., 2011. Silencing microRNA-155 ameliorates experimental autoimmune encephalomyelitis. *The Journal of ...*, 187(5), pp.2213–2221.
- Mutch, W.J. et al., 1986. Parkinson's disease in a Scottish city. *British medical journal (Clinical research ed.)*, 292(6519), pp.534–536.
- Nalls, M.A. et al., 2014. Large-scale meta-analysis of genome-wide association data identifies six new risk loci for Parkinson's disease. *Nature Genetics*, 46(9), pp.989–993.
- Neumann, J. et al., 2009. Glucocerebrosidase mutations in clinical and pathologically proven Parkinson's disease. *Brain*, 132(7), pp.1783–1794.
- Ng, C. et al., 2009. Parkin Protects against LRRK2 G2019S Mutant-Induced Dopaminergic Neurodegeneration in Drosophila. *Journal of Neuroscience*, 29(36), pp.11257–11262.
- Nguyen, H.N. et al., 2011. LRRK2 mutant iPSC-derived da neurons demonstrate increased susceptibility to oxidative stress. *Cell Stem Cell*, 8(3), pp.267–280.
- Nicklas, W.J., Vyas, I. & Heikkila, R.E., 1985. Inhibition of NADH-linked oxidation in brain mitochondria by 1-methyl-4-phenyl-pyridine, a metabolite of the neurotoxin, 1-methyl-4-phenyl-1,2,5,6-tetrahydropyridine. *Life Sciences*, 36(26), pp.2503–2508.
- Ning, H. et al., 2010. MicroRNA regulation of neuron-like differentiation of adipose tissue-derived stem cells. *Differentiation*, 78(5), pp.253–259.
- Nisticò, R. et al., 2011. Paraquat- and rotenone-induced models of Parkinson's disease. *International Journal of Immunopathology and Pharmacology*, 24(2), pp.313–322.
- Niu, Y. et al., 2015. Early Parkinson's disease symptoms in α -synuclein transgenic monkeys. *Human Molecular Genetics*, 24(8), pp.2308–2317.
- Noble, S. et al., 2015. Transgenic Zebrafish Expressing mCherry in the Mitochondria of Dopaminergic Neurons. *Zebrafish*, 12(5), p.zeb.2015.1085.
- Noyce, A.J. et al., 2012. Meta-analysis of early nonmotor features and risk factors for Parkinson disease. *Annals of Neurology*, 72(6), pp.893–901.
- Nunes, I. et al., 2003. Pitx3 is required for development of substantia nigra dopaminergic neurons. *Proceedings of the National Academy of Sciences of the United States of America*, 100(7), pp.4245–50.
- O'Connell, R.M. et al., 2009. Inositol phosphatase SHIP1 is a primary target of miR-155. *Proceedings of the National Academy of Sciences of the United States of America*, 106(17), pp.7113–8.
- O'Connell, R.M. et al., 2007. MicroRNA-155 is induced during the macrophage inflammatory response. *Proceedings of the National Academy of Sciences of the United States of America*, 104(5), pp.1604–9.
- O'Connell, R.M. et al., 2010. MicroRNA-155 promotes autoimmune inflammation by enhancing inflammatory T cell development. *Immunity*, 33(4), pp.607–619.
- Obeso, J.A. et al., 2008. Functional organization of the basal ganglia: therapeutic implications for Parkinson's disease. *Movement disorders : official journal of the Movement Disorder Society*, 23 Suppl 3, pp.S548–S559.
- de Oliveira, S. et al., 2013. Cxcl8 (IL-8) mediates neutrophil recruitment and behavior in the zebrafish inflammatory response. *Journal of immunology (Baltimore, Md. : 1950)*, 190(8), pp.4349–59.

- Packer, A.N. et al., 2008. The bifunctional microRNA miR-9/miR-9* regulates REST and CoREST and is downregulated in Huntington's disease. *The Journal of neuroscience : the official journal of the Society for Neuroscience*, 28(53), pp.14341–6.
- Paisán-Ruíz, C. et al., 2004. Cloning of the gene containing mutations that cause PARK8-linked Parkinson's disease. *Neuron*, 44(4), pp.595–600.
- Panicker, L.M. et al., 2014. Gaucher iPSC-derived macrophages produce elevated levels of inflammatory mediators and serve as a new platform for therapeutic development. *Stem cells (Dayton, Ohio)*, pp.1–16.
- Paquet, D. et al., 2009. A zebrafish model of tauopathy allows in vivo imaging of neuronal cell death and drug evaluation. *Journal of Clinical Investigation*, 119(5), pp.1382–1395.
- Pardridge, W.M., 2005. The blood-brain barrier: Bottleneck in brain drug development. *NeuroRX*, 2(1), pp.3–14.
- Parisiadou, L. et al., 2009. Phosphorylation of ezrin/radixin/moesin proteins by LRRK2 promotes the rearrangement of actin cytoskeleton in neuronal morphogenesis. *The Journal of neuroscience : the official journal of the Society for Neuroscience*, 29(44), pp.13971–13980.
- Park, J. et al., 2006. Mitochondrial dysfunction in Drosophila PINK1 mutants is complemented by parkin. *Nature*, 441(7097), pp.1157–1161.
- Parkinson, J., 1817. An essay on the shaking palsy. *Sherwood, Neely, and Jones, London*.
- Parkinson, J., 2002. An essay on the shaking palsy. 1817. *The Journal of neuropsychiatry and clinical neurosciences*, 14(2), pp.223–236; discussion 222.
- Parkinson's UK, 2009. Parkinson's prevalence in the United Kingdom.
- Pathak, S. et al., 2015. MiR-155 modulates the inflammatory phenotype of intestinal myofibroblasts by targeting SOCS1 in ulcerative colitis. *Experimental & Molecular Medicine*, 47(5), p.e164.
- Patron, J.P. et al., 2012. MiR-133b targets antiapoptotic genes and enhances death receptor-induced apoptosis. *PLoS one*, 7(4), p.e35345.
- Pavese, N. et al., 2006. Microglial activation correlates with severity in Huntington disease: A clinical and PET study. *Neurology*, 66(11), pp.1638–1643.
- Peng, C. et al., 2007. Overexpression of pitx3 upregulates expression of BDNF and GDNF in SH-SY5Y cells and primary ventral mesencephalic cultures. *FEBS letters*, 581(7), pp.1357–61.
- Peng, C. et al., 2011. Pitx3 is a critical mediator of GDNF-induced BDNF expression in nigrostriatal dopaminergic neurons. *The Journal of ...*, 31(36), pp.12802–12815.
- Peschansky, V.J. & Wahlestedt, C., 2014. Non-coding RNAs as direct and indirect modulators of epigenetic regulation. *Epigenetics*, 9(1), pp.3–12.
- Peterson, S.M. et al., 2014. Common features of microRNA target prediction tools. *Frontiers in Genetics*, 5(FEB), pp.1–10.
- Petri, R. et al., 2013. miRNAs in brain development. *Experimental Cell Research*.
- Pfeiffer, R.F., 2012. Autonomic dysfunction in Parkinson's disease. *Expert Review of Neurotherapeutics*, 12(6), pp.697–706.
- Polymeropoulos, M.H. et al., 1997. Mutation in the α -Synuclein Gene Identified in Families with Parkinson's Disease Mutation in the β -Synuclein Gene Identified in Families with Parkinson's Disease. *Science*, 276(June), pp.2045–2047.

- Poon, H.F. et al., 2007. Cocaine-induced oxidative stress precedes cell death in human neuronal progenitor cells. *Neurochemistry International*, 50(1), pp.69–73.
- Porras, G., Li, Q. & Bezdard, E., 2012. Modeling Parkinson's Disease in Primates: The MPTP Model. *Cold Spring Harbor Perspectives in Medicine*, 2(3), pp.a009308–a009308.
- Postlethwait, J. et al., 2004. Subfunction partitioning, the teleost radiation and the annotation of the human genome. *Trends in Genetics*, 20(10), pp.481–490.
- Postlethwait, J.H., 2000. Zebrafish Comparative Genomics and the Origins of Vertebrate Chromosomes. *Genome Research*, 10(12), pp.1890–1902.
- Postuma, R.B. et al., 2011. Olfaction and color vision identify impending neurodegeneration in rapid eye movement sleep behavior disorder. *Annals of neurology*, 69(5), pp.811–818.
- Poulopoulos, M., Levy, O.A. & Alcalay, R.N., 2012. The neuropathology of genetic Parkinson's disease. *Movement Disorders*, 27(7), pp.831–842.
- Prince, V.E. & Pickett, F.B., 2002. Splitting pairs: the diverging fates of duplicated genes. *Nature reviews. Genetics*, 3(11), pp.827–837.
- Qiu, C., Kivipelto, M. & Von Strauss, E., 2009. Epidemiology of Alzheimer's disease: Occurrence, determinants, and strategies toward intervention. *Dialogues in Clinical Neuroscience*, 11(2), pp.111–128.
- Qiu, T. et al., 2014. MiR-145, miR-133a and miR-133b inhibit proliferation, migration, invasion and cell cycle progression via targeting transcription factor Sp1 in gastric cancer. *FEBS Letters*, 588(7), pp.1168–1177.
- Rajput, A.H., Rozdilsky, B. & Rajput, A., 1991. Accuracy of clinical diagnosis in parkinsonism-- a prospective study. *The Canadian journal of neurological sciences. Le journal canadien des sciences neurologiques*, 18(3), pp.275–278.
- Ramesh, T. et al., 2010. A genetic model of amyotrophic lateral sclerosis in zebrafish displays phenotypic hallmarks of motoneuron disease. *Disease models & mechanisms*, 3(9-10), pp.652–662.
- Ramirez, A. et al., 2006. Hereditary parkinsonism with dementia is caused by mutations in ATP13A2, encoding a lysosomal type 5 P-type ATPase. *Nature genetics*, 38(10), pp.1184–1191.
- Ramonet, D. et al., 2011. Dopaminergic Neuronal loss, Reduced Neurite Complexity and Autophagic Abnormalities in Transgenic Mice Expressing G2019S Mutant LRRK2. *PLoS ONE*, 6(4).
- Razin, A. & Riggs, A.D., 1980. DNA methylation and gene function. *Science (New York, N.Y.)*, 210(4470), pp.604–610.
- Ren, G. et al., 2011. Disruption of LRRK2 does not cause specific loss of dopaminergic neurons in zebrafish. *PloS one*, 6(6), p.e20630.
- Ricciarelli, R. et al., 2007. Vitamin E and neurodegenerative diseases. *Molecular Aspects of Medicine*, 28(5-6), pp.591–606.
- Richardson, J.R. et al., 2007. Obligatory role for complex I inhibition in the dopaminergic neurotoxicity of 1-methyl-4-phenyl-1,2,3,6-tetrahydropyridine (MPTP). *Toxicological Sciences*, 95(1), pp.196–204.
- Rink, E. & Wullimann, M.F., 2002. Development of the catecholaminergic system in the early zebrafish brain: an immunohistochemical study. *Brain research. Developmental brain research*, 137(1), pp.89–100.

- Rink, E. & Wullimann, M.F., 2001. The teleostean (zebrafish) dopaminergic system ascending to the subpallium (striatum) is located in the basal diencephalon (posterior tuberculum). *Brain Research*, 889(1-2), pp.316–330.
- Robertson, A.L. et al., 2014. A zebrafish compound screen reveals modulation of neutrophil reverse migration as an anti-inflammatory mechanism. *Science translational medicine*, 6(225), p.225ra29.
- Robu, M.E. et al., 2007. P53 Activation By Knockdown Technologies. *PLoS Genetics*, 3(5), pp.787–801.
- Rodriguez, A. et al., 2007. Requirement of bic/microRNA-155 for Normal Immune Function. *Science*, 316(5824), pp.608–611.
- Rodriguez-Pallares, J. et al., 2007. Mechanism of 6-hydroxydopamine neurotoxicity: The role of NADPH oxidase and microglial activation in 6-hydroxydopamine-induced degeneration of dopaminergic neurons. *Journal of Neurochemistry*, 103(1), pp.145–156.
- Van Rompuy, A.S. et al., 2014. Long-Term Overexpression of Human Wild-Type and T240R Mutant Parkin in Rat Substantia Nigra Induces Progressive Dopaminergic Neurodegeneration. *Journal of Neuropathology and Experimental Neurology*, 73(2), pp.159–174.
- Rosenberg, M.I. et al., 2006. MyoD inhibits Fstl1 and Utrn expression by inducing transcription of miR-206. *Journal of Cell Biology*, 175(1), pp.77–85.
- Rossi, A. et al., 2015. Genetic compensation induced by deleterious mutations but not gene knockdowns. *Nature*.
- Rovelet-Lecrux, A. et al., 2006. APP locus duplication causes autosomal dominant early-onset Alzheimer disease with cerebral amyloid angiopathy. *Nature genetics*, 38(1), pp.24–26.
- Russell, A.P. et al., 2013. Disruption of skeletal muscle mitochondrial network genes and miRNAs in amyotrophic lateral sclerosis. *Neurobiology of Disease*, 49(1), pp.107–117.
- Ryan, B.J. et al., 2015. Mitochondrial dysfunction and mitophagy in Parkinson's: from familial to sporadic disease. , 40(4).
- Sætrom, P., Snøve, O. & Rossi, J.J., 2007. Epigenetics and MicroRNAs. *Pediatric Research*, 61(5 Part 2), p.17R–23R.
- Sala-Cirtog, M., Marian, C. & Anghel, A., 2015. New insights of medicinal plant therapeutic activity—The miRNA transfer. *Biomedicine & Pharmacotherapy*, 74, pp.228–232.
- Sallinen, V. et al., 2010. Dopaminergic cell damage and vulnerability to MPTP in Pink1 knockdown zebrafish. *Neurobiology of Disease*, 40(1), pp.93–101.
- Sallinen, V. et al., 2009. MPTP and MPP+ target specific aminergic cell populations in larval zebrafish. *Journal of Neurochemistry*, 108(3), pp.719–731.
- Sanchez-Simon, F.M. et al., 2010. Morphine regulates dopaminergic neuron differentiation via miR-133b. *Molecular pharmacology*, 78(5), pp.935–942.
- Sanders, L.H. et al., 2014. LRRK2 mutations cause mitochondrial DNA damage in iPSC-derived neural cells from Parkinson's disease patients: Reversal by gene correction. *Neurobiology of Disease*, 62, pp.381–386.
- Satake, W. et al., 2009. Genome-wide association study identifies common variants at four loci as genetic risk factors for Parkinson's disease. *Nature genetics*, 41(12), pp.1303–1307.
- Savica, R. et al., 2009. Medical records documentation of constipation preceding Parkinson

- disease: A case-control study. *Neurology*, 73(21), pp.1752–1758.
- Saxonov, S., Berg, P. & Brutlag, D.L., 2006. A genome-wide analysis of CpG dinucleotides in the human genome distinguishes two distinct classes of promoters. *Proceedings of the National Academy of Sciences*, 103(5), pp.1412–1417.
- Schaefer, A. et al., 2007. Cerebellar neurodegeneration in the absence of microRNAs. *The Journal of experimental medicine*, 204(7), pp.1553–8.
- Schapira, A.H. et al., 1989. Mitochondrial complex I deficiency in Parkinson's disease. *Lancet*, 1(8649), p.1269.
- Schapira, A.H. V, 2015. Glucocerebrosidase and Parkinson disease: Recent advances. *Molecular and cellular neurosciences*, 66(Pt A), pp.37–42.
- Schiffer, N.W. et al., 2007. Identification of anti-prion compounds as efficient inhibitors of polyglutamine protein aggregation in a zebrafish model. *Journal of Biological Chemistry*, 282(12), pp.9195–9203.
- Schlachetzki, J.C.M. & Hüll, M., 2009. Microglial activation in Alzheimer's disease. *Current Alzheimer research*, 6(6), pp.554–563.
- Schmidt, R., Strähle, U. & Scholpp, S., 2013. Neurogenesis in zebrafish - from embryo to adult. *Neural development*, 8, p.3.
- Schonrock, N. et al., 2010. Neuronal microRNA deregulation in response to Alzheimer's disease amyloid- β . *PLoS ONE*, 5(6).
- Schrag, A. & Schott, J.M., 2006. Epidemiological, clinical, and genetic characteristics of early-onset parkinsonism. *Lancet Neurology*, 5(4), pp.355–363.
- Seibler, P. et al., 2011. Mitochondrial Parkin recruitment is impaired in neurons derived from mutant PINK1 induced pluripotent stem cells. *The Journal of neuroscience : the official journal of the Society for Neuroscience*, 31(16), pp.5970–5976.
- Semina, E. V et al., 2000. Deletion in the promoter region and altered expression of Pitx3 homeobox gene in aphakia mice. *Human molecular genetics*, 9(11), pp.1575–1585.
- Sheng, D. et al., 2010. Deletion of the WD40 domain of LRRK2 in Zebrafish causes Parkinsonism-like loss of neurons and locomotive defect. *PLoS genetics*, 6(4), p.e1000914.
- Sherer, T.B. et al., 2003. Subcutaneous rotenone exposure causes highly selective dopaminergic degeneration and alpha-synuclein aggregation. *Experimental neurology*, 179(1), pp.9–16.
- Shi, X. et al., 2005. Zebrafish pitx3 is necessary for normal lens and retinal development. *Mechanisms of development*, 122(4), pp.513–27.
- Shimakami, T. et al., 2012. Base Pairing between Hepatitis C Virus RNA and MicroRNA 122 3' of Its Seed Sequence Is Essential for Genome Stabilization and Production of Infectious Virus. *Journal of Virology*, 86(13), pp.7372–7383.
- Shimura, H. et al., 2001. Ubiquitination of a new form of alpha-synuclein by parkin from human brain: implications for Parkinson's disease. *Science (New York, N.Y.)*, 293(5528), pp.263–269.
- Shin, J.H. et al., 2011. PARIS (ZNF746) repression of PGC-1 α contributes to neurodegeneration in parkinson's disease. *Cell*, 144(5), pp.689–702.
- Shulman, J.M., De Jager, P.L. & Feany, M.B., 2011. Parkinson's disease: genetics and pathogenesis. *Annual review of pathology*, 6, pp.193–222.

- Simon-Sanchez, J., Schulte, C. & Bras, J., 2009. Genome-wide association study reveals genetic risk underlying Parkinson's disease. ... *genetics*, 41(12), pp.1308–1312.
- Singleton, A.B. et al., 2003. alpha-Synuclein locus triplication causes Parkinson's disease. *Science (New York, N.Y.)*, 302(5646), p.841.
- Sinha, M., Mukhopadhyay, S. & Bhattacharyya, N.P., 2012. Mechanism(s) of alteration of micro rna expressions in huntington's disease and their possible contributions to the observed cellular and molecular dysfunctions in the disease. *NeuroMolecular Medicine*, 14(4), pp.221–243.
- Skibinski, G. et al., 2014. Mutant LRRK2 toxicity in neurons depends on LRRK2 levels and synuclein but not kinase activity or inclusion bodies. *The Journal of neuroscience : the official journal of the Society for Neuroscience*, 34(2), pp.418–33.
- Sleeman, I.J., Boshoff, E.L. & Duty, S., 2012. Fibroblast growth factor-20 protects against dopamine neuron loss in vitro and provides functional protection in the 6-hydroxydopamine-lesioned rat model of Parkinson's disease. *Neuropharmacology*, 63(7), pp.1268–1277.
- Smidt, M.P. et al., 2000. A second independent pathway for development of mesencephalic dopaminergic neurons requires Lmx1b. *Nature neuroscience*, 3(4), pp.337–341.
- Spencer, A.H. et al., 2011. The prevalence and clinical characteristics of punding in Parkinson's disease. *Movement disorders : official journal of the Movement Disorder Society*, 26(4), pp.578–586.
- Spillantini, M.G. et al., 1997. Alpha-synuclein in Lewy bodies. *Nature*, 388(6645), pp.839–840.
- Stamey, W., Davidson, A. & Jankovic, J., 2008. Shoulder pain: a presenting symptom of Parkinson disease. *Journal of clinical rheumatology : practical reports on rheumatic & musculoskeletal diseases*, 14(4), pp.253–254.
- Staton, A. a & Giraldez, A.J., 2011. Use of target protector morpholinos to analyze the physiological roles of specific miRNA-mRNA pairs in vivo. *Nature protocols*, 6(12), pp.2035–49.
- Sternberg, E.J. et al., 2013. Postural and Intention Tremors: A Detailed Clinical Study of Essential Tremor vs. Parkinson's Disease. *Frontiers in Neurology*, 4.
- Streisinger, G. et al., 1981. Production of clones of homozygous diploid zebra fish (*Brachydanio rerio*). *Nature*, 291(5813), pp.293–296.
- Su, W. et al., 2013. The p53 Transcription Factor Modulates Microglia Behavior through MicroRNA-Dependent Regulation of c-Maf. *The Journal of Immunology*, 192(1), pp.358–366.
- Su, W., Aloj, M.S. & Garden, G.A., 2015. MicroRNAs mediating CNS inflammation: Small regulators with powerful potential. *BRAIN, BEHAVIOUR, AND IMMUNITY*.
- Summerton, J.E., 2007. Morpholino, siRNA, and S-DNA compared: impact of structure and mechanism of action on off-target effects and sequence specificity. *Current topics in medicinal chemistry*, 7(7), pp.651–660.
- Sun, Y. et al., 2012. Zebrafish chemical screening reveals the impairment of dopaminergic neuronal survival by cardiac glycosides. *PLoS ONE*, 7(4), pp.1–11.
- Suwelack, D. et al., 2004. Neuronal expression of the transcription factor Gli1 using the Talpha1 alpha-tubulin promoter is neuroprotective in an experimental model of Parkinson's disease. *Gene therapy*, 11(24), pp.1742–1752.

- Swygert, S.G. & Peterson, C.L., 2014. Chromatin dynamics: Interplay between remodeling enzymes and histone modifications. *Biochimica et Biophysica Acta - Gene Regulatory Mechanisms*, 1839(8), pp.728–736.
- Taylor, T.N., Greene, J.G. & Miller, G.W., 2011. Behavioral phenotyping of mouse models of Parkinson's disease. *Behavioral neuroscience*, 211(1), pp.1–10.
- Thai, T.-H. et al., 2007. Regulation of the Germinal Center Response by MicroRNA-155. *Science*, 316(5824), pp.604–608.
- Thomas, B. & Flint Beal, M., 2007. Parkinson's disease. *Human Molecular Genetics*, 16(R2).
- Thounaojam, M.C. et al., 2014. MicroRNA 155 regulates Japanese encephalitis virus-induced inflammatory response by targeting Src homology 2-containing inositol phosphatase 1. *Journal of virology*, 88(9), pp.4798–810.
- Tong, M., Dong, M. & de la Monte, S.M., 2010. Brain Insulin-Like Growth Factor and Neurotrophin Resistance in Parkinson's Disease and Dementia with Lewy Bodies: Potential Role of Manganese Neurotoxicity. , 16(3), pp.585–599.
- Tong, Y. et al., 2009. R1441C mutation in LRRK2 impairs dopaminergic neurotransmission in mice. *Proceedings of the National Academy of Sciences of the United States of America*, 106(34), pp.14622–14627.
- Del Tredici, K. & Braak, H., 2012. Lewy pathology and neurodegeneration in premotor Parkinson's disease. *Movement Disorders*, 27(5), pp.597–607.
- Varshney, G.K. et al., 2015. High-throughput gene targeting and phenotyping in zebrafish using CRISPR / Cas9. , pp.1030–1042.
- Venderova, K. et al., 2009. Leucine-rich repeat kinase 2 interacts with Parkin, DJ-1 and PINK-1 in a *Drosophila melanogaster* model of Parkinson's disease. *Human Molecular Genetics*, 18(22), pp.4390–4404.
- Verdin, H. et al., 2014. Novel and recurrent PITX3 mutations in Belgian families with autosomal dominant congenital cataract and anterior segment dysgenesis have similar phenotypic and functional characteristics. *Orphanet journal of rare diseases*, 9(1), p.26.
- Verstraeten, A., Theuns, J. & Van Broeckhoven, C., 2015. Progress in unraveling the genetic etiology of Parkinson disease in a genomic era. *Trends in genetics : TIG*, 31(3), pp.140–9.
- Vigorito, E. et al., 2013. miR-155: An ancient regulator of the immune system. *Immunological Reviews*, 253, pp.146–157.
- Vila, M., Ramonet, D. & Perier, C., 2008. Mitochondrial alterations in Parkinson's disease: New clues. *Journal of Neurochemistry*, 107(2), pp.317–328.
- Vilariño-Güell, C. et al., 2014. DNAJC13 mutations in Parkinson disease. *Human molecular genetics*, 23(7), pp.1794–801.
- Visanji, N.P. et al., 2013. The prion hypothesis in Parkinson's disease: Braak to the future. *Acta neuropathologica communications*, 1(1), p.2.
- Vitner, E.B. et al., 2012. Contribution of brain inflammation to neuronal cell death in neuronopathic forms of Gaucher's disease. *Brain*, 135, pp.1724–1735.
- Volpicelli, F. et al., 2012. Direct regulation of Pitx3 expression by Nurr1 in culture and in developing mouse midbrain. *PLoS ONE*, 7(2).
- van der Walt, J.M. et al., 2004. Fibroblast growth factor 20 polymorphisms and haplotypes strongly influence risk of Parkinson disease. *American journal of human genetics*, 74(6), pp.1121–1127.

- Wang, G. et al., 2008. Variation in the miRNA-433 Binding Site of FGF20 Confers Risk for Parkinson Disease by Overexpression of α -Synuclein. *The American Journal of Human Genetics*, 82(2), pp.283–289.
- Wang, H. et al., 2013. One-Step Generation of Mice Carrying Mutations in Multiple Genes by CRISPR/Cas-Mediated Genome Engineering. *Cell*, 153(4), pp.910–918.
- Wang, P. et al., 2010. Inducible microRNA-155 feedback promotes type I IFN signaling in antiviral innate immunity by targeting suppressor of cytokine signaling 1. *Journal of immunology (Baltimore, Md. : 1950)*, 185(10), pp.6226–6233.
- Wen, D. et al., 2013. MiR-133b acts as a tumor suppressor and negatively regulates FGFR1 in gastric cancer. *Tumor Biology*, 34(2), pp.793–803.
- Wen, L. et al., 2008. Visualization of monoaminergic neurons and neurotoxicity of MPTP in live transgenic zebrafish. *Developmental biology*, 314(1), pp.84–92.
- West, A.B. et al., 2005. Parkinson's disease-associated mutations in leucine-rich repeat kinase 2 augment kinase activity. *Proceedings of the National Academy of Sciences of the United States of America*, 102(46), pp.16842–16847.
- West, A.B. et al., 2007. Parkinson's disease-associated mutations in LRRK2 link enhanced GTP-binding and kinase activities to neuronal toxicity. *Human Molecular Genetics*, 16(2), pp.223–232.
- West, R.J.H. et al., 2015. Neurophysiology of Drosophila models of Parkinson's disease. *Parkinson's disease*, 2015, p.381281.
- Westhoff, J.H. et al., 2013. Development of an automated imaging pipeline for the analysis of the zebrafish larval kidney. *PLoS ONE*, 8(12), pp.1–13.
- Wider, C. et al., 2009. FGF20 and Parkinson's disease: no evidence of association or pathogenicity via alpha-synuclein expression. *Movement disorders : official journal of the Movement Disorder Society*, 24(3), pp.455–459.
- Wienholds, E. & Kloosterman, W., 2005. MicroRNA expression in zebrafish embryonic development. *Science*, (July), pp.310–311.
- Wiklund, E.D. et al., 2011. Coordinated epigenetic repression of the miR-200 family and miR-205 in invasive bladder cancer. *International Journal of Cancer*, 128(6), pp.1327–1334.
- Wilkinson, R.N. et al., 2012. Hedgehog signaling via a calcitonin receptor-like receptor can induce arterial differentiation independently of VEGF signaling in zebrafish. *Blood*, 120(2), pp.477–488.
- Williams, A.H. et al., 2009. MicroRNA control of muscle development and disease. *Current Opinion in Cell Biology*, 21(3), pp.461–469.
- Williams, A.H. et al., 2009. MicroRNA-206 delays ALS progression and promotes regeneration of neuromuscular synapses in mice. *Science (New York, N.Y.)*, 326(5959), pp.1549–1554.
- Williams, D.R., Watt, H.C. & Lees, A.J., 2006. Predictors of falls and fractures in bradykinetic rigid syndromes: a retrospective study. *Journal of neurology, neurosurgery, and psychiatry*, 77(4), pp.468–473.
- Williams, T. et al., 2012. Recent advances in the utility and use of the General Practice Research Database as an example of a UK Primary Care Data resource. *Therapeutic Advances in Drug Safety*, 3(2), pp.89–99.
- Wilms, H. et al., 2003. Activation of microglia by human neuromelanin is NF-kappaB dependent and involves p38 mitogen-activated protein kinase: implications for

- Parkinson's disease. *The FASEB journal : official publication of the Federation of American Societies for Experimental Biology*, 17(3), pp.500–502.
- Wittbrodt, J.N., Liebel, U. & Gehrig, J., 2014. Generation of orientation tools for automated zebrafish screening assays using desktop 3D printing. , pp.1–6.
- Wittmann, C. et al., 2012. Facilitating Drug Discovery: An Automated High-content Inflammation Assay in Zebrafish. *Journal of Visualized Experiments*, 222(65), pp.1–7.
- Woodard, C.M. et al., 2014. iPSC-Derived Dopamine Neurons Reveal Differences between Monozygotic Twins Discordant for Parkinson's Disease. *Cell Reports*, 9(4), pp.1173–1182.
- Wu, D.C. et al., 2002. Blockade of microglial activation is neuroprotective in the 1-methyl-4-phenyl-1,2,3,6-tetrahydropyridine mouse model of Parkinson disease. *The Journal of neuroscience : the official journal of the Society for Neuroscience*, 22(5), pp.1763–1771.
- Wu, D.-C. et al., 2003. NADPH oxidase mediates oxidative stress in the 1-methyl-4-phenyl-1,2,3,6-tetrahydropyridine model of Parkinson's disease. *Proceedings of the National Academy of Sciences of the United States of America*, 100(10), pp.6145–6150.
- Xi, Y. et al., 2010. Impaired dopaminergic neuron development and locomotor function in zebrafish with loss of pink1 function. *European Journal of Neuroscience*, 31(4), pp.623–633.
- Xi, Y., Yu, M., et al., 2011. Transgenic zebrafish expressing green fluorescent protein in dopaminergic neurons of the ventral diencephalon. *Developmental dynamics : an official publication of the American Association of Anatomists*, 240(11), pp.2539–47.
- Xi, Y., Noble, S. & Ekker, M., 2011. Modeling neurodegeneration in zebrafish. *Current neurology and neuroscience reports*, 11(3), pp.274–82.
- Xu, L., Chen, W.-F. & Wong, M.-S., 2009. Ginsenoside Rg1 protects dopaminergic neurons in a rat model of Parkinson's disease through the IGF-I receptor signalling pathway. *British journal of pharmacology*, 158(3), pp.738–748.
- Yamaguchi, H. & Shen, J., 2007. Absence of dopaminergic neuronal degeneration and oxidative damage in aged DJ-1-deficient mice. *Molecular neurodegeneration*, 2, p.10.
- Yan, C.H. et al., 2011. Lmx1a and Lmx1b function cooperatively to regulate proliferation, specification, and differentiation of midbrain dopaminergic progenitors. *The Journal of neuroscience : the official journal of the Society for Neuroscience*, 31(35), pp.12413–12425.
- Yang, X., 2015. Applications of CRISPR-Cas9 mediated genome engineering. *Military Medical Research*, 2(1), p.11.
- Yang, Y. et al., 2006. Mitochondrial pathology and muscle and dopaminergic neuron degeneration caused by inactivation of Drosophila Pink1 is rescued by Parkin. *Proceedings of the National Academy of Sciences of the United States of America*, 103(28), pp.10793–10798.
- Yin, V.P. et al., 2008. Fgf-dependent depletion of microRNA-133 promotes appendage regeneration in zebrafish. *Genes and Development*, 22(6), pp.728–733.
- Yin, V.P. et al., 2012. Regulation of zebrafish heart regeneration by miR-133. *Developmental Biology*, 365(2), pp.319–327.
- Yin, W.Z. et al., 2014. Down-regulation of MicroRNA-205 promotes gastric cancer cell proliferation. *European Review for Medical and Pharmacological Sciences*, 18(7), pp.1027–1032.

- Yu, Y. et al., 2012. MicroRNA miR-133b is essential for functional recovery after spinal cord injury in adult zebrafish. , 33(9), pp.1587–1597.
- Zesiewicz, T.A., Sullivan, K.L. & Hauser, R.A., 2006. Nonmotor symptoms of Parkinson's disease. *Expert review of neurotherapeutics*, 6(12), pp.1811–1822.
- Zhang, Y., Wang, Z. & Gemeinhart, R.A., 2013. Progress in microRNA delivery. *Journal of Controlled Release*, 172(3), pp.962–974.
- Zhao, H. et al., 2013. MiR-133b is down-regulated in human osteosarcoma and inhibits osteosarcoma cells proliferation, migration and invasion, and promotes apoptosis. *PLoS ONE*, 8(12), pp.1–11.
- Zhao, Y. et al., 2014. MiR-133b is frequently decreased in gastric cancer and its overexpression reduces the metastatic potential of gastric cancer cells. *BMC cancer*, 14(1), p.34.
- Zimprich, A. et al., 2011. A mutation in VPS35, encoding a subunit of the retromer complex, causes late-onset parkinson disease. *American Journal of Human Genetics*, 89(1), pp.168–175.
- Zimprich, A. et al., 2004. Mutations in LRRK2 cause autosomal-dominant parkinsonism with pleomorphic pathology. *Neuron*, 44(4), pp.601–607.
- Zovoilis, A. et al., 2011. microRNA-34c is a novel target to treat dementias. *The EMBO journal*, 30(20), pp.4299–308.
- Züchner, S. et al., 2006. Mutations in the novel mitochondrial protein REEP1 cause hereditary spastic paraplegia type 31. *American journal of human genetics*, 79(2), pp.365–369.